UCLA
UCLA Electronic Theses and Dissertations

Title

Icosahedral Boron Clusters: Building Blocks In Luminescent Materials

Permalink

Author

Kirlikovali, Kent Ozan

Publication Date

2019

UNIVERSITY OF CALIFORNIA

Los Angeles

Icosahedral Boron Clusters:

Building Blocks in Luminescent Materials

A dissertation submitted in partial satisfaction of the

requirements for the degree Doctor of Philosophy

in Chemistry

by

Kent Ozan Kirlikovali

2019

ABSTRACT OF THE DISSERTATION

Icosahedral Boron Clusters:

Building Blocks in Luminescent Materials

by

Kent Ozan Kirlikovali

Doctor of Philosophy in Chemistry

University of California, Los Angeles, 2019

Professor Alexander Michael Spokoyny, Chair

This dissertation describes the development of unique ligand scaffolds incorporating icosahedral carboranes, a robust group of organomimetic clusters that provide a variety of tunable frameworks not attainable with standard aromatic ligands, for use in luminescent transition metal complexes. Specifically, we have targeted blue phosphorescent Ir(III)- and Pt(II)-based emitters in the context of organic light-emitting diode (OLED) applications. OLEDs incorporating these types of emitters have achieved remarkable efficiencies in recent years, leading to the development of thinner and less energy-intensive television screens, mobile phone displays, and solid-state lighting sources. In order to realize the full potential of OLED-based devices on a global scale, critical issues related to efficiency and lifetime of blue OLEDs must be addressed.

Chapter One provides a brief history of lighting technology and the current status of OLED technology. An overview of blue phosphorescent Ir(III)- and Pt(II)-based emitters is discussed, including key design parameters and current challenges associated with this class of emitters. Lastly, a background on boron cluster chemistry is provided.

Chapter Two describes a new class of robust and highly luminescent *bis*(heteroleptic) Ir(III) complexes containing weakly coordinating *nido*-carboranyl substituents. These ligands associate with the cationic Ir(III) center through primarily electrostatic interactions. Importantly, the observed quantum yields for these complexes correspond to a 10-fold increase compared to those of previously reported Ir(III) complexes with carboranyl-based ligands featuring covalent interactions between the cluster and the Ir(III) center.

Chapter Three introduces a dianionic, strong field ancillary ligand framework based on 1,1′-bis-*o*-carborane (bc). A blue phosphorescent Pt(II) complex featuring the bc ligand is studied. The bc ligand remains photophysically innocent in all visible transitions, and it provides sufficient steric bulk to preclude parasitic intermolecular Pt(II)···Pt(II) interactions.

Chapter Four details the synthesis of two isomeric Pt(II) complexes featuring the bc ligand. Control over the mode of chelation of the bc ligand to the Pt(II) center enables the fine-tuning of the electronic properties of the resulting Pt(II) complexes by virtue of vertex-differentiated coordination chemistry of carborane-based ligands.

Chapter Five presents current progress towards luminescent metal complexes featuring multidentate carborane-based ligand architectures. This class of ligands should result in more rigid metal complexes with improved emission efficiency and greater stability. Ultimately, this work presents potentially new avenues for designing efficient blue phosphorescent emitters through the use of tunable carborane-based ligand scaffolds.

The dissertation of Kent Ozan Kirlikovali is approved.

Benjamin Joel Schwartz

Robin L. Garrell

Dante A. Simonetti

Alexander Michael Spokoyny, Committee Chair

University of California, Los Angeles

2019

Thank you for everything, Mom and Dad.

I love you guys.

TABLE OF CONTENTS

CHAPTER 3: Luminescent Metal Complexes Featuring Photophysically Innocent Boron Cluster Ligands

CHAPTER 4: Fine-Tuning Electronic Properties of Luminescent Pt(II) Compleses *via* Vertex-Differentiated Coordination of Sterically Invariant Carborane-Based Ligands

LIST OF FIGURES

LIST OF TABLES

LIST OF ABBREVIATIONS

2-MeTHF = 2-Methyltetrahydrofuran
acac = Acetylacetonate
bc = 1,1′-bis-o-carborane dianion
bph = Biphenyl
bpy = 2,2′-Bipyridine
cod = 1,5-Cyclooctadiene
CV = Cyclic voltammetry
DME = 1,2-Dimethoxyethane
dppe = 1,2-Diphenylphosphinoethane
dtb-bpy = 4,4′-Di-$tert$-butyl-2,2′-bipyridine
Et_2O = Diethyl ether
^{F2}ppy = 2-(2,4-Difluorophenyl)pyridine
Fc = Ferrocene
H_2-bc = 1,1′-Bis-o-carborane
KHMDS = Potassium hexamethyldisilazide
MTBE = Methyl $tert$-butyl ether
N^nBu_4 = Tetra-n-butylammonium
NEt_4 = Tetraethylammonium
NHC = N-heterocyclic carbene
NMR = Nuclear magnetic resonance
oCB = o-Carborane
OLED = Organic light-emitting diode
TADF = Thermally activated delayed fluorescence
THF = Tetrahydrofuran
Ph = Phenyl
ppy = 2-Phenylpyridine
py = Pyridine
^tBu = $tert$-Butyl
tebc = 9,9′,12,12′-Tetra-ethyl-1,1′-bis(o-carborane)
Tol = Toluene
TGA = Thermogravimetric analysis
VT = Variable temperature

ACKNOWLEDGMENTS

It's finally hitting me that this whole graduate school thing is coming to an end, and it feels pretty surreal recognizing that I've finally reached this point. I've learned so much about myself through all the ups and downs of graduate school, and there's absolutely no way I would have survived without the support from some amazing people around me. I must first thank Alex, my advisor, for his mentorship that enabled me to mature into a competent, thoughtful scientist (or so I'd like to think, anyway). Alex created a highly collaborative and interdisciplinary research environment that constantly challenges everyone fortunate enough to join his group. When I started at UCLA, I didn't fully appreciate the importance of effectively communicating ideas, and I thought all the important work was done in lab. I'd be lying if I said I never put together a bad figure or never bombed a public presentation (I actually did more of both than I'd care to admit), but Alex always took the time to work with me and teach me how to craft a story for a specific audience in a way that made the research engaging and worth listening to. It was definitely a process, but I'm forever indebted to Alex for holding me, as well as everyone else in the group, to this high standard. I'd also like to thank other faculty members in the department, especially those on my committee, Prof. Ben Schwartz, Prof. Robin Garrell, and Prof. Dante Simonetti, who have been involved throughout my graduate career.

There's no way I would have excelled in the lab without the mentorship provided by all of our amazing post docs, Dr. Liban Saleh, Dr. Jon Axtell, Dr. Xin Mu, and Dr. Julia Stauber. All of you have all spent countless hours with me helping me design experiments and analyze data, and you've kept me on track by allowing me to constantly solicit career and life advice. Your perpetual presence in the lab has played a massive part in my growth as a chemist, and I have no doubt that every other student in our group would share this sentiment.

Starting up the lab with the other grad students in the first crop, Rafal Dziedzic, Dahee Jung, Marco Messina, Elaine Qian, and Alex Wixtrom, was an adventure I wouldn't trade for anything. I think I can finally look back on all those late nights in lab with Yams not Yangers playing on the radio and smile. I was fortunate enough to mentor multiple undergraduate students, Alice Phung, Aly Gonzalez, and Michelle Ko, as well as one graduate student, Kierstyn Anderson, which was a rewarding experience that we all learned from (I think). Kierstyn, take care of our hood, and just remember to ask yourself this question whenever you're stuck trying to solve a problem: "What would Jon do?" To all the other current grad students, Jessica Logan, Nick Bernier, Harry Mills, Mary Waddington, Zeeshan Parvez, Rebecca Kubena, and Hayden Montgomery, you guys are in good hands. I've had a blast getting to know all of you, from the random nights out to the multiple Vegas and Mammoth retreats and every 4 hour group meeting in between, and I'm excited to see the awesome work this group will produce in the coming years.

I've had the pleasure of being a TA for some great professors throughout my time at UCLA, especially Dr. Johnny Pang and Dr. Roshini Ramachandran (the ultimate post-doc/professor hybrid). I learned a lot about myself while preparing for and teaching these classes, and I always felt I had endless support from you both. Thank you for the great experiences.

I'd like to thank my undergraduate advisors, Prof. Mark Thompson and Peter Djurovich, for their continuous guidance throughout my time at both USC and UCLA. I had an incredible undergraduate research experience that solidified my desire to pursue a Ph.D., and the fact that I have been going back there at least 2-3 times per year to run experiments while at UCLA illustrates their continuous support for me. Also, I must say SCIP lived up to all the hype.

I'm 100% certain I wouldn't be where I am now if it wasn't for the awesome group of friends around me: my roommates, the Marina/Montana boys, the fantasy football squad, the Coachella/Rufus crews, and countless other wonderful people in my life. The transition into grad school was a rough one at times, but you always had my back. You picked me up when I was down and celebrated with me when I felt like I was on top of the world. I owe a lot of my success and personal growth over this time in my life to you guys. I'm stoked for the final celebration and to see what the future holds for all of us.

I've had plenty of outside support from Peter Kassel and Ayala Ofek, especially during this transition out of graduate school and into the unknown world outside of Southern California. Thank you for always listening and for helping me through it.

Lastly, I want to thank my parents for always being there for me. You led by example and showed me what hard work and commitment can accomplish. You always encouraged me to follow my dreams and sacrificed for me so that I had the option to do whatever I wanted with my life. I've always felt this freedom, and I still gravitated towards chemistry (thanks, Dad, for all the awesome chemistry demos when I was a kid!). I've been so incredibly fortunate to have two loving and supporting parents. Thank you for everything. I love you guys.

Chapter One is a version of Kirlikovali, K. O.; Spokoyny, A. M. "The Long Lasting Blues: A New Record for Phosphorescent Organic Light-Emitting Diodes." *Chem* **2017**, *3,* 385-387.

Chapter Two is a version of Axtell, J. C.; Kirlikovali, K. O.; Djurovich, P. I.; Jung, D.; Nguyen, V. T.; Munekiyo, B.; Royappa, A. T.; Rheingold, A. L.; Spokoyny, A. M. "Blue Phosphorescent Zwitterionic Iridium(III) Complexes Featuring Weakly Coordinating *nido*-Carborane-based Ligands." *J. Am. Chem. Soc.* **2016**, *138*, 15758-15765. Axtell, Kirlikovali,

Djurovich, Jung, and Nguyen were responsible for experimental work. Royappa and Rheingold were responsible for X-ray crystallographic studies.

Chapter Three is a version of Kirlikovali, K. O.; Axtell, J. C.; Gonzalez, A.; Phung, A. C.; Khan, S. I.; Spokoyny, A. M. "Luminescent Metal Complexes Featuring Photophysically Innocent Boron Cluster Ligands." *Chem. Sci.* **2016**, *7*, 5132-5138. Kirlikovali, Axtell, Gonzalez, and Phung were responsible for experimental work. Khan was responsible for X-ray crystallographic studies.

Chapter Four is a version of Kirlikovali, K. O.; Axtell, J. C.; Djurovich, P. I.; Anderson, K.; Rheingold, A. L.; Spokoyny, A. M. "Fine-Tuning Electronic Properties of Luminescent Pt(II) Complexes *via* Coordination of 1,1′-Bis(*o*-carborane)." *Organometallics* **2018**, *37*, 3122-3131. Kirlikovali, Axtell, Djurovich, and Anderson were responsible for experimental work. Rheingold was responsible for X-ray crystallographic studies.

Chapter Five contains unpublished results. Dr. Jonathan C. Axtell and Kierstyn Anderson contributed to the experimental studies.

BIOGRAPHICAL SKETCH

Education

University of Southern California   Chemistry   B.S. (5/2014)

Professional Experience

7/2013 – 8/2013   Research Assistant, Myriant, Boston, MA.
Project: Analytical Methods to Monitor Succinic Acid Production.

11/2011 – 7/2013   Undergraduate Researcher, Department of Chemistry, USC.
Advisor: Mark E. Thompson.
Research Specialization: Zinc Dipyrrin Complexes for Organic
Photovoltaic Devices.

6/2010 – 8/2010   Research Assistant, Integrated Polymer Industries (IPI), Irvine, CA.
Project: Development of Solidifiers for CO-110 IPI-SuperLamina™
(Polymer Sealant for Concrete Surfaces).

Selected Awards and Honors

IPMI Student Award Winner (International Precious Metals Institute, 03/2018)
Ralph & Charlene Bauer Inorganic Chemistry Award (UCLA, 01/2018)
Link Foundation Energy Fellowship, Honorable Mention (Link Foundation Energy Program, 04/2017)
Research Pitch Competition Award (UCLA, 12/2015).

Graduate Teaching Assistant (UCLA)

2014 – 2019   **Chemistry 174** (3x) – advanced inorganic chemistry, lab; **Chemistry C179/C279**;
bioinorganic chemistry, lecture; **Chemistry 172/272** – advanced inorganic chemistry II,
lecture; **Chemistry 20L** (2x) – general chemistry I, lab, **Chemistry 30AL** – general
chemistry II, lab; **Chemistry 14A** (2x) – general chemistry I, lecture; **Chemistry 14B** –
general chemistry II, lecture; **Chemistry 14BL** (2x) – general and organic chemistry, lab;
Chem 3 – general chemistry for non-chemistry majors, lecture.

Peer-Reviewed Publications (* - denotes co-first authorship)

1. Yruegas, S.; Axtell, J. C.; Kirlikovali, K. O.; Spokoyny, A. M.; Martin, C. D. "Synthesis of 9-Borafluorene Analogues Featuring a Three-Dimensional 1,1'-Bis(*o*-carborane) Backbone." *Chem. Commun.* **2019**, *55*, 2892-2895.
2. Anderson, K. P.; Mills, H. A.; Mao, C.; Kirlikovali, K. O.; Axtell, J. C.; Rheingold, A. L.; Spokoyny, A. M. "Improved Synthesis of Icosahedral Carboranes Containing Exohedral B-C and C-C Bonds." *Tetrahedron* **2019**, *75,* 187-191. *(Special Issue on Frustrated Lewis Acids and Organoboranes).* Preprint: https://doi.org/10.26434/chemrxiv.7252586.v1.
3. Kirlikovali, K. O.; Axtell, J. C.; Djurovich, P. I.; Anderson, K.; Rheingold, A. L.; Spokoyny, A. M. "Fine-Tuning Electronic Properties of Luminescent Pt(II) Complexes *via* Coordination of 1,1′-Bis(*o*-carborane)." *Organometallics* **2018**, *37*, 3122-3131. *Preprint: https://doi.org/10.26434/chemrxiv.6670739.v1*
4. Kirlikovali, K. O.; Cho, E.; Downard, T. J.; Grigoryan, L.; Han, Z.; Hong, S.; Jung, D.; Quintana, J. C.; Reynoso, V.; Ro, S.; Shen, Y.; Swartz, K.; Ter Sahakyan, E.; Wixtrom, A. I.; Yoshida, B.; Rheingold, A. L.; Spokoyny, A. M. "Buchwald-Hartwig Amination Using Pd(I) Dimer Precatalysts Supported by Biaryl Phosphine Ligands." *Dalton Trans.* **2018**, *47,* 3684-3688. *(Winter 2017, Chemistry 174 Independent Course Project). Preprint: https://dx.doi.org/10.26434/chemrxiv.5758551.v1*
5. Kirlikovali, K. O.; Spokoyny, A. M. "The Long Lasting Blues: A New Record for Phosphorescent

Organic Light-Emitting Diodes." *Chem* **2017**, *3,* 385-387. *(Preview Article)*

6. Axtell, J. C.; <u>Kirlikovali, K. O.</u>; Dziedzic, R. M.; Gembicky, M.; Rheingold, A. L.; Spokoyny, A. M. "Magnesium Reagents Featuring a 1,1'-Bis(*o*-Carborane) Ligand Platform." *Eur. J. Inorg. Chem.* **2017**, 4411-4416. *(VIP - Very Important Paper and Cover Article)*
7. Axtell, J. C.; <u>Kirlikovali, K. O.</u>; Jung, D.; Dziedzic, R. M.; Rheingold, A. L.; Spokoyny, A. M. "Metal-Free Peralkylation of the *closo*-Hexaborate Anion." *Organometallics* **2017**, *36,* 1204-1210.
8. Axtell,* J. C.; <u>Kirlikovali,* K. O.</u>; Djurovich, P. I.; Jung, D.; Nguyen, V. T.; Munekiyo, B.; Royappa, A. T.; Rheingold, A. L.; Spokoyny, A. M. "Blue Phosphorescent Zwitterionic Iridium(III) Complexes Featuring Weakly Coordinating *nido*-Carborane-based Ligands." *J. Am. Chem. Soc.* **2016**, *138*, 15758-15765.
9. Messina, M. S.; Axtell, J. C.; Wang, Y.; Chong, P.; Wixtrom, A. I.; <u>Kirlikovali, K. O.</u>; Upton, B. M.; Hunter, B. M.; Shafaat, O. S.; Khan, S. I.; Winkler, J. R.; Gray, H. B.; Alexandrova, A. N.; Maynard, H. D.; Spokoyny, A. M. "Visible-Light-Induced Olefin Activation Using 3D Aromatic Boron-Rich Cluster Photooxidants." *J. Am. Chem. Soc.* **2016***, 138, 6952-6955.*
10. <u>Kirlikovali, K. O.</u>; Axtell, J. C.; Gonzalez, A.; Phung, A. C.; Khan, S. I.; Spokoyny, A. M. "Luminescent Metal Complexes Featuring Photophysically Innocent Boron Cluster Ligands." *Chem. Sci.* **2016**, *7*, 5132-5138.
11. Bartynski, A.; Trinh, C.; <u>Kirlikovali, K. O.</u>; Thompson, M. E. "Multichromophoric Energy Sensitization of C_{60} for Organic Photovoltaics." *Appl. Phys. Lett.* **2014**, *105*, 113305.
12. Trinh, C.; <u>Kirlikovali, K. O.</u>; Das, S.; Ener, M. E.; Gray, H. B.; Djurovich, P.; Bradforth, S. E.; Thompson, M. E. "Symmetry-Breaking Charge Transfer of Visible Light Absorbing Systems: Zinc Dipyrrins." *J. Phys. Chem. C.* **2014**, *118*, 21834-21845.
13. Trinh, C.; <u>Kirlikovali, K. O.</u>; Bartynski, A. N.; Tassone, C. J.; Toney, M. F.; Burkhard, G. F.; McGehee, M. D.; Djurovich, P. I.; Thompson, M. E. "Efficient Energy Sensitization of C_{60} and Application to Organic Photovoltaics." *J. Am. Chem. Soc*. **2013**, *135*, 11920-11928.

Selected Public Presentations
1. "Polydentate Boron Cluster Ligands: Synthesis and Applications in Luminescent Pt(II) Complexes." Organometallics Gordon Research Conference, Salve Regina University, Newport, RI, July 2018 (poster).
2. "The Chemistry of Precious Metals: From Luminescent Materials to Catalysis." International Precious Metals Institute National Conference, San Antonio, TX, June 2018 (invited talk).
3. "Blue Phosphorescent Pt(II) and Ir(III) Complexes Featuring Carborane-based Ligands for OLED Applications." Photochemisrty Gordon Research Conference, Bates College, Lewiston, ME, July 2017 (poster).
4. "Blue Phosphorescent Zwitterionic Ir(III) Complexes Featuring Weakly Coordinating Ligands." ACS National Meeting, San Francisco, CA, April 2017 (talk).
5. "Photophysically Innocent Boron Cluster Ligand Scaffolds for Light-Emitting Diode Materials." ACS National Meeting, San Diego, CA, April 2016 (talk).

Patents and Patent Applications
1. Spokoyny, Maynard, Qian, Messina, Wixtrom, Axtell, <u>Kirlikovali</u>, Gonzalez. "Novel Three-Dimensional Boron-Rich Clusters." US Patent US20190047871A1. February 14, 2019.

CHAPTER 1 – GENERAL INTRODUCTION

1.1 History of Lighting Technology

Thomas Edison revolutionized lighting in the late 19th century with the invention of the first commercially practical incandescent light bulb, a considerable improvement on the oil lamps and candles that were used up to that time. Incandescent bulbs generate light by passing electricity through a wire filament until it is hot enough to radiate visible light; as a result, more than 95% of the energy is lost as heat, and a majority of the light emitted is in the invisible infrared region (Table 1.1).[1,2] Fluorescent light bulbs, up to five times more efficient and an order of magnitude longer-lasting than incandescent bulbs (Table 1.1), have been favored over incandescent bulbs since their commercialization in the early 1940s.[1] Applying an electric current through a fluorescent bulb excites mercury vapor, which then emits ultraviolet (UV) radiation that hits a phosphor coating, ultimately resulting in the emission of visible light. Significant drawbacks include the use of mercury, which presents a health hazard and complicates safe disposal procedures, and the fundamental limitation of luminous efficacy to 90 lm/W,[1,2] which is due to the intrinsic loss of energy when converting UV photons to visible photons (commercial fluorescent bulbs produce about 70 lm/W, Table 1.1). Until the development of white light-emitting diodes (LEDs), fluorescent bulbs remained the most efficient sources of light available.

Table 1.1 Performance comparison of three ubiquitous sources of light.

Source	Luminous Efficacy[a] (lm/W)	Energy Efficiency[b]	Lifetime[c] (hours)
Incandescent	16	2%	10^3
Fluorescent	70	10%	10^4
LED	300	45%	10^5

[a]Visible light source efficiency detected by the human eye. [b]Source efficiency based on the electricity conversion (a 100%-efficient lamp produces 680 lm/W). [c]The average lifespan of the source. Data obtained from Reference 1.

LEDs are currently the most efficient sources of light, with luminous efficacy values exceeding 300 lm/W and lifetimes (~10^5 hours) that are orders of magnitude longer than those of fluorescent and incandescent bulbs (Table 1.1).[1,2] In LEDs, multiple layers of carefully engineered inorganic semiconductors directly convert electricity into photons; the energy of the photon, and therefore the color of light emitted, can be tuned by varying the band gap of the semiconductor. White light can be produced by using a blue LED to excite a phosphor, which then produces the remaining portion of the visible spectrum (similar to fluorescent bulbs), or by combining red, green, and blue LEDs in a single device. With lighting accounting for 20-30% of the world's energy consumption, mass production of white LEDs has significantly contributed to worldwide energy conservation. In addition to more efficient solid-state lighting, larger and brighter lighting panels, screens, and displays have also resulted from the continued improvement in the efficiency of LEDs.[1-3]

1.2 Overview of Organic Light-Emitting Diodes (OLED) Technology

Organic light-emitting diodes (OLEDs) do not rely on inorganic semiconductors, but rather thin layers of small organic molecules (10s – 100s of nm thick) sandwiched between metal electrodes (Figure 1.1). OLEDs have multiple advantages over their inorganic counterparts:[3-5] they are orders of magnitude thinner and lighter, which enables the development of transparent devices, they can be applied to flexible plastic substrates resulting in screens and displays that can be rolled up, and they are brighter than inorganic LEDs because multiple thin, emissive layers can be deposited on a single device. OLED television screens and mobile phone displays have gained popularity in recent years as thinner and less energy-intensive alternatives to their non-organic counterparts; however, the operational lifetime of blue OLEDs is limited to hundreds of hours, reducing their utility in these applications. Similar to the blue LED, a long-

2

lasting blue OLED must be created before we can realize the full potential of OLEDs in these applications.
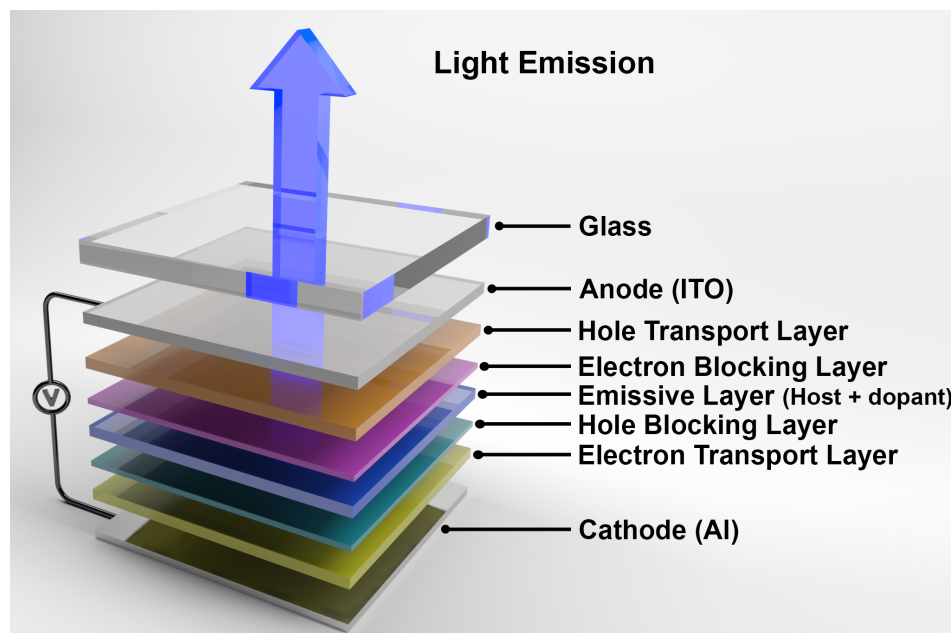
Figure 1.1 Typical architecture for an organic light-emitting diode (OLED) device.

OLED devices can generate light from purely organic molecules (fluorescent, Figure 1.2A) or organometallic molecules (phosphorescent, Figure 1.2B). Light emission in OLEDs proceeds *via* recombination of electrons and holes and leads to the formation of 25% singlet excitons and 75% triplet excitons.[3] Fluorescent emitters, usually highly conjugated organic molecules, are unable to access the triplet excitons and the remaining 75% of triplet excitons are lost as heat instead of the desired generation of light. Thermally activated delayed fluorescence (TADF) is an emerging type of purely organic OLED[6-10] that can achieve nearly 100% internal quantum efficiency.[11-14] To achieve TADF, the energy gap between singlet and triplet states is minimized so that the two spin states thermally equilibrate, resulting in a reversible intersystem crossing in which non-radiative triplet excitons can up-convert to radiative singlet excitons. Though researchers have fabricated TADF OLED devices with external quantum efficiencies (EQE) comparable to those of PHOLEDs (~20%),[6-8,12] highly conjugated organic emitter

molecules are still susceptible to bond-breaking degradation pathways, especially for molecules used in high-energy blue OLEDs.

A

2-CzPN
Ref. 6

DMAC-DPS
Ref. 11

DABNA-2
Ref. 12

B

Firpic
Ref. 75

***fac*-Ir(pmp)₃**
Ref. 61

***fac*-Ir(dmp)₃**
Ref. 59
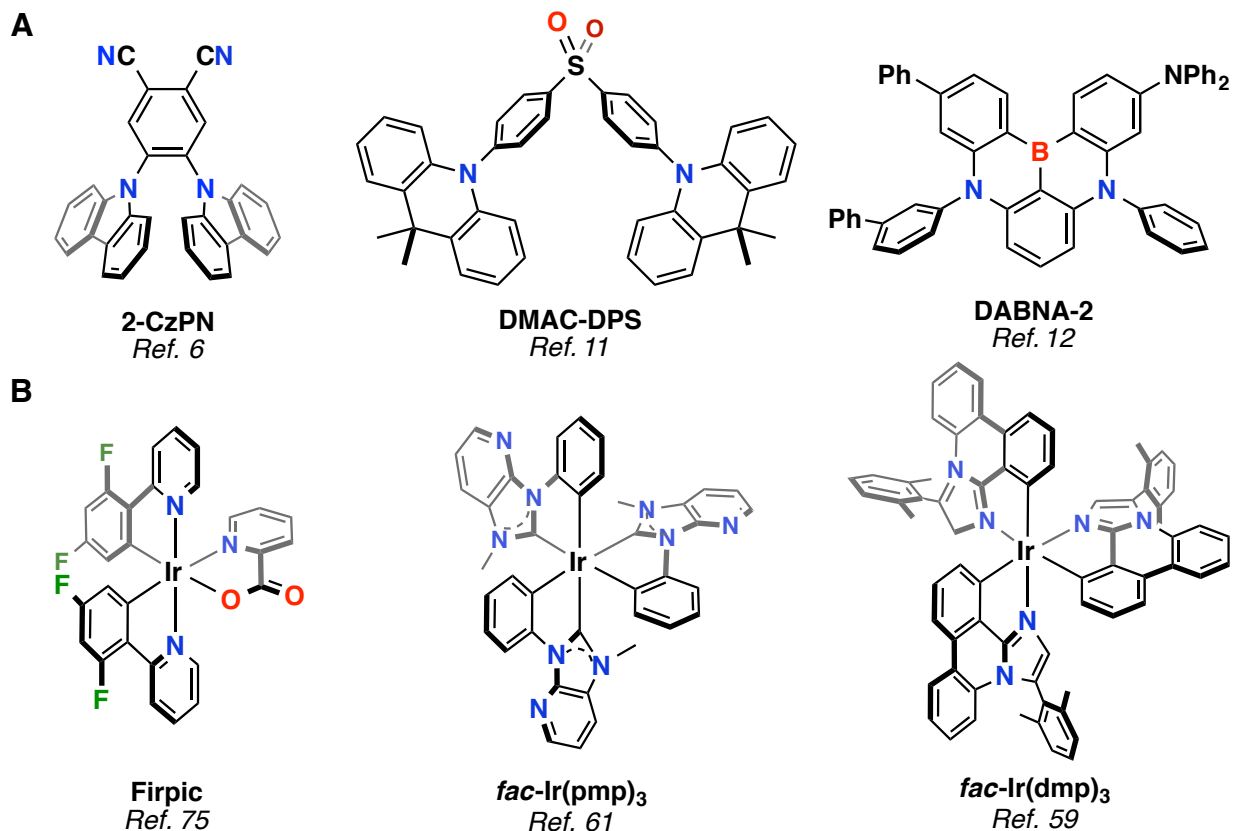
Figure 1.2 Structures of representative molecules that comprise (A) efficient blue TADF OLEDs and (B) cyclometallated Ir(III) complexes that comprise the current state-of-the-art blue PHOLEDs.

Phosphorescent emitters, typically cyclometallated Pt(II)[3-5,15-35,54] and Ir(III)[3-5,36-53,55-58] complexes, are able to access triplet excited sates via spin-orbit coupling (SOC) which result in *radiative* pathways from the excited triplet state to the singlet ground state.[3] In this process of triplet harvesting, there is a quantitative transfer of excitation energy to emitting triplets; therefore, OLEDs with phosphorescent emitters (PHOLEDs) can reach efficiencies up to four times higher than OLEDs containing fluorescent emitters.[54-58] Indeed, PHOLEDs have been experimentally shown to achieve nearly 100% internal efficiency,[57] providing an excellent platform. Currently, red and green PHOLEDs are industrially sound with device lifetimes

upwards of 10^6 hours; however, blue PHOLEDs were only recently optimized to operate efficiently for hundreds of hours at the brightness required for industrial applications—orders of magnitude away from the necessary device lifetime for implementation in screens and displays.[59,60] Furthermore, the efficiency of blue PHOLEDs dramatically drops when operated at high current densities to achieve the brightness necessary for television and lighting applications,[61-64] mainly due to long excited state lifetimes leading to increased bimolecular annihilation.[63,64] To date, blue PHOLEDs have yet to meet the required Commision Internationale de l'Eclairage (CIE) coordinates of (0.14, 0.08), the standard blue defined by the National Television Standards Committee (NTSC), though few are approaching this benchmark.[15-17,43,61,62,65] The design of phosphorescent OLED molecules with wide enough band gaps for blue emission, high quantum yields, suitable lifetimes, and sufficient kinetic stability remains a grand challenge in the field.

1.3 Design of Ir(III)- and Pt(II)-Based Phosphorescent Emitters

Historically, Ir(III) complexes have been favored over Pt(II) for PHOLED applications as many early examples of Pt(II) complexes showed low emission quantum yields. Recently, the development of Pt(II) complexes employing tetradentate ligand scaffolds has resulted in blue PHOLEDs with high color purity and efficiencies comparable to blue Ir(III)-based PHOLEDs.[15,16,62] Rigid multidentate ligands suppress non-radiative decay pathways by minimizing molecular distortions, leading to highly efficient phosphorescent emission.[16-23] Additionally, this ligand architecture has been used to make Pt(II) complexes with extremely narrow emission bands (less than 20 nm at full-width-half-max), a highly desirable characteristic of emitters used for PHOLEDs that is difficult to achieve with bidentate and tridentate ligand

designs.[16,23] Furthermore, this class of ligands yields Pt(II) complexes with high thermal and electrochemical stability with no potential for isomerization.
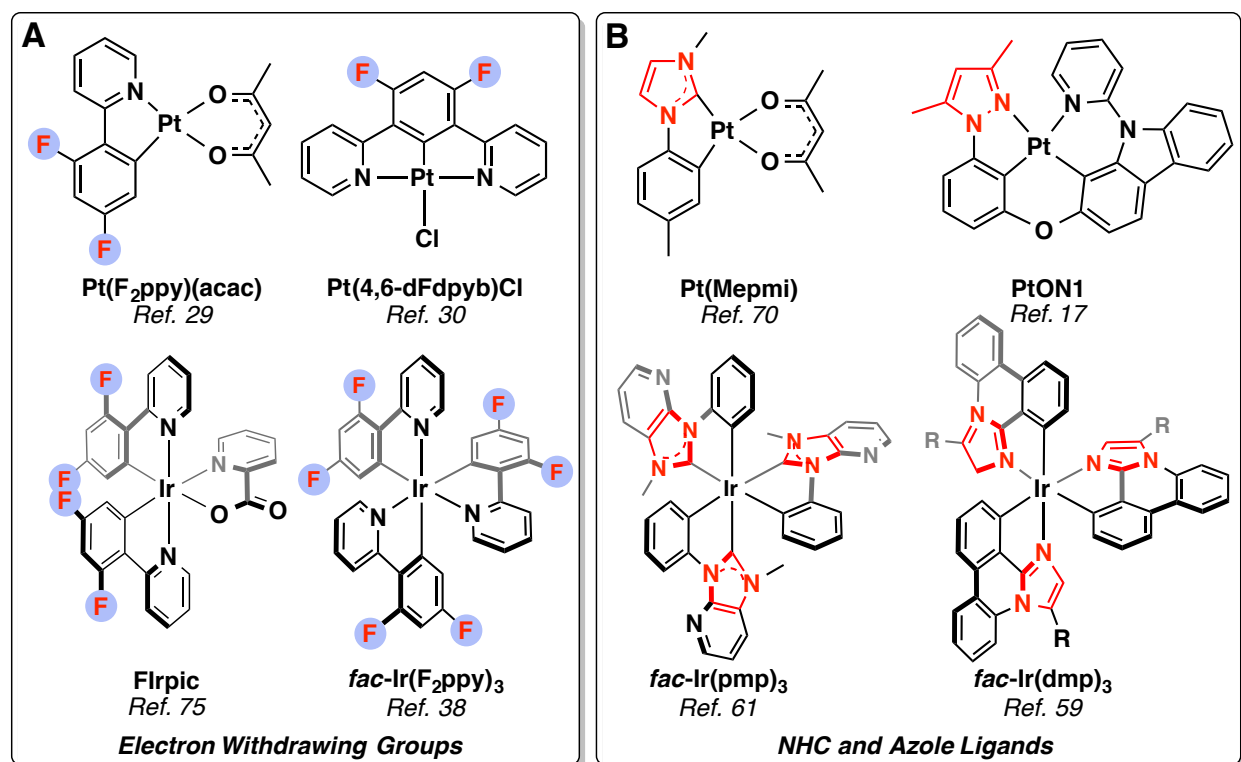
Figure 1.3 Key design strategies for blue phosphorescent Pt(II) and Ir(III) complexes. (A) Introducing electron withdrawing groups on the phenyl rings, and (B) replacing pyridyl groups with azole and imidazole/N-heterocyclic carbene (NHC) groups. For *fac*-Ir(dmp)$_3$, R = 2,6-dimethylphenyl.

The emissive properties of Pt(II) complexes used in PHOLEDs can be tuned by varying the electronic nature of the ligands surrounding the metal center. Functionalizing the cyclometallating phenyl unit with electron withdrawing groups is known to decrease the energy of the HOMO level, resulting in an increased HOMO-LUMO gap and hypsochromically shifted emission (Figure I.3A).[3-5,66,67] Conversely, the introduction of strong-field ligands, such as *N*-heterocyclic carbenes (NHCs),[15,16,61,62,66-74] or electron-accepting ligands with high reduction potentials, such as pyrazoles,[17,20,23,24,85] destabilizes the LUMO and increases its energy, again resulting in a larger HOMO-LUMO gap and blue-shifted emission (Figure I.3B). All of these

strategies, however, feature several key limitations. Though blue PHOLEDs incorporating fluorinated metal complexes have been shown to achieve high efficiencies, the sky-blue emission color is too unsaturated to be used in displays.[61,62,66,67] Furthermore, the fluorinated Ir(III) complex **FIrpic** (Figure 1.2B and 1.3A) and similar Pt(II) species (Figure 1.3A) have been shown to have poor electrochemical stability in PHOLED devices, greatly inhibiting the lifetime of the device.[75-79] Free fluoride ions and the corresponding fluoride-free complexes were found among the degradation products, suggesting the radical degradation product that forms after this cleavage harms the PHOLED device. Many of the azole- and NHC-based complexes used in deep blue PHOLEDs (Figure 1.2B, *fac*-**Ir(pmp)₃** and *fac*-**Ir(dmp)₃**) exhibit exceptional quantum yields ($\phi > 80\%$) with relatively short excited state lifetimes ($\tau < 5$ μs); however, these PHOLEDs undergo a significant drop in efficiency when operated at the high brightness needed for display applications.[15-17,73,74]

In general, many square planar Pt(II) complexes are susceptible to aggregation as a consequence of the lack of steric bulk above and below the square plane, leading to intermolecular Pt(II)···Pt(II) interactions that bring about luminescence quenching and red-shifting of the solid-state emission frequency.[22,80-83] Molecular designs that incorporate bulky functional groups are often used to address this issue, but these substituents often extend in the square plane with limited three-dimensionality and may have undesired effects on the photophysical properties depending on the type of functional group used.[17,25-30,84-88] For example, using a large phenyl group may increase intermolecular distances enough to mitigate unfavorable Pt(II)···Pt(II) interactions, but the extended π-network will delocalize the excited-state triplet and result in a red shifted emission.[18,27-32,85,88] Furthermore, in prototypical mixed ligand complexes, (L)(L′)Pt(II), the HOMO is generally both metal- and ligand-based (Pt(II) and L) while the

7

LUMO is located on the remaining ligand (L′).[89,90] This ultimately complicates the predictability of ligand effects on emission properties.

1.4 Background on Boron Cluster Chemistry

The majority of existing OLED materials are constructed from carbon-rich building blocks. Potential alternatives to these species, which can potentially mitigate the above-mentioned limitations, are boron-rich clusters, specifically icosahedral carboranes.[91] Neutral icosahedral carboranes (formula $C_2B_{10}H_{12}$) represent a unique class of structures that have been previously shown to provide a convenient entry for constructing extremely robust ligands.[92-123] Unlike many conventional borane and borate reagents classically employed in organic chemistry, these polyhedral boron species exhibit phenomenal stability profiles outmatching most of the existing organic-based building blocks. These molecules are stable towards air and moisture, resist decomposition when heated at extremely high temperatures and can be synthesized on a multi-kilogram scale. The $C_2B_{10}H_{12}$ carborane structural platform exists in a form of three isomers (C atom either in the *ortho*, *meta*, or *para* position and further abbreviated in the text as *o-*, *m-* and *p*-carborane, respectively – Figure 1.4). Cage isomerization involves the thermally induced migration of skeletal carbon atoms away from each other, as exemplified in the quantitative conversion of the 1,2 isomer to the 1,7 isomer at 450 $^{\circ}$C, and subsequently, the rearrangement of the 1,7 species to the 1,12 isomer at higher temperatures (T > 600 $^{\circ}$C). These materials are accessible on a multi-kilogram scale in a two step-synthesis starting from sodium borohydride (NaBH$_4$) using decaborane as an intermediate (Figure 1.4).
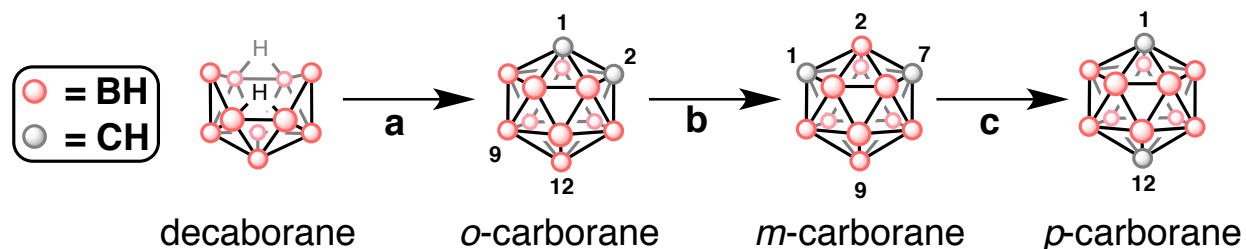
Figure 1.4 Synthesis of icosahedral carboranes ($C_2B_{10}H_{12}$). Synthesis conditions: (a) base, acetylene gas; (b) thermolysis at 450 $^{\circ}$C; (c) thermolysis at 600 $^{\circ}$C.

These molecules create a new class of non-classical bonding motifs and, therefore, their structures cannot be described through the classical organic bond diagrams, where a connecting line between two atoms would indicate a single two-electron bonding interaction. Instead, the proper description of the bonding scenarios exhibited by these species is best described by applying the Wade-Mingos rules and the associated concept of 3D aromaticity. Carborane-based ligands are synthetically appealing, given that it is possible to place functional groups at specific carbon and boron vertices of the cluster moiety, thus allowing for a large range of tunability. Furthermore, these species feature extraordinarily large HOMO-LUMO gaps in their unfunctionalized form (~ 8 eV), making them photophysically innocent in the context of designing metal-based phosphorescent emitters.[124]

1.5 References

1. Nobel Media AB. "The Nobel Prize in Physics 2014 - Popular Information. Blue LEDs — Filling the world with new light." *Nobelprize.org*, **2014**.
2. Nobel Media AB. "The Nobel Prize in Physics 2014 - Advanced Information. Efficient blue light-emitting diodes leading to bright and energy-saving white light sources." *Nobelprize.org*, **2014**.
3. H. Yersin, Ed. *Highly Efficient OLEDs with Phosphorescent Materials*; Wiley-VCH: Weinheim, **2008**.
4. P.-T. Chou, Y. Chi. "Phosphorescent Dyes for Organic Light-Emitting Diodes." *Chem. Eur. J.* **2007**, *13*, 380-395.
5. Y. Chi, P.-T. Chou. "Transition-metal phosphors with cyclometalating ligands: fundamentals and applications." *Chem. Soc. Rev.* **2010**, *39*, 638-655.

6. H. Uoyama, K. Goushi, K. Shizu, H. Nomura, C. Adachi. "Highly efficient organic light-emitting diodes from delayed fluorescence." *Nature* **2012**, *492*, 234-238.

7. S. Y. Lee, T. Yasuda, Y. S. Yang, Q. Zhang, C. Adachi. "Luminous Butterflies: Efficient Exciton Harvesting by Benzophenone Derivatives for Full-Color Delayed Fluorescence OLEDs." *Angew. Chem. Int. Ed.* **2014**, *53*, 6402-6406.

8. M. P. Gaj, C. Fuentes-Hernandez, Y. Zhang, S. R. Marder, B. Kippelen. "Highly Efficient Organic Light-Emitting Diodes from Thermally Activated Delayed Fluorescence Using a Sulfone-Carbazole Host Material." *Org. Electron.* **2015**, *16*, 109-112.

9. K. Kawasumi, T. Wu, T. Zhu, H. S. Chae, T. V. Voorhis, M. A. Baldo, T. M. Swager. "Thermally Activated Delayed Fluorescence Materials Based on Homoconjugation Effect of Donor-Acceptor Triptycenes." *J. Am. Chem. Soc.* **2015**, *137*, 11908-11911.

10. S. Feuillastre, M. Pauton, L. Gao, A. Desmarchelier, A. J. Riives, D. Prim, D. Tondelier, B. Geffroy, G. Muller, G. Clavier, G. Pieters. "Design and Synthesis of New Circularly Polarized Thermally Activated Delayed Fluorescence Emitters." *J. Am. Chem. Soc.* **2016**, *138*, 3990-3993.

11. Q. Zhang, B. Li, S. Huang, H. Nomura, H. Tanaka, C. Adachi. "Efficient Blue Organic Light-Emitting Diodes Employing Thermally Activated Delayed Fluorescence." *Nature Photonics* **2014**, *8*, 326-332.

12. T. Hatakeyama, K. Shiren, K. Nakajima, S. Nomura, S. Nakatsuka, K. Kinoshita, J. Ni, Y. Ono, T. Ikuta. "Ultrapure Blue Thermally Activated Delayed Fluorescence Molecules: Efficient HOMO-LUMO Separation by the Multiple Resonance Effect." *Adv. Mater.* **2016**, *28*, 2777–2781.

13. Q. Zhang, J. Li, K. Shizu, S. Huang, S. Hirata, H. Miyazaki, C. Adachi. "Design of Efficient Thermally Activated Delayed Fluorescence Materials for Pure Blue Organic Light Emitting Diodes." *J. Am. Chem. Soc.* **2012**, *134*, 14706-14709.

14. F. B. Dias, K. N. Bourdakos, V. Jankus, K. C. Moss, K. T. Kamtekar, V. Bhalla, J. Santos, M. R. Bryce, A. P. Monkman. "Triplet Harvesting with 100% Efficiency by Way of Thermally Activated Delayed Fluorescence in Charge Transfer OLEDs." *Adv. Mater.* **2013**, *25*, 3707-3714.

15. T. Fleetham, Z. Wang, J. Li. "Efficient Deep Blue Electrophosphorescent Devices Based on Platinum(II) Bis(n-methyl-imidazolyl)benzene Chloride." *Org. Electron.* **2012**, *13*, 1430-1435.

16. T. Fleetham, G. Li, L. Wen, J. Li. "Efficient "Pure" Blue OLEDs Employing Tetradentate Pt Complexes with a Narrow Spectral Bandwidth." *Adv. Mater.* **2014**, *26*, 7116-7121.

17. X.-C. Hang, T. Fleetham, E. Turner, J. Brooks, J. Li. "Highly Efficient Blue-Emitting Cyclometalated Platinum(II) Compexes by Judicious Molecular Design." *Angew. Chem., Int. Ed.* **2013**, *52*, 6753-6756.

18. M.-Y. Yuen, S. C. F. Kui, K.-H. Low, C.-C. Kwok, S. S.-Y. Chui, C.-W. Ma, N. Zhu, C.-M. Che. "Synthesis, Photophysical and Electrophosphorescent Properties of Fluorene-Based Platinum(II) Complexes." *Chem. Eur. J.* **2010**, *16*, 14131-14141.

19. G. Li, T. Fleetham, J. Li. "Efficient and Stable White Organic Light-Emitting Diodes Employing a Single Emitter." *Adv. Mater.* **2014**, *26*, 2931-2936.

20. E. Turner, N. Bakken, J. Li. "Cyclometallated Platinum Complexes with Luminescent Quantum Yields Approaching 100%." *Inorg. Chem.* **2013**, *52*, 7344-7351.

21. T. Fleetham, G. Li, J. Li. "Efficient Red-Emitting Platinum Complex with Long Operational Stability." *ACS Appl. Mater. Interfaces* **2015**, *7*, 16240-16246.

22. T. Fleetham, L. Huang, J. Li. "Tetradentate Platinum Complexes for Efficient and Stable Excimer-Based White OLEDs." *Adv. Mater.* **2014**, *24*, 6066-6073.

23. G. Li, T. Fleetham, E. Turner, X.-C. Hang, J. Li. "Highly Efficient and Stable Narrow-Band Phosphorescent Emitters for OLED Applications." *Adv. Optical Mater.* **2015**, *3*, 390-397.

24. D. A. K. Vezzu, J. C. Deaton, J. S. Jones, L. Bartolotti, C. F. Harris, A. P. Marchetti, M. Kondakova, R. D. Pike, S. Huo. "Highly Luminescent Tetradentate Bis-Cyclometalated Platinum Complexes: Design, Synthesis, Structure, Photophysics, and Electroluminescence Application." *Inorg. Chem.* **2010**, *49*, 5107-5119.

25. S.-Y. Chang, J. Kavitha, S.-W. Li, C.-S. Hsu, Y. Chi, Y.-S. Yeh, P.-T. Chou, G.-H. Lee, A. J. Carty, Y.-T. Tao, C.-H. Chien. "Platinum(II) Complexes with Pyridyl Azolate-Based Chelates: Synthesis, Structural Characterization, and Tuning of Photo- and Electrophosphorescence." *Inorg. Chem.* **2006**, *45*, 137-146.

26. C.-M. Che, S.-C. Chan, H.-F. Xiang, M. C. W. Chan, Y. Liu, Y. Wang. "Tetradentate Schiff Base Platinum(II) Complexes as New Class of Phosphorescent Materials for High-Efficiency and White-Light Electroluminescent Devices." *Chem. Commun.* **2004**, 1484-1485.

27. J. Kavitha, S.-Y. Chang, Y. Chi, J.-K. Yu, Y.-H. Hu, P.-T. Chou, S.-M. Peng, G.-H. Lee, Y.-T. Tao, C.-H. Chien, A. J. Carty. "In Search of High-Performance Platinum(II) Phosphorescent Materials for the Fabrication of Red Electroluminescent Devices." *Adv. Funct. Mater.* **2005**, *15*, 223-229.

28. W. Sotoyama, T. Satoh, N. Sawatari, H. Inoue. "Efficient Organic Light-Emitting Diodes with Phosphorescent Platinum Complexes Containing N^C^N-coordinating Tridentate Ligand." *Appl. Phys. Lett.* **2005**, *86*, 153505.

29. J. Brooks, Y. Babayan, S. Lamansky, P. I. Djurovich, I. Tsyba, R. Bau, M. E. Thompson. "Synthesis and Characterization of Phosphorescent Cyclometallated Platinum Complexes." *Inorg. Chem.* **2002**, *41*, 3055-3066.

30. A. F. Rausch, L. Murphy, J. A. G. Williams, H. Yersin. "Improving the Performance of Pt(II) Complexes for Blue Light Emission by Enhancing the Molecular Rigidity." *Inorg. Chem.* **2012**, *51*, 312-319.

31. S.-Y. Chang, Y.-M. Cheng, Y. Chi, Y.-C. Lin, C.-M.-Jiang, G.-H. Lee, P.-T. Chou. "Emissive Pt(II) Complexes Bearing Both Cyclometallated Ligand and 2-Pyridyl Hexafluoropropoxide Ancillary Chelate." *Dalton Trans.* **2008**, 6901-6911.

32. Z. M. Hudson, C. Sun, M. G. Helander, H. Amarne, Z.-H. Lu, S. Wang. "Enhancing Phosphorescence and Electrophosphorescence Efficiency of Cyclometallated Pt(II) Compounds with Triarylboron." *Adv. Funct. Mater.* **2010**, *20*, 3426-3439.

33. H. Na, A. Maity, T. S. Teets. "Postsynthetic Systematic Electronic Tuning of Organoplatinum Photosensitizers via Secondary Coordination Sphere Interactions." *Organometallics* **2016**, *35*, 2267-2274.

34. E. Kabir, C.-H. Wu, J. I.-C. Wu, T. S. Teets. "Heteroleptic Complexes of Cyclometalated Platinum with Triarylformazanate Ligands." *Inorg. Chem.* **2016**, *55*, 956-963.

35. U. S. Bhansali, E. Polikarpov, J. S. Swensen, W.-H. Chen, H. Jia, D. J. Gaspar, B. E. Gnade, A. B. Padmaperuma, M. A. Omary. "High-Efficiency Turquoise-Blue Electrophosphorescence from a Pt(II)-Pyridyltriazolate Complex in a Phosphine Oxide Host." *Appl. Phys. Lett.* **2009**, *95*, 233304.

36. S. Lamansky, P. Djurovich, D. Murphy, F. Abdel-Razzaq, H.-E. Lee, C. Adachi, P. E. Burrows, S. R. Forrest, M. E. Thompson. "Highly Phosphorescent Bis-Cyclometalated

Iridium Complexes: Synthesis, Photophysical Characterization, and Use in Organic Light Emitting Diodes." *J. Am. Chem. Soc.* **2001**, *123*, 4304-4312.

37. S. Lamansky, P. Djurovich, D. Murphy, F. Abdel-Razzaq, R. Kwong, I. Tsyba, M. Bortz, B. Mui, R. Bau, M. E. Thompson. "Synthesis and Characterization of Phosphorescent Cyclometalated Iridium Complexes." *Inorg. Chem.* **2001**, *40*, 1704-1711.

38. A. B. Tamayo, B. D. Alleyne, P. I. Djurovich, S. Lamansky, I. Tsyba, N. N. Ho, R. Bau, M. E. Thompson. "Synthesis and Characterization of Facial and Meridional Tris-cyclometalated Iridium(III) Complexes." *J. Am. Chem. Soc.* **2003**, *125*, 7377-7387.

39. A. Tsuboyama, H. Iwawaki, M. Furugori, T. Mukaide, J. Kamatani, S. Igawa, T. Moriyama, S. Miura, T. Takiguchi, S. Okada, M. Hoshino, K. Ueno. "Homoleptic Cyclometalated Iridium Complexes with Highyl Efficient Red Phosphorescence and Application to Organic Light-Emitting Diode." *J. Am. Chem. Soc.* **2003**, *125*, 12971-12979.

40. T. Sajoto, P. I. Djurovich, A. Tamayo, M. Yousufuddin, R. Bau, M. E. Thompson. "Blue and Near-UV Phosphorescence from Iridium Complexes with Cyclometalated Pyrazolyl or *N*-Heterocyclic Carbene Ligands." *Inorg. Chem.* **2005**, *44*, 7992-8003.

41. M. S. Lowry, S. Bernhard. "Synthetically Tailored Excited States: Phosphorescent, Cyclometalated Iridium(III) Complexes and Their Applications." *Chem. Eur. J.* **2006**, *12*, 7970-7977.

42. K. Dedeian, J. Shi, E. Forsythe, D. C. Morton, P. Y. Zavalij. "Blue Phosphorescence from Mixed Cyano—Isocyanide Cyclometalated Iridium(III) Complexes." *Inorg. Chem.* **2007**, *46*, 1603-1611.

43. L. Xiao, Z. Chen, B. Qu, J. Luo, S. Kong, Q. Gong, J. Kido. "Recent Progress on Materials for Electrophosphorescent Organic Light-Emitting Devices." *Adv. Mater.* **2017**, *23*, 926-952.

44. F. J. Coughlin, M. S. Westrol, K. D. Oyler, N. Byrne, C. Kraml, E. Zysman-Colman, M. S. Lowry, S. Bernhard. "Synthesis, Separation, and Circularly Polarized Luminescence Studies of Enantiomers of Iridium(III) Luminophores." *Inorg. Chem.* **2008**, *47*, 2039-2048.

45. Y. You, S. Y. Park. "Phosphorescent Iridium(III) Complexes: Toward High Phosphorescence Quantum Efficiency Through Ligand Control." *Dalton Trans.* **2009**, 1267-1282.

46. T. Sajoto, P. I. Djurovich, A. B. Tamayo, J. Oxgaard, W. A. Goddard III, M. E. Thompson. "Temperature Dependence of Blue Phosphorescent Cyclometalated Ir(III) Complexes." *J. Am. Chem. Soc.* **2009**, *131*, 9813-9822.

47. J. C. Deaton, R. H. Young, J. R. Lenhard, M. Rajeswaran, S. Huo. "Photophysical Properties of the Series *fac*- and *mer*-(1-Phenylisoquinolinato-N^C$^{2'}$)$_{3-x}$Iridium(III) (x = 1—3)." *Inorg. Chem.* **2010**, *49*, 9151-9161.

48. S. A. Moore, D. L. Davies, M. M. Karim, J. K. Nagle, M. O. Wolf, B. O. Patrick. "Photophysical Behaviour of Cyclometallated Iridium(III) Complexes with Phosphine(terthiophene) Ligands." *Dalton Trans.* **2013**, *42*, 12354-12363.

49. T. Yu, Y. Cao, W. Su, C. Zhang, Y. Zhao, D. Fan, M. Huang, K. Yue, S. Z. D. Cheng. "Synthesis, Structure, Photo- and Electro- Luminescence of an Iridium(III) Complex with a Novel Carbazole Functionalized β-diketone Ligand." *RSC Adv.* **2014**, *4*, 554-562.

50. K. B. Klubek, S.-C. Dong, L.-S. Liao, C. W. Tang, L. J. Rothberg. "Investigating Blue Phosphorescent Iridium Cyclometallated Dopant with Phenyl-Imidazole Ligands." *Org. Electron.* **2014**, *15*, 3127-3136.

51. N. Deligonul, A. R. Browne, J. A. Golen, A. L. Rheingold, T. G. Gray. "Cyclometalated Iridium(III) Complexes of Azadipyrromethene Chromophores." *Organometallics* **2014**, *33*, 637-643.

52. A. Maity, L. Q. Le, Z. Zhu, J. Bao, T. S. Teets. "Steric and Electronic Influence of Aryl Isocyanides on the Properties of Iridium(III) Cyclometalates." *Inorg. Chem.* **2016**, *55*, 2299-2308.

53. R. D. Sanner, N. J. Cherepy, V. G. Young Jr. "Blue Light Emission from Cyclometallated Iridium(III) Cyano Complexes: Syntheses, Crystal Structures, and Photophysical Properties." *Inorg. Chim. Acta.* **2016**, *440*, 165-171.

54. M. A. Baldo, D. F. O'Brien, Y. You, A. Shoustikov, S. Sibley, M. E. Thompson, S. R. Forrest. "Highly Efficient Phosphorescent Emission from Organic Electroluminescent Devices." *Nature* **1998**, *395*, 151-154.

55. M. A. Baldo, S. Lamansky, P. E. Burrows, M. E. Thompson, S. R. Forrest. "Very High-Efficiency Green Organic Light-Emitting Devices Based on Electrophosphorescence." *Appl. Phys. Lett.* **1999**, *75*, 4-6.

56. C. Adachi, M. A. Baldo, S. R. Forrest, M. E. Thompson. "High-Efficiency Organic Electrophosphorescent Devices with Tris(2-phenylpyridine)iridium Doped into Electron-transporting Materials." *Appl. Phys. Lett.* **2000**, *77*, 904-906.

57. C. Adachi, M. A. Baldo, M. E. Thompson, S. R. Forrest. "Nearly 100% Internal Phosphorescence Efficiency in an Organic Light-Emitting Device." *J. Appl. Phys.* **2001**, *90*, 5048-5051.

58. M. Ikai, S. Tokito, Y. Sakamoto, T. Suzuki, Y. Taga. "Highly Efficient Phosphorescence from Organic Light-Emitting Devices with an Exciton-block Layer." *Appl. Phys. Lett.* **2001**, *79*, 156-158.

59. Y. Zhang, J. Lee, J., S. R. Forrest. "Tenfold Increase in the Lifetime of Blue Phosphorescent Organic Light-Emitting Diodes." *Nature Commun.* **2014**, *5*, 5008.

60. R. C. Kwong, M. R. Nugent, L. Michalski, T. Ngo, K. Rajan, Y.-J. Tung, M. S. Weaver, T. X. Zhou, M. Hack, M. E. Thompson, S. R. Forrest, J. J. Brown. "High Operational Stability of Electrophosphorescent Devices." *Appl. Phys. Lett.* **2002**, *81*, 162-164.

61. J. Lee, H.-F. Chen, T. Batagoda, C. Coburn, P. I. Djurovich, M. E. Thompson, S. R. Forrest. "Deep Blue Phosphorescent Organic Light-Emitting Diodes with Very High Brightness and Efficiency." *Nature Mat.* **2015**, *15*, 92-98.

62. T. B. Fleetham, L. Huang, K. Klimes, J. Brooks, J. Li. "Tetradentate Pt(II) Complexes with 6-Membered Chelate Rings: A New Route for Stable and Efficient Blue Organic Light Emitting Diodes." *Chem. Mater.* **2016**, *28*, 3276-3282.

63. M. A. Baldo, C. Adachi, S. R. Forrest. "Transient Analysis of Organic Electrophosphorescence. II. Transient Analysis of Triplet-Triplet Annihilation." *Phys. Rev. B* **2000**, *62*, 10967.

64. N. C. Giebink, B. W. D'Andrade, M. S. Weaver, P. B. Mackenzie, J. J. Brown, M. E. Thompson, S. R. Forrest. "Intrinsic Luminance Loss in Phosphorescent Small-Molecule Organic Light Emitting Devices Due to Bimolecular Annihilation Reactions." *J. Appl. Phys.* **2008**, *103*, 044509.

65. L. Xiao, Z. Chen, B. Qu, J. Luo, S. Kong, Q. Gong, J. Kido. "Recent Progresses on Materials for Electrophosphorescent Organic Light-Emitting Devices." *Adv. Mater.* **2011**, *23*, 926-952.

66. C.-F. Chang, Y.-M. Cheng, Y. Chi, Y.-C. Chiu, C.C. Lin, G.-H. Lee, P.-T. Chou, C.-C. Chen, C.-H. Chang, C.-C. Wu. "Highly Efficient Blue-Emitting Iridium(III) Carbene Complexes and Phosphorescent OLEDs." *Angew. Chem. Int. Ed.* **2008**, *47*, 4542-4545.

67. Y.-C. Chiu, J.-Y. Hung, Y. Chi, C.-C. Chen, C.-H. Chang, C.-C. Wu, Y.-M. Cheng, Y.-C. Yu, G.-H. Lee, P.-T. Chou. "En Route to High External Quantum Efficiency (~12%) Organic

True-Blue-Light-Emitting Diodes Employing Novel Design of Iridium(III) Phosphors." *Adv. Mater.* **2009**, *21*, 2221-2225.

68. C. Schildknecht, sljasfld. "Novel Deep-Blue Emitting Phosphorescent Emitter." *PROC SPIE Int. Soc. Opt. Eng.* **2005**, *5937*, 59370E.

69. R. Visbal, M. C. Gimeno. "N-heterocyclic Carbene Metal Complexes: Photoluiminescence and Applications." *Chem. Soc. Rev.* **2014**, *43*, 3551-3574.

70. Y. Unger, D. Meyer, O. Molt, C. Schildknecht, I. Münster, G. Wagenblast, T. Strassner. "Green-Blue Emitters: NHC-Based Cyclometalated [Pt(C^C*)(acac)] Complexes." *Angew. Chem. Int. Ed.* **2010**, *49*, 10214-10216.

71. A. Tronnier, A. Risler, N. Langer, G. Wagenblast, I. Münster, T. Strassner. "A Phosphorescent C^C* Cyclometalated Platinum(II) Dibenzothiophene NHC Complex." *Organometallics* **2012**, *31*, 7447-7452.

72. A. Tronnier, A. Poethig, E. Herdtweck, T. Strassner. "C^C* Cyclometalated Platinum(II) NHC Complexes with β-Ketoimine Ligands." *Organometallics* **2014**, *33*, 898-908.

73. H. Sasabe, J.-I. Takamatsu, T. Motoyama, S. Watanabe, G. Wagenblast, N. Langer, O. Molt, E. Fuchs, C. Lennartz, J. Kido. "High-Efficiency Blue and White Organic Light-Emitting Devices Incorporating a Blue Iridium Carbene Complex." *Adv. Mater.* **2010**, *22*, 5003-5007.

74. K.-Y. Lu, H.-H. Chou, C.-H.Hsieh, Y.-H. O. Yang, H.-R. Tsai, H.-Y. Tsai, L.-C. Hsu, C.-Y. Chen, I.-C. Chen, C.-H. Cheng. "Wide-Range Color Tuning of Iridium Biscarbene Complexes from Blue to Red by Different N^N Ligands: an Alternative Route for Adjusting the Emission Colors." *Adv. Mater.* **2011**, *23*, 4933-4937.

75. E. Baranoff, F. E. Curchod. "FIrpic: Archetypal Blue Phosphorescent Emitter for Electroluminescence." *Dalton Trans.* **2015**, *44*, 8318-8329.

76. S. Scholz, R. Meerheim, K. Walzer, K. Leo. "Chemical Degradation Mechanisms of Organic Semiconductor Devices." *Proc. SPIE* **2008**, *6999*, 69991B.

77. V. Sivasubramaniam, F. Brodkorb, S. Hanning, H. P. Loebl, V. van Elsbergen, H. Boerner, U. Scerf, M. Kreyenschmidt. "Fluorine Cleavage of the Light Blue Heteroleptic Triplet Emitter FIrpic." *J. Fluorine Chem.* **2009**, *130*, 640-649.

78. I. R. de Moraes, S. Scholz, B. Lüssem, K. Leo. "Analysis of Chemical Degradation Mechanism Within Sky Blue Phosphorescent Organic Light Emitting Diodes by Laser-Desorption/Ionization Time-of-Flight Mass Spectrometry." *Org. Electron.* **2011**, *12*, 341-347.

79. R. Seifert, I. R. de Moraes, S. Scholz, M. C. Gather, B. Lüssem, K. Leo. "Chemical Degradation Mechanisms of Highly Efficient Blue Phosphorescent Emitters Used for Organic Light Emitting Diodes." *Org. Electron.* **2013**, *14*, 115-123.

80. D. Bandyopadhyay, P. Bandyopadhyay, A. Chakravorty, F. A. Cotton, L. R. Falvello. "Isomeric Bis[(phenylazo)acetaldoximato]platinum(II) Compounds." *Inorg. Chem.* **1983**, *22*, 1315-1321.

81. L. Chassot, E. Müller, A. von Zelewsky. "cis-Bis(2-phenylpyridine)platinum(II) (CBPPP): a Simple Molecular Platinum Compound." *Inorg. Chem.* **1984**, *23*, 4249-4253.

82. M. Ghedini, D. Pucci, A. Crispini, G. Barberio. "Oxidative Addition to Cyclometalated Azobenzene Platinum(II) Complexes: A Route to Octahedral Liquid Crystalline Materials." *Organometallics* **1999**, *18*, 2116-2124.

83. K. E. Dungey, B. E. Thompson, N. A. P. Kane-Maguire, L. L. Wright. "Photobehavior of (α-Diimine)dimesitylplatinum(II) Complexes." *Inorg. Chem.* **2000**, *39*, 5192-5196.

84. B. Wang, F. Liang, H. Hu, Y. Liu, Z. Kang, L.-S. Liao, J. Fan. "Strongly Phosphorescent Platinum(II) Complexes Supported by Tetradentate Benzazole-Containing Ligands." *J. Mater. Chem. C* **2015**, *3*, 8212-8218.

85. H. Li, J. Ding, Z. Xie, Y. Cheng, L. Wang. "Synthesis, Characterization, and Electrophosphorescent Properties of Mononuclear Platinum(II) Complexes Based on 2-Phenylbenzoimidazole Derivatives." *J. Organomet. Chem.* **2009**, *694*, 2777-2785.

86. S.-Y. Chang, J. Kavitha, J.-Y. Hung, Y. Chi, Y.-M. Cheng, E. Y. Li, P.-T. Chou, G.-H. Lee. "Luminescent Platinum(II) Complexes Containing Isoquinoiinyl Indazolate Ligands: Synthetic Reaction Pathway and Photophysical Properties." *Inorg. Chem.* **2007**, *46*, 7046-7074.

87. R. C. Kwong, S. Sibley, T. Dubovoy, M. Baldo, S. R. Forrest, M. E. Thompson. "Efficient, Saturated Red Organic Light Emitting Devices Based on Phosphorescent Platinum(II) Porphyrins." *Chem. Mater.* **1999**, *11*, 3709-3713.

88. J. Zhang, F. Zhao, X. Zhu, W.-K. Wong, D. Ma, M.-Y. Wong. "New Phosphorescent Platinum(II) Schiff Base Complexes for PHOLED Applications." *J. Mater. Chem.* **2012**, *22*, 16448-16457.

89. D. P. Rillema, A. J. Cruz, C. Moore, K. Siam, A. Jehan, D. Base, T. Nguyen, W. Huang. "Electronic and Photophysical Properties of Platinum(II) Biphenyl Complexes Containing 2,2'-Bipyridine and 1,10-Phenanthroline Ligands." *Inorg. Chem.* **2013**, *52*, 596-607.

90. D. P. Rillema, S. R. Stoyanov, A. J. Cruz, H. Nguyen, C. Moore, W. Huang, K. Siam, A. Jehan, V. KomReddy. "HOMO-LUMO Energy Gap Control in Platinum(II) Biphenyl Complexes Containing 2,2'Bipyridine ligands." *Dalton Trans.* **2015, *44*,** 17075-17090.

91. R. N. Grimes. *Carboranes*, 2nd ed.; Academic Press: Cambridge, 2011.

92. M. F. Hawthorne, D. C. Young, T. D. Andrews, D. V. Howe, R. L. Pilling, A. D. Pitts, M. Reintjes, L. F. Warren Jr., P. A. Wegner. "p-Dicarbollyl Derivatives of the Transition Metals. Metallocene Analogs." *J. Am. Chem. Soc.* **1968**, *90*, 879-896.

93. M. F. Hawthorne, G. B. Dunks. "Metallocarboranes that Exhibit Novel Chemical Features." *Science* **1972**, *178*, 462-471.

94. D. J. Crowther, N. C. Baenziger, R. F. Jordan. "Group 4 Metal Dicarbollide Chemistry. Synthesis, Structures, and Reactivity of Electrophilic Alkyl Complexes (Cp*)(C$_2$B$_9$H$_{11}$)M(R), M = Hf, Zr." *J. Am. Chem. Soc.* **1991**, *113*, 1455-1457.

95. O. Tutusaus, C. Viñas, R. Núñez, F. Teixidor, A. Demonceau, S. Delfosse, A. F. Noels, I. Mata, E. Molins. "The Modulating Possibilities of Dicarbollide Clusters: Optimizing the Kharasch Catalysts." *J. Am. Chem. Soc.* **2003**, *125*, 11830-11831.

96. T. C. Li, A. M. Spokoyny, C. She, O. K. Farha, C. A. Mirkin, T. J. Marks, J. T. Hupp. "Ni(III)/(IV) Bis(dicarbollide) as a Fast, Noncorrosive Redox Shuttle for Dye-Sensitized Solar Cells." *J. Am. Chem. Soc.* **2010**, *132*, 4580-4582.

97. E. L. Hoel, M. F. Hawthorne. "Preparation of B-σ-carboranyl Iridium Complexes by Oxidative Addition of Terminal Boron-Hydrogen Bonds to Iridium(I) Species." *J. Am. Chem. Soc.* **1975**, *97*, 6388-6395.

98. E. H. S. Wong, M. F. Hawthorne. "Hydrido Complexes of Ruthenium with Carborane Ligands." *Inorg. Chem.* **1978**, *17*, 2863-2866.

99. A. K. Saxena, N. S. Hosmane. "Recent Advances in the Chemistry of Carborane Metal Complexes Incorporating d- and f-block Elements." *Chem. Rev.* **1993**, *93*, 1081-1124.

100. A. M. Spokoyny, C. W. Machan, D. J. Clingerman, M. S. Rosen, M. J. Wiester, R. D. Kennedy, C. L. Stern, A. A. Sarjeant, C. A. Mirkin. "A Coordination Chemistry Dichotomy for Icosahedral Carborane-Based Ligands." *Nat. Chem.* **2011**, *3*, 590-596.

101. Weller, A. "Ligand Design: The Two Faces of Carboranes." *Nature. Chem.* **2011**, *3*, 577-578.

102. A. M. Spokoyny, C. D. Lewis, G. Teverovskiy, S. L. Buchwald. "Extremely Electron-Rich, Icosahedral Carborane-Based Phosphinoboranes." *Organometallics* **2012**, *31*, 8478-8481.

103. A. M. Spokoyny. "New Ligand Platforms Featuring Boron-Rich Clusters as Organomimetic Substituents." *Pure & Appl. Chem.* **2013**, *85*, 903-919.

104. C. A. Lugo, C. Moore, A. Rheingold, V. Lavallo. "Synthesis of a Hybrid *m*-Terphenyl/*o*-Carborane Building Block: Applications in Phosphine Ligand Design." *Inorg. Chem.* **2015**, *54*, 2094–2096.

105. J. Estrada, S. E. Lee, S. McArthur, A. El-Hellani, F. S. Tham, V. Lavallo. "Resisting B—H Oxidative Addition: The Divergent Reactivity of the *o*-Carborane and Carba-*closo*-dodecaborate Ligand Substituents." *J. Organomet. Chem.* **2015,** *798*, 214-217.

106. B. J. Eleazer, M. D. Smith, D. V. Peryshkov. "Metal- and Ligand-Centered Reactivity of *meta*-Carboranyl-Backbone Pincer Complexes of Rhodium." *Organometallics* **2016**, *35*, 106-112.

107. Y. Quan, Z. Xie. "Palladium-Catalyzed Regioselective Diarylation of *o*-Carboranes By Direct Cage B—H Activation." *Angew. Chem.* **2016**, *128*, 1317-1320.

108. A. R. Popescu, F. Teixidor, C. Viñas. "Metal Promoted Charge and Hapticities of Phosphines: the Uniqueness of Carboranylphosphines." *Coord. Chem. Rev.* **2014**, *269*, 54-84.

109. B. Xu, Y.-P. Wang, Z.-J. Yao, G.-X. Jin. "Metal-induced B—H Bond Activation: Reaction Between Half-sandwich Ir and Rh Complexes with Carboranylthioamide." *Dalton Trans.* **2015**, *44*, 1530-1533.

110. J. Kahlert, L. Böhling, A. Brockhinke, H.-G. Stammler, B. Neumann, L. M. Rendina, P. J. Low, L. Weber, M. A. Fox. "Syntheses and Reductions of *C*-dimesitylboryl-1,2-dicarba-*closo*-dodecaboranes." *Dalton Trans.* **2015**, *44*, 9766-9781.

111. P. A. Jelliss, J. Mason, J. M. Nazzoli, J. H. Orlando, A. Vinson, N. P. Rath, M. J. Shaw. "Synthesis and Characterization of Ruthenacarborane Complexes Incorporating Chelating *N*-Donor Ligands: Unexpected Luminescence from the Complex [3-CO-3,3-{k^2-Me$_2$N(CH$_2$)$_2$NMe$_2$}-*closo*-3,1,2-RuC$_2$B$_9$H$_{11}$]." *Inorg. Chem.* **2006**, *45*, 370-385.

112. S. W. Buckner, M. J. Fischer, P. A. Jelliss, R. Luo, S. D. Minteer, N. P. Rath, A. Siemiarczuk. "Dual Fluorescence from an *Isonido* Re^{III} Rhenacarborane Phosphine Complex, [7,10-m-H-7-CO-7,7-(PPh$_3$)$_2$-*isonido*-7,8,9-ReC$_2$B$_7$H$_9$]." *Inorg. Chem.* **2006**, *45*, 7339-7347.

113. R. A. Wiesboeck, M. F. Hawthorne. "Dicarbaundecaborane(13) and Derivatives." *J. Am. Chem. Soc.* **1964**, *86*, 1642-1643.

114. D. A. Owen, M. F. Hawthorne. "Novel Chelated Biscarborane Transition Metal Complexes Formed Through Carbon-Metal σ Bonds." *J. Am. Chem. Soc.* **1970**, *92*, 3194-3196.

115. M. F. Hawthorne, D. A. Owen. "Chelated Biscarborane Transition Metal Derivatives Formed Through Carbon-Metal σ Bonds." *J. Am. Chem. Soc.* **1971**, *93*, 873-880.

116. L. I. Zakharkin, A. I. Kovredov. "Formation of Biscarboranes During Reactions of Lithium Carboranes with Copper Salts." *Bull. Acad. Sci. USSR, Div. Chem. Sci.* **1973***, 22,* 1396.

117.   H. J. Bae, H. Kim, K. M. Lee, T. Kim, M. Eo, Y. S. Lee, Y. Do, M. H. Lee. "Heteroleptic Tris-Cyclometalated Iridium(III) Complexes Supported by an *o*-Carboranyl-Pyridine Ligand." *Dalton Trans.* **2013**, *42*, 8549-8552.

118.   Bis-carboranes that feature both C—C and B—C bonds: X. Yang, W. Jiang, C. B. Knobler, M. D. Mortimer, M. F. Hawthorne. "The Synthesis and Structural Characterization of Carborane Oligomers Connected by Carbon-Carbon and Carbon-Boron Bonds Between Icosahedra." *Inorg. Chim. Acta* **1995**, *240*, 371-378.

119.   D. E. Harwell, M. D. Mortimer, C. B. Knobler, F. A. L. Anet, M. F. Hawthorne. "Auracarboranes with and without Au—Au Interactions: An Unusually Strong Aurophilic Interaction." *J. Am. Chem. Soc.* **1996**, *118*, 2679-2685.

120.   J. C. Axtell, K. O. Kirlikovali, P. I. Djurovich, D. Jung, V. T. Nguyen, B. Munekiyo, A. T. Royappa, A. L. Rheingold, A. M. Spokoyny. "Blue Phosphorescent Zwitterionic Iridium(III) Complexes Featuring Weakly Coordinating nido-Carborane-Based Ligands." *J. Am. Chem. Soc.* **2016**, *138*, 15758-15765.

121.   S. Ren, Z. Xie. "A Facile and Practical Synthetic Route to 1,1′-Bis(*o*-carborane)." *Organometallics* **2008**, *27,* 5167–5168.

122.   A. M. Projhorov, P. A. Slepukhin, V. L. Rusinov, V. N. Kalinin, D. N. Kozhevnikov. "2,2′-Bipyridinyl carboranes as *B,N,N*-Ligands in cyclometallated complexes of platinum(II)." *Chem. Commun.* **2011**, *47*, 7713-7715.

123.   A. M. Prokhorov, T. Hofbeck, R. Czerwieniec, A. F. Suleymanova, D. N. Kozhevnikov, H. Yersin. "Brightly Luminescent Pt(II) Pincer Complexes with a Sterically Demanding Carboranyl-Phenylpyridine Ligand: A New Material Class for Diverse Optoelectronic Applications." *J. Am. Chem. Soc.* **2014**, *136*, 9637–9642.

124.   K. O. Kirlikovali, J. C. Axtell, A. Gonzalez, A. C. Phung, S. I. Khan, A. M. Spokoyny. "Luminescent Metal Complexes Featuring Photophysically Innocent Strong-Field Chelating Boron Cluster Ligands" *Chem. Sci.* **2016**, *7*, 5132-5138.

CHAPTER 2 – BLUE PHOSPHORESCENT ZWITTERIONIC IRIDIUM(III) COMPLEXES FEATURING WEAKLY COORDINATING *NIDO*-CARBORANE-BASED LIGANDS

2.1 Introduction

The past two decades have seen a surge in the development of fluorescent[1] and phosphorescent[2] emitters with ever-increasing efficiency and color purity. In particular, the continued development of efficient Ir(III)-based phosphorescent compounds, currently targeted for their potential use in organic light-emitting diodes (OLEDs),[3] represents a vital component of this research. Previous work has shown that ligand choice is crucial for optimizing luminescence efficiencies, emission wavelengths, and emitter stability in these devices (see Appendix A).[1,2] Still, despite the significant progress that has been made so far,[4] efficient and long-lasting blue phosphorescent emitters have remained largely elusive.[5]

A) Covalent Metal-Ligand Bonds

B) Weakly Coordinating, Non-Covalent Interaction

Prevalent construct for phosphorescent Ir(III) emitters

R = F, H
R′ = CH₃, H

This work
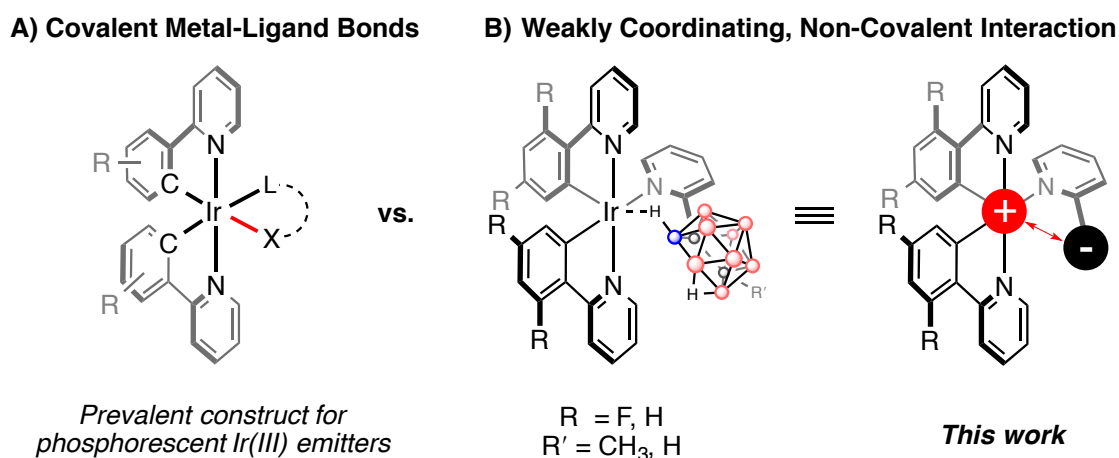
Figure 2.1 New design approach for luminescent metal complexes in which a weakly-coordinating ligand is employed.

The prevailing design principle for Ir(III)-based phosphorescent systems leverages *covalently*-bound strong- and weak-field (chelating) donor ligands to deliver the desired

properties of the luminescent species (Figure 2.1A). This strategy would seem intuitive, given the well-recognized non-radiative decay pathways of excited-state Ir(III) species *via* ligand labilization/loss or excited-state distortions.[6] Researchers have attempted to address this issue by using cyclometallated *N*-heterocyclic carbenes (NHCs) as L-type ligands to increase the energy barrier for non-radiative thermal deactivation.[2f-h] In contrast to this convention, here we introduce a fundamentally new approach whereby strongly blue emitting and highly stable phosphorescent Ir(III) compounds are generated by employing weakly coordinating/non-covalently bound ligands derived from robust carborane clusters.

Carboranes,[7] a class of icosahedral boron-based clusters recognized for their high stability[8] and unique electronic properties,[9,10] have recently been utilized as ligand components of emissive Pt(II)- and Ir(III)-based molecules towards implementation as dopants in OLEDs[11] and as fluorophores in cell imaging.[12] The distinctive electronic influence of carboranes – which behave as electron-withdrawing groups if bound through carbon and electron-releasing groups if bound through boron – provide a unique opportunity for isosteric electronic variation.[9,13] Since complete control over vertex functionalization of carboranes is still a largely unsolved problem, researchers in the field of OLED development have employed more easily accessible *C*-functionalized carborane scaffolds to perturb the electronic manifold of metal-based phosphors. However, despite the electronic extremes accessible through carborane as a ligand, very few[14] phosphorescent metal-based molecules have been developed that contain carborane directly bound to a metal center or that contain deboronated (*e.g. nido*) analogues;[15] rather, carboranyl substituents are most commonly installed on the periphery of the ligand scaffolds where direct interaction of the metal and the carborane is not possible (see Appendix A for a brief summary of such emitters).[16] As part of our ongoing studies of the organometallic chemistry of carboranes,

we considered that deboronated carboranes, which are formally anionic, might be successfully employed as weakly coordinating/non-covalent ligands in building zwitterionic Ir(III)-based phosphorescent molecules.

2.2 Results and Discussion

2.2.1 Synthesis

We began our studies in pursuit of generating *bis*(heteroleptic) Ir(III) phosphors with a *nido*-carboranylpyridine ligand. A common tactic employed in designing metal-based phosphorescent molecules involves the installation of strong field ligands such as carbanions or *N*-heterocyclic carbenes to stabilize metal-based orbitals; it is also known, however, that the filled *d*-orbitals may also be stabilized if electron density is removed from the metal center,[17] either as a consequence of electron-withdrawing ligands or if the metal center bears a formal positive charge. In both cases, the HOMO-LUMO gaps are widened, opening the possibility for blue-shifted, radiative excited-state decay. We reasoned that the dominant steric profile of the *nido*-carboranyl scaffold amidst an otherwise rigid octahedral metal environment might minimize metal-cage interactions such that the metal holds a greater proportion of the formal positive charge. In addition, the diffuse nature of the negatively charged *nido*-carboranyl substituent would give poor directionality for interaction with the metal, thereby maintaining the desired ionic/non-covalent interaction by restricting electron-sharing with the Ir(III) center.

To test this hypothesis, we synthesized ligand **1a**. The intermediate carboranylpyridine (Figure 2.2A, Compound **1b**) has been synthesized previously: one reported method requires Sonagashira coupling of 2-bromopyridine with dimethylethynyl carbinol, followed by condensation of 2-ethynylpyridine with decaborane, affording the desired product in ~28% yield

(22% yield over two steps).[18] More recently, Valliant and co-workers reported an alternative synthesis of **1b** from decaborane which requires the use of 10 mol% of a Ag(I)-based catalyst.[19]

A

B

R = F; R' = CH₃ (**2a, 73%**)
R = F; R' = H (**2b, 77%**)
R = H; R' = CH₃ (**2c, 90%**)
R = H; R' = H (**2d, 82%**)

C

2a

D

— **2a**
— **2b**
— **2c**
— **2d**
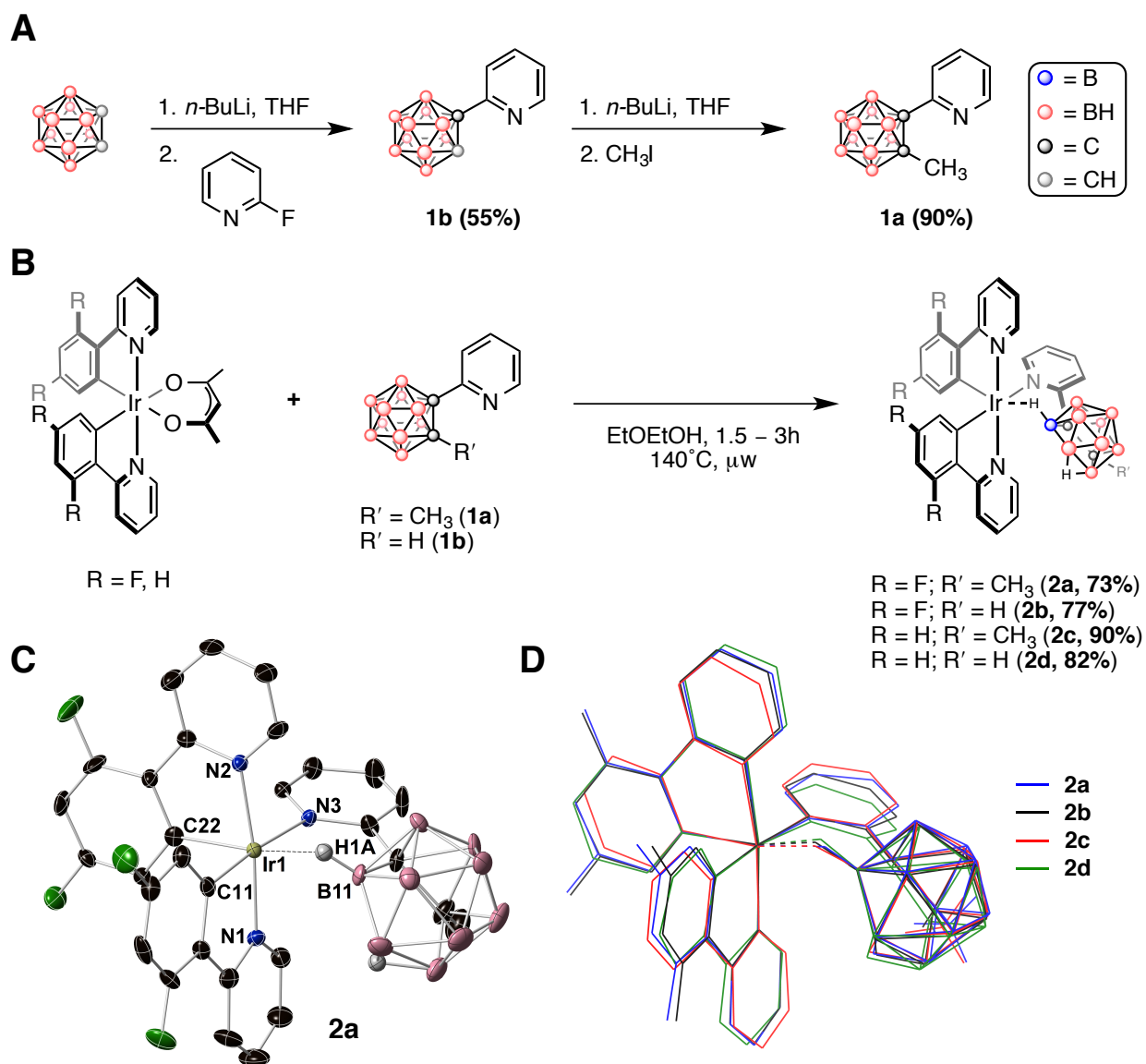
Figure 2.2 (A) Synthesis of carborane-based ligand precursors; (B) Ir(III) compounds containing a nido-carboranylpyridine ligand. (C) Solid-state structure of **2a** (Carboranyl label corresponds to IUPAC numbering scheme) (D) Structure similarities of **2a–2d** are shown by superimposed stick models of the single crystal X-ray structures. Summary of the select bond distances and angles for structures **2a–2d** can be found in Appendix A (Figures A2 and A3 and Table A1).

Since *C*-metallated carboranyls (e.g. 1-Li-*o*-C₂B₁₀H₁₁) can easily be generated, we considered that such a species might be successfully employed in S$_N$Ar-type reactivity with 2-fluoropyridine, a substrate documented to undergo substitution with a range of O-, N-, S-, and C-

21

based nucleophiles.[20] Though few examples of electron-deficient arenes undergoing nucleophilic substitution by metal carboranyl compounds exist[21] – none of which include heterocyclic arenes – we found that treatment of commercially available *o*-carborane with *n*-BuLi followed by addition of 2-fluoropyridine affords the desired ligand in a single step in 55% yield. Importantly, this protocol circumvents the use of the toxic decaborane precursor and metal-based catalysis. Subsequent deprotonation of **1b** followed by treatment with methyl iodide affords **1a** in good yield.

Treatment of Ir(^{F2}ppy)$_2$(acac)[22] with **1a** under either microwave conditions or in an oil bath in 2-ethoxyethanol (EtOEtOH) for 3h (Figure 2.2B) results in the formation of a golden yellow solution which emits blue under ultraviolet (UV) excitation (365 nm) at 77 K. Notably, this reaction is significantly faster and higher yielding than those generally observed for the synthesis of Ir(III) bis(heteroleptic) cyclometallates.[2f] ^{11}B NMR spectroscopy revealed that the resulting product contained a deboronated carborane, which was identified from the diagnostic resonances in the -30 to -40 ppm range.

The solvent in this reaction was then was removed *in vacuo* and the resulting solid was subjected to additional spectroscopic characterization. The ^{1}H NMR spectrum of the sample dissolved in CDCl$_3$ showed diagnostic, upfield (~ -3.5 to -4.5 ppm) chemical shifts, characteristic of a hydride on the open face of a deboronated *o*-carborane. Precipitation of the Ir(III) species from hexanes afforded **2a** in 73% yield after purification. X-ray diffraction analysis of single crystals of the product (**2a**), grown from a concentrated EtOH solution at -15˚C, confirmed the presence of the *nido*-carboranyl group (Figure 2.2C). The deboronation of *o*-carborane is known to proceed through treatment with metal alkoxide or hydroxide bases in alcohol solvent;[23] we therefore suggest that the nature of the reaction solvent, in addition to the

precoordination of **1a** to the Ir(III) center through pyridine, aids the observed deboronation.[24] Indeed, heating **1a** in EtOEtOH under the reaction conditions but in the absence of Ir(^{F2}ppy)$_2$(acac) does not result in deboronation (or any other observable decomposition products). Additionally, heating Ir(^{F2}ppy)$_2$(acac) and **1a** in a non-protic solvent (1,2-dimethoxyethane or acetonitrile) under otherwise identical reaction conditions results in < 10% conversion to **2a**.

In order to probe the effect of the *nido*-carboranyl ligand on the luminescent properties of Ir(III)-based compounds, we synthesized several derivatives featuring modified phenylpyridine (ppy) and carborane-based ligands. The deboronation of **1a** *en route* to formation of **2a** led us to question the necessity of protecting the remaining carboranyl C–H vertex of **1b**, particularly considering that *C*-functionalized *o*-carboranes containing electron-releasing substituents are generally *more* stable toward deboronation than the parent *o*-carborane.[25] **2b**–**2d** were synthesized in an analogous manner to **2a** (Figure 2B) and we find that no C–H activation is observed under the reaction conditions by using non-methylated ligand **1b** as a precursor. X-ray crystallographic analysis of single crystals of **2b**–**2d** confirmed the presence of the *nido*-carboranyl ligand fragments as in **2a**. As expected, the structures of **2a**–**2d** are closely related, as seen from the superimposed wireframe plots shown in Figure 2.2D. Compound **2b**, which contains a proton at the 2-position of the carborane cage, emits blue both in the solid state and in solution at 77 K under handheld UV light. Compounds **2c** and **2d**, which contain unfunctionalized ppy ligands, emit blue-green in solution at 77 K under UV excitation (*vide infra*). **2d** also exhibits bright green emission in the solid state.

2.2.2 Photophysical Data

To our knowledge, **2a–2d** are the first examples of luminescent iridium(III) compounds that employ a cyclometallated ligand which associates with the metal through weakly-coordinating/non-covalent interactions, despite a large number of cationic, luminescent iridium complexes having been reported. Many of these cationic Ir(III) species exist as formal salts,[2g,26] while comparatively few zwitterionic species, which also contain formally cationic Ir(III) centers, have been documented.[12,27] In contrast to **2a–2d**, the negatively charged component of these previously reported "inner-salt complexes"[27a] is distal to the metal center and the coordination environment around the Ir(III) center falls in line with the more traditional construct containing covalent metal-ligand bonds (Figure 2.1A).
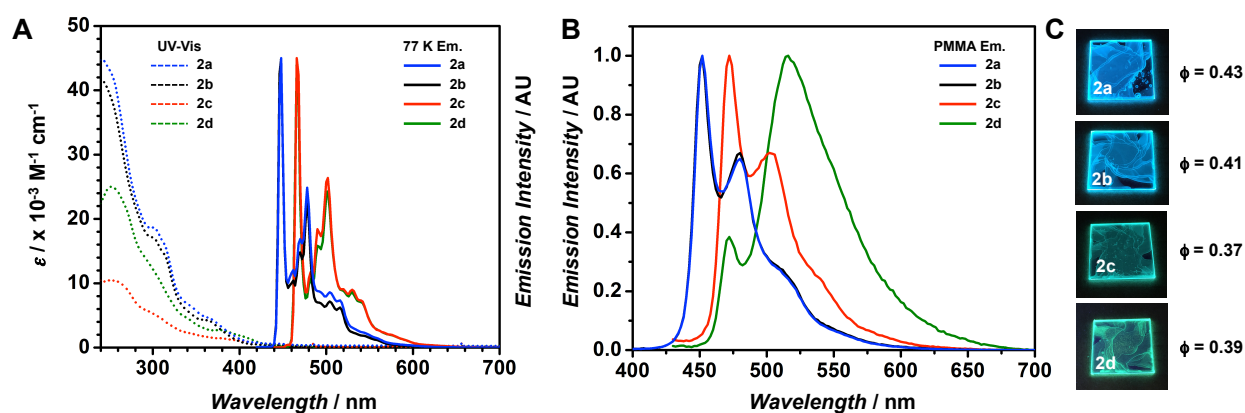
Figure 2.3 (A) UV-Vis absorption (dotted line) and 77 K emission (solid line) spectra for **2a-2d**. UV-Vis measurements were recorded in CH_2Cl_2 at 1×10^{-5} M and 77 K emission spectra were obtained from solutions of 2-MeTHF. (B) Emission spectra of 2 wt.% PMMA films of **2a-2d** (λ_{exc} = 400 nm). (C) Pictures of 2 wt.% PMMA films of **2a-2d** when irradiated with UV light (λ_{exc} = 365 nm).

A suite of photophysical studies were carried out on **2a–2d** to evaluate the influence of the *nido*-carboranylpyridine ligand framework on the luminescent properties, excited state lifetime, and thermal stability of the title compounds. The absorption and emission spectra of **2a–2d** are presented in Figure 2.3 with corresponding data presented in Figure 2.4A. All compounds exhibit strong absorption bands from 250–330 nm attributed to the spin-allowed $^1\pi$—π^*

transitions (^{1}LC) on the ppy ligands. The broad, lower intensity bands that extend from 340–420 nm arise from spin-allowed ^{1}MLCT and spin-forbidden ^{3}MLCT transitions that are consistent with previously reported Ir(III) complexes.[2]

All complexes are weakly emissive in fluid solutions of deaerated 2-MeTHF with quantum yields (φ) less than 0.01 at room temperature, but become strongly luminescent at 77 K and when doped in PMMA films (Figure 2.4A and Appendix A). This behavior has been observed with other previously reported *mer*-Ir(C^N)$_3$ (C^N = monoanionic cyclometalating ligand) complexes.[2f] Interestingly, only **2b** and **2d**, which do not contain CH$_3$ groups bound to the 2-position of the *nido*-carboranyl fragment, exhibit observable emission as neat solids. This observation could also be ascribed to aggregation in the solid state due to a lesser degree of steric bulk on the carborane to prevent such interactions. A similar observation has been made by Lee and co-workers in Ir(III)-based emitters containing *C*-substituted carboranes.[28]
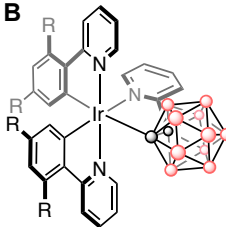
A	Abs. λ_{max}[a] [ε x 10^{-3} (M^{-1}cm^{-1})]	Em. λ_{max}[b,c] (nm)	ϕ_{PL}[b,d]	τ[b,e] (µs)	k_r[f] (x 10^5 s^{-1})	k_{nr}[f] (x 10^5 s^{-1})	k_r/k_{nr}
2a	253 [25], 338 [4.6], 279 [2.7]	452 (448)	0.43	3.35 (5.65)	1.3	1.7	0.76
2b	260 [10], 309 [4.7], 382 [1.4]	451 (447)	0.41	3.62 (6.38)	1.1	1.6	0.69
2c	244 [45], 302 [19], 367 [4.5]	472 (466)	0.37	3.02 (5.11)	1.2	2.1	0.57
2d	243 [41], 301 [17], 363 [4.3]	525 (466)	0.39	2.96 (5.19)	1.3	2.1	0.62
3a	255 [32], 306 [12], 377 [4.7]	463 (459)	0.070	0.62	1.1	15	0.07
3b	256 [39], 347 [6.4], 396.4 [4.4]	489 (483)	0.035	0.71	0.49	14	0.04

Figure 2.4 (A) [a]UV-Vis absorption spectra were measured in CH$_2$Cl$_2$ (1 x 10^{-5} M). [b]Emission maxima, quantum yields, and excited state lifetimes were measured in 2 wt% PMMA films. Spectra recorded in 2-MeTHF at 77 K are marked with parentheses. [c]Highest energy peaks are reported in this table. [d]Quantum yields were measured using an integrating sphere under N$_2$. [e]Excited-state lifetimes values in PMMA films are obtained from the weighted average of a bi-exponential decay. [f]Calculated for PMMA films according to the equations $k_r = \phi/\tau$ and $k_{nr} = (1-\phi)/\tau$, where k_r is the radiative rate constant, k_{nr} is the non-radiative rate constant, φ is the quantum yield, and τ is the excited-state lifetime. (B) Structures of Ir(III) complexes featuring covalently-bound carboranyl ligand reported by Lee *et al.* (Ref 14a).

At 298 K, the excited state lifetimes (τ) of **2a–2d** in fluid solution display multi-exponential decays with nano- and microsecond components. The dynamic behavior suggests a possible equilibration between other triplet states before deactivation and is currently under further investigation. Upon cooling 2-MeTHF solutions of **2a–2d** to 77 K, τ becomes first order and ranges from 5.11 μs (**2c**) to 6.38 μs (**2d**). Low temperature emission spectra for **2a–2d** all display well-defined vibronic features consistent with emission from a ligand-centered triplet state. Introduction of the CH_3 group to the *nido*-carboranyl-pyridyl ligand has a negligible effect on the luminescence as the E_{0-0} energies and vibronic structure for **2a/2b** and **2c/2d** are nearly indistinguishable (Figure 2.3A). In PMMA films at room temperature the vibronic manifold in the emission spectra for **2a-c** redshift and broaden relative to the corresponding spectra at 77 K (Figure 2.3B). In contrast, the low solubility for **2d** is evidenced in a spectrum that displays a broad, red-shifted band at 525 nm. This new feature indicates that **2d** aggregates prior to solvent evaporation despite filtering solutions before casting the PMMA film (see Appendix A for further discussion). Indeed, Lee and co-workers have noted that substituted carboranyl components of Ir(III)-based emitters can help prevent solid-state quenching at higher concentrations.[16f,h] The quantum yields for all four complexes drastically increase upon doping in PMMA films, ranging from 0.37 to 0.43 (Figure 4A).

Methylation of the *nido*-carboranyl fragment has little effect on photophysical properties when these complexes are doped in PMMA films since ϕ, τ, and the emission frequencies for **2a/2b** and **2c/2d** are roughly identical. Conveniently, the carboranyl moiety can be functionalized to address solubility issues, such as in the case of **2d** to **2c**, without significant effect on the emission properties. This is a significant advantage of the carborane-based framework in the context of the described system.

From the excited-state lifetimes and quantum yields of **2a**–**2d** doped in the PMMA matrices, the radiative (k_r) and non-radiative (k_{nr}) rate constants can be deduced (Figure 2.4A). The k_r values observed are between 1.1×10^5 s^{-1} and 1.3×10^5 s^{-1}, with k_{nr} values ranging from 1.6×10^5 s^{-1} to 2.1×10^5 s^{-1}. To elucidate the effect of the *nido*-carboranylpyridine ligand, these values were compared to those of related complexes doped in PMMA films reported by Lee and coworkers, **3a** and **3b** (Figure 2.4B).[14a] Though $\phi < 0.10$ for **3a** and **3b** in the PMMA films, the shorter τ values for these compounds yield k_r values roughly similar to those of **2a**–**2d**. In contrast, the k_{nr} values for **2a**–**2d** are more than an *order of magnitude lower* than those of **3a** and **3b**. The ratio of k_r/k_{nr} for **2d** is ~16 times greater than that for the related compound **3b** (0.64 and 0.04, respectively). Therefore, despite the weakly coordinating nature of the carboranyl fragment to the Ir(III), **2a**–**2d** exhibit significantly lower values for k_{nr} and hence up to a *10-fold increase* in quantum yields compared to values reported for related molecules with covalent Ir(III)–carborane interactions. This newly developed electrostatic framework thus potentially offers a counterintuitive yet useful concept in engineering efficient Ir(III) emitters for OLED devices.

2.2.3 Electrochemistry and Thermogravimetric Analysis

Cyclic voltammetry (CV) plots of **2a**–**2c** are presented in Figure 2.5A with the associated data summarized in Table 2.1. Compared to **3a** and **3b**, **2a**–**2c** have analogous reductive behavior as all complexes display a single, irreversible reduction wave from -2.26 V to -2.39 V versus the ferrocenium/ferrocene redox couple. Introduction of the methyl group on the *nido*-carboranyl ligand has negligible influence on the reduction potential, as E^{Red} for **2a** and **2b** are 2.27 V and 2.26 V, respectively. In contrast, the Ir(III) complexes bearing the *nido*-carboranyl ligands are up to 0.32 V more difficult to oxidize than their covalent analogues (**3a** and **3b**) and feature two

irreversible oxidation waves. The first oxidation potential ($E^{Ox,1}$) decreases from 1.14 V (**2b**) to 1.05 V (**2a**), likely due to the electron-releasing inductive effect of the methyl group. Furthermore, the second oxidation potential ($E^{Ox,2}$) is roughly the same at 1.48 V for **2a** and 1.50 V for **2b**. On the basis of density functional theory (DFT) calculations (*vide infra*), reduction likely occurs on the ppy ligand,[2f,29] whereas the two unique oxidations involve removal of an electron from both the *nido*-carboranyl fragment and the Ir(III) center.
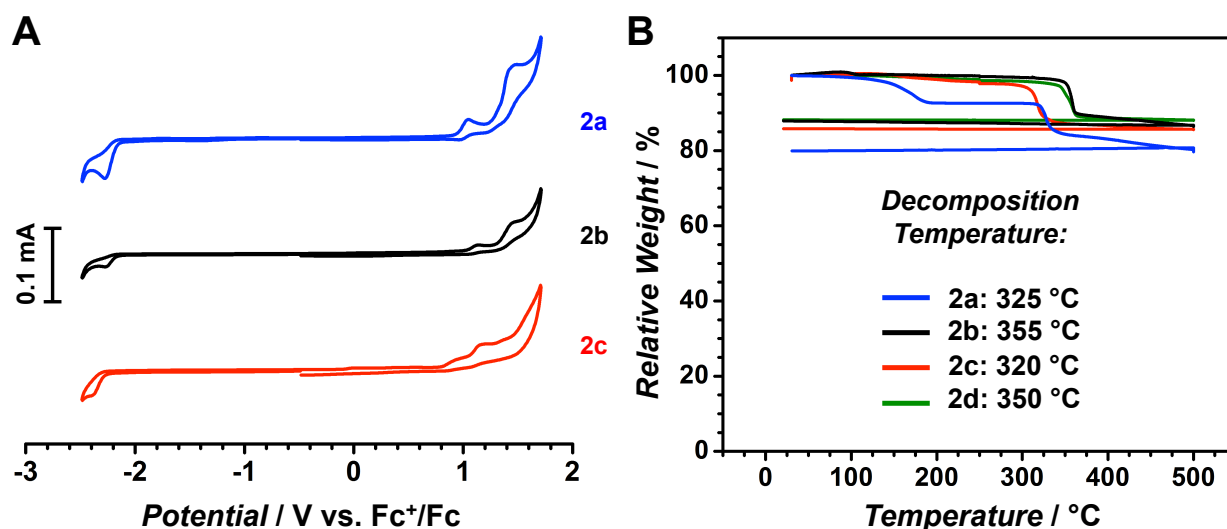
Figure 2.5 (A) Stacked cyclic voltammograms of **2a–2c** with scale bar of 0.1 mA. Referenced to Fc[+]/Fc in MeCN with a glassy carbon working electrode, scan rate = 0.1 V/s. Low solubility of **2d** prevented electrochemical characterization. (B) Thermogravimetric analysis (TGA) plots of **2a–2d** with corresponding temperatures of decomposition listed below. Mass loss at ~140°C for **2a** corresponds to loss of residual EtOEtOH.

Table 2.1 Electrochemical Properties for **2a–2c** and Related Compounds.[a,b]

Compound	E^{Red} (V)	$E^{Ox,1}$ (V)	$E^{Ox,2}$ (V)	ΔE (V)[d]
2a	-2.27	1.05	1.48	3.32
2b	-2.26	1.14	1.50	3.40
2c	-2.39	0.94	1.20	3.33
3a[e]	-2.30	0.94[f]	—	3.24
3b[e]	-2.39	0.62[c,f]	—	3.01

[a]Values reported relative to the ferrocenium/ferrocene redox couple (Fc[+]/Fc) at 0.5 mM, scan rate = 0.1 V/s. [b]Low solubility of **2d** hindered electrochemical characterization. [c]Reversible. [d]ΔE = $E^{Ox,1}$ − E^{Red}. [e]From Ref. 14a. [f]Values correspond to first (and only) oxidation reported.

A series of zwitterionic Ir(III)-based phosphors have been previously probed electrochemically[27a] and were shown to display shifts to more positive potentials (1.09 V – 1.58 V vs. Fc/Fc$^+$) compared to typical Ir(III)-based phosphors containing a formally neutral Ir(III) center (~0.9 V vs. Fc$^+$/Fc). Cyclic voltammetry measurements of independently synthesized deboronated analogue of **1b** (**4a**, see Appendix A) were performed, which show the first oxidation wave centered at 0.57 V vs. Fc$^+$/Fc. We therefore suggest that the first oxidation is centered on the *nido*-carboranyl fragment (whose oxidation is pushed to more positive potentials upon association to the metal center) and the second oxidation corresponds to a metal-centered Ir(III)/(IV) couple. Despite the apparent electrostatic interaction between the carboranyl ligand and the Ir(III) center, **2a–2d** have proven to be very thermally stable. Thermogravimetric analysis (TGA) shows the onset of mass loss occurring from 320°C – 355°C for these compounds (Figure 2.5B). Importantly, the introduction of methyl substitution on the carborane (**2a** and **2c**) does not significantly affect decomposition temperatures.

2.2.4 Structural and Computational Analysis

The electronic structures of **2a–2d** calculated using density functional theory (DFT) provide further insights into the observed photophysical phenomena. Ground-state geometries of **2a–2d** were optimized from the coordinates obtained from their crystallographically-derived X-ray data and subsequent single point calculations were carried out with the B3LYP functional and TZP basis set (Figure 2.6A and 2.6B). The bond angles and distances of the optimized structures compare favorably with the experimentally determined metrics based on X-ray crystallography (Appendix A, Figure A4). The calculated energies corresponding to the first triplet excited state (T_1) to singlet ground state (S_0) are consistent with those measured in solution at 77 K (see SI for the summary of calculated values). As expected, the HOMO levels

for **2a** and **2b**, which contain fluorinated ppy ligands, are located slightly lower in energy than those for **2c** and **2d**; similarly, the LUMO levels for **2a** and **2b** are slightly higher in energy than those for **2c** and **2d**. Finally, the experimentally-observed emission data is consistent with the energy levels calculated for **2a**–**2d** (see Appendix A, Table A3). Analysis of the solid state structure of **2a**, which will be treated in the following discussion as a representative example given the structural similarity of **2a**–**2d** (See Figure 2.2D and Figures A2 and A3, Appendix A), displays a *meridional* (*mer*) arrangement of the pyridine ligands. A long Ir⋯B(11) distance of 2.528(6) Å is found, which is longer than the sum of the covalent radii of the two atoms (2.07 Å) based on literature values,[30] suggesting no appreciable covalent metal-ligand bonding interaction. These distances are also systematically longer by ~ 0.3 Å than those in Ir(III)-based complexes in which B–H agostic interactions are normally invoked.[31,32] In addition, the Ir–H(1A) bond distance (1.935(9) Å) also well exceeds the sum of the covalent radii (1.54 Å) of Ir(III) and H atoms. The B(11)–H(1A) bond distance of 1.007(2) Å is nearly identical to those of the other terminal B–H bonds on the boron cluster scaffold in **2a**, suggesting that this bond (in addition to the analogous bonds in **2b**–**2d**) is not strongly activated by the Ir(III) center.
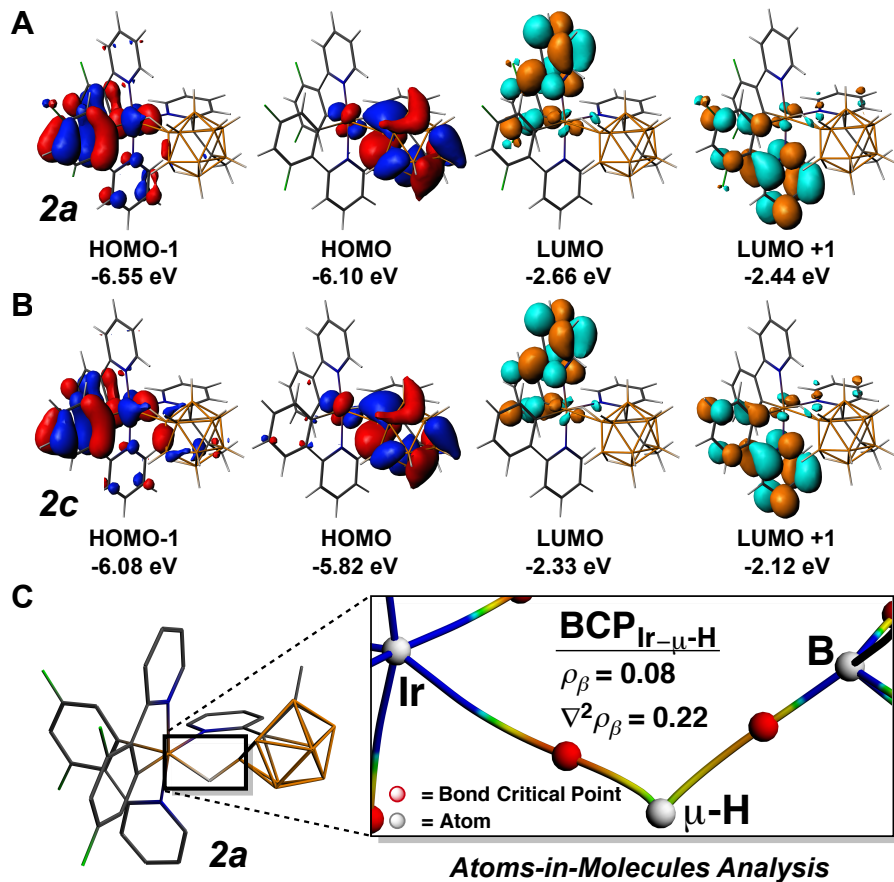
Figure 2.6 Frontier orbital diagrams of (A) **2a** and (B) **2c**. HOMO-1, HOMO, LUMO, and LUMO+1 diagrams were calculated from the geometry-optimized singlet state. (C) AIM analysis of **2a**. Electron density and Laplacian density values at the bond critical point suggest primarily electrostatic interactions between the *nido*-carboranyl fragment and the Ir(III) center.

Infrared (IR) spectroscopy suggests only weak coordination of the bridging hydride to the metal center: solid-state IR spectra reveal broad resonances in the expected B–H region ~2500 cm^{-1}, which correspond to the cage B–H stretches, with some fine structure observed (Appendix A, Figure A7). An additional but very weak resonance is observed for **2a–2d** ~2100 cm^{-1} which is suggestive of a weak Ir–m-H–B stretching band. Such M–m-H–B interactions have been noted previously with carboranes.[24b,32] In particular, Reed[33] and Teixidor[34] observed similar stretching frequencies in $[CB_{11}H_{12}]^{-}$ (~2380 cm^{-1}) and *nido*-carborane-based (2119–2077 cm^{-1}) systems, respectively, and have also ascribed these bands to weak interactions of carboranyl B–H bonds with cationic metal centers. Hawthorne observed slightly lower B–H stretching frequencies

(~1965 cm^{-1}) for a *nido*-carborane anion associated to Ir(III) through two B–*μ*-H–Ir interactions.[35] Given the rigid steric profile of the ppy ligands around octahedral iridium center and the bulk of the carboranyl ligand, we suggest that the bridging hydride interacts with the metal to complete its preferred octahedral geometry but that the primary mode of association results from ion pairing between the formally anionic *nido*-carborane and the formally cationic Ir(III) center (Figure 2.1B). ^{11}B NMR resonances for **2a–2c** (**2d** is too insoluble to observe defined ^{11}B signatures) contain several broad features at room temperature, where B–H coupling is not well-resolved. A variable temperature (VT) ^{11}B NMR study of **2a** revealed that these resonances further broaden upon cooling to -60˚C (see Appendix A, Figure A10) and sharpen upon heating to 60˚C, implicating fluxional behavior of the *nido*-carboranyl-metal interaction. At higher temperatures, it is revealed that one doublet in the ^{11}B NMR contains a slightly smaller coupling constant (~80 Hz) relative to the rest (~ 130 – 140 Hz); the ^{1}H NMR data also shows a partially resolved quartet (~ -3.5 ppm) with a $^{1}J_{BH}$ value of ~ 80Hz. Given that the spectrum broadens upon cooling, the observation of this B–H coupling is a snapshot of a fluxional process that is fast on the NMR timescale and indicates that the M–*μ*-H–B is appreciable at some point during this dynamic process. Overall, these data support an electrostatic description interaction between the Ir(III) center and the *nido*-carboranyl ligand in the solid state and in solution as opposed to a covalent Ir–*nido*-carboranyl bond model.

Importantly, using DFT, we were able to further probe the interaction between Ir(III) and the *nido*-carboranyl fragment in **2a–2d** using the Quantum Theory of Atoms in Molecules (QTAIM) analysis, which has been used to evaluate different types of bonding (*e.g.* covalent, electrostatic) interactions between atoms.[36] The results suggest that minimal covalency exists between Ir(III) and either H(1A) or B(11) in **2a** (Figure 2.6C) or **2b–2d** (Appendix A, Table A4).

First, no bond critical point (BCP) is observed between Ir and B(11) in any of the four title compounds. This is consistent with the long Ir–B(11) distances found crystallographically (which extend beyond the sum of the covalent radii of the two atoms) and further supports an electrostatic description of the interaction between the carboranyl ligand and the metal center as evidenced by the VT ^{11}B NMR study of **2a** (*vide supra*; see Appendix A).

Second, while a BCP is found in **2a**–**2d** between Ir and H(1A), the value of the electron density (r_b) at this point is ~0.08 for all compounds. In general, r_b values of 0.2 or greater are indicative of covalent interactions, whereas values of less than 0.1 signify non-covalent interactions such as van der Waals, hydrogen bonding, or electrostatic interactions. The Laplacian of the electron density at the BCP ($\nabla^2 r_b$) signifies the relative concentration or depletion of electron density along and perpendicular to the bond path at the BCP. Positive values generally indicate the depletion of electron density at the BCP, which is indicative of closed-shell bonding interactions, such as ionic and hydrogen bonding. Values of ~ 0.22 are obtained for all structures, strongly suggesting closed shell/electrostatic interactions between the carboranyl ligand fragment and Ir(III).

2.3 Conclusions

The concept of using electrostatically bound ligands for Ir(III)-based phosphors is introduced for the first time. The experimental and computational data suggest that the use of bulky, weakly coordinating, non-covalent ligand frameworks is a viable option for stable and emissive phosphorescent molecules based on Ir(III). Importantly, structural modification of the weakly-coordinating ligand can be carried out without detrimentally affecting the photophysical properties of the resulting complex: the inclusion of a methyl group at the *C*-vertex of the *nido*-carboranyl ligand in **2a** and **2c** does not strongly influence the emission wavelength relative to

the non-methylated counterparts (**2b** and **2d**, respectively); importantly, however, methylation does improve the solubility of **2a** and **2c** relative to **2b** and **2d**. This orthogonality is a potentially useful handle for optimizing the physical/materials properties of this class of Ir(III)-based phosphors without significantly modulating the excited-state characteristics when employed as a component of an OLED construct, particularly given the non-triviality of engineering dopant-host layer compatibility.[37] Recent reports of straightforward methods to functionalize *boron* vertices of carboranes[38] with vertex precision also provide potentially powerful strategies for modulating structural and photophysical properties of Ir(III) species with *B*-substituted carborane-based ligands. Ultimately, the utility of boron cluster-based weakly-coordinating ligands in phosphorescent molecules demonstrated here sets the precedent for the exploration of this motif using other tunable boron cluster congeners that similarly present appreciable steric bulk and overall negative charge.[39] In particular, functionalized *closo*- boron clusters, such as the anionic carba-*closo*-dodecaboranes and charge-compensated *closo*-dodecaborates, are prime candidates for further study within this context, as these bulky, *closo*- clusters are generally more stable than *nido*- or *arachno*- derivatives and are themselves widely used as non-coordinating anions. A deeper understanding of the structure-function relationships of strategically designed, weakly-coordinating carborane-based ligands on the materials and photophysical properties of metal-based luminescent molecules will potentially promote the discovery of new, efficient emitters for application in light-emitting devices.

2.4 Experimental

2.4.1 General considerations

All experiments were performed under ambient conditions unless otherwise noted. Tetrahydrofuran (THF) and acetonitrile (CH$_3$CN) used for cyclic voltammetry were sparged with argon and passed through activated alumina prior to use. All post-Schlenk work-up and characterization was performed under ambient conditions. The "ambient conditions" for this manuscript refer to room temperature (20 - 25 °C) and uncontrolled laboratory air. Thin-layer chromatography (TLC) samples for carborane-containing compounds were stained with 1 wt. % PdCl$_2$ in 6M HCl and were developed with heat.

2.4.2 Materials

Deuterated solvents were purchased from Cambridge Isotope Laboratories and were stored over 3Å molecular sieves under ambient conditions. 2-ethoxyethanol (EtOEtOH), [Ir(^{F2}ppy)$_2$(m-Cl)]$_2$ (Cat. # 749230), [Ir(ppy)$_2$(m-Cl)]$_2$ (CAS # 92220-65-0), methyl iodide (with copper stabilizer) tetrabutylammonium hexafluorophosphate (≥99.0%, electrochemical grade), tetrabutylammonium bromide, potassium hydroxide, diethyl ether (Et$_2$O), methylene chloride (CH$_2$Cl$_2$), ethanol (EtOH) and hexanes were purchased from Sigma-Aldrich. 1,2-dimethoxyethane was purchased from Sigma Aldrich and stored on the benchtop over 3Å molecular sieves. 2-Fluoropyridine and 1,2-difluorobenzene were purchased from Oakwood Chemicals. *o*-carborane was purchased from Boron Specialties, LLC. Glass-backed Silica Gel 60 GLA TLC plates and Celite were purchased from Fisher Scientific. All reagents were used as received unless otherwise indicated. Na(acac) was synthesized in a N$_2$-filled glovebox by treatment of a THF solution of acetylacetone with 1.5eq. NaH at room temperature with stirring

for 24h. After 24h, the mixture was filtered through Celite and the filtrate was dried *in vacuo* to give the desired product. The resulting salt was stored outside the box in a desiccator.

2.4.3 Instruments

^{1}H NMR spectra were obtained on a Bruker AV500 or a Bruker AV400 spectrometer; ^{13}C{^{1}H} NMR spectra were obtained on a Bruker AV500 or Brucker DRX500 spectrometer; ^{11}B and ^{31}P NMR spectra were obtained on a Bruker DRX500 spectrometer; ^{19}F NMR spectra were obtained on a Bruker AV300 spectrometer. MestReNova (Version 10.0.0-14411) software was used to process the NMR data. ^{1}H and ^{13}C{^{1}H} NMR spectra were referenced to residual solvent resonances in deuterated solvents (CDCl$_3$: ^{1}H, 7.260 ppm; ^{13}C, 73.840 ppm; Acetone-d^6: ^{1}H, 2.050 ppm; ^{13}C, 29.84 ppm. Note: due to high humidity H$_2$O resonances are often present). ^{11}B and ^{19}F and NMR spectra were referenced to external BF$_3$·Et$_2$O (0 ppm) and C$_6$H$_5$F (-113.15 ppm) standards, respectively. Mass spectrometry data was acquired using a Waters LCT Premier mass spectrometer by direct injection. UV−Vis spectra were recorded on a Hewlett-Packard 4853 diode array spectrometer. Phosphorescence lifetime measurements for **2a**–**2d** were performed by a time-correlated single-photon counting method using an IBH fluorocube lifetime instrument equipped with a 405 nm LED excitation source. Quantum yield measurements were carried out using a Hamamatsu C9920 system equipped with a xenon lamp, calibrated integrating sphere, and model C10027 photonic multichannel analyzer. Steady-state emission measurements of **2a**–**2d** as solids, in the thin film, and in solution at 77 K were performed using a Photon Technology International QuantaMaster spectrofluorimeter. Microwave reactions were performed in glass 10 mL microwave reactor vials purchased from CEM with silicone/PTFE caps equipped with a stir bar using a CEM Discover SP microwave synthesis reactor.

2.4.4 Preparation of PMMA Thin Films

A solution of PMMA (0.100 g, 35 kDa) in toluene (1.0 mL) was thermally sonicated for 1 hour at 40°C, or until PMMA was completely dissolved. Next, **2a–2d** (2 mg, 2 wt. %) was added to the solution and sonicated for an additional 5 minutes, yielding a yellow solution. The solution of **2a–2d**/PMMA was spin coated on a quartz substrate (3-5 drops, 800-1,000 RPM, 30 seconds), and this was repeated (~ 4−6 times) until the film was thick enough emit light under λ = 365 nm excitation in a dark room under ambient conditions. Due to low solubility, the solution of **2a**/PMMA was passed through a 0.20 mm syringe filter prior to spin coating.

2.4.5 Determination of Molar Extinction Coefficients

Extinction coefficients were determined through a series of 5 dilutions with a maximum absorption between 0.1 and 0.7.

2.4.6 X-ray data collection and processing parameters

For **2a–2d**, a single crystal was mounted on a nylon loop using perfluoropolyether oil and cooled rapidly to 100 K with a stream of cold dinitrogen. Diffraction data were measured using a Bruker APEX-II CCD diffractometer using Mo-$K\alpha$ radiation. The cell refinement and data reduction were carried out using Bruker SAINT and the structure was solved with SHELXS-97. All subsequent crystallographic calculations were performed using SHELXL-2013.

2.4.7 Cyclic voltammetry

Cyclic voltammetry was performed on **2a–2d** and using a CH Instruments Model 600D potentiostat with a glassy carbon disc working electrode, platinum wire counter electrode, and Ag/AgCl wire reference in a saturated solution of KCl in MeCN. All experiments were conducted in 0.1M [N^{n}Bu$_4$]PF$_6$/CH$_3$CN with 0.5 mM analyte concentrations. CH$_3$CN solutions

were degassed by sparging with argon for 10 minutes, and the cyclic voltammetry was performed under constant flow of argon or nitrogen gas. A scan rate of 0.1 mV/s was used with ferrocene as an internal standard.

2.4.8 DFT Calculation Details

All optimized geometries were calculated from crystallographic data and optimized with DFT calculations using standard triple-ξ polarization (TZP) basis sets available in the Amsterdam Density Functional 2014.04 Rev. 44409 (ADF)[a-c] software suite, with Becke[d] and Perdew[e] (BP) Slater-type orbitals (STOs) on a 6 core Apple computer. The local density approximation (LDA) was made with BP and exchange and correlation corrections available by default in the ADF 2014.04 suite. Single point calculations were performed using the B3LYP[f,g] level of theory and a TZP basis set. All-electron basis sets were used for all atoms (cores remained un-frozen). Electron spins were restricted for S_0 calculations, and electron spins were unrestricted for T_1 calculations. Relativistic correlations were made using Zero-Order Relativistic Approximation (ZORA)[h-j] for Ir (**2a–2d**).

References for DFT calculations:

a) te Velde, G.; Bickelhaupt, F. M.; Baerends, E. J.; Guerra, C. F.; van Gisbergen, S. J. A.; Snijders, J. G.; Ziegler, T. *J. Comput. Chem.* **2001**, *22*, 931; b) Guerra, C. F.; Snijders, J. G.; te Velde, G.; Baerends, E. J. *Theor. Chem. Acc.* **1998**, *99*, 391; c) Baerends, E. J.; Ziegler, T.; Autschbach, J.; Bashford, D.; Bérces, A.; Bickelhaupt, F. M.; Bo, C.; Boerrigter, P. M.; Cavallo, L.; Chong, D. P.; Deng, L.; Dickson, R. M.; Ellis, D. E.; van Faassen, M.; Fan, L.; Fischer, T. H.; Fonseca Guerra, C.; Franchini, M.; Ghysels, A.; Giammona, A.; van Gisbergen, S. J. A.; Götz, A. W.; Groeneveld, J. A.; Gritsenko, O. V.; Grüning M.; Gusarov, S.; Harris, F. E.; van den Hoek, P.; Jacob, C. R.; Jacobsen, J.; Jensen, L.; Kaminski, J. W.; van Kessel, G.; Kootstra, F.;

Kovalenko, A.; Krykunov, M. V.; van Lenthe, E.; McCormack, D. A.; Michalak, A.; Mitoraj, M.; Morton, S. M.; Neugebauer, J.; Nicu, V. P.; Noodleman, L.; Osinga, V. P.; Patchkovskii, S.; Pavanello, M.; Philipsen, P. H. T.; Post, D.; Pye, C. C.; Ravenek, W.; Rodríguez, J. I.; Ros P.; Schipper, P. R. T.; van Schoot, H.; Schreckenbach, G.; Seldenthuis, J. S.; Seth, M.; Snijders, J. G.; Solà, M. Swart, M.; Swerhone, D.; te Velde, G.; Vernooijs, P.; Versluis, L.; Visscher, L.; Visser, O.; Wang, F.; Wesolowski, T. A.; van Wezenbeek, E. M.; Wiesenekker, G.; Wolff, S. K.; Woo, T. K.; Yakovlev, A. L. *ADF 2014/GUI 2014*; SCM: Amsterdam, **2014**; d) Becke, A. D. *Phys. Rev. A* **1988**, *38*, 3098; e) Perdew, J. P. *Phys. Rev. B* **1986**, *33*, 8822; f) Becke, A. D. *J. Chem. Phys.* **1993**, *98*, 5648; g) Lee, C.; Yang, W. Parr, R. G. *Phys. Rev. B* **1988**, *37*, 785; h) van Lenthe, E.; Baerends, E. J.; Snijders, J. G. *J. Chem. Phys.* **1993**, *99*, 4597; i) van Lenthe, E.; Baerends, E. J.; Snijders, J. G. *J. Chem. Phys.* **1994**, *101*, 9783; j) van Lenthe, E.; Ehlers, A.; Baerends, E. J. *J. Chem. Phys.* **1999**, *110*, 8943.

2.4.10 Synthetic Procedures

2.4.10.1 2-(2-CH$_3$-C$_2$B$_{10}$H$_{11}$)C$_5$H$_4$N (1a)

2-*o*-Carboranylpyridine (101mg, 0.456 mmol) was added to a 50mL Schlenk flask and the flask was evacuated and backfilled with N$_2$. Dry THF (15mL) was added and the resulting solution was cooled to -78˚C. n-BuLi (2.5M in hexanes, 191 mL, 0.479 mmol) was added via syringe and the resulting mixture was stirred at -78˚C for 1h. After 1h, the solution (at this point slightly yellow) was stirred at room temperature for 2h. After 2h, the solution was cooled to 0˚C and methyl iodide (31mL, 0.502 mmol) was added via syringe, giving the solution a deep purple color. The solution was removed from the ice bath and was allowed to stir at room temperature for two hours, over which time the solution gradually decolorized. After two hours, the pale purple solution was diluted with acetone and the solvent was then removed under vacuum. The

39

residue was charged with Et_2O and the mixture was filtered through a pad of silica gel. The filtrate was dried *in vacuo* to afford the desired product as a white solid (97mg, 90%). ^{1}H NMR ($CDCl_3$, 500 MHz) δ 8.61 (d, 1H, py), 7.75 (m, 2H, py), 7.37 (m, 1H, py), 3.0 − 1.5 (br m, 10H, BH), 1.76 (s, 3H, CH_3); ^{13}C NMR ($CDCl_3$, 125 MHz) 149.42, 137.36, 125.67, 124.78, 80.85, 77.02, 23.55; ^{11}B NMR ($CDCl_3$, 160 MHz) 2.66 (d, 1B), 4.98 (d, 1B), 9.88 (m, 8B). Expected mass: 233.2553; Found 233.2560.

2.4.10.2 2-(2-H-$C_2B_{10}H_{11}$)C_5H_4N (1b)

o-Carborane (250mg, 1.73 mmol) was charged to a Schlenk flask with ~20mL THF. The resulting solution was cooled to 0˚C and nBuLi (2.5M in hexanes, 763mL) dropwise. The resulting mixture was stirred at 0˚C for 15 minutes. The solution was removed from the ice bath and was stirred at room temperature for 10min, after which time the solution was heated to 70˚C in an oil bath for 2h. After 2h, the solution was cooled to 0˚C and 2-fluoropyridine (164mL, 1.91 mmol) was added dropwise via syringe. The mixture was stirred at 0˚C for 15 min and was then heated to 70˚C in an oil bath for 2h. After 2h, the red/yellow mixture was diluted with acetone (~10mL) and then the solvents were removed *in vacuo*. The residue was charged with CH_2Cl_2 and H_2O. The H_2O layer was neutralized with NH4Cl, and the organic layer was subsequently washed 2x with H_2O. The organic layer was dried over $MgSO_4$, filtered through Celite, and dried *in vacuo*. The residue was then eluted through a silica column with 9:1 hexanes:acetone to remove any remaining *o*-carborane contaminant. Fractions containing the desired product were combined and the solvent was removed under vacuum. The white product was afforded in 55% yield. All NMR spectra match those of the original report (Coult, F.; Fox, M. A.; Gill, W. R.; Herbertson, P. L.; Hugh MacBride, J. A.; Wade, K. *J. Organomet. Chem.* **1993**, *462*, 19).

2.4.10.3 Ir(ppy)₂(acac)

[Ir(ppy)₂(μ-Cl)]₂ (0.150 g, 0.139 mmol), Na(acac) (0.041 g, 0.336 mmol), 3.5 mL 1,2-dimethoxyethane, and small stir bar were combined in a 10 mL microwave tube. The mixture was stirred at 140°C for 2 hours to yield a yellow-brown slurry. The reaction product was transferred to a vial and the remaining contents in the microwave tube were washed out with ethanol, then solvents were removed *in vacuo*. The dark yellow solid was dissolved in minimal CH_2Cl_2 and the solution was passed through a pad of Celite. CH_2Cl_2 was removed *in vacuo* to yield the desired product (0.154 g, 92%). ^{1}H NMR (500 MHz, acetone-*d*6), ppm: δ 8.56 (d, 2H, *J* = 5.8 Hz), 8.07 (d, 2H, *J* = 7.9 Hz), 7.91 (t, 2H, *J* = 7.8 Hz), 7.64 (d, 2H, *J* = 7.8 Hz), 7.33 (t, 2H, *J* = 6.6 Hz), 6.75 (t, 2H, *J* = 7.4 Hz), 6.60 (t, 2H, *J* = 7.4 Hz), 6.22 (d, 2H, *J* 3.8 Hz), 5.27 (s, 1H), 1.69 (s, 6H). Chemical shifts match those of the previously reported preparation of this compound (Lamansky, S.; Djurovich, P. I.; Murphy, D.; Abdel-Razzaq, F.; Kwong, R.; Tsyba, I.; Bortz, M.; Mui, B.; Bau, R.; Thompson, M. E. *Inorg. Chem.* **2001**, *40*, 1704).

2.4.10.4 Ir([F2]ppy)₂(acac)

This compound was previously reported by Thompson and co-workers (Tamayo, A.; Alleyne, B. D.; Djurovich, P. I.; Lamansky, S.; Tsyba, I.; Ho, N. N.; Bau, R.; Thompson, M. E. *J. Am. Chem. Soc.* **2003**, *125*, 7377) but NMR characterization was not provided. Here we report a modified synthesis and provide full NMR characterization: [Ir([F2]C^N)₂Cl]₂ (200mg, 0.164 mmol) and Na(acac) (50mg, 0.411mmol) were charged to a 10mL glass microwave tube with a stirbar, followed by 2mL 1,2-dimethoxyethane. The contents were heated in the microwave with stirring at 140°C for 2h. The resulting mixture, which contained a yellow precipitate, was dried *in vacuo*, charged with CH_2Cl_2, and filtered through Celite. The Celite pad was washed with CH_2Cl_2 until the filtrate ran clear. The filtrate was evaporated to dryness to afford the desired

product in 95% yield. ^{1}H NMR (CDCl$_3$, 500 MHz) δ 8.44 (d, 2H, Ar), 8.25 (d, 2H, Ar), 7.79 (t, 2H, Ar), 7.19 (t, 2H, Ar), 6.33 (ddd, 2H, Ar), 5.66 (dd, 2H, Ar), 5.26 (s, 1H, CH), 1.81 (s, 6H, CH$_3$); ^{13}C NMR (CDCl$_3$, 125 MHz) 184.87, 165.20 (d, $^2J_{CF}$ = 7.0 Hz), 162.63 (dd, $^1J_{CF}$ = 230 Hz, $^3J_{CF}$ = 12 Hz), 160.59 (dd, $^1J_{CF}$ = 233 Hz, $^3J_{CF}$ = 13 Hz), 151.14 (d, $^3J_{CF}$ = 7 Hz), 147.92, 137.73, 128.50 (m), 122.48 (d, $^2J_{CF}$ = 19 Hz), 121.48, 114.95 (dd, $^2J_{CF}$ = 17 Hz, $^3J_{CF}$ = 3 Hz), 100.57, 97.18 (t, $^2J_{CF}$ = 27 Hz), 28.56; ^{19}F{^{1}H} NMR (CDCl$_3$, 282 MHz) -108.86 (q, 2F), -111.12 (jt, 2F).

2.4.10.5 Ir(^{F2}ppy)$_2$(2-(2-CH$_3$-C$_2$B$_9$H$_{10}$)C$_5$H$_4$N) (2a)

Ir(^{F2}ppy)$_2$(acac) (29mg, 0.0432 mmol) and **1a** (13mg, 0.0561 mmol) were charged to a 10mL glass microwave tube with a stirbar, followed by 500μL EtOEtOH and 20mL deionized H$_2$O. The yellow mixture was heated to 140°C for 2h to give a clear yellow solution. The resulting solution was concentrated *in vacuo* to give a yellow residue. The residue was twice charged with hexanes and dried under vacuum. The residue dissolved in CH$_2$Cl$_2$ and was eluted through a silica plug (~5 cm). The yellow solution was then dried under vacuum. The resulting residue was then charged with hexanes (~2mL) and isolated on a fritted funnel and washed with warm hexanes to provide the yellow product (27mg, 73%). X-ray quality crystals were grown from a concentrated EtOH solution at -15°C. **^{1}H NMR** (CDCl$_3$, 400 MHz) δ 9.05 (d, 1H, Ar), 8.44 (d, 1H, Ar), 8.40 (d, 1H, Ar), 7.97 (t, 1H, Ar), 7.90 (t, 1H, Ar), 7.84 (d, 1H, Ar), 7.72 (t, 1H, Ar), 7.58 (d, 1H, Ar), 7.51 (d, 1H, Ar), 7.27 (t, 1H, Ar), 7.17 (t, 1H, Ar), 6.96 (t, 1H, Ar), 6.60 (t, 1H, Ar), 6.44 (t, 1H, Ar), 5.65 (d, 1H, Ar), 5.60 (d, 1H, Ar), 3.0 – 0.5 (br, 8H, BH), 1.57 (s, 3H, CH$_3$), -3.3 – -4.2 (br, 2H, BH); **^{13}C NMR** (125 MHz) 165.53 (d, J_{FC} = 6.5 Hz), 164.51, 163.93 (dd, J_{FC} = 258 Hz, J_{FC} = 13 Hz), 163.35 (d, J_{FC} = 6.6 Hz), 162.84 (dd, J_{FC} = 258 Hz, J_{FC} = 12 Hz), 161.73 (dd, J_{FC} = 260 Hz, J_{FC} = 12 Hz), 161.12 (J_{FC} = 260 Hz, J_{FC} = 12 Hz), 155.83,

153.89, 150.44, 148.46, 146.34, 139.10, 138.88, 137.82, 128.20 (m), 128.07, 127.30 (m), 124.86,

124.70, 124.38, 124.15, 124.03, 123.87, 123.26, 99.66 (t, J_{FC} = 26 Hz), 99.27 (t, J_{FC} = 22 Hz),

74.23, 53.44, 22.69; **^{19}F NMR** (CDCl$_3$, 282 MHz) -104.92 (q, 1F), -106.98 (q, 1F), -107.66 (jt,

1F), -109.46 (d, 1F); **^{11}B NMR** (CDCl$_3$, 160 MHz) -6.10 (br, 2B), -11.90 – -14.00 (m, 4B), -

21.70 – -25.00 (m, 2B), -31.50 – -34.50 (m, 2B).

2.4.10.6 Ir(^{F2}ppy)$_2$(2-(2-H-C$_2$B$_9$H$_{11}$)C$_5$H$_4$N) (2b)

Ir(^{F2}ppy)$_2$(acac) (40mg, 0.0596 mmol) and **1b** (17mg, 0.0715 mmol) were charged to a

10mL glass microwave tube with a stirbar, followed by 500μL EtOEtOH. The yellow mixture

was heated to 140°C for 1.5h to give a yellow solution with an emissive yellow solid. The

resulting mixture was dried *in vacuo* to give a yellow residue. Et$_2$O (2mL) was added and the

mixture was chilled at -15°C overnight. The solid was isolated on a fritted glass funnel and was

rinsed four times with hexanes and dried *in vacuo*; this process was repeated with the dried

filtrate. Yield (2 crops): 36mg, 77%. X-ray quality crystals were grown from a concentrated

CH$_2$Cl$_2$ solution at -15°C. **^{1}H NMR** ((CD$_3$)$_2$CO, 400 MHz) δ 9.21 (d, 1H, Ar), 8.51 (d, 1H, Ar),

8.47 (d, 1H, Ar), 8.21 (m, 2H, Ar), 7.91 (m, 2H, Ar), 7.65 (d, 1H, Ar), 7.62 (d, 1H, Ar), 7.56 (m,

2H, Ar), 7.17 (ddd, 1H, Ar), 6.78 (ddd, 1H, Ar), 6.61 (dd, 1H, Ar), 5.74 (dd, 1H, Ar), 5.64 (dd,

1H, Ar), 3.00-1.00 (br m, 9H, BH), 2.43 (s, 1H, CH), -3.0 – -4.5ppm (br m, 2H, BH); **^{13}C NMR**

((CD$_3$)$_2$CO, 500 MHz) 168.89, 164.04 (dd, J_{CF} = 137 Hz; J_{CF} = 13 Hz), 163.63 (dd, J_{CF} = 172

Hz, J_{CF} = 7 Hz), 162.64 (d, J_{CF} = 8Hz), 162.54 (d, J_{CF} = 8Hz), 161.14 (dd, J_{CF} = 150 Hz, J_{CF} = 12

Hz), 161.58 (dd, J_{CF} = 225 Hz, J_{CF} = 12 Hz), 155.94, 153.79, 150.44, 149.08, 147.43 (d, J_{CF} =

7Hz), 139.79, 139.60, 139.24, 128.63 (m), 127.55 (m), 125.48, 125.01, 124.60, 124.54, 124.22

(d, J_{CF} = 4 Hz), 124.06 (d, J_{CF} = 5 Hz), 114.03 (dd, J_{CF} = 18Hz, J_{CF} = 3 Hz), 112.31 (dd, J_{CF} = 18

Hz, J_{CF} = 3 Hz), 99.18 (t, J_{CF} = 27 Hz), 98.58 (J_{CF} = 27Hz), 77.16, 45.31; **^{11}B NMR** ((CD$_3$)$_2$CO,

160 MHz) -5.94 (d, 1B), -16.27 (m, 4B), -23.60 – -27.50 (2 doublets, 2B), -31.81 (d, 1B), -35.59 (d, 1B); ^{19}F NMR ((CD$_3$)$_2$CO, 282 MHz) -107.17 (q, 1F), -109.02 (q, 1F), -109.11 (jt, 1F), -111.19 (jt, 1F).

2.4.10.7 Ir(ppy)$_2$(2-(2-CH$_3$-B$_9$H$_{10}$)-py) (2c)

Ir(ppy)$_2$(acac) (0.040 g, 0.066 mmol), **1a** (0.020 g, 0.082 mmol), 1.5 mL EtOEtOH, and small stir bar were combined in a 10 mL microwave vial. The mixture was stirred at 140°C for 1.5 hours to yield a yellow slurry. The reaction product was transferred to a vial and the remaining contents in the microwave tube were washed out with EtOH, then solvents were removed *in vacuo*. The yellow solid was dissolved in minimal CH$_2$Cl$_2$ and passed through a short silica plug. The yellow solution was concentrated to dryness, and the resulting solid was washed with hexanes (5 x 10 mL) to remove any remaining **1a**. The yellow product (40mg, 82%) was dried under vacuum overnight. ^{1}H NMR ((CD$_3$)$_2$CO-d$_6$, 500 MHz) δ 9.03 (d, 1H, Ar), 8.33 (d, 1H, Ar), 8.29 (d, 1H, Ar), 8.12–8.05 (m, 3H, Ar), 7.94 (dd, 1H, Ar), 7.88 (m, 1H, Ar), 7.78 (dd, 1H, Ar), 7.67 (d, 1H, Ar), 7.63 (dd, 1H, Ar), 7.49 (ddd, 1H, Ar), 7.41 (ddd, 1H, Ar), 7.09 (ddd, 1H, Ar), 7.04 (ddd, 1H, Ar), 6.87 (tdd, 2H, Ar), 6.73 (td, 1H, *Ar*), 6.24 (dd, 1H, Ar), 6.21 (dd, 1H, Ar), 1.61 (s, 3H, CH), 0.35-2.80 (br. m., 9B, BH), -3.03 (q, 1H, BH, J_{B-H}= 83.2 Hz), -3.55 (br. s, 1H, BH); ^{11}B NMR ((CD$_3$)$_2$CO-d$_6$, 160 MHz), ppm: δ -5.96 (d, 1B), -11.53 (br, 4B), -21.37 (d, 1B), -23.15 (d, 1B), -31.09 (d, 1B), -33.34 (d, 1B); ^{13}C NMR ((CD$_3$)$_2$CO-d$_6$, 125 MHz), ppm: δ 169.22, 167.54, 164.84, 154.04, 151.35, 150.23, 145.62, 144.58, 144.11, 139.38, 139.29, 138.72, 132.99, 131.45, 130.84, 130.01, 128.64, 126.20, 125.25, 125.09, 124.94, 124.58, 123.70, 123.03, 121.39, 121.22, 68.31, 54.97, 22.82. Single crystals for X-ray diffraction analysis were grown from slow vapor diffusion of pentane into dichloromethane at room temperature.

2.4.10.8 Ir(ppy)$_2$(2-(2-H-B$_9$H$_{11}$)-py) (2d)

Ir(ppy)$_2$(acac) (0.040 g, 0.066 mmol), **1b** (0.017 g, 0.077 mmol), 1.5 mL EtOEtOH, and small stir bar were combined in a 10 mL microwave vial. The mixture was stirred at 140°C for 1.5 hours to yield a yellow slurry. The reaction product was transferred to a vial and the remaining contents in the microwave tube were washed out with EtOH, then solvents were removed *in vacuo*. The yellow solid was then washed with Et$_2$O (5 x 2 mL) and vacuum dried overnight to yield the desired product (43mg, 90%). **^{1}H NMR** ((CD$_3$)$_2$CO-d$_6$, 500 MHz) δ 9.16 (d, 1H, Ar), 8.34 (d, 1H, Ar), 8.28 (d, 2H, Ar), 8.09 (m, 2H, Ar), 7.94 (d, 1H, Ar), 7.86 (ddd, 1H, Ar), 7.83 (d, 1H, Ar), 7.79 (d, 1H, Ar), 7.62 (d, 1H, Ar), 7.51 (dd, 1H, Ar), 7.44 (m, 2H, Ar), 7.07 (ddd, 1H, Ar), 7.03, (ddd, 1H, Ar), 6.86 (m, 2H, Ar), 6.74 (td, 1H, Ar), 6.25, (d, 1H, Ar), 6.16 Hz (d, 1H, Ar), 2.85-0.5 (br. m, 9B, BH), 2.36 (s, 1H, CH), -3.17 (m, 1H, BH, $J_{B–H}$ = 83.6 Hz), -3.84 (br. s, 1H, BH); **2d** is too insoluble to obtain meaningful ^{11}B and ^{13}C NMR spectra. Single crystals for X-ray diffraction analysis were grown from the slow evaporation of a concentrated solution of hot 1,2-difluorobenzene.

2.4.10.9 Tetrabutylammonium 2-(nido-7,8-o-carboranyl)pyridine (4a)

1b (100mg, 0.452 mmol) was charged to a roundbottom flask with 10mL EtOH and KOH (112mg, 2.00 mmol). The resulting solution was heated to 55°C overnight to afford a cloudy, colorless mixture. The solvent was removed in vacuo and the residue was charged with ~20mL H$_2$O. To this solution was added tetrabutylammonium bromide (146 mg, 0.542 mmol) in 4mL H$_2$O. The resulting white suspension was stirred vigorously for 30min at room temperature, after which time the white solid was isolated on a fritted funnel and dried *in vacuo* to give white product (175mg, 85%). **^{1}H NMR** (CDCl$_3$, 400 MHz) δ 8.28 (d, 1H, Ar), 7.44 – 7.34 (m, 2H, Ar), 6.91 (t, 1H, Ar), 3.16 (m, 8H, NBu$_4$), 1.62 (m, 8H, NBu$_4$), 1.44 (sextet, 8H, NBu$_4$), 1.01 (t, 12H,

NBu$_4$), 3.2 – 0.5 (br m, BH), -2.26 (br s, 1H, BH) (Broad nature of B-H peaks skews integration values slightly); ^{13}**C NMR** (CDCl$_3$, 125 MHz) 163.39, 147.42, 135.38, 120.86, 119.72, 77.37, 59.07, 43.64, 24.11, 19.79, 13.77; ^{11}**B{^{1}H} NMR** (CDCl$_3$, 160 MHz) -8.82, -10.15, -13.12, -16.20, -18.62, -23.04, -32.67, -35.24.
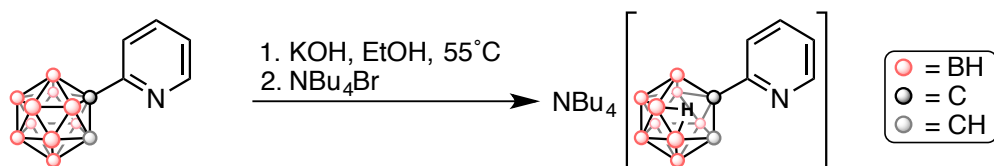
2.5 Appendix A

2.5.1 Additional Characterization Data

closo-
o-carborane
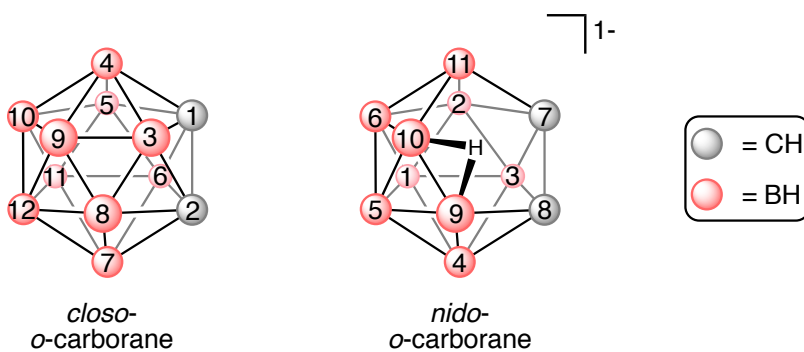
nido-
o-carborane

Figure A1 Numbering scheme for *closo-o*-carborane (left) and *nido-o*-carborane (right).

2a   **2b**
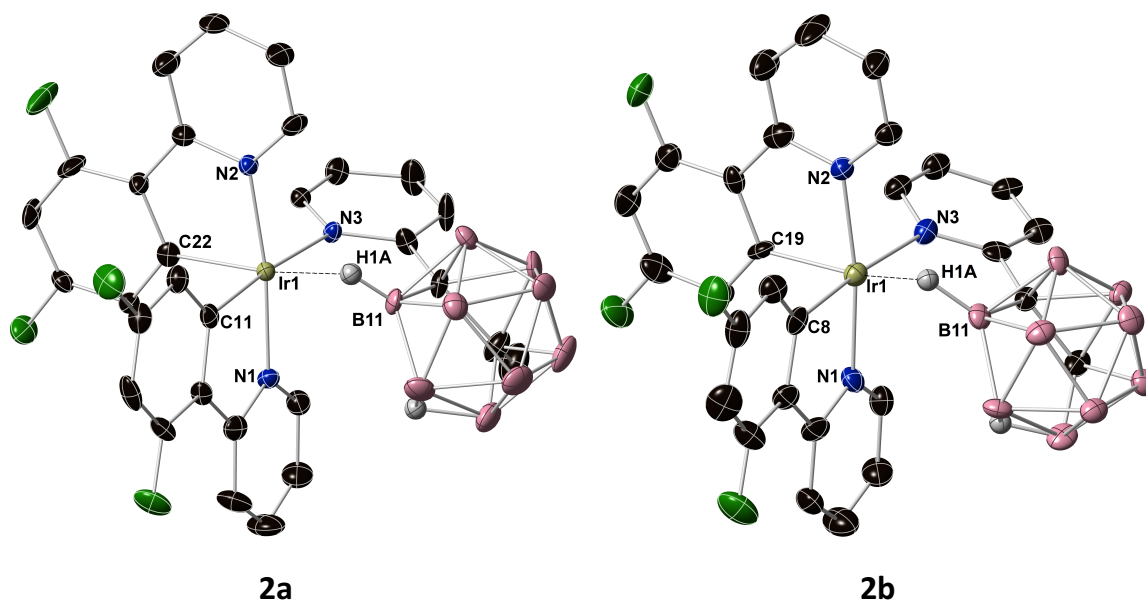
Figure A2 X-ray crystal structures of **2a** (left) and **2b** (right) (Protons (except for Ir–μ-H–B) have been omitted for clarity). Long Ir(1)–B(11) distances (2.528(6) Å, 2.504(1) Å) and Ir(1)–μ-H distances (1.935(9) Å, 1.665(6) Å) for **2a** and **2b**, respectively, suggest negligible covalent bonding interactions between Ir(1) and either H(1A) or B(11) in **2a** and **2b**.

2c   **2d**
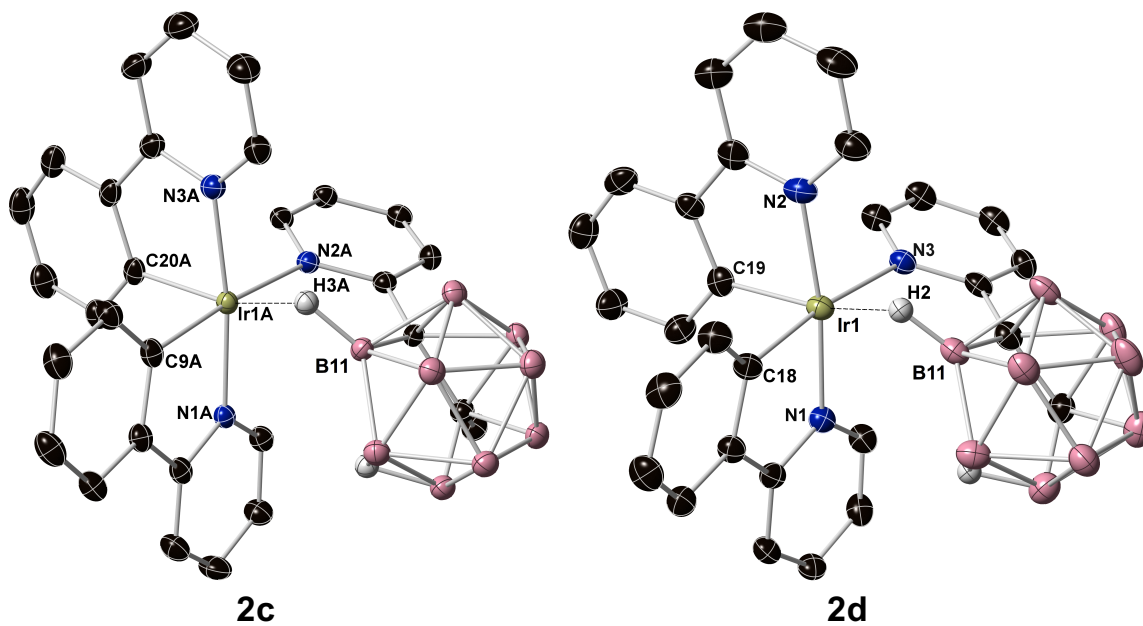
Figure A3 X-ray crystal structures of **2c** (left) and **2d** (right) (Protons (except for Ir–μ-H–B) have been omitted for clarity). Long Ir(1)–B(11) distances (2.521(7) Å, 2.501(6) Å) and Ir(1)–μ-H distances (1.769(5) Å, 1.790(0) Å) for **2c** and **2d**, respectively, suggest negligible covalent bonding interactions between Ir(1) and either μ-H or B(11) in **2c**/**2d**.

47

Table A1 Selected bond distances for **2a**–**2d**.

Compound	Ir(1)–B(11) (Å)	Ir(1)–μ-H (Å)	μ-H–B(11) (Å)
2a	2.528(6)	1.935(9)	1.007(2)
2b	2.504(1)	1.665(6)	1.192(8)
2c	2.521(7)	1.769(5)	1.242(4)
2d	2.501(6)	1.790(0)	1.144(6)

2a: Ir(1)–C(11), 2.011(5); Ir(1)–C(22), 2.020(3); Ir(1)–N(1), 2.044(6); Ir(1)–N(2), 2.050(7); Ir(1)–N(3), 2.177(2).

2b: Ir(1)–C(8), 2.012(2); Ir(1)–C(19), 2.012(6); Ir(1)–N(1), 2.052(4); Ir(1)–N(2), 2.066(6); Ir(1)–N(3), 2.177(7).

2c: Ir(1A)–C(9A), 2.020(4); Ir(1A)–C(20A), 2.013(6); Ir(1A)–N(1A), 2.044(4); Ir(1A)–N(2A), 2.192(9); Ir(1A)–N(3A), 2.050(8).

2d: Ir(1)–C(18), 2.019(1); Ir(1)–C(19), 2.029(2); Ir(1)–N(1), 2.049(7); Ir(1)–N(2), 2.059(5); Ir(1)–N(3), 2.169(1).
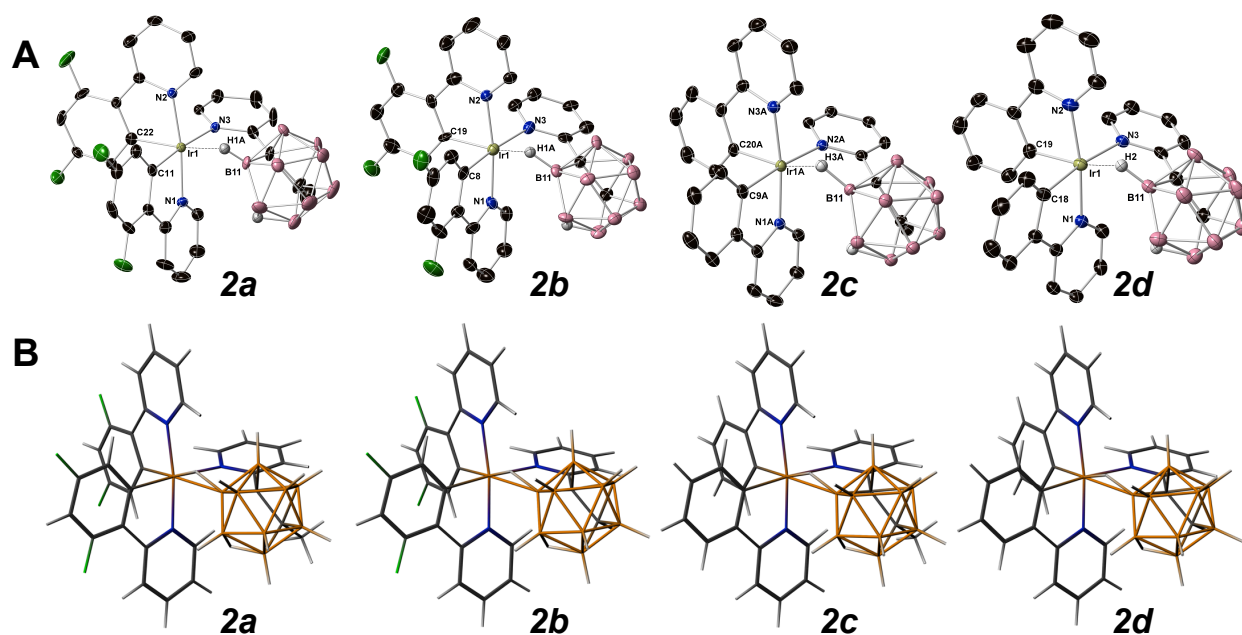
Figure A4 Comparison between (A) single crystal X-ray structures and (B) geometry-optimized structures of **2a**–**2d**.
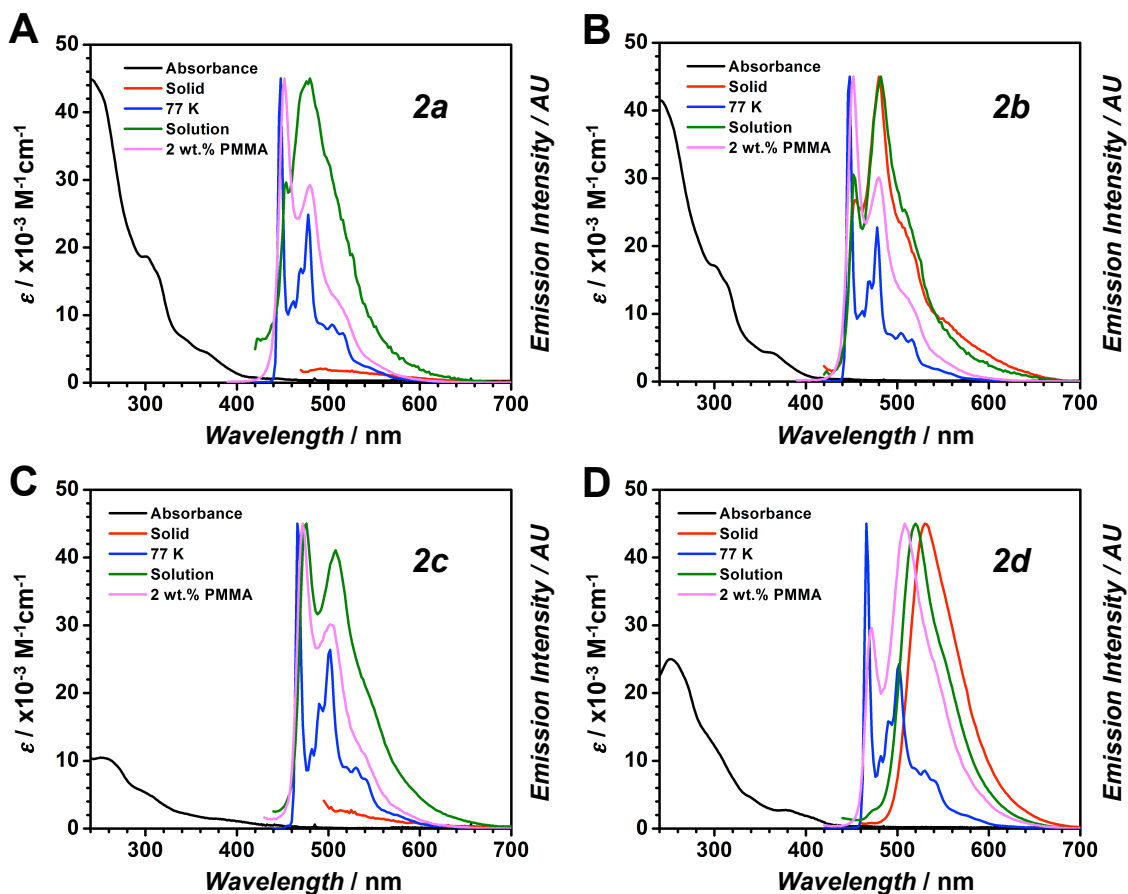
Figure A5 UV-Vis absorption (black line) and emission spectra for **2a-2d**. UV-Vis measurements were recorded in CH_2Cl_2 at 1×10^{-5} M. Solution-based emission spectra at 298 K (green line) and 77 K (blue line) were obtained from solutions of 2-MeTHF. Emission spectra for 2 wt.% PMMA films and neat solids are labeled with purple and red lines, respectively.

Table A2 Photophysical data for **2a–2d**.

| | Emission l$_{max}$ (nm) | | | | ϕ_{PL} | | τ (μs)^c | |
	Solid, 298 K^a	Solution, 77 K	Solution 298 K^b	2 wt.% PMMA	2-MeTHF, 298 K^b	2 wt. % PMMA^b	2-MeTHF, 77 K	2 wt.% PMMA^{b,d}
2a	–	448, 478	453, 480	452, 480	0.006	0.43	5.65	3.35
2b	454, 480	447, 478	452, 482	451, 480	0.008	0.41	6.38	3.62
2c	–	466, 502	475, 508	475, 503	0.008	0.37	5.11	3.02
2d^e	530	466, 503	520	472, 508	0.11^f	0.39	5.19	2.96

^{a}**2a** and **2c** are non-emissive as solids at 298 K. ^{b}Under N$_2$. ^{c}Observed wavelength at emission maximum. ^{d}Weighted average of a multi-exponential decay. ^{e}Solutions of **2d** filtered through 0.22 mm syringe filter prior to solution-based lifetime measurements and preparation of PMMA films.^{f}Relatively high ϕ likely a result of low solubility and aggregation.
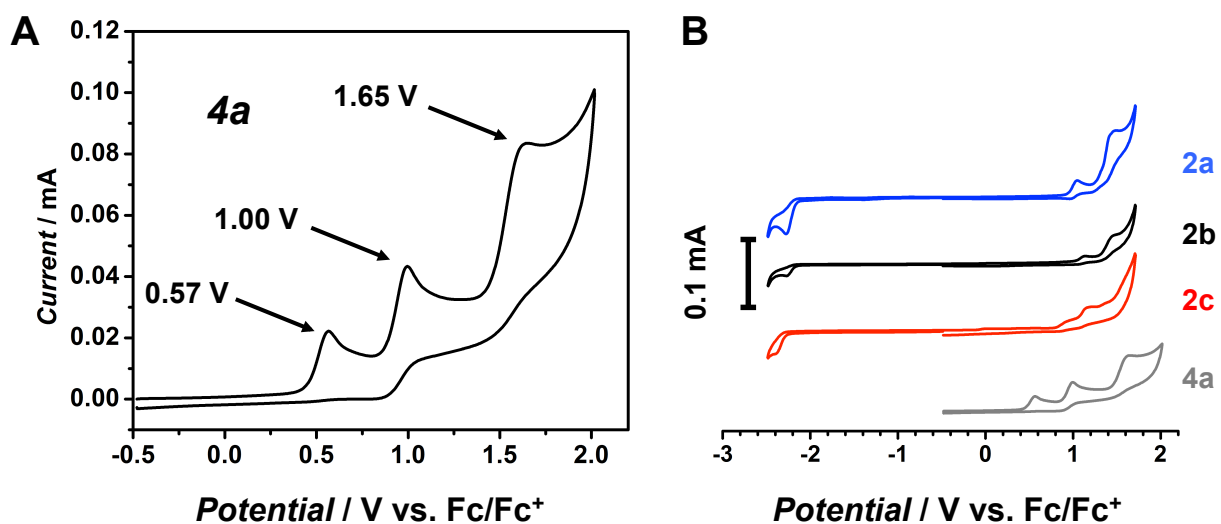
Figure A6 Cyclic voltammagram of (A) the oxidative wave of **4a** and (B) stacked cyclic voltammograms of **2a-2c** and **4a** with scale bar of 0.1 mA. Scan rate = 0.1 V/s, 0.1 M [^{n}Bu$_4$N][PF$_6$], 1 mM analyte concentration in MeCN, versus Fc$^+$/Fc.

	B–H (cm^{-1})	Ir–μ-H–B (cm^{-1})
2a	2535	2086
2b	2544	2090
2c	2532	2018
2d	2534	2081
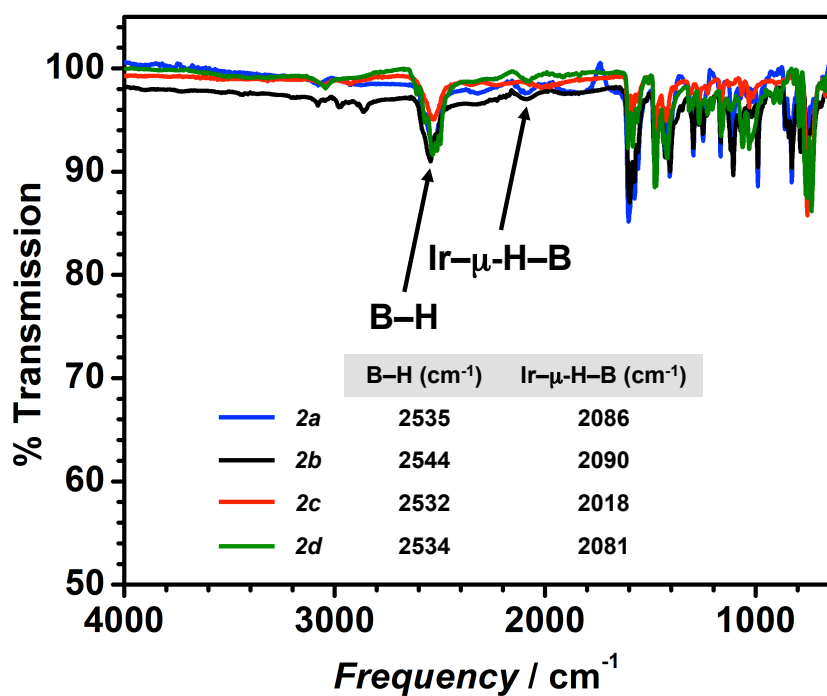
Figure A7 Solid-state infrared (IR) spectroscopy on **2a–2d** with corresponding B–H and Ir–μ-H–B stretches labeled.

2.5.2 Discussion of Aggregation of 2d vs. 2a-2c

The highest frequency transition for both **2a** and **2b** undergoes a small blue-shift (5 nm) when the 298 K solution emission spectra are compared to the corresponding 77 K spectra (Figure A4A-A4B), whereas **2d** displays a 54 nm blue-shift from 520 nm at 298 K to 466 nm at 77 K (Figure A4D). **2c** displays a blue-shift of 9 nm as the highest frequency peak shifts from 475 nm in 2-MeTHF at 298 K to 466 nm at 77 K (Figure A4C). The broad, featureless shape of the 298 K solution spectrum of **2d** is indicative of aggregation in solution. In contrast, methylated analogue **2c** retains vibronic features in the 298 K solution emission spectrum, reinforcing this hypothesis.

a) Würthner, F.; Kaiser, T. E.; Saha-Möller, C. R. *Angew. Chem., Int. Ed.* **2011**, *50,* 3376; b) Lamansky, S.; Djurovich, P.; Murphy, D.; Abdel-Razzaq, F.; Kwong, R.; Tsyba, I.; Bortz, M.; Mui, B.; Bau, R.; Thompson, M. E. *Inorg. Chem.* **2001**, *40*, 1704; c) Li, G.; Wu, Y.; Shan, G.; Che, W.; Zhu, D.; Song, B.; Yan, L.; Su, Z. Bryce, M. R. *Chem. Commun.* **2014**, *50*, 6977; d) Hong, Y.; Lam, J. W. Y.; Tang, B. Z. *Chem. Soc. Rev.* **2011**, *40*, 5361.

2.5.3 Additional Discussion of DFT Calculations

For all compounds, the highest occupied molecular orbital (HOMO) is both metal- and carborane-centered; for **2c** and **2d**, small contributions to the HOMO from one of the phenylpyridine ligands are also detected (Figure A8). The lowest unoccupied molecular orbital (LUMO) for all compounds are located on the phenylpyridine ligands with minor contributions from the Ir(III) center and no significant contribution from the carboranylpyridine ligand (Figure A8).

A subtle deviation from the consistent electronic structure across all compounds comes with the calculated triplet (T_0) spin density. While for **2a–2c**, in which the triplet is delocalized across the entire molecule, **2d** revels a triplet spin density located primarily on one of the phenylpyridine rings and Ir(III) center. Lee and co-workers noted (ref below) that a significant

contribution to non-radiative rate decay in their tethered carborane-containing Ir(III) systems derives from the elasticity of the C-C bond of the *o*-carborane moieties, on which a significant portion of the triplet state LUMO resides. In contrast, we observe no contribution of the *nido*-carboranyl fragment to the LUMO manifold.

Lee, Y. H.; Park, J.; Lee, J.; Lee, S. U.; Lee, M. H. *J. Am. Chem. Soc.* **2015**, *137*, 8018.

Table A3 DFT results.

Compound	HOMO-1 (eV)	HOMO (eV)	LUMO (eV)	LUMO+1 (eV)	Triplet (eV)	Calculated DE^{a} (eV)	Calculated DE^{a} (nm)	Experimental DE^{b} (nm)
2a	-6.58	-6.10	-2.66	-2.44	-3.30	2.80	443	448
2b	-6.59	-6.20	-2.65	-2.41	-3.35	2.85	447	447
2c	-6.08	-5.82	-2.33	-2.12	-3.21	2.61	477	466
2d	-6.10	-5.91	-2.37	-2.13	-3.42	2.49	498	466

$^{a}\Delta E = E_{Triplet} - E_{HOMO}$. ^{b}Determined from the highest frequency peak in the corresponding 77 K emission spectrum.
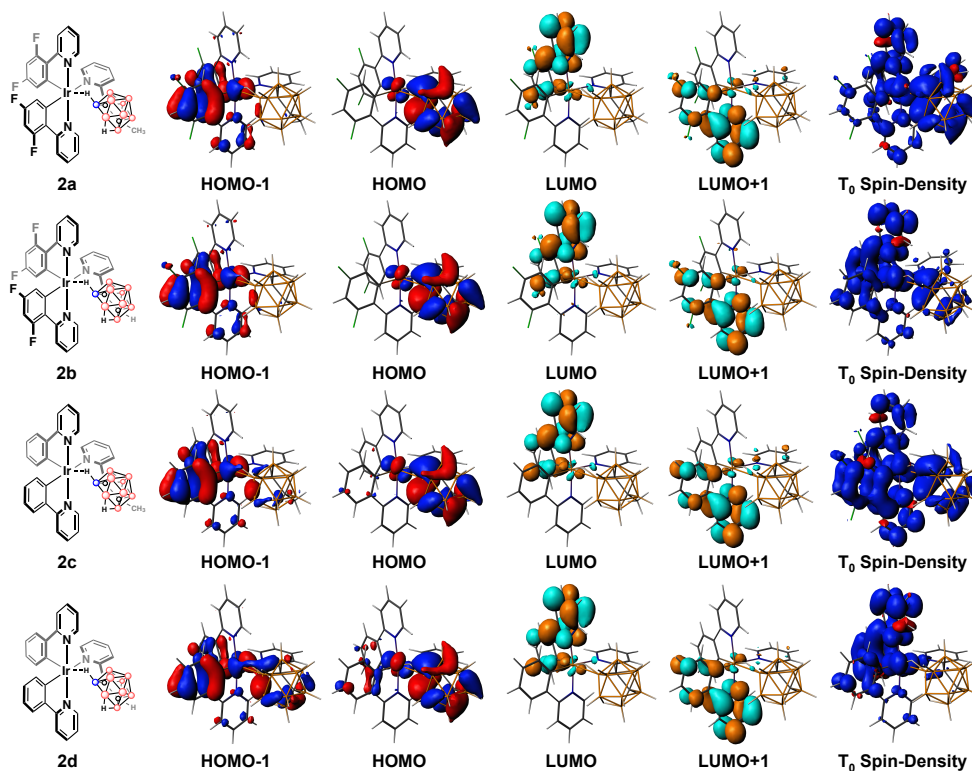
Figure A8 HOMO-1, HOMO, LUMO, LUMO+1, and T_0 spin-density diagrams for **2a**–**2d**.
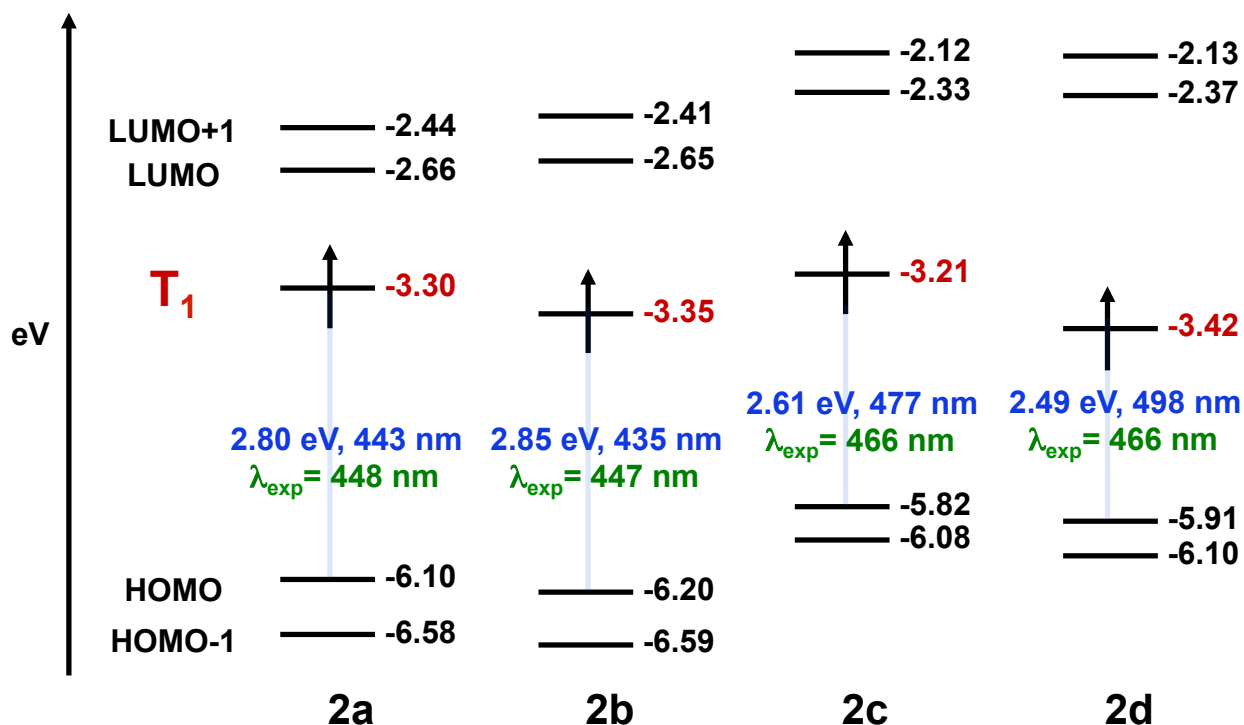
Figure A9 Diagram of energy levels for **2a**–**2d** determined by DFT calculations.

2.5.4 Additional Discussion of AIM Data/Bonding of *nido*-carboranyl Ligand to Ir(III)

In solution, a subtle reduction in the ^{11}B–^{1}H coupling value is observed (seen most clearly in the ^{11}B NMR spectrum of **2a**) for one peak in the ^{11}B NMR spectrum, which we tentatively assign to B–μ-H ($^1J_{BH}$ ~75Hz) relative to the other ^{11}B–^{1}H coupling constants in this spectrum (~130Hz – 140Hz). These observations are reminiscent of C–H agostic interactions that have been documented in high oxidation state Ta, Mo, and W alkylidenes (*e.g.*) (references a–g below), in which geometric/structural distortions are clearly observed through both X-ray crystallographic analysis as well as ^{1}H and ^{13}C NMR spectroscopy. Covalency is generally presumed in these instances (reference *g* below), whereas in the present case, based on computational data, covalent, η^2-type interactions between Ir(III) and μ-H do not seem to be present for **2a**–**2d**. Clear geometric distortions, which are straightforwardly observed in high oxidation state, early transition metal systems mentioned above, are not clear in the solid-state

structures for **2a**–**2d**. Furthermore, the Ir–μ-H–B angle in this case is far more obtuse (~110° – 120°) compared to the M–μ-H–CR angles (ca. 50° for *syn* rotamers, M = Mo/W) observed in the aforementioned alkylidenes in which the carbon atoms are directly bound to the metal; such obtuse angles observed in the case for **2a**–**2d** are likely a result of the steric bulk of the *nido*-carboranyl cage in the rigid environment of two phenylpyridine ligands bound to Ir(III). Such steric restrictions likely prevent electron density from the B–H bond effectively interacting with Ir(III), at least to an extent in which B(11) interacts with the Ir(III) center in any way. This weaker interaction is also reflected in the fluxionality of **2a** at different temperatures (see NMR below). It should be noted that while the Ir–μ-H distances in **2a**–**2d** range from 1.935(9) Å in **2a** (longest) to 1.665(6) Å in **2b** (shortest), the hydride is located far beyond the distance expected for a formal bond to the Ir(III) center (~1.5 – 1.6 Å) (references *h–j* below). Lavallo also observed similar interactions with a carboranylphosphine and a cationic iridium metal center suggested to be in a 3+ oxidation state (reference *k* below). While Ir–H and B–μ-H distances are comparable to those observed in **2a**–**2d**, the Ir–B bond distances implicated in agostic-type interactions reported by Lavallo are shorter (2.467(3) Å and 2.491(3) Å) than those observed here (2.504(1) Å – 2.528(6) Å). The phosphorus donor enforces a closer interaction of the carboranyl moiety with the metal, forming a 5-membered chelate whereas in the present case a six-membered chelate is formed in which Ir–B distances are longer. The fluxional behavior of the ligand observed in the variable temperature ^{11}B NMR spectra (see NMR data below) suggests that if Ir–μ-H–B agostic interactions are present between the ligand and the metal, they are likely very weak.

a) Schultz, A. J.; Williams, J. M.; Schrock, R. R.; Rupprecht, G. A.; Fellmann, J. D. *J. Am. Chem. Soc.* **1797**, *101*, 1593; b) Poater, A.; Solans-Monfort, X.; Clot, E.; Copéret, C.; Eisenstein, O. *Dalton Trans.* **2006**, 3077; c) Pedersen, S. F.; Schrock, R. R. *J. Am. Chem. Soc.* **1982**, *104*, 7483; d) Freundlich, J. S.; Schrock, R. R.; Cummins, C. C.; Davis, W. M. *J. Am. Chem. Soc.* **1994**, *116*, 6476; e) Cole, J. M.; Howard, J. A. K.; McIntyre, G. J.; Gibson, V. C.; Walker, G. L. P. *Chem. Commun.* **1998**, 1829; f) Goddard, R. J.; Hoffman, R.; Jemmis, E. D. *J. Am. Chem. Soc.* **1980**, *102*, 7667; g) Brookhart, M.; Green, M. L. H. *J. Organomet. Chem.* **1983**, *250*, 395; h) Salomon, M. A.; Braun, T.; Krossing, I. *Dalton Trans.* **2008**, 5197; i) Chiu, Y.-C.; Lin, C.-H.; Hung, J.-Y.; Chi, Y.; Cheng, Y.-M.; Wang, K.-W.; Chung, M.-W.; Lee, G.-H.; Chou, P.-T. *Inorg. Chem.* **2009**, *48*, 8164; j) Kaesz, H. D.; Saillant, R. B. *Chem. Rev.* **1972**, *3*, 231; k) El-Hellani, A.; Kefalidis, C. E.; Tham, F. S.; Maron, L.; Lavallo, V. *Organometallics* **2013**, *32*, 6887.

Table A4 QTAIM results.

Compound	Values at Ir–μ-H Bond Critical Point (BCP)	
	$r_b{}^a$	$\nabla^2 r_b{}^b$
2a	0.0885	0.2202
2b	0.0875	0.2210
2c	0.0863	0.2185
2d	0.0854	0.2198

[a]Value of electron density at the BCP; $r_b < 0.1$ indicates an electrostatic interaction. [b]Laplacian of electron density at the BCP; positive values for $\nabla^2 r_b$ indicate depletion of electron density at BCP.

2.5.6 Variable Temperature ^{11}B NMR study of 2a
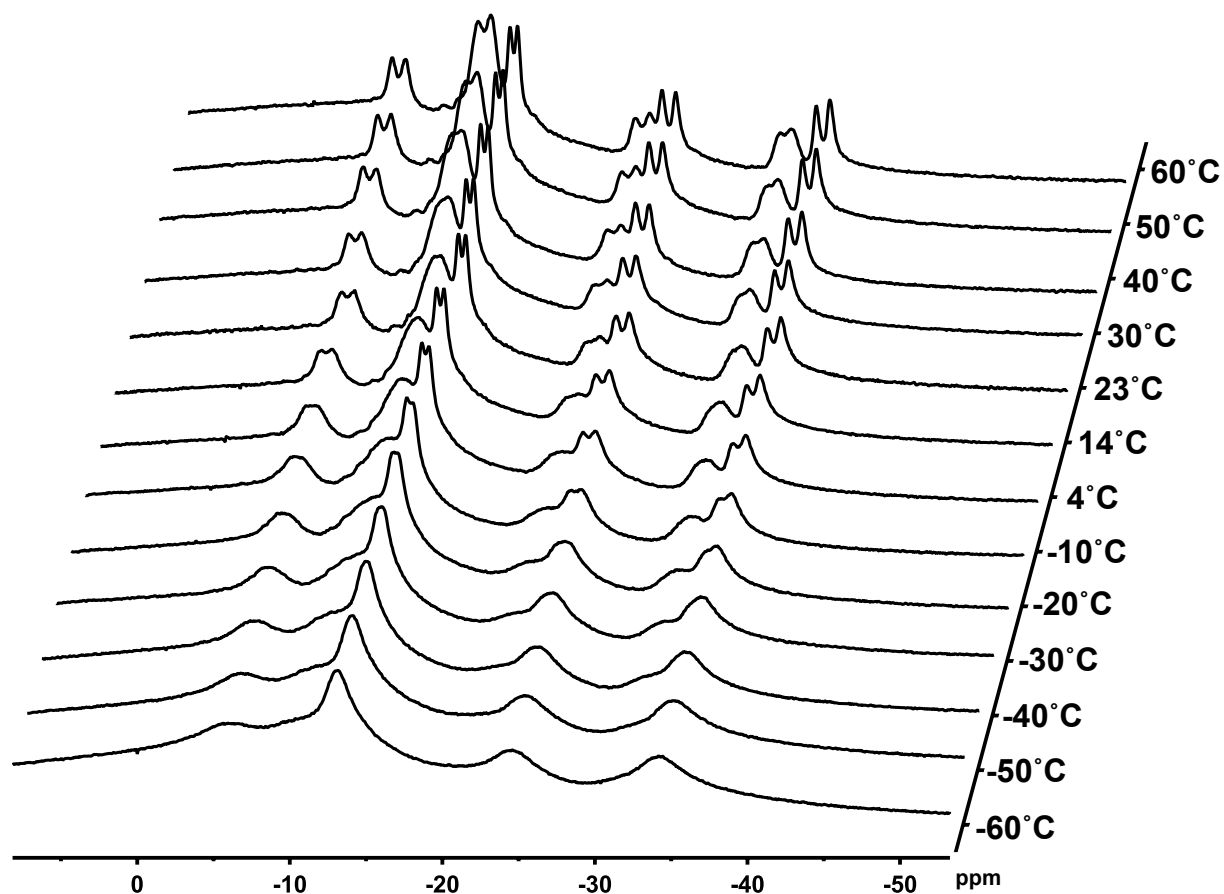
Figure A10 Variable temperature (VT) ^{11}B NMR study of **2a** in CDCl$_3$.

2.5.7 Photophysical Data for Selected Ir(III) Emitters in Literature

Table A5 Photophysical data for selected carborane-containing Ir(III) emitters.

Compound	Em. λ_{max}[a] (nm)	ϕ_{PL}[a] (solution)	τ[a] (ms)	Solvent	ϕ_{PL}[b] (PMMA)	Reference
1	520	0.46	0.47	CH$_2$Cl$_2$	–	a
2	503	0.83	1.22	Toluene	0.20	b
3	488	0.98	0.87	Toluene	0.35	c
4	507	0.41	0.38	Toluene	–	d
5	526	0.96	1.32	Toluene	0.36	e

[a]Measured in deaerated solutions at 298 K. [b]PMMA films doped with 4-8 wt.% Ir(III) complexes.
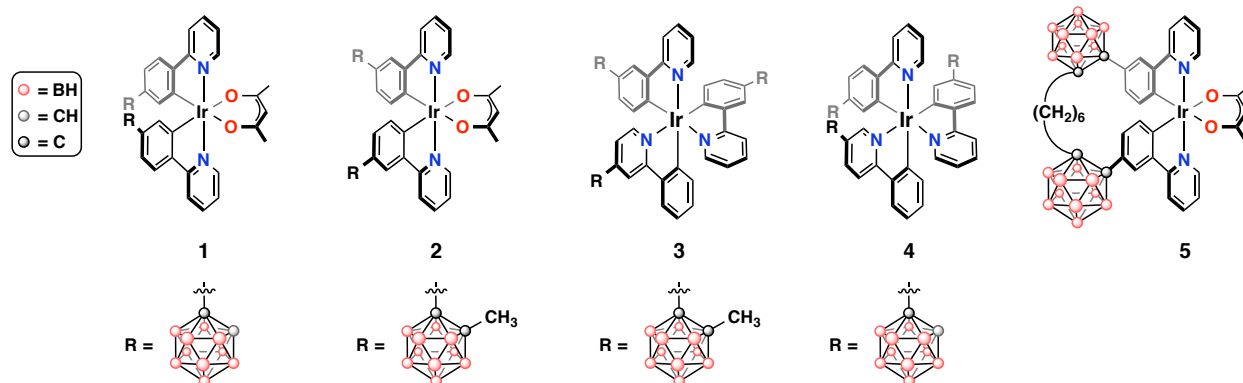
Figure A11 Structures of carborane-containing Ir(III) emitters in Table A5.

Table A6 Photophysical data for selected efficient blue Ir(III) emitters.

Compound	Em. λ_{max}[a] (nm)	ϕ_{PL}[a] (solution)	τ[a] (ms)	Solvent	Reference
6	418	0.76	1.2	2-MeTHF	f
7	468	0.80	1.7	CH$_2$Cl$_2$	g
8	466	0.98	1.7	2-MeTHF	h
9	475	0.93	2.6	2-MeTHF	h
10	445	0.90	2.3	THF	i

[a]Measured in deaerated solutions at 298 K.
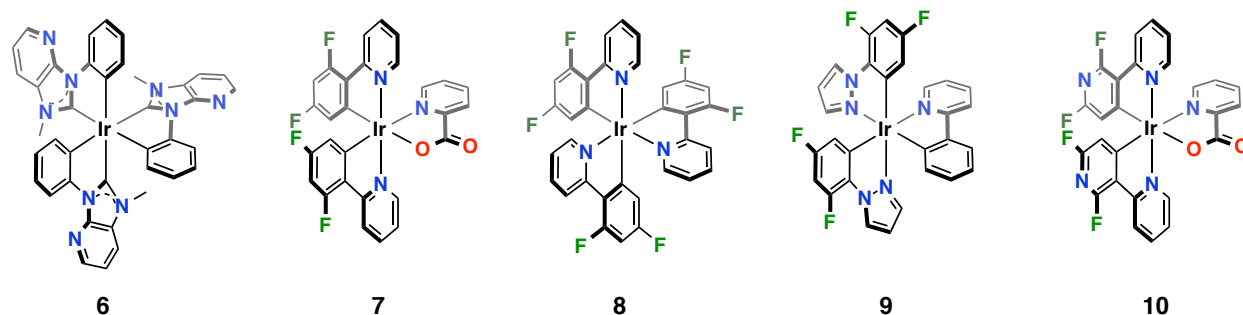
Figure A12 Structures of selected efficient blue Ir(III) emitters in Table S6.

References:
a) Shi, C.; Sun, H.; Jiang, Q.; Zhao, Q.; Wang, J.; Huang, W.; Yan, H. *Chem. Commun.* **2013**, *49*, 4746; b) Zhu, L.; Tang, X.; Yu, Q.; Lv, W.; Yan, H.; Zhao, Q.; Huang, W. *Chem. Eur. J.* **2015**, *21*, 4721; c) Kim, Y.; Park, S.; Lee, Y. H.; Jung, J.; Yoo, S.; Lee, M. H. *Inorg. Chem.* **2016**, *55*, 909; d) Shi, C.; Sun, H.; Tang, X.; Lv, W.; Yan, H.; Zhao, Q.; Wang, J.; Huang, W. *Angew. Chem., Int. Ed.* **2013**, *52*, 13434; e) Lee, Y. H.; Park, J.; Lee, J.; Lee, S. U.; Lee, M. H. *J. Am. Chem. Soc.* **2015**, *137*, 8018; f) Lee, J.; Chen, H.-F.; Batagoda, T.; Coburn, C.; Djurovich, P. I.; Thompson, M. E.; Forrest, S. R. *Nat. Mater.* **2016**, *15*, 92; g) Baranoff, E.; Curchod, B. F. E. *Dalton Trans.* **2015**, *44*, 8318; h) Sajoto, T.; Djurovich, P. I.; Tamayo, A. B.; Oxgaard, J.; Goddard III, W. A.; Thompson, M. E. *J. Am. Chem. Soc.* **2009**, *131*, 9813; i) Kang, Y.; Chang,

Y.-L.; Lu, J.-S.; Ko, S.-B.; Rao, Y.; Varlan, M.; Lu, Z.-H.; Wang, S. *J. Mater. Chem.* C **2013**, *1*, 441.

2.5.8 Luminescent Ir(III) Complexes with [CB$_{11}$H$_{11}$]$^-$-based ligands

In order to expand this class of zwitterionic Ir(III) complexes featuring weakly-coordinating carborane-based ligands, we turned our attention to formally anionic carba-*closo*-dodecaborane ligands ([CB$_{11}$H$_{12}$]$^-$). Relative to *nido*-carboranyl species, these anionic *closo*-carboranyl clusters are generally more stable. We were interested in studying luminescent Ir(III) compounds containing the formally anionic *closo*-carboranyl ligands in order compare the materials and photophysical properties of these zwitterionic Ir(III) complexes to those of the *nido*-carboranyl-based zwitterionic Ir(III) species.
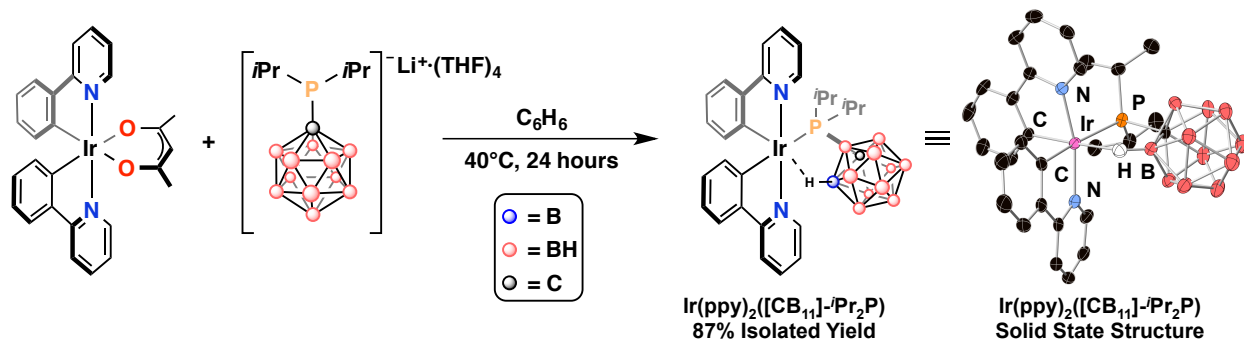
Figure A13 Synthetic scheme for Ir(ppy)$_2$([CB$_{11}$]-^{i}Pr$_2$P) (left), and X-ray crystal structure (right). Protons (except for Ir–μ-H–B) have been omitted for clarity. Long Ir–B distances (2.81(2) Å) and Ir–μ-H distances (1.99(7) Å) for this molecule suggest negligible covalent bonding interactions between Ir and either μ-H or B.

A mixture of Ir(ppy)$_2$(acac) and [(CB$_{11}$H$_{11}$)-^{i}Pr$_2$P][Li(THF)$_4$] was stirred in benzene at 40°C for 24 hours under N$_2$ (Figure A13), resulting in a yellow solution that emits green under ultraviolet (UV) excitation (λ_{exc} = 365 nm). The solvent was removed *in vacuo* to yield a yellow solid, which was then redissolved in CH$_2$Cl$_2$ and passed through a pad of Celite. Upon solvent removal, the crude product was further purified *via* silica column chromatography and isolated in 87% yield. X-ray diffraction analysis of single crystals of the product, grown from the slow

evaporation of a concentrated solution of diethyl ether at room temperature, confirmed the structure (Figure A13). The Ir–μ-H distance for Ir(ppy)$_2$([CB$_{11}$]-^{i}Pr$_2$P) (1.99(7) Å) is comparable to the analogous distances determined for **2a**–**2d** (1.935(9)–1.665(6) Å; Table A1).
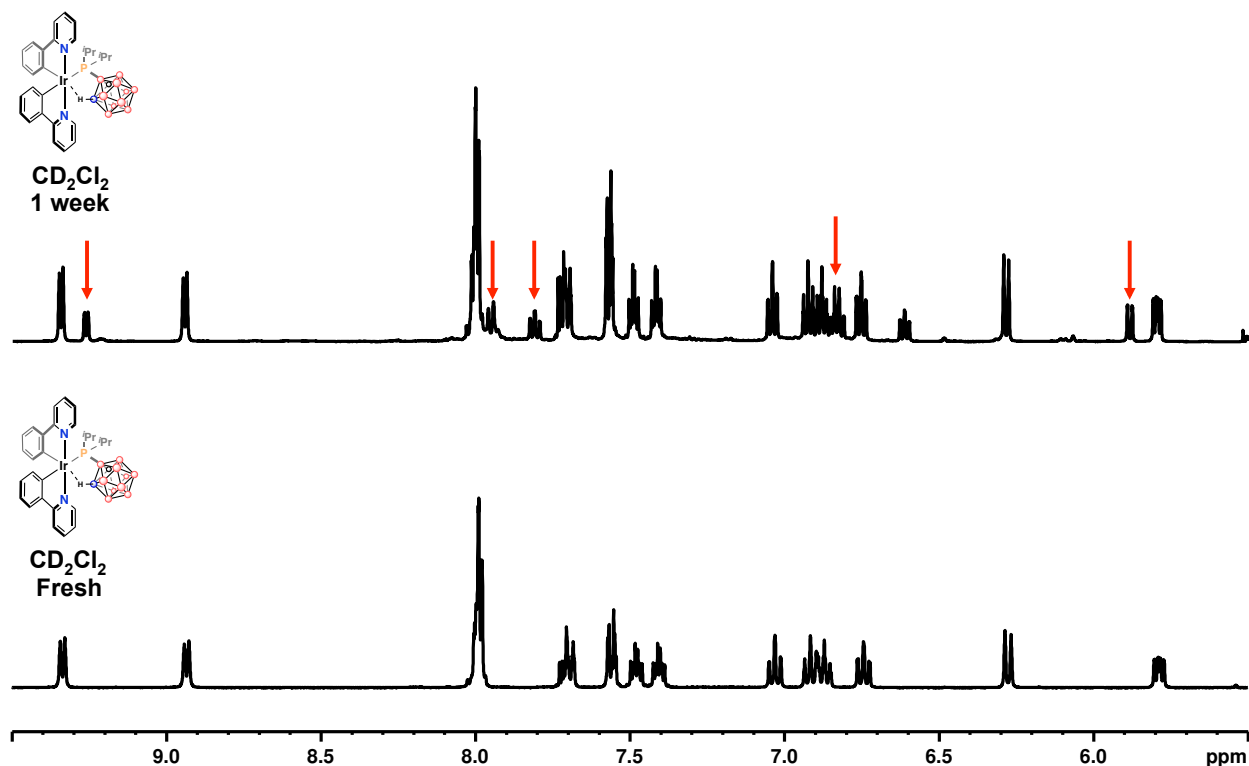
Figure A14 Stacked ^{1}H NMR plots for Ir(ppy)$_2$[(CB$_{11}$H$_{11}$)-^{i}Pr$_2$P] dissolved in CD$_2$Cl$_2$, freshly prepared (bottom), and the same sample after exposure to ambient conditions (stored on the benchtop) for 1 week (top). Red arrows highlight new peaks that have formed.

Ir(ppy)$_2$[(CB$_{11}$H$_{11}$)-^{i}Pr$_2$P] did not exhibit long-term stability in CD$_2$Cl$_2$ solution (Figure A14). Upon exposure to ambient conditions for 1 week, new chemical shifts were observed in the ^{1}H NMR spectrum for this compound, corresponding to the formation of a new species in solution (Figure A14, top). Due to the weakly coordinating nature of the [CB$_{11}$H$_{11}$]$^-$ moiety, we hypothesized the ligand was slowly displaced by solvent and shifted to the outer sphere of the metal complex. To probe this hypothesis, we dissolved a sample of Ir(ppy)$_2$([CB$_{11}$]-^{i}Pr$_2$P) in CD$_3$CN, which should more readily displace a weakly coordinating ligand due to the more Lewis Basic nature of CD$_3$CN relative to the [CB$_{11}$H$_{11}$]$^-$ species. Upon dissolution of

Ir(ppy)$_2$[(CB$_{11}$H$_{11}$)-^{i}Pr$_2$P] in CD$_3$CN, the major species observed by ^{31}P NMR spectroscopy is a

singlet at δ = 43.47, corresponding to free [(CB$_{11}$H$_{11}$)-^{i}Pr$_2$P)]$^-$, with Ir(ppy)$_2$[(CB$_{11}$H$_{11}$)-^{i}Pr$_2$P] no

longer observed (Figure A15). These data suggest the formation of

[Ir(ppy)$_2$(CD$_3$CN)$_2$][(CB$_{11}$Cl$_{11}$)-^{i}Pr$_2$P)], in which two CD$_3$CN displace the caboranyl-phosphine

ligand.
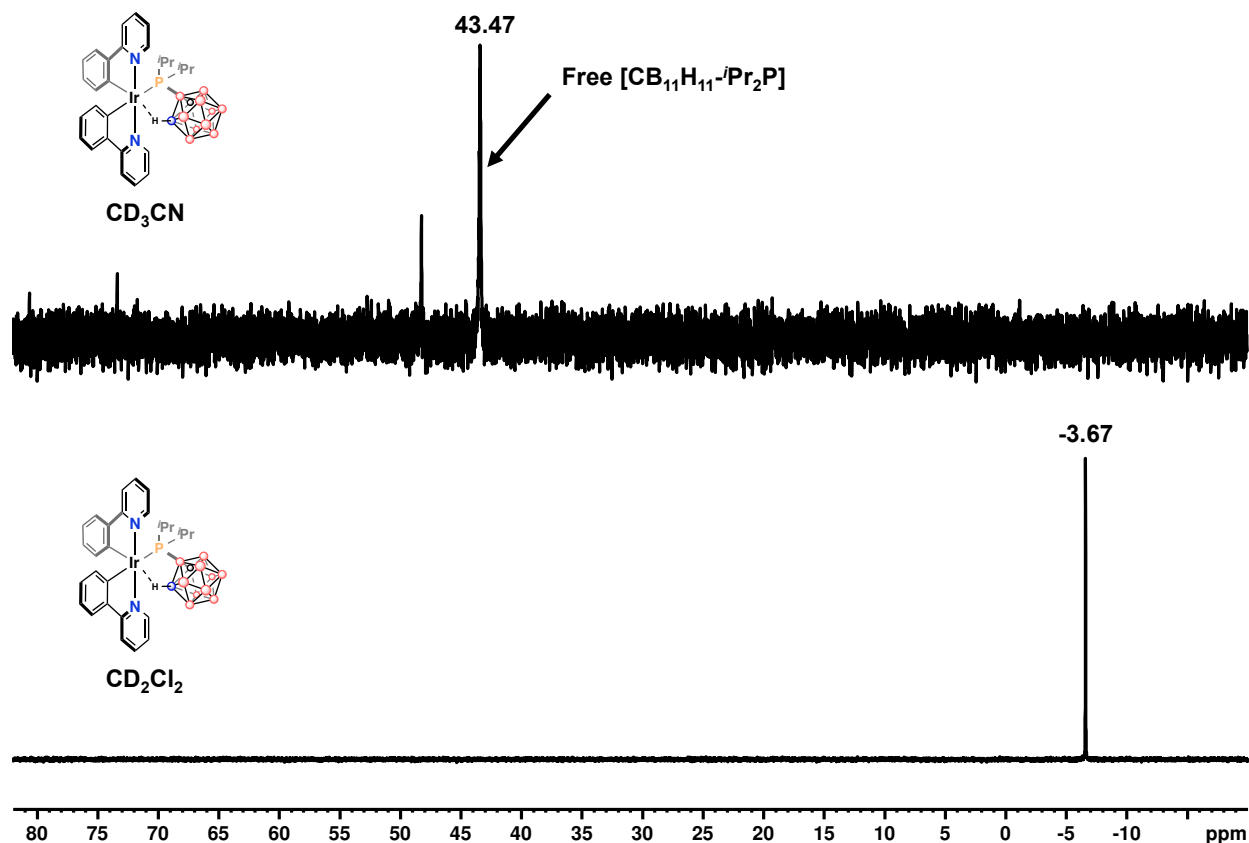
Figure A15 ^{31}P NMR data for Ir(ppy)$_2$[(CB$_{11}$H$_{11}$)-^{i}Pr$_2$P] dissolved in CD$_3$CN (top) and CD$_2$Cl$_2$ (bottom). Upon dissolution of Ir(ppy)$_2$[(CB$_{11}$H$_{11}$)-^{i}Pr$_2$P] in CD$_3$CN, the major species observed *via* ^{31}P NMR spectroscopy is the free ligand, [(CB$_{11}$H$_{11}$)-^{i}Pr$_2$P].

The ^{1}H NMR spectrum of Ir(ppy)$_2$[(CB$_{11}$H$_{11}$)-^{i}Pr$_2$P] dissolved in CD$_3$CN shows the

presence of one major species in solution, and it is consistent with the ^{1}H NMR data for

[Ir(ppy)$_2$(CH$_3$CN)$_2$][BF$_4$] dissolved in CD$_2$Cl$_2$ (Figure A16). Based on these observations, the

[(CB$_{11}$H$_{11}$)-^{i}Pr$_2$P)]$^-$ ligand may be too weakly coordinating to generate robust, luminescent Ir(III)

complexes; however, studies on chlorinated ([(CB$_{11}$Cl$_{11}$)-^{i}Pr$_2$P)]$^-$) or pyridyl ([(CB$_{11}$H$_{11}$)-pyr]$^-$;

pyr = 2-pyridyl) analogues in the context of luminescent Ir(III) complexes may still be warranted.
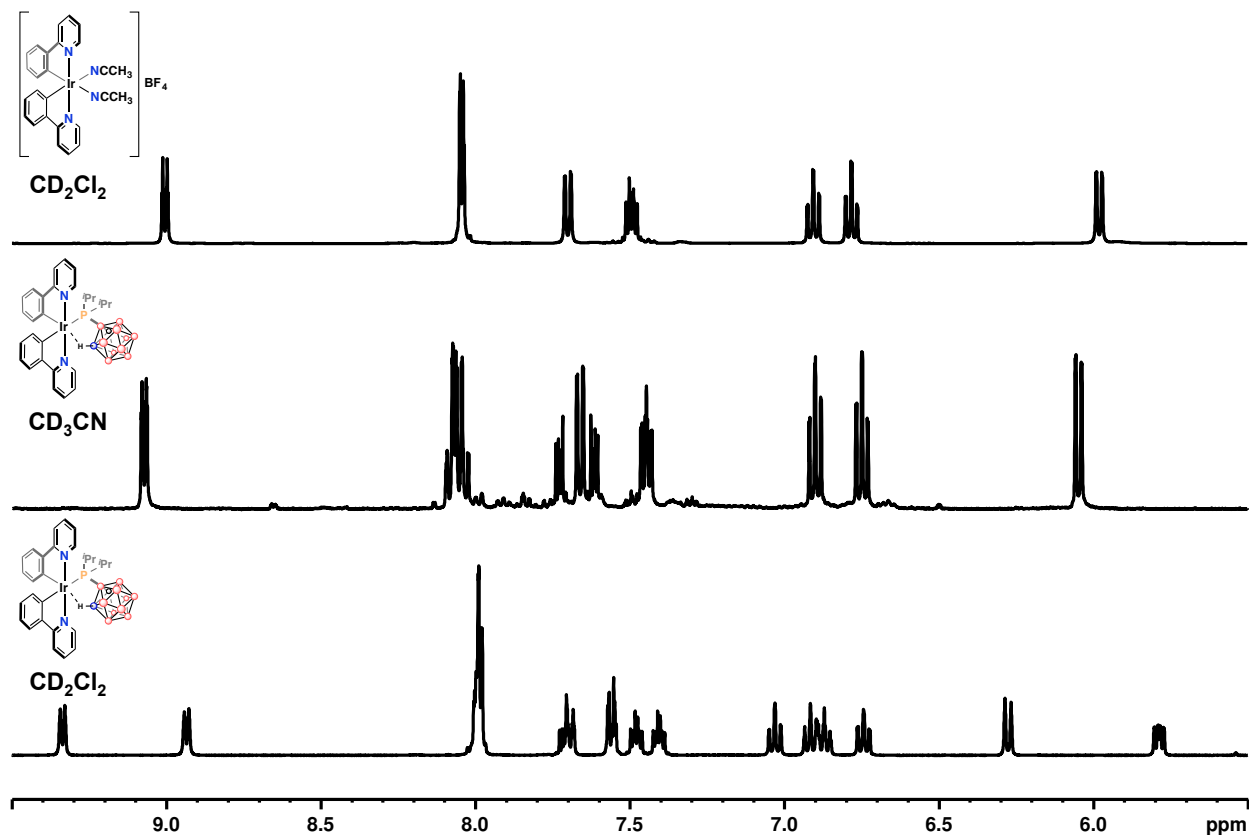
Figure A16 Stacked ^{1}H NMR plots for [Ir(ppy)$_2$(CH$_3$CN)$_2$][BF$_4$] dissolved in CD$_2$Cl$_2$ (top), Ir(ppy)$_2$[(CB$_{11}$H$_{11}$)-^{i}Pr$_2$P] dissolved in CD$_3$CN (middle), and Ir(ppy)$_2$[(CB$_{11}$H$_{11}$)-^{i}Pr$_2$P] dissolved in CD$_2$Cl$_2$ (bottom).

2.5.8.1 Synthesis and Characterization of Ir(ppy)$_2$[(CB$_{11}$H$_{11}$)-^{i}Pr$_2$P]

A mixture of Ir(ppy)$_2$(acac) (0.020 g, 0.033 mmol) and [(CB$_{11}$H$_{11}$)-^{i}Pr$_2$P][Li(THF)$_4$] (0.020 g, 0.037 mmol) were combined in a 20 mL scintillation vial. The mixture was dissolved in benzene (2 mL) and stirred in a dinitrogen-filled glovebox at 40°C for 24 hours. The resulting yellow solution exhibited green emission under ultraviolet (UV) excitation (λ_{exc} = 365 nm). The solvent was removed *in vacuo* to yield a yellow solid, which was then dissolved in minimal CH$_2$Cl$_2$ and passed through a pad of Celite. Upon solvent removal, the crude product was further

purified *via* silica column chromatography (R_f = 0.50, eluent = 2:1 CH$_2$Cl$_2$:hexanes). The product was concentrated to dryness, dried under vacuum for 4 hours, and isolated in 87% yield.

¹H NMR (CD$_2$Cl$_2$, 400 MHz), ppm: δ 9.34 (d, 1H, Ar), 8.93 (d, 1H, Ar), 8.02–7.96 (m, 4H, Ar), 7.671–7.68 (m, 1H, Ar), 7.57–7.52 (m, 1H, Ar), 7.50–7.46 (m, 1H, Ar), 7.43–7.38 (m, 1H, Ar), 7.03 (td, 1H, Ar), 6.94–6.84 (m, 2H, Ar), 6.74 (td, 1H, Ar), 6.28 (d, 1H, Ar), 5.82–5.76 (m, 1H, Ar), 2.94–2.83 (m, 1H, CH–^{i}Pr), 1.69–1.62 (m, 1H, CH–^{i}Pr), 1.56–1.45 (m, 3H, CH$_3$–^{i}Pr), 1.31–1.24 (m, 6H, CH$_3$–^{i}Pr), 0.42–0.31 (m, 3H, CH$_3$–^{i}Pr), 2.81–0.5 (br, 10H, CH–carborane), -2.9 – -4.0 (br q, 1H, Ir–μ-H). **¹¹B NMR** (CD$_2$Cl$_2$, 160 MHz), ppm: δ -1.66 (d, 2H), -8.1 – -17.7 (br m, 7H), -22.2 (d, 2H); **³¹P NMR** (CD$_2$Cl$_2$, 200 MHz), ppm: δ -3.7. Single crystals for X-ray diffraction were grown from the slow evaporation of a concentrated solution of diethyl ether at room temperature.
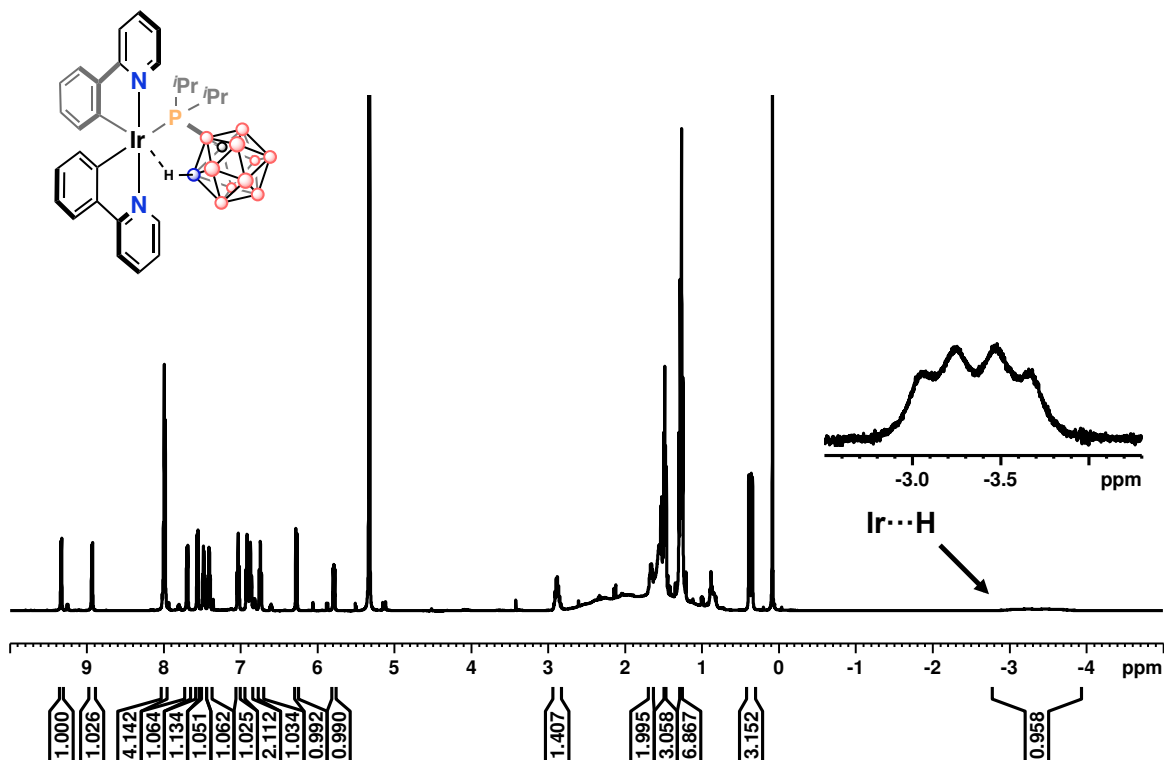
Figure A17 ¹H NMR data for Ir(ppy)$_2$[(CB$_{11}$H$_{11}$)-^{i}Pr$_2$P] (CD$_2$Cl$_2$, 400 MHz).
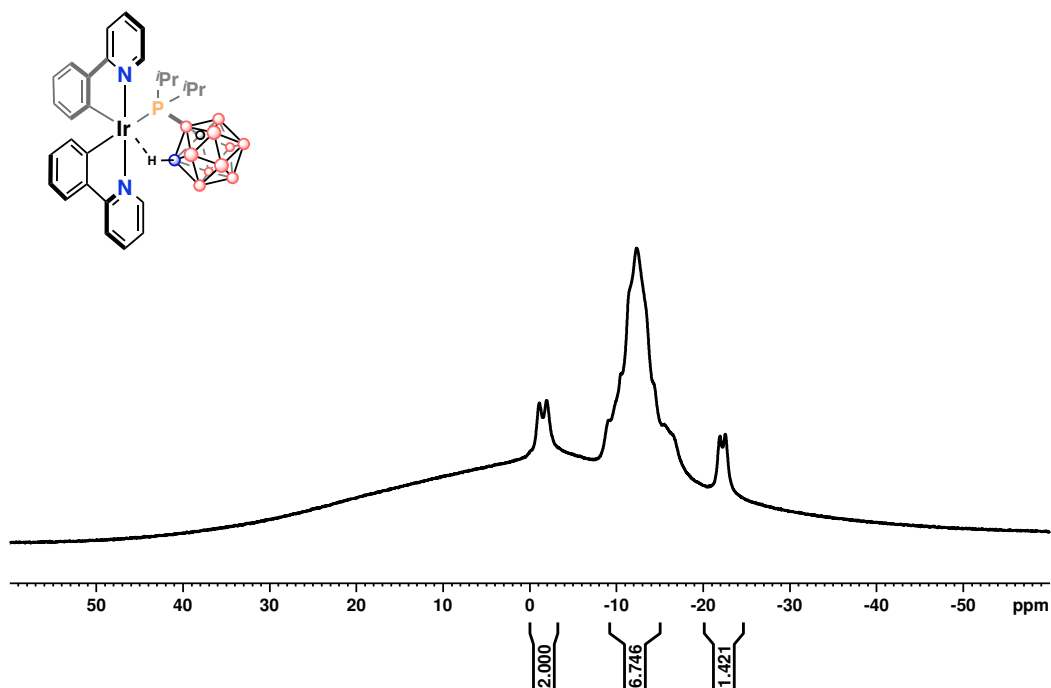
Figure A18 ^{11}B NMR data for Ir(ppy)$_2$[(CB$_{11}$H$_{11}$)-^{i}Pr$_2$P] (CD$_2$Cl$_2$, 160 MHz).
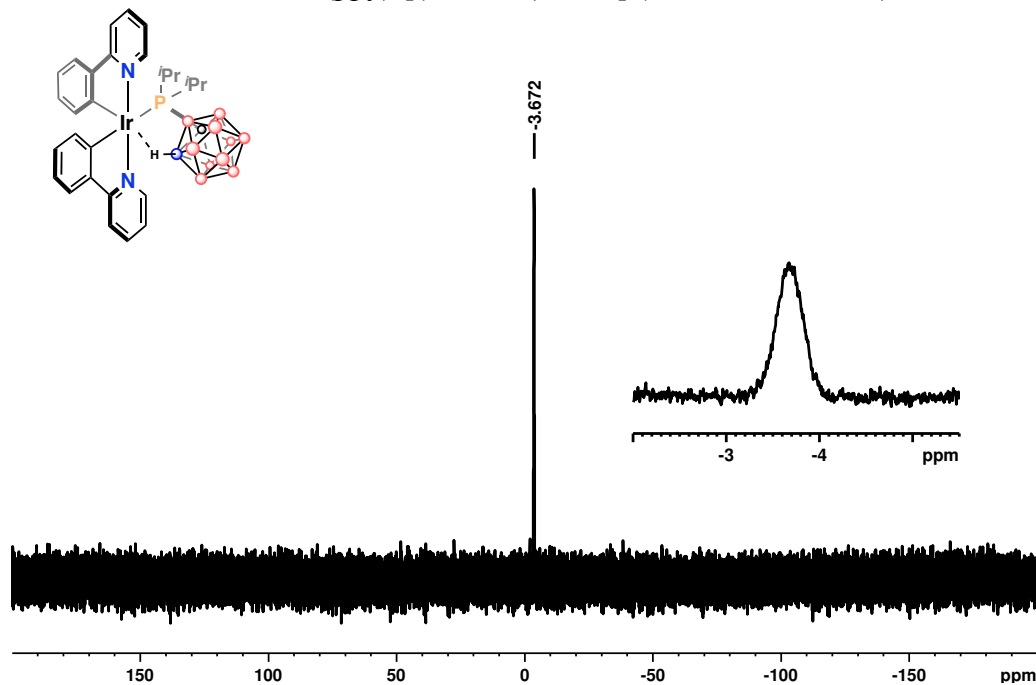
Figure A19 ^{31}P NMR data for Ir(ppy)$_2$[(CB$_{11}$H$_{11}$)-^{i}Pr$_2$P] (CD$_2$Cl$_2$, 200 MHz).

2.6 References

1. For selected examples of blue OLEDs incorporating fluorescent emitters, see: a) Uoyama, H.; Goushi, K.; Shizu, K.; Nomura, H.; Adachi, C. *Nature* **2012**, *492*, 234; b) Méhes, G.;

Nomura, H.; Zhang, Q.; Nakagawa, T.; Adachi, C. *Angew. Chem. Int. Ed.* **2012**, *51*, 11311; c) Lee, S. Y.; Yasuda, T.; Yang, Y. S.; Zhang, Q.; Adachi, C. *Angew. Chem. Int. Ed.* **2014**, *53*, 6402; d) Kawasumi, K.; Wu, T.; Zhu, T.; Chae, H. S.; Van Voorhis, T.; Baldo, M. A.; Swager, T. M. *J. Am. Chem. Soc.* **2015**, *137*, 11908; e) Zhang, Q.; Li, B.; Huang, S.; Nomura, H.; Tanaka, H.; Adachi, C. *Nature Photonics* **2014**, *8*, 326; f) Feuillastre, S.; Pauton, M.; Gao, L.; Desmarchelier, A.; Riives, A. J.; Prim, D.; Tondelier, D.; Geffroy, B.; Muller, G.; Clavier, G; Pieters, G. *J. Am. Chem. Soc.* **2016**, *138*, 3990; g) Li, K.; Guan, X.; Ma, C.-W.; Chen, Y.; Che, C.-M. *Chem. Commun.* **2011**, *47*, 9075.

2. For selected examples of phosphorescent emitters for OLED applications, see: a) H. Yersin, Ed. *Highly Efficient OLEDs with Phosphorescent Materials*; Wiley-VCH: Weinheim, **2008**.; b) P.-T. Chou, Y. Chi *Chem. Eur. J.* **2007**, *13*, 380; c) Y. Chi, P.-T. Chou *Chem. Soc. Rev.* **2010**, *39*, 638; d) Lamansky, S.; Djurovich, P.; Murphy, D.; Abdel-Razzaq, F.; Lee, H.-E.; Adachi, C.; Burrows, P. E.; Forrest, S. R.; Thompson, M. E. *J. Am. Chem. Soc.* **2001**, *123*, 4304; e) Lamansky, S.; Djurovich, P.; Murphy, D.; Abdel-Razzaq, F.; Kwong, R.; Tsyba, I.; Bortz, M.; Mui, B.; Bau, R.; M. E. Thompson. *Inorg. Chem.* **2001**, *40*, 1704; f) Tamayo, A. B.; Alleyne, B. D.; Djurovich, P. I.; Lamansky, S.; Tsyba, I.; Ho, N. N.; Bau, R.; Thompson, M. E. *J. Am. Chem. Soc.* **2003**, *125*, 7377; g) Sajoto, T.; Djurovich, P. I.; Tamayo, A.; Yousufuddin, M.; Bau, R.; Thompson, M. E. *Inorg. Chem.* **2005**, *44*, 7992; h) Chang, C.-F.; Cheng, Y.-M.; Chi, Y.; Chiu, Y.-C.; Lin, C.-C.; Lee, G.-H.; Chou, P.-T.; Chen, C.-C.; Chang, C.-H.; Wu, C.-C. *Angew. Chem. Int. Ed.* **2008**, *47*, 4542; i) Tsuboyama, A.; Iwawaki, H.; Furugori, M.; Mukaide, T.; Kamatani, J.; Igawa, S.; Moriyama, T.; Miura, S.; Takiguchi, T.; Okada, S.; Hoshino, M.; Ueno, K. *J. Am. Chem. Soc.* **2003**, *125*, 12971; j) Maity, A.; Le, L. Q.; Zhu, Z.; Bao, J.; Teets, T. S. *Inorg. Chem.* **2016**, *55*, 2299; k) Fleetham, T.; Wang, Z.; Li, J. *Org. Electron.* **2012**, *13*, 1430; l) Turner, E.; Bakken, N.; Li, J. *Inorg. Chem.* **2013**, *52*, 7344; m) Saris, P. J. G.; Thompson, M. E. *Org. Lett.* **2016**, *18*, 3960; n) Kui, S. C. F.; Chow, P. K.; Cheng, G.; Kwok, C.-C.; Kwong, C. L.; Low, K.-H.; Che, C.-M. *Chem. Commun.* **2013**, *49*, 1497; o) Hudson, Z. M.; Sun, C.; Helander, M. G.; Amarne, H.; Lu, Z.-H.; Wang, S. *Adv. Chem. Mater.* **2010**, *20*, 3426; p) Ko, S.-B.; Park, H.-J.; Gong, S.; Wang, X.; Lu, Z.-H.; Wang, S. *Dalton Trans.* **2015**, *44*, 8433.

3. Tremblay, J.-F. The rise of OLED displays. Chemical & Engineering News, July 11, 2016, p. 30-34. (URL: http://cen.acs.org/articles/94/i28/rise-OLED-displays.html)

4. a) Zhang, Y.; Lee, J.; Forrest, S. R. *Nat. Commun.* **2014**, *5*, 5508; b) Fleetham, T.; Li, G.; Wen, L.; Li, J. *Adv. Mater.* **2014**, *26*, 7116; c) Lee, J.; Chen, H.-F.; Batagoda, T.; Coburn, C.; Djurovich, P. I.; Thompson, M. E.; Forrest, S. R. *Nat. Mater.* **2016**, *15*, 92; d) Fleetham, T. B.; Huang, L.; Klimes, K.; Brooks, J.; Li, J. *Chem. Mater.* **2016**, *28*, 3276.

5. a) Giebink, N. C.; D'Andrade, B. W.; Weaver, M. S.; Mackenzie, P. B.; Brown, J. J.; Thompson, M. E.; Forrest, S. R. *J. Appl. Phys.* **2008**, *103*, 044509; b) Seifert, R.; de Moraes, I. R.; Scholz, S.; Gather, M. C.; Lüssem, B.; Leo, K. *Org. Electron.* **2013**, *14*, 115; c) Holmes, R. J.; Forrest, S. R.; Tung, Y.-J.; Kwong, R. C.; Brown, J. J.; Garon, S.; Thompson, M. *Appl. Phys. Lett.* **2003**, *82*, 2422.

6. a) Sajoto, T.; Djurovich, P. I.; Tamayo, A. B.; Oxgaard, J.; Goddard III, W. A.; Thompson, M. E. *J. Am. Chem. Soc.* **2009**, *131*, 9813; b) Zhou, X.; Burn, P. L.; Powell, B. J. *Inorg. Chem.* **2016**, *55*, 5266; c) Yang, L.; Okuda, F.; Kobayashi, K.; Nozaki, K.; Tanabe, Y.; Ishii, Y.; Haga, M. *Inorg. Chem.* **2008**, *47*, 7154.

7. a) Heying, T. L.; Ager, Jr., J. W.; Clark, S. L.; Mangold, D. J.; Goldstein, H. L.; Hillman, M.; Polak, R. J.; Szymanski, J. W. *Inorg. Chem.* **1963**, *2*, 1089; b) Fein, M. M.; Grafstein, D.;

Paustian, J. E.; Bobinski, J.; Lichstein, B. M.; Mayes, N.; Schwartz, N. N.; Cohen, M. S. *Inorg. Chem.* **1963**, *2*, 1115; c) Fein, M. M.; Bobinski, J.; Nayes, N.; Schwartz, N.; Cohen, M. S. *Inorg. Chem.* **1963**, *2*, 1111; d) Zakharkin, L. I.; Stanki, V. I.; Brattsev, V. A.; Chapovskii, Y. A.; Klimova, A. I.; Okhlobystin, O. Y.; Ponomarenko, A. A.; *Dolk. Akad. Nauk. SSSR* **1964**, *155*, 1119; e) Hawthorne, M. F.; Andrews, T. D.; Garrett, P. M.; Olsen, F. P.; Reintjes, M.; Tebbe, F. N.; Warren, L. F.; Wegner, P. A.; Young, D. C. *Inorg. Synth.* **1967**, *10*, 91; f) Grimes, R. N. *Carboranes*, 3rd ed; Academic Press, 2016.

8. a) Lipscomb, W. N. *Boron Hydrides*; Benjamin: New York, 1963; b) Schleyer, P. v. R.; Najafian, K. *Inorg. Chem.* **1998**, *37*, 3454; c) Chen, Z.; King, R. B. *Chem. Rev.* **2005**, *105*, 3613; d) King, R. B. *Chem. Rev.* **2001**, *101*, 1119.

9. Spokoyny, A. M.; Machan, C. W.; Clingerman, D. J.; Rose, M. S.; Wiester, M. J.; Kennedy, R. D.; Stern, C. L.; Sarjeant, A. A.; Mirkin, C. A. *Nature Chem.* **2011**, *3*, 590.

10. a) Grimes, R. N. *Dalton Trans.* **2015**, *44*, 5939; b) Tsang, M. Y.; Viñas, C.; Teixidor, F.; Planas, J. G.; Conde, N.; SanMartin, R.; Herrero, M. T.; Domínguez, E.; Lledós, A.; Vidossich, P.; Choquesillo-Lazarte, D. *Inorg. Chem.* **2014**, *53*, 9284; c) Gabel, D. *Pure Appl. Chem.* **2015**, *87*, 173; d) Teixidor, F.; Sillanpää, R.; Pepidol, A. *Chem. Eur. J.* **2015**, *21*, 12778; e) Eleazer, B. J.; Smith, M. D.; Peryshkov, D. V. *Organometallics* **2016**, *35*, 106; f) Schwartz, J. J.; Mendoza, M. A.; Wattanatorn, N.; Zhao, Y.; Nguyen, V. T.; Spokoyny, A. M.; Mirkin, C. A.; Baše, T.; Weiss, P. S. *J. Am. Chem. Soc.* **2016**, *138*, 5957; g) Kennedy, R. D.; Peng, Y.; Clingerman, D. J.; Mondloch, J.; Krungleviciute, V.; Wilmer, C. E.; Sarjeant, A. A.; Snurr, J.; Hupp, T.; Yildirim, T.; Farha, O. K.; Mirkin, C. A. *Chem. Mater.* **2013**, *25*, 3539.

11. a) Mukherjee, S.; Thilagar, P. *Chem. Commun.* **2016**, *52*, 1070; b) Li, X.; Yan, H.; Zhao, Q. *Chem. Eur. J.* **2016**, *22*, 1888; c) Kirlikovali, K. O.; Axtell, J. C.; Gonzalez, A.; Phung, A. C.; Khan, S. I.; Spokoyny, A. M. *Chem. Sci.* **2016**, *7*, 5132.

12. Jiang, W.; Gao, Y.; Sun, Y.; Ding, F.; Xu, Y.; Bian, Z.; Li, F.; Bian, J.; Huang, C. *Inorg. Chem.* **2010**, *49*, 3252.

13. a) Weller, A. *Nature Chem.* **2011**, *3*, 577; b) Spokoyny, A. M.; Lewis, C. D.; Teverovskiy, G.; Buchwald, S. L. *Organometallics* **2012**, *31*, 8478.

14. a) Bae, H. J.; Kim, H.; Lee, K. M.; Kim, T.; Eo, M.; Lee, Y. S.; Do, Y.; Lee, M. H. *Dalton Trans.* **2013,** *42*, 8549; b) Kim, T.; Lee, J.; Lee, S. U.; Lee, M. H. *Organometallics* **2015**, *34*, 3455; c) Prokhorov, A. M.; Slepukhin, P. A.; Rusinov, V. L.; Kalinin, V N.; Kozhevnikov, D. N. *Chem. Commun.* **2011**, *47*, 7713; d) Prokhorov, A. M.; Hofbeck, T.; Czerwieniec, R.; Suleymanova, A. F.; Kozhevnikov, D. N.; Yersin, H. *J. Am. Chem. Soc.* **2014**, *136*, 9637.

15. a) Shi, C.; Tu, D.; Yu, Q.; Liang, H.; Liu, Y.; Li, Z.; Yan, H.; Zhao, Q.; Huang, W. *Chem. Eur. J.* **2014**, *20*, 16550; b) Visbal, R.; Ospino, I.; López-de-Luzuriaga, J. M.; Laguna, A.; Gimeno, M. C. *J. Am. Chem. Soc.* **2013**, *135*, 4712; c) Visbal, R.; López-de-Luzuriaga, J. M.; Laguna, A.; Gimeno, M. C. *Dalton Trans.* **2014**, *43*, 328; d) Czerwieniec, R.; Hofbeck, T.; Crespo, O.; Laguna, A.; Gimeno, M. C.; Yersin, H. *Inorg. Chem.* **2010**, *49*, 3764; e) Crespo, O.; Gimeno, M. C.; Jones, P. G.; Laguna, A.; López-de-Luzuriaga, J. M.; Monge, M.; Pérez, J. L.; Ramón, M. A. *Inorg. Chem.* **2003**, *42*, 2061; f) Crespo, O.; Gimeno, M. C.; Laguna, A.; Lehtonen, O.; Ospino, I.; Pyykkö, P.; Villacampa, M. D. *Chem. Eur. J.* **2014**, *20*, 3120.

16. a) Shi, C.; Sun, H.; Jiang, Q.; Zhao, Q.; Wang, J.; Huang, W.; Yan, H. *Chem. Commun.* **2013**, *49*, 4746; b) Kim, T. Kim, H.; Lee, K. M.; Lee, Y. S.; Lee, M. H. *Inorg. Chem.* **2013**, *52*, 160; c) Shi, C.; Sun, H.; Tang, X.; Lv, W.; Yan, H.; Zhao, Q.; Wang, J.; Huang, W. *Angew. Chem. Int. Ed.* **2013**, *52*, 13434; d) Lee, Y. H.; Park, J.; Lee, J.; Lee, S. U.; Lee, M.

H. *J. Am. Chem. Soc.* **2015**, *137*, 8018; e) Zhu, L.; Tang, X.; Yu, Q.; Lv, W.; Yan, H.; Zhao, Q.; Huang, W. *Chem. Eur. J.* **2015**, *21*, 4721; f) Lee, Y. H.; Park, J.; Jo, S.-J.; Kim, M.; Lee, J.; Lee, S. U.; Lee, M. H. *Chem. Eur. J.* **2015**, *21*, 2052; g) Park, J.; Lee, Y. H.; Ryu, J. Y.; Lee, J.; Lee, M. H. *Dalton Trans.* **2016**, *45*, 5667; h) Kim, Y.; Park, S.; Lee, Y. H.; Jung, J.; Yoo, S.; Lee, M. H. *Inorg. Chem.* **2016**, *55*, 909.

17. Li, J.; Djurovich, P. I.; Alleyne, B. D.; Tsyba, I.; Ho, N. N.; Bau, R.; Thompson, M. E. *Polyhedron* **2004**, *23*, 419.

18. a) Ames, D. E.; Bull, D.; Takundwa, C. *Synthesis* **1981**, 364; b) Coult, F.; Fox, M. A.; Gill, W. R.; Herbertson, P. L.; Hugh MacBride, J. A.; Wade, K. *J. Organomet. Chem.* **1993**, *462*, 19.

19. El-Zaria, M. E.; Keskar, K.; Genady, A. F.; Ioppolo, J. A.; McNulty, J.; Valliant, J. F. *Angew. Chem., Int. Ed.* **2014**, *53*, 5156.

20. a) Fort, Y.; Forgione, P. *E-Eros Encyclopedia of Reagents for Organic Synthesis* "2-Fluoropyridine" **2007**; b) Cherng, Y.-J. *Tetrahedron* **2002**, *58*, 4931.

21. a) Zakharkin, L. I.; Lebedev, V. N. *Bull. Acad. Sci. USSR, Div. Chem. Sci.* **1970**, *19*, 914; b) Zakharkin, L. I.; Lebedev, V. N. *Bull. Acad. Sci. USSR, Div. Chem. Sci.* **1972**, *21*, 2273; c) Henly, T. J.; Knobler, C. B.; Hawthorne, M. F. *Organometallics* **1992**, *11*, 2313; d) Ohta, K.; Ogawa, T.; Endo, Y. *Bioorg. & Med. Chem. Lett.* **2012**, *22*, 4728; e) Tricas, H.; Colon, M.; Ellis, D.; Macgregor, S. A.; McKay, D.; Rosair, G. M.; Welch, A. J.; Glukhov, I. V.; Rossi, F.; Laschi, F.; Zanello, P. *Dalton Trans.* **2011**, *40*, 4200; f) Ohta, K.; Goto, R.; Endo, Y. *Tetrahedron Lett.* **2005**, *46*, 483.

22. Lamansky, S.; Djurovich, P. I.; Murphy, D.; Abdel-Razzaq, F.; Kwong, R.; Tsyba, I.; Bortz, M.; Mui, B.; Bau, R.; Thompson, M. E. *Inorg. Chem.* **2001**, *40*, 1704. (See SI for NMR characterization).

23. a) Wiesboeck, R. A.; Hawthorne, M. F. *J. Am. Chem. Soc.* **1964**, *86*, 1642; b) Hawthorne, M. F.; Young, D. C.; Garrett, P. M.; Owen, D. A.; Schwerin, S. G.; Tebbe, F. N.; Wegner, P. A. *J. Am. Chem. Soc.* **1968**, *90*, 862; c) Plešek, J.; Heřmánek, S.; Štíbr, B.; Waksman, L.; Sneddon, L. G. *Inorg. Synth.* **1983**, *22*, 231.

24. a) Mei, M.; Chan, H.-S.; Xie, Z. *Organometallics* **2011**, *30*, 3449; b) Teixidor, F.; Núñez, R.; Flores, M. A.; Demonceau, A.; Viñas, C. *J. Organomet. Chem.* **2000**, *614-615*, 48.

25. a) Zakharkin, L. I.; Kirillova, V. S. *Bull. Acad. Sci. USSR, Div. Chem. Sci.* **1975**, 2484; b) Schaeck, J. J.; Kahl, S. B. *Inorg. Chem.* **1999**, *38*, 204.

26. Ladouceur, S.; Zysman-Colman, E. *Eur. J. Inorg. Chem.* **2013**, 2985.

27. a) Darmawan, N.; Yang, C.-H.; Mauro, M.; Frohlich, R.; De Cola, L.; Chang, C.-H.; Wu, Z.-J.; Tai, C.-W. *J. Mater. Chem. C* **2014**, *2*, 2569; b) Byun, Y.; Lyu, Y.-Y.; Das, R. R.; Kwon, O.; Lee, T.-W.; Park, Y. J. *Appl. Phys. Lett.* **2007**, *91*, 211106; c) Jiang, W.; Gao, Y.; Sun, Y.; Ding, F.; Xu, Y.; Bian, Z.; Li, F.; Bian, J.; Huang, C. *Inorg. Chem.* **2010**, *49*, 3252; d) Li, J.; Djurovich, P. I.; Alleyne, B. D.; Tsyba, I.; Ho, N. N.; Bau, R.; Thompson, M. E. *Polyhedron* **2004**, *23*, 419.

28. Bae, H. J.; Chung, J.; Kim, H.; Park, J.; Lee, K. M.; Koh, T.-W.; Lee, Y. S.; Yoo, S.; Do, Y.; Lee, M. H. *Inorg. Chem.* **2014**, *53*, 128.

29. Dedeian, K.; Shi, J.; Shepherd, N.; Forstyhe, E.; Morton, D. C. *Inorg. Chem.* **2005**, *44*, 4445.

30. Pyykkö, P.; Atsumi, M. *Chem. Eur. J.* **2009**, *15*, 186.

31. a) Drover, M. W.; Bowes, E. G.; Schafer, L. L.; Love, J. A.; Weller, A. S. *Chem. Eur. J.* **2016**, *22*, 6793; b) Brugos, J.; Cabeza, J. A.; Garciá-Álvarez, P.; Kennedy, A. R.; Pérez-Carreño, E.; Van der Maelen, J. F. *Inorg. Chem.* **2016**, *55*, 8905; c) Stevens, C. J.;

Dallanegra, R.; Chaplin, A. B.; Weller, A. S.; Macgregor, S. A.; Ward, B.; McKay, D.; Alcaraz, G.; Sabo-Etienne, S. *Chem. Eur. J.* **2011**, *17*, 3011; d) Tang, C. Y.; Thompson, A. L.; Aldridge, S. *J. Am. Chem. Soc.* **2010**, *132*, 10578.

32. a) El-Hellani, A.; Kefalidis, C. E.; Tham, F. S.; Maron, L.; Lavallo, V. *Organometallics* **2013**, *32*, 6887; b) Rifat, A.; Patmore, N. J.; Mahon, M. F.; Weller, A. S. *Organometallics* **2002**, *21*, 2856; c) Crowther, D. J.; Borkowsky, S. L.; Swenson, D.; Meyer, T. Y.; Jordan, R. F. *Organometallics* **1993**, *12*, 2897; d) Núñez, R.; Viñas, C.; Teixidor, F.; Abad, M. M. *Appl. Organometal. Chem.* **2003**, *17*, 509; e) Riley, L. E.; Chan, A. P. Y.; Taylor, J.; Man, W. Y.; Ellis, D.; Rosair, G. M.; Welch, A. J.; Sivaev, I. B. *Dalton Trans.* **2016**, *45*, 1127; f) Mhinzi, G. S.; Litster, S. A.; Redhouse, A. D.; Spencer, J. L. *J. Chem. Soc., Dalton Trans.* **1991**, 2769.

33. a) Shelly, K.; Finster, D. C.; Lee, Y. J.; Scheidt, W. R.; Reed, C. A. *J. Am. Chem. Soc.* **1985**, *107*, 5955; b) Shelly, K.; Reed, C. A. *J. Am. Chem. Soc.* **1986**, *108*, 3117.

34. Teixidor, F.; Flores, M. A.; Viñas, C.; Sillanpää, R.; Kivekäs, R. *J. Am. Chem. Soc.* **2000**, *122*, 1963.

35. Doi, J. A.; Teller, R. G.; Hawthorne, M. F. *J. Chem. Soc., Chem. Comm.* **1980**, 80.

36. a) Bader, R. F. W. *Chem. Rev.* **1991**, *91*, 893; b) For QTAIM analysis of boron-containing clusters, carboranes, and electron-deficient cluster species, see "Properties of atoms in molecules: structures and reactivities of boranes and carboranes" Bader, R. F. W.; Legare, D. A. *Can J. Chem.* **1992**, *70*, 657; c) Bader, R. F. W. *Atoms in Molecules: A Quantum Theory*, Oxford University Press: New York, 1990.

37. a) J. S.; Polikarpov, E.; Von Ruden, A.; Wang, L.; Sapochak, L. S.; Padmaperuma, A. B. *Adv. Funct. Mater.* **2011**, *21*, 3250; b) Tsang, D. P.-K.; Chan, M.-Y.; Tam, A. Y.-Y.; Yam, W.-W. *Org. Electron.* **2011**, *12*, 1114; c) Veinot, J. G. C.; Marks, T. J. *Acc. Chem. Res.* **2005**, *38*, 632.

38. Recently published methodology: a) Dziedzic, R. M.; Saleh, L. M. A.; Axtell, J. C.; Martin, J. L.; Stevens, S. L.; Royappa, A. T.; Rheingold, A. L.; Spokoyny, A. M. *J. Am. Chem. Soc.* **2016**, *138*, 9081; b) Zhao, D.; Xie, Z. *Angew. Chem. Int. Ed.* **2016**, *55*, 3166; c) Lyu, H.; Quan, Y.; Xie, Z. *Angew. Chem. Int. Ed.* **2016**, *55*, 11840; d) Zhao, D.; Xie, Z. *Chem. Sci.* **2016**, *7*, 5635; e) Kabytaev, K. Z.; Everett, T. A.; Safronov, A. V.; Sevryugina, Y. V.; Jalisatgi, S. S.; Hawthorne, M. F. *Eur. J. Inorg. Chem.* **2013**, *14*, 2488; f) Sevryugina, Y.; Julius, R. L.; Hawthorne, M. F. *Inorg. Chem.* **2010**, *49*, 10627; g) Lugo, C. A.; Moore, C. E.; Rheingold, A. L.; Lavallo, V. *Inorg. Chem.* **2015**, *54*, 2094; h) Kracke, G. R.; VanGordon, Y. V.; Sevryugina, Y. V.; Kueffer, P. J.; Kabytaev, K.; Jalisatgi, S. S.; Hawthorne, M. F. *Chem. Med. Chem.* **2015**, *10*, 62; i) Wingen, L. M.; Scholz, M. S. *Inorg. Chem.* **2016**, *55*, 8274; j) Cao, K.; Xu, T.-T.; Wu, J.; Jiang, L.; Yang, J. *Chem. Commun.* **2016**, *52*, 11446; k) Olid, D.; Núñez, R.; Viñas, C.; Teixidor, F. *Chem. Soc. Rev.* **2013**, *42*, 3318; l) Safronov, A.; Kabytaev, K. Z.; Jalisatgi, S. S.; Hawthorne, M. F. *Dalton Trans.* **2014**, *43*, 12647; m) Kabytaev, K. Z.; Safronov, A. V.; Jalisatgi, S. S.; Hawthorne, M. F. *J. Organomet. Chem.* **2014**, *749*, 106; n) Kabytaev, K. Z.; Safronov, A. V.; Sevryugina, Y. V.; Barnes, C. L.; Jalisatgi, S. S.; Hawthorne, M. F. *Inorg. Chem.* **2015**, *54*, 4143; o) Safronov, A. V.; Sevryugina, Y. V.; Jalisatgi, S. S.; Kennedy, R. D.; Barnes, C. L.; Hawthorne, M. F. *Inorg. Chem.* **2012**, *51*, 2629; p) Beletskaya, I. P.; Bregadze, V. I.; Kabytaev, K. Z.; Zhigareva, G. G.; Petrovskii, P. V.; Glukhov, I. V.; Starikova, Z. A. *Organometallics* **2007**, *26*, 2340.

39. a) Lavallo, V.; Wright II, J. H.; Tham, F. S.; Quinlivan, S. *Angew. Chem.* **2013**, *52*, 3172; b) Kultyshev, R. G.; Liu, J.; Liu, S.; Tjarks, W.; Soloway, A. H.; Shore, S. G. *J. Am. Chem. Soc.*

2002, *124*, 2614; c) Beletskaya, I. P.; Bregadze, V. I.; Ivushkin, V. A.; Petrovskii, P. V.; Sivaev, I. B.; Sjöberg, S.; Zhigareva, G. G. *J. Organomet. Chem.* **2004**, *689*, 2920; d) Kultyshev, R. G.; Lui, S.; Leung, H. T.; Liu, J.; Shore, S. G. *J. Am. Chem. Soc.* **2003**, *42*, 3199; e) Himmelspach, A.; Reiss, G. J.; Finze, M. *Inorg. Chem.* **2012**, *51*, 2679; f) Douvris, C.; Michl, J. *Chem. Rev.* **2013**, *113*, PR179; g) Preetz, W.; Peters, G. *Eur. J. Inorg. Chem.* **1999**, *11*, 1831; h) Semioshkin, A.; Brellochs, B.; Bregadze, V. *Polyhedron* **2004**, *23*, 2135; i) Olid, D.; Núñez, R.; Viñas, C.; Teixidor, F. *Chem. Soc. Rev.* **2013**, *42*, 3318; j) Peymann, T.; Knobler, C. B.; Hawthorne, M. F. *Inorg. Chem.* **2000**, *39*, 1163; k) Grüner, B.; Janoušek, Z.; King, B. T.; Woodford, J. N.; Wang, C. H.; Všetečka, V.; Michl, J. *J. Am. Chem. Soc.* **1999**, *121*, 3122; l) Zhang, Y.; Liu, J.; Duttwyler, S. *Eur. J. Inorg. Chem.* **2015**, 5158; m) Konieczka, S. Z.; Himmelspach, A.; Hailmann, M.; Finze, M. *Eur. J. Inorg. Chem.* **2013**, 134; n) Bolli, C.; Derendorf, J.; Jenne, C.; Scherer, H.; Sindlinger, C. P.; Wegener, B. *Chem. Eur. J.* **2014**, *20*, 13783; o) Wong, Y. O.; Smith, M. D.; Peryshkov, D. V. *Chem. Eur. J.* **2016**, *22*, 6764; p) Ivanov, S. V.; Lupinetti, A. J.; Solntsev, K. A.; Strauss, S. H. *J. Fluorine Chem.* **1988**, *89*, 65; q) Ivanov, S. V.; Davis, J. A.; Miller, S. M.; Anderson, O. P.; Strauss, S. H. *Inorg. Chem.* **2003**, *42*, 4489; r) *Boron Hydride Chemistry*; Earl L. Muetterties, Ed. Academic Press, Inc: New York, New York, 1975; s) Ramírez-Contreras, R.; Bhuvanesh, N.; Zhou, J.; Ozerov, O. V. *Angew. Chem. Int. Ed.* **2013**, *52*, 10313; t) Press, L. P.; McCulloch, B. J.; Gu, W.; Chen, C.-H.; Foxman, B. M.; Ozerov, O. V. *Chem. Commun.* **2015**, *51*, 14034; u) Ramírez-Contreras, R.; Ozerov, O. V. *Dalton Trans.* **2012**, *41*, 7842.

CHAPTER 3 – LUMINESCENT METAL COMPLEXES FEATURING PHOTOPHYSICALLY INNOCENT BORON CLUSTER LIGANDS

3.1 Introduction

Many square planar platinum complexes containing chelating biaryl ligands have been established as efficient phosphorescent emitters, making them desirable dopants in organic light-emitting diodes (OLEDs).[1,2] The emissive properties of these Pt(II) complexes can be tuned by varying the electronic nature of the ligands surrounding the metal center; however, complete control over desired photophysical properties is still limited. For example, these square planar complexes are susceptible to aggregation as a consequence of the lack of steric bulk above and below the square plane, leading to intermolecular Pt(II)···Pt(II) interactions that bring about luminescence quenching and red-shifting of the solid-state emission frequency.[2,3] Furthermore, in prototypical mixed ligand complexes, (L)(L′)Pt(II), the HOMO is generally both metal- and ligand-based (Pt(II) and L) while the LUMO is located on the remaining ligand (L′).[4] This ultimately complicates the predictability of ligand effects on emission properties. A class of compounds that could kinetically stabilize the Pt(II) square planar framework without participating in electronic transitions would prove very useful for creating improved phosphorescent emitters for the next generation of OLED devices.

Icosahedral dicarba-*closo*-dodecaboranes ($C_2B_{10}H_{12}$, carborane) are robust, charge-neutral boron clusters that are often viewed as 3D aromatic analogues of arenes. Unfunctionalized carborane species have an extremely large HOMO-LUMO gap (~8 eV, see Appendix B),[5] making them potentially useful building blocks for probing their photophysical innocence in the context of metal-based phosphorescent emitters. This is especially appealing given the available functionalization routes through either carbon or boron vertices in these

clusters, enabling the synthesis of tailored ligand frameworks for transition metal complexes.[6] For example, Lee and co-workers have recently demonstrated that κ^2-C,N-bound 1-(2-pyridyl)-*o*-carboranyl[7a] and κ^2-C,P-bound 1-(^{i}Pr$_2$PCH$_2$)-*o*-carboranyl[7b] can be strong ancillary ligands that contribute to the electronic stabilization of bis(heteroleptic) Ir(III) species (see Appendix B for molecular structures), leading to an arylpyridine-dominant phosphorescent emission. From DFT calculations and analysis of the emission spectra, these authors determined the C-bound *o*-carboranyl unit remains uninvolved in electronic transitions and that phosphorescent emission results from MLCT of the Ir(III)-based HOMO to the arylpyridine-based LUMO. Furthermore, several groups have functionalized biaryl ligands with C-connected carboranyl moieties (*ortho*, *meta*, *para*, and *nido*) to tune luminescent properties[8] (see Appendix B for molecular structures). To the best of our knowledge, attempts to design a tunable, exclusively carborane-based ligand scaffold for phosphorescent emitter molecules have not been explored thus far.[9] Such a ligand framework would be an ideal system for a rational design of metal-based luminescent complexes (*vide supra*).

In 1964, Hawthorne reported the first synthesis of 1,1′-bis(*o*-carborane) (**2**),[10a] effectively a 3D analogue of biphenyl (Figure 3.1), and in 1973, Zakharkin showed that the oxidative coupling of two *o*-carboranes (**1**) through carbon vertices yields **2**.[10d] Later, Hawthorne demonstrated that the deprotonation of **2** results in a dianionic species **bc**, which was shown to bind several transition metals in bidentate or monodentate fashions.[10b-f] Ligand **bc** possesses similar electronic and physical properties as the parent *o*-carborane (see Appendix B), and behaves as a robust transition metal ligand. More recently, several groups have improved the synthesis of **2**[10j] and further expanded the series of heteroleptic late-transition metal complexes

containing **bc**.[11] However, fundamental electronic characterization and potential applications for these compounds as electronic materials have yet to be disclosed.
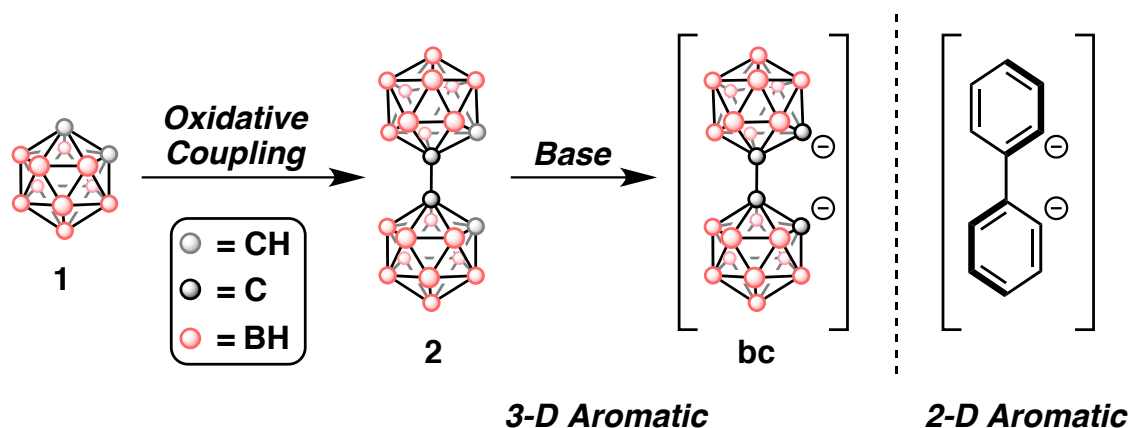
Figure 3.1 Oxidative coupling of *o*-carborane (**1**) yields 1,1′-bis-*o*-carborane (**2**). Deprotonation of **2** yields the dianionic **bc** ligand, which can be conceptually thought of as a 3-D aromatic analogue of a dianionic biphenyl ligand (**bph**).

Two monoanionic bidentate ligands are commonly used in Pt(II) architectures employed for OLEDs, but there are few examples of Pt(II)-based emitters containing a dianionic bidentate ligand and a neutral bidentate ligand.[12] One such example is Pt(bph)(bpy)[12a-c] (where bph = biphenyl, bpy = 2,2′-bipyridine, see Appendix B for a molecular structure). We hypothesized that employing **bc** in place of bph could introduce sufficient steric bulk above and below the square plane to eliminate intermolecular Pt(II)···Pt(II) interactions, which are often responsible for non-radiative decay pathways that lower luminescent efficiency.[2,3] Additionally, the lack of an exposed π-aromatic system in **bc** should help in reducing these undesirable intermolecular interactions and unwanted substitution and degradation pathways. Furthermore, the high-lying LUMO of **bc** should be inaccessible for orbital mixing and MLCT processes. Therefore, the **bc** ligand was hypothesized to provide kinetic stability while maintaining photophysical innocence in the context of designing OLEDs. Finally, emission originating from a single ligand will yield greater color purity, as mixing of emissions from multiple delocalized excited states will not be

possible. Together, these properties should allow for the rational tuning of other ancillary ligands without electronic interference from **bc**.

3.2 Results and Discussion

To test our hypothesis, we first proceeded to evaluate the photophysical behavior of **bc** as a ligand in a series of d^8 model transition metal complexes of the type M(bc)(dppe) (M = Ni(II), Pd(II), Pt(II); dppe = 1,2-bis(diphenylphosphino)ethane; Figure 3.2). The dilithio salt of **bc** (Li$_2$[**bc**]) was generated in THF and transferred into a slurry of M(dppe)Cl$_2$ in THF at -80 °C. The reaction was allowed to slowly warm to room temperature overnight, yielding a dark brown solution. Pure compounds were isolated in the yields reported in Figure 3.2 as crystalline yellow-orange solids after purification using column chromatography on silica or alumina (see Appendix B). All reactions can be easily monitored via ^{31}P NMR spectroscopy. For example, **3a** and **3b** exhibit a significant (>10 ppm) upfield shift in their observed ^{31}P NMR singlet resonance compared to the starting metal-based precursors (see Appendix B). These results are also consistent with the recent work by Welch and co-workers who independently synthesized **3a**.[11a] Observed $^1J_{\text{Pt-P}}$ coupling values for **3c** change significantly compared to the starting material, exhibiting a decrease of 1133 Hz ($^1J_{\text{Pt-P}}$ value changes from 3624 Hz to 2491 Hz). The substantial reduction in the magnitude of the $^1J_{\text{Pt-P}}$ coupling for **3c** can be attributed to the strong ligand field of **bc** versus that of the chloride ligands.[13]
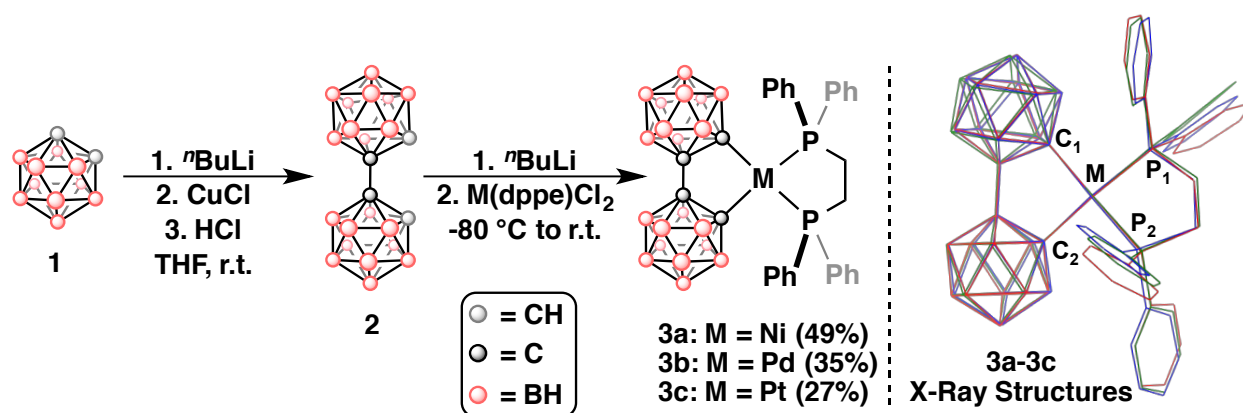
Figure 3.2 Left: Synthesis of M(bc)(dppe), where M = Ni (**3a**), Pd (**3b**), Pt (**3c**). The synthesis of **2** was adapted from Reference 10j. Right: Stacked X-ray crystal structures of compounds **3a-3c** (CCDC 1446940-1446942), illustrating structural similarity down the group. Red = **3a**, Green = **3b**, Blue = **3c** (see Appendix B for thermal ellipsoid plots of **3a-3c**).

To demonstrate that the **bc** framework is structurally similar to the biphenyl (bph) framework, we compared bond distances, angles, and molecular geometries of **3a-3c** to those of a series of cyclometallated M(bph)(L^L) in reported X-ray crystal structures, and determined that **bc** does not influence the intramolecular geometry much differently than the bph ligand. Furthermore, the M—P bond lengths in **3a-3c** are also consistent with the strong-field ligand nature of **bc** in these complexes (see Appendix B for specific discussion).

UV-Vis spectroscopic measurements were performed on **3a-3c** and revealed strong transitions in the UV region below 360 nm corresponding to π-π* transitions on the ligand. UV-Vis spectra of **3a-3c** also feature weaker intensity transitions in the visible region ranging from 400-500 nm that result from M(II)-(dppe) MLCT. DFT calculations were performed on the geometry optimized X-ray crystal structure inputs of **3a-3c** in order to confirm the nature of the observed electronic transitions (see Appendix B). Our computational studies reveal an almost entirely metal-based HOMO and dppe ligand-based LUMO with negligible contribution from the **bc** ligand in all frontier orbitals. As we hypothesized previously, **bc** chelated to the d[8] transition

73

metals in our model complexes remains uninvolved in all MLCT-based visible transitions, suggesting its photophysical innocence in the UV-Vis region.

Next, we sought to synthesize a Pt(II)-bpy (bpy = 2,2′-bipyridine) complex chelated by **bc**, as Pt(II) complexes containing this class of ligands are known to exhibit phosphorescent emission.[12a-c] Starting with the addition of Li₂[**bc**] to a slurry of Pt(bpy)Cl₂, a large amount of emissive, insoluble product was obtained. The extremely low solubility of this product in common organic solvents hampered its characterization. In order to potentially circumvent this issue, we then chose the 4,4′-di-*tert*-butyl-2,2′-bipyridine (dtb-bpy) ligand as an alternative, anticipating more favorable solubility properties. Using the same synthetic route yielded, again, a largely insoluble, emissive solid (Figure 3.3A). After dissolving the crude product in hot 1,2-difluorobenzene and passing the solution through a Celite plug, a non-emissive solid was left on the Celite; a yellow solid that emitted blue-green under UV excitation (365 nm) remained after all volatiles were removed *in vacuo*. Surprisingly, ^{1}H NMR spectroscopic data suggests that the isolated product consists of a mixture of two species (**4a/4b**) with a **bc** ligand chelated to the Pt(II) center in both κ^2-C,C-bound (**4a**) and κ^2-B,C-bound modes (**4b**) (Fig. 3). The κ^2-C,C-bound species **4a**, derived from the symmetric binding of the **bc** ligand, is consistent with the presence of three resonances of equal integration in the aromatic region (dtb-bpy ligand) of the ^{1}H NMR spectrum (Figure 3.3B, label A). The six remaining resonances in the aromatic region (Figure 3.3B, label B) of the ^{1}H NMR spectrum are consistent with an asymmetric κ^2-B,C-bound **bc** species **4b** (*vide infra*). From the relative integration of these two sets of resonances, we estimate that the produced mixture contained a ratio of 1.4:1.0 of **4a** to **4b**. Repeated attempts to optimize this reaction produced the same mixture in varying ratios of **4a** and **4b** (see Appendix B). Attempts to drive the formation of one isomer from the mixture of isomers while heating

under forcing conditions produced no observable change in both ^{1}H and ^{11}B NMR spectra. Notably, during the preparation of this manuscript, Welch and co-workers reported the synthesis of a series of Ru(II) complexes chelated by the κ^2-B,C-bound **bc** ligand.[11c] The authors explained this B—Ru bond formation results from a competitive B—H activation process, which we think is reminiscent of the observed formation of **4b** in this work.
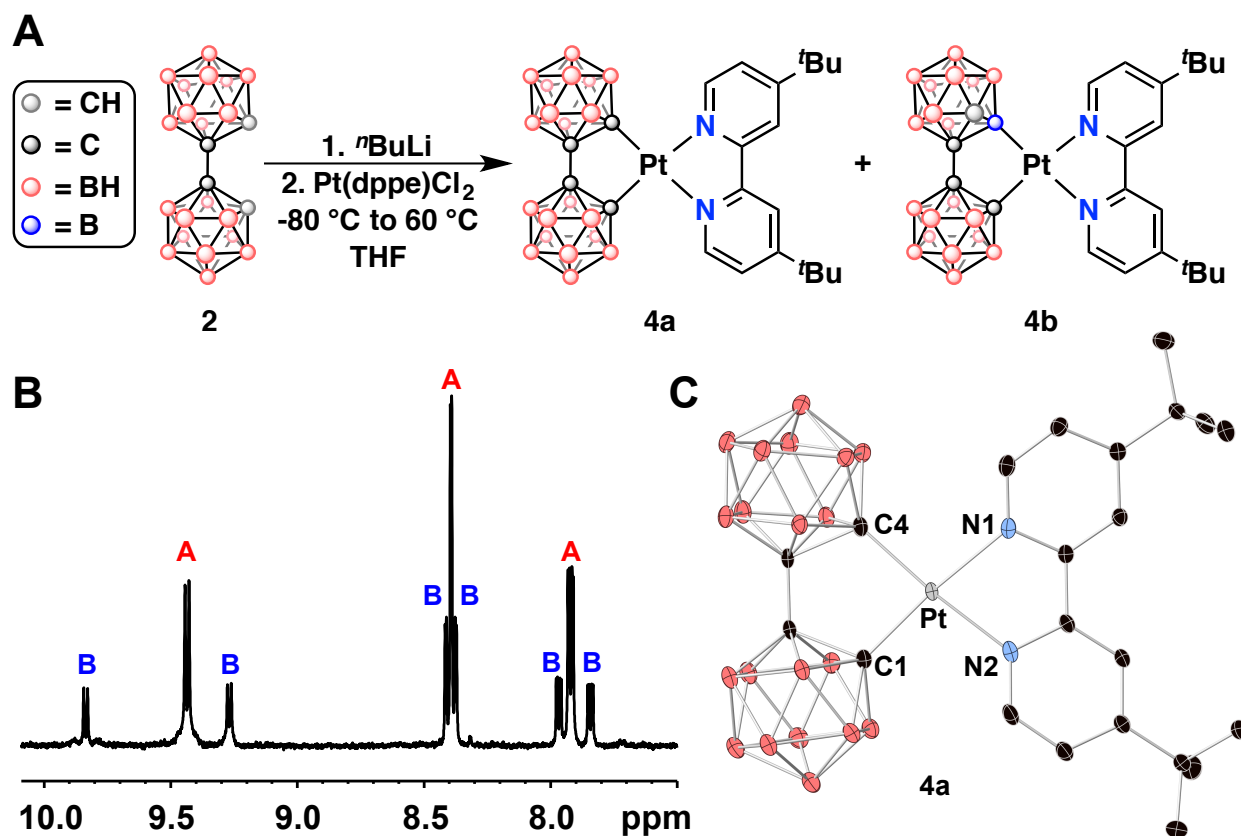
Figure 3.3 (A) Synthesis of the Pt(bc)(dtb-bpy) complex leads to a mixture containing two product isomers featuring a κ^2-C,C-bound **bc** (**4a**) and κ^2-B,C-bound **bc** (**4b**). (B) ^{1}H NMR spectrum of the aryl region for the isolated mixture of **4a** (label A) and **4b** (label B). (C) Single crystal X-ray structure of **4a** drawn with 50% thermal ellipsoid probability (CCDC 1446943). H atoms are omitted for clarity.

A mixture of **4a** and **4b** was dissolved in hot 2-MeTHF and allowed to cool to room temperature, yielding single crystals of **4a** (Figure 3.3C). The molecule adopts a minimally distorted square planar geometry with the C—Pt—N$_{trans}$ angles at 174.2(7)° and 173.0(8)°. The

bulky **bc** ligand forces the molecule to pack "head-to-tail" with Pt(II)···Pt(II) distances ranging between 5.87(0) Å and 5.52(0) Å (see Appendix B), which far exceed the reported 3.15—3.76 Å expected for intermolecular Pt(II)···Pt(II) interactions[2,3] (see Appendix B for further discussion about the single crystal X-ray structure of **4a**).

Given that the **bc** framework is amenable to substitution, we hypothesized that functionalizing this scaffold with alkyl groups would increase the solubility of the resulting Pt(II) complexes, ultimately allowing us to better characterize these emissive species. We therefore installed ethyl groups at the B(9) and B(12) positions of the parent 9,12-B-diiodo-*o*-carborane (**5**) using Kumada cross-coupling conditions producing bis(alkylated) species **6** (Figure 3.4A and Appendix B). Compound **6** was then subjected to Cu-mediated oxidative coupling conditions, ultimately producing the tetralkylated-**bc** (**7**) in 50% isolated yield (Figure 3.4A and Appendix B).[10j] Compound **7** was dilithiated and added to Pt(dtb-bpy)Cl$_2$ in a similar manner as with **2** (Figure 3.4A). Surprisingly, after the reaction mixture was stirred for a day at 60 °C, predominantly a κ^2-B,C-bound isomer **8** was observed by ^{1}H and 2D ^{13}C-^{1}H HSQC NMR spectroscopy (> 80%). Purification of the resulting mixture further afforded pure κ^2-B,C-bound species as a pale orange solid which exhibits blue-green emission in the solid state and, as hypothesized, is extremely soluble in the majority of common organic solvents. To our knowledge, this is the first reported example of a functionalized **bc** bound to a metal.[10i]

Crystals of **8** suitable for X-ray analysis were grown by slow evaporation of diethyl ether over the course of one week. The diffraction study confirmed the presence of the asymmetric isomer with one Pt—C bond and one Pt—B(4) bond (Figure 3.4B). At 2.07(3) Å, the B(4)—Pt bond is slightly longer than the 2.03(6) Å C—Pt bond. Furthermore, the greater *trans* influence of the carborane-based boryl moiety[14] can be seen in the elongation of the Pt—N bond lengths:

76

the Pt—N(1) bond is 2.17(5) Å, whereas the Pt—N(2) bond is only 2.05(3) Å. As a result of the asymmetric binding of the **bc**-based ligand in **8**, one carborane cage rotates and forces the ethyl group about 30° out of the plane created by C—Pt—B(4), whereas the other 3 ethyl groups sit in the square plane (Figure 3.4C). This protruding ethyl group likely forces the dtb-bpy out of the square plane, causing the molecule to adopt a slightly distorted square planar structure; however, bond angles of 176.5(5)° for C—Pt—N(2) and 168.8(2)° for B(4)—Pt—N(1) are well within the range of corresponding angles in previously reported 4-coordinate Pt(bph)(N^N) compounds (see Appendix B).
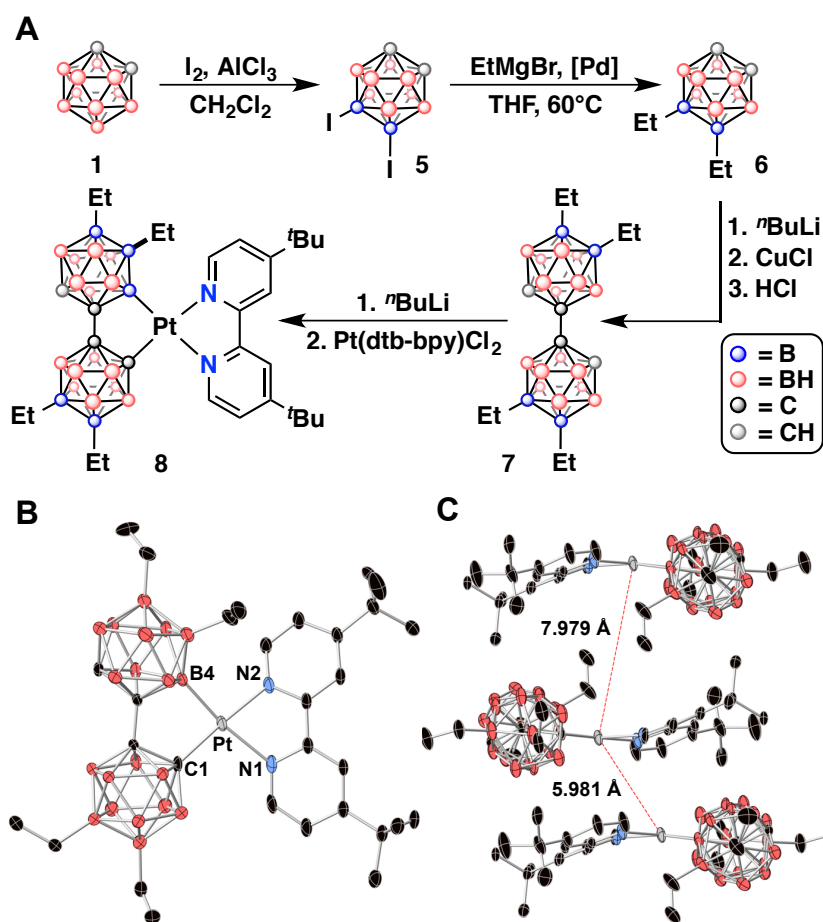
Figure 3.4 (A) Synthetic route to 9,9′,12,12′-tetraethyl-1,1′-bis(*o*-carborane) (**7**), syntheses of **5** and **6** from References 6k. (B) X-ray crystal structure of **8** (CCDC 1446944) with thermal ellipsoids drawn at 50% probability, H atoms omitted for clarity. (C) Stacking of **8** with Pt(II)···Pt(II) distances of 5.981 Å and 7.979 Å.

Importantly, the intermolecular Pt(II)···Pt(II) distances were augmented even more in the solid-state than in **4a** through the introduction of ethyl groups, yielding Pt(II)···Pt(II) distances of 5.891 Å (when ethyl groups face away from each other) and 7.979 Å (when ethyl groups point towards each other), effectively preventing any potential intermolecular Pt(II)···Pt(II) interactions (Figure 3.4C). Furthermore, the solid-state packing adopts a "head-to-tail" arrangement such that dtb-bpy lies above and below the **bc**-based ligand in the crystal lattice, eliminating the potential for any π—π stacking interactions, which have also been reported to result in deleterious non-radiative emission quenching.[2c,3d]

Cyclic voltammetry (CV) of **8** reveals a reversible, one-electron reduction ($E_{1/2}^{Red}$ = -1.92 V) and an irreversible one-electron oxidation (E^{Ox} = 0.85 V), as shown in Table 3.1 and Figure 3.5A. This electrochemical behavior is consistent with other square planar Pt(II) species undergoing a reversible ligand-centered reduction and irreversible metal-centered oxidation.[2-4,12a,12c,15a] Further, DFT calculations support these data (*vide infra*).

Table 3.1 Electrochemical data for **8** and related compounds from literature.[a]

Compound	$E_{1/2}^{Red}$ (V)	E^{Ox} (V)	Solvent	Reference
8	-1.92[c]	0.85[d]	MeCN	This work
Pt(bph)(bpy)[b]	-1.87[c]	-0.33[d]	MeCN	12a
Pt(bph)(en)[b]	-2.13[c]	0.25[d]	CH$_2$Cl$_2$	12c

[a]Values reported relative to the ferrocenium/ferrocene couple (Fc$^+$/Fc). [b]Values were corrected according to Reference 15b. [c]Reversible. [d]Irreversible.

Though electrochemical characterization for heteroleptic Pt(II) complexes bound by a dianionic bidentate ligand and a neutral bidentate ligand are scarce, Table 3.1 presents redox potentials for two such examples, Pt(bph)(bpy) and Pt(bph)(en) (where en = 1,2-ethylenediamine).[15b] The reduction potential for **8** is similar to the other two compounds (Table 3.1, Column 2); however, the oxidation potential of **8** is significantly greater (Table 3.1, Column

3). This is consistent with the strong field ligand character of the **bc-**based framework**,** which should make it more difficult to remove an electron from the Pt(II) HOMO level in **8**.

Table 3.2 Photophysical Data of **8** from solution-based[a] and solid-state[b] measurements.

Medium	Em. λ_{max} (nm)	ϕ^c	τ^d (μs)	k_r^f (10^4 s^{-1})	k_{nr}^f (10^4 s^{-1})
77 K	456, 486, 514	—	11.4	—	—
PMMA Film	497	0.07	4.24^e	1.67	22.1
Neat Solid	476, 505, 540	0.03	0.94^e	3.20	103.1

[a]Solutions at room temperature were non-emissive, and 77 K spectra were measured in 2-MeTHF. [b]PMMA film was prepared as 2 wt. %, neat solid was **8** in powder form. [c]Quantum yields were measured using an integrating sphere under N_2. [d]77 K lifetime was measured in 2-MeTHF, PMMA film and neat solid lifetimes were measured in the absence of air. [e]Values obtained from the weighted average of a multi-exponential decay. [f]Calculated according to the equations $k_r = \phi/\tau$ and $k_{nr} = (1-\phi)/\tau$, where k_r is the radiative rate constant, k_{nr} is the non-radiative rate constant, ϕ is the quantum yield, and τ is the luminescence lifetime.

Similar to **4a**/**4b**, we observed that **8** emits an intense blue-green color upon irradiation with a table-top UV lamp at 365 nm at room temperature. Given the improved solubility properties of **8**, we were able to carry out a detailed series of photophysical measurements in order to ascertain the efficiency and nature of this luminescent behaviour. The UV-Vis and phosphorescent emission spectra for **8** are presented in Figure 3.5B with corresponding data in Table 3.2. The absorption spectrum reveals strong transitions in the UV region ($\leq$330 nm) that arise from π—π* transitions on the dtb-bpy ligand. The broad, lower intensity band from 340-420 nm can be assigned to both singlet and triplet metal-to-ligand charge transfers ([1]MLCT and [3]MLCT). Compound **8** is non-emissive in solution at room temperature, suggesting emission might be thermally quenched through interaction with solvent molecules. However, at 77 K in 2-MeTHF, bright blue phosphorescence is observed (λ_{max} = 485 nm, τ = 11.4 μs). The well-defined vibrational features suggest ligand-centered emission resulting from an MLCT.[1a]
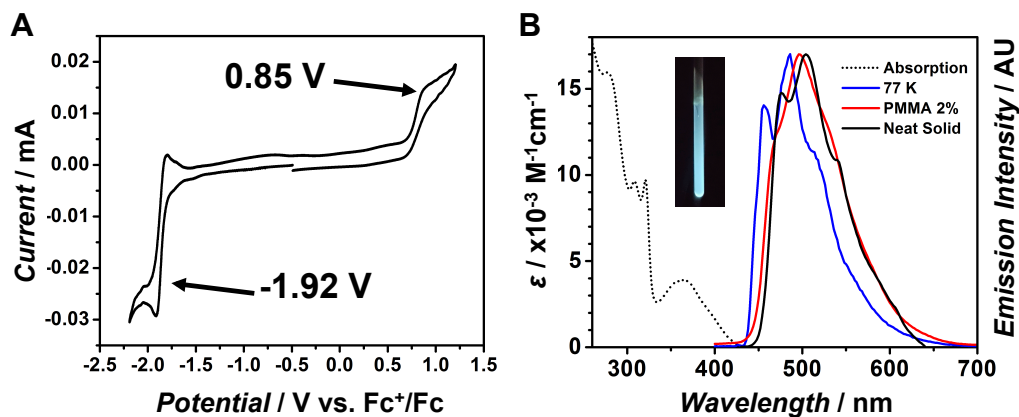
Figure 3.5 (A) Cyclic voltammagram of **8** versus Fc$^+$/Fc in MeCN with a glassy carbon working electrode, scan rate = 0.1 V/s. (B) UV-Vis absorption spectrum in CH$_2$Cl$_2$ (dotted line) and emission spectra of **8** in 2-MeTHF at 77 K (blue), 2 wt. % PMMA film (red), and neat solid (black), λ_{exc} = 380 nm; inset: picture of **8** in 2-MeTHF at 77 K (λ_{exc} = 365 nm).

Similarly, the neat solid **8** also exhibits an emission profile with a resolved vibronic fine structure, further suggesting the ligand-centered emission. Compared to the emission profile from the neat solid, emission from the solution at 77 K is hypsochromically shifted by roughly 20 nm. This shift is expected as vibrational relaxations to a lower energy excited state will not be favorable at lower temperatures, resulting in a higher energy, blue-shifted emission observed for **8** at 77 K in 2-MeTHF. When **8** is doped in a PMMA matrix (2 wt. %), the emission profile is broadened and the peak is blue-shifted by about 8 nm versus the emission of the neat solid. The excited-state lifetime (τ) for **8** increases as the environment becomes more rigid. This increase is significant, going from 0.94 ms as a neat solid, to 4.24 μs doped in PMMA, further to 11.4 μs at 77 K. This evidence suggests that decreasing vibrational motion through a more rigid and ordered surrounding environment can preserve the excited state, possibly by minimizing the energy loss via non-radiative relaxation pathways.[1a]

From the measured excited state lifetimes and quantum yields for **8** doped in the PMMA matrix and neat solid, the radiative rate constant (k$_r$) and non-radiative rate constant (k$_{nr}$) could be calculated (Table 3.2). Though k$_r$ for the doped PMMA film is half that of the neat solid, k$_{nr}$

for the doped PMMA film decreased by about a factor of 5, which supports the trend seen for measured τ values (*vide supra*). Additionally, the doped PMMA film exhibits a quantum yield (ϕ) more than twice that of the neat solid, as well as a lifetime that is about 4.5 times greater. Based on these data, it is likely that the PMMA film decreases access to a non-radiative decay pathway through its behavior as a rigid matrix.

To further our understanding of the photophysical properties of **8**, we performed a DFT computational study at the BP86-D3 level using the TZP basis set (Figure 3.6). The optimized geometry of the singlet state displays a slightly distorted square planar structure, which is in agreement with the obtained single crystal X-ray structure. The frontier orbital diagram indicates a HOMO and HOMO-1 almost completely localized on the Pt(II) with negligible contribution from the **bc** fragment. Both the LUMO and LUMO+1 are isolated on dtb-bpy, which corroborates the observed ligand-centered phosphorescence of **8** without observed contribution from the **bc** fragment. The optimized geometry of the triplet state, however, reveals an almost tetrahedral structure that is extremely distorted from the favorable square planar geometry seen in the ground state (Figure 3.6). In the excited state, the complex twists via a non-radiative decay pathway, resulting in a large value for k_{nr}. This hypothesis supports the observed decrease in k_{nr} from the pure solid to the PMMA matrix: as the rigidity of the environment increases, the geometry of the molecule will be more difficult to distort. These calculations suggest that future molecular designs should incorporate a large degree of steric bulk to potentially minimize this excited state distortion, thereby improving phosphorescence efficiency in these compounds.
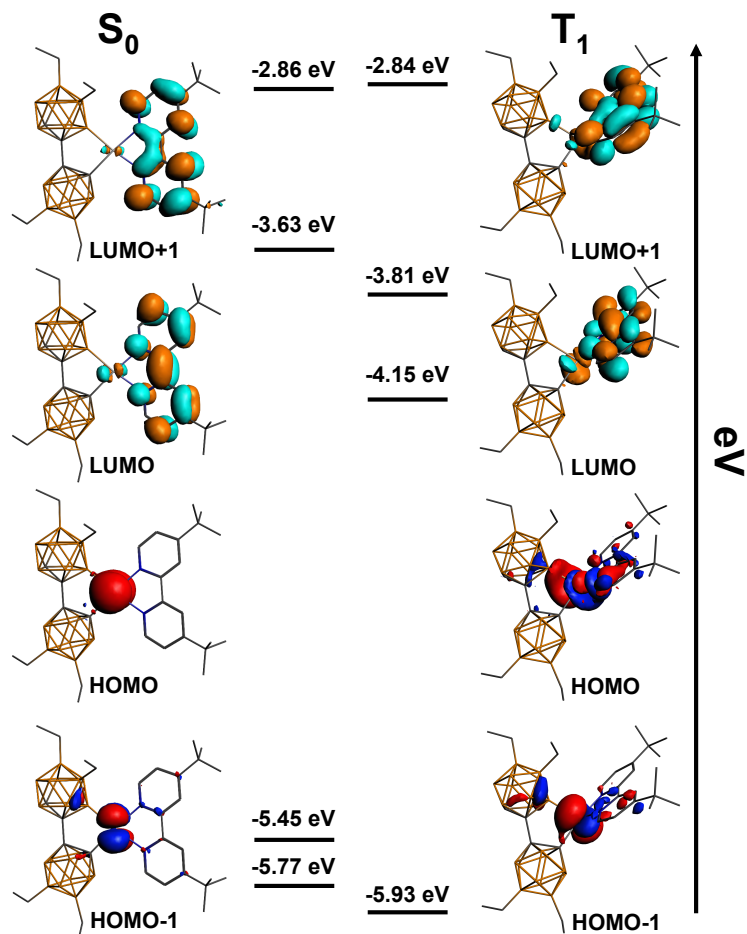
Figure 3.6 Frontier orbitals of **8** based on optimized geometries of S_0 and T_1 states (BP86-D3, TZP).

In general, phosphorescent blue OLEDs suffer from short lifetimes (~600 hours) relative to their red and green counterparts (10^6 hours).[16a] Several groups have previously investigated the degradation of blue OLEDs and found that the decomposition of the phosphorescent dopant molecules occurs during regular use, greatly inhibiting the overall lifetime and efficiency of the device.[16b-e] Thermogravimetric analysis of **8** suggests the **bc** ligand framework remains intact upon heating to 500°C (see Appendix B). This observation suggests that chelating boron cluster scaffolds may be potentially appropriate ligands that can ameliorate previously described stability issues in OLED devices.

3.3 Conclusions

In conclusion, for the first time, we have presented a detailed study on the behavior of 1,1′-bis(*o*-carborane) as a dianionic ligand (**bc**) in group 10 metal complexes. From the synthesis and characterization of model complexes, we have discovered that unlike the structurally reminiscent biphenyl ligand, **bc** displays a unique photophysical innocence and remains uninvolved in relevant photophysical transitions when bound to the group 10 transition metals. Furthermore, since **bc** introduces sufficient steric bulk above and below the square plane of the metal center, it effectively shuts down undesired intermolecular interactions in the solid-state. For Pt(II) complexes featuring phosphorescent emission properties, this unique ligand design aspect allowed us to remove any possible Pt(II)···Pt(II) interactions, which commonly lead to luminescence quenching. The organomimetic[6e,17] properties of carboranes in general, and **bc** in particular, enabled us to rationally tune the processability of a blue phosphorescent emitting Pt(II) species. We are currently investigating the substitution of carborane-based ligands with bulkier functional groups that will minimize the excited state distortion. This work opens a new avenue in designing luminescent materials with improved properties incorporating robust and photophysically innocent multidentate ligand platforms.

3.4 Appendix B

3.4.1 General Considerations

All experiments were performed air and moisture free under an atmosphere of nitrogen using standard Schlenk and cannula techniques. THF used for reactions and MeCN used for cyclic voltammetry was purified and dried using a Grubbs column.[1] All post-Schlenk work-up and characterization was performed under ambient conditions. The "ambient conditions" for this

manuscript refer to room temperature (20 - 25 °C) and uncontrolled laboratory air. Thin-layer chromatography (TLC) samples for carborane-containing compounds were stained with 1 wt. % $PdCl_2$ in 6M HCl and were developed with heat. Elemental analyses were carried out by Atlantic Microlab, Inc. in Norcross, GA.

3.4.2 Materials

Deuterated solvents were purchased from Cambridge Isotope Laboratories and used as received. MilliQ water described in this manuscript refers to purified potable water with a resistivity at 25 °C of ≤18.2 MΩ·cm. $Pd(cod)Cl_2$[2] and $Pt(cod)Cl_2$[3] were made according to literature procedures. O-carborane ($1,2$-$C_2B_{10}H_{12}$) was purchased from Boron Specialties (USA). $K_2[PtCl_6]$, $PdCl_2$, $Ni(dppe)Cl_2$, 1,2-bis(diphenylphosphino)ethane (dppe), 2,2′-bipyridine (bpy), 4,4′-di-*tert*-butyl-2,2′-bipyridine (dtb-bpy), 1,5-cyclooctadiene (cod), iodine, ethyl magnesium bromide, $Pd(PPh_3)_2Cl_2$, and tetrabutylammonium hexafluorophosphate (≥99.0%, electrochemical grade) were purchased from Sigma-Aldrich. Glass-backed Silica Gel 60 GLA TLC plates were purchased from Fisher Scientific. Aluminum oxide (activated, basic, Brockmann Grade I, 58 Å, 60 mesh powder) was purchased from Alfa Aesar. All reagents were used as received unless otherwise indicated.

3.4.3 Instruments

^1H NMR spectra were obtained on a Bruker AV500 or a Bruker AV400 spectrometer; $^{13}C\{^1H\}$ NMR spectra were obtained on a Bruker AV500 spectrometer; ^{11}B and ^{31}P NMR spectra were obtained on a Bruker DRX500 spectrometer. Bruker Topspin software was used to process the NMR data. ^1H and $^{13}C\{^1H\}$ NMR spectra were referenced to residual solvent resonances in deuterated solvents (CD_2Cl_2: ^1H, 5.320 ppm; ^{13}C, 53.840 ppm; $CDCl_3$: ^1H, 7.260 ppm; ^{13}C, 73.840 ppm; THF-d^8: ^1H, 5.020 ppm; ^{13}C, 61.500 ppm; Note: due to high humidity

H_2O resonances are often present). ^{11}B and ^{31}P and NMR spectra were referenced to $BF_3 \cdot Et_2O$ (0 ppm) and H_3PO_4 (0 ppm) standards, respectively. Mass spectrometry data was acquired using a Thermo Instruments Exactive Plus with IonSense ID-CUBE DART source instrument (compound **4a** and **4b**), and a Thermo Scientific[TM] Q-Exactive[TM] Plus instrument with a quadrupole mass filter and Orbitrap mass analyzer (compound **8**). UV−Vis spectra were recorded on a Hewlett-Packard 4853 diode array spectrometer. Phosphorescence lifetime measurements for **8** were performed by a time-correlated single-photon counting method using an IBH fluorocube lifetime instrument equipped with a 405 nm LED excitation source. Quantum yield measurements were carried out using a Hamamatsu C9920 system equipped with a xenon lamp, calibrated integrating sphere, and model C10027 photonic multichannel analyzer. Steady-state emission measurements of **8** as a solid, in the thin film, and in solution at 77 K were performed using a Photon Technology International QuantaMaster spectrofluorimeter.

3.4.4 Preparation of PMMA Thin Films

A solution of PMMA (0.085 g, 120 kDa) in toluene (1.5 mL) was thermally sonicated for 3 hours at 40°C, or until PMMA was completely dissolved. Next, **8** (0.0017 mg, 2 wt. %) was added to the solution and sonicated for 5 minutes, yielding an orange solution. The solution of **8**/PMMA was spin coated on a quartz substrate (3-5 drops, 800-1,000 RPM, 30 seconds), and this was repeated until the film was thick enough emit light under $\lambda = 365$ nm excitation in a dark room under ambient conditions.

3.4.5. Determination of Molar Extinction Coefficients

Extinction coefficients were determined through a series of 5 dilutions with a maximum absorption between 0.1 and 0.7.

3.4.6 X-ray Data Collection and Processing Parameters

For **3a-3c**, **4a**, and **8** a single crystal was mounted on a nylon loop using perfluoropolyether oil and cooled rapidly to 100 K with a stream of cold dinitrogen. Diffraction data were measured using a Bruker APEX-II CCD diffractometer using Mo-$K\alpha$ radiation. The cell refinement and data reduction were carried out using Bruker SAINT and the structure was solved with SHELXS-97. All subsequent crystallographic calculations were performed using SHELXL-2013.

3.4.7 Cyclic voltammetry

Cyclic voltammetry was performed on **8** and using a CH Instruments Model 600D potentiostat with a glassy carbon disc working electrode, platinum wire counter electrode, and Ag/AgCl wire reference in a saturated solution of KCl in MeCN. All experiments were conducted in 0.1M [N^nBu_4]PF_6/MeCN with 0.5 mM analyte concentrations. MeCN solutions were degassed by sparging with argon for 10 minutes, and the cyclic voltammetry was performed under constant flow of argon gas. A scan rate of 0.1 mV/s was used with ferrocene as an internal standard.

3.4.8 DFT Calculations

All optimized geometries were calculated from crystallographic data and optimized with DFT calculations using standard triple-ξ polarization (TZP) basis sets available in the Amsterdam Density Functional 2014.04 Rev. 44409 (ADF)[4] software suite, with Becke[5] and Perdew[6] (BP) Slater-type orbitals (STOs) on a 6 core Apple computer. The local density approximation (LDA) was made with BP and exchange and correlation corrections available by default in the ADF 2014.04 suite. Single point calculations were performed using BP86 level of theory with the Grimme D3 dispersion correction[7] and a TZP basis set. Electron cores were

frozen to 2p for Ni, Pd, and Pt; 1s for B, C, and N; and 2s for P atoms. Electron spins were restricted for S_0 calculations, and electron spins were unrestricted for T_1 calculations. Relativistic correlations were made using Zero-Order Relativistic Approximation (ZORA) for Pt (**3c** and **8**).

3.4.9 Experimental

3.4.9.1 1,1′-Bis(*o*-carborane) (2)

O-carborane (5.00 g, 34.67 mmol) was added to a 500mL Schlenk flask, which was then evacuated and backfilled with N_2 three times. Dry toluene (200 mL) was transferred *via* cannula, and the contents were stirred to give a slightly cloudy white solution. Next, ⁿBuLi (28.4 mL, 71.0 mmol, 2.5 M in hexane) was added slowly *via* syringe. The solution immediately turned milky white and the mixture was allowed to stir at room temperature for 21 hours. CuCl powder (9.44 g, 95.3 mmol) was then added, causing the reaction mixture to immediately turn gray and then dark red over the course of 30 minutes. This suspension was stirred for 3 days, after which toluene was removed by rotary evaporation. CH_2Cl_2 (50 mL) and aqueous HCl (120 mL, 12 M) were added and stirred vigorously for 3 hours, or until the color turned green (indicating the formation of CuCl). The organic layer was separated, and the aqueous layer was washed with CH_2Cl_2 (3 x 100mL). The combined organic fractions were dried over Na_2SO_4, filtered, and dried *in vacuo*, yielding a light brown solid (4.60 g). This crude product was purified by stepwise vacuum sublimation: sublimation under dynamic vacuum (0.20 Torr) at 75°C for 1 hour yielded crystals of unreacted *o*-carborane. After removal, the remaining solid was heated to 180˚C under dynamic vacuum (0.20 Torr) for 1-2 hours. Pure product in the form of white crystals was isolated from the cold finger and dried under vacuum overnight (3.61 g, 73%). **¹H NMR** (CD$_2$Cl$_2$, 500 MHz): δ 3.90 (s, 2H, CH$_{cage}$), 3.40-1.40 (br. m, 18H, BH); **¹¹B NMR** (CD$_2$Cl$_2$, 160

MHz): 2.38 (4B), -8.98 (2B), -10.00 (6B), -11.17 (4B), 12.24 (2B), -13.29 (2B); ^{13}**C NMR** (CD$_2$Cl$_2$, 125 MHz): 72.31, 63.25. Synthesis adapted from Reference 8.

3.4.9.2 9,12-diiodo-o-carborane (5)

To a 200 mL Schlenk flask was added *o*-carborane (2.88 g, 20.0 mmol) and one equivalent I$_2$ (5.08 g, 20.0 mmol). The flask was evacuated and backfilled with N$_2$ at least three times to remove residual moisture. Dry CH$_2$Cl$_2$ (100 mL) was transferred to the reaction vessel *via* cannula and the contents of the flask were stirred to give a purple solution. Next, AlCl$_3$ (0.533 g, 4.0 mmol) was added under positive N$_2$ flow, and the reaction was refluxed until the color fades to pale yellow (~2-3 hours). A second equivalent of I$_2$ (5.08 g, 20.0 mmol) and AlCl$_3$ (0.267g, 2.0 mmol) were added, and the reaction was heated to 45°C and allowed to reflux overnight. The next day, the dark brown reaction mixture was diluted with H$_2$O (50 mL, or until effervescence subsided), and unreacted I$_2$ was quenched with Na$_2$SO$_3$ (0.708 g, 5.62 mmol). After stirring for 10 minutes, the purple organic layer was separated and the aqueous layer was washed with CH$_2$Cl$_2$ (40 mL x 3) and dried over MgSO$_4$. If the solution is still colored, activated charcoal can be added. This solution was passed through a silica plug and eluted with CH$_2$Cl$_2$ to give a light gray solution. Solvent was then removed by rotary evaporation, yielding a lavender solid. The crude product was then sublimed under vacuum (150-160°C, 5-6 hours, 0.20 Torr) to afford a white solid (6.52 g, 82%) on the cold finger, which was isolated and dried under vacuum overnight before further use. Alternatively, the crude product can be purified by recrystallization by layering CH$_2$Cl$_2$ with an equal volume of hexane and storing at -20°C. After 3-4 hours, the white crystals can be filtered off and washed with cold hexane. ^{1}**H NMR** (CDCl$_3$, 500 MHz) δ 3.99 (s, 2H, CH), 3.50-1.80 (m, 9H, BH); ^{11}**B NMR** (CDCl$_3$, 160 MHz): -5.50 (d, 2B), -12.67 (d,

4B), -14.01 (s, 3B), -14.89 (s, 1B); ^{13}C NMR (CDCl$_3$, ppm): 51.71. Synthesis adapted from Reference 9.

3.4.9.3 9,12-diethyl-o-carborane (6)

To a 50 mL Schlenk flask was added 9,12-diiodo-o-carborane (1.98 g, 5.00 mmol) and PdCl$_2$(PPh$_3$)$_2$ (0.07091 g, 0.10 mmol). The flask was left under vacuum for 30 minutes, then backfilled with N$_2$. Dry THF (20 mL) was added *via* cannula, and the flask was stirred in an ice bath for 10 minutes. EtMgBr (7.9 mL, 3.0 M, 23.7 mmol) was then slowly added. The resulting mixture was gently refluxed for 10 days and monitored by GC-MS. The reaction was cooled to room temperature and quenched with H$_2$O, then charged with diethyl ether (150 mL). The organic layer was separated, and the aqueous layer was extracted with diethyl ether (3 x 80mL). Aqueous HCl (5%, 30 mL) was added to the organic layer, and the organic layer was separated and solvent removed *via* rotary evaporation. The crude product was purified *via* silica column chromatography (ethyl acetate:hexanes 1:9). Solvent was removed under vacuum to afford the desired product as a low-melting red solid (0.250g, 31%). ^{1}**H NMR** (CD$_2$Cl$_2$, 500 MHz) δ 3.47 (2H, s, CH$_{cage}$), 3.00-1.20 (8H, br. m, BH), 0.89 (t, 6H, CH$_3$), 0.71 (q, 4H, CH$_2$); ^{11}**B NMR** (CD$_2$Cl$_2$, 160 MHz): 9.64 (s, 2B), -8.43 (d, 2B), -14.24 (d, 4B), -16.21 (d, 2B); ^{13}**C NMR** (CDCl$_3$, 125 MHz): 47.71, 13.52, 9.35 (br). Synthesis adapted from Reference 9.

3.4.9.4 9,9′,12,12′-Tetra-ethyl-1,1′-bis(o-carborane) (7)

To a clean 25 mL Schlenk flask, 9,12-diethyl-o-carborane (0.500 g, 2.50 mmol) was added, and the flask was cooled to -78 °C. The flask was evacuated and backfilled with N$_2$ five times, followed by the addition of dry toluene (10 mL) *via* cannula, yielding a yellow solution. Next, ^{n}BuLi (2.1 mL, 5.25 mmol, 2.5 M in hexanes) was added *via* syringe. The mixture, which immediately turned clear and gradually acquired a yellow color, was allowed to warm and was

89

stirred at room temperature for 24 hours. CuCl was added (0.680 g, 6.87 mmol), and the resulting dark green suspension was allowed to stir for 3 days. Toluene was then removed under reduced pressure, and CH_2Cl_2 (5 mL) and aqueous HCl (15 mL, 10 M) were added and stirred vigorously to quench the resulting dark green reaction mixture. The mixture was allowed to stir until the aqueous layer turned light green (~3 h). The organic layer was separated, and the aqueous layer was washed with CH_2Cl_2 (3 x 15mL). The combined organic fractions were dried over Na_2SO_4, filtered, and concentrated to dryness yielding a yellow-orange solid. The crude product was eluted through a pad of silica with hexanes and concentrated to dryness, yielding a pale yellow solid (0.385 g). Minimal pentane (2-3 mL) was added to the solid and stored in the freezer (-20°C) for recrystallization. The next day, pentane was decanted yielding white crystals. The supernatant was stored in the freezer and decanted after four hours, and this process was repeated once more yielding pure white crystals (Total: 0.231 g, 46%). **^{1}H NMR** (CD_2Cl_2, 500 MHz) δ 3.72 (s, 2H, cage CH), 3.4-1.2 (br. m, 16H, BH), 0.86 (m, 12H, CH_3), 0.69 (m, 8H, CH_2); **^{11}B NMR** (CD_2Cl_2, 160 MHz): 10.04 (s, 4B), -8.58 (d, 4B), -12.09 (m, 12B); **^{13}C NMR** (CD_2Cl_2, 125 MHz): 65.48, 56.19, 13.32, 8.36. Single crystals for X-ray diffraction analysis were grown from a concentrated solution of pentane stored in a freezer at -15 °C overnight.

3.4.9.5 Pd(dppe)Cl$_2$

Pd(cod)Cl$_2$ (0.286 g, 1.00 mmol) and CH_2Cl_2 (6 mL) were combined and stirred in a large *vial* to give a yellow slurry, and 1,2-bis(diphenylphosphino)ethane (dppe, 0.398 g, 1.00 mmol) was then added. The color quickly changed to a lighter shade of yellow. After 15 minutes, hexane (14 mL) was added, and the *vial* was capped and stored in the freezer (-20°C) for 4 hours. The solid was filtered and washed with pentane (5 mL x 3) yielding the pale yellow product

(0.517 g, 90%). **¹H NMR** (CD$_2$Cl$_2$, 400 MHz): 7.87 (8H, m), 7.60 (4H, m), 7.53 (8H, m), 2.47 (4H, d, CH$_2$); **³¹P NMR** (CD$_2$Cl$_2$, 121 MHz): 64.7. Synthesis adapted from Reference 10.

3.4.9.6 Pt(dppe)Cl$_2$

Pt(cod)Cl$_2$ (0.374 g, 1.00 mmol) and CH$_2$Cl$_2$ (6 mL) were combined and stirred in a large *via*l to give a white slurry, and 1,2-bis(diphenylphosphino)ethane (dppe, 0.398 g, 1.00 mmol) was then added. After 15 minutes, hexane (14 mL) was added, and the *via*l was capped and stored in the freezer (-20°C) for 4 hours. The solid was filtered and washed with pentane (5 mL x 3) yielding the white product (0.576 g, 87%). **¹H NMR** (CD$_2$Cl$_2$, 400 MHz): 7.86 (8H, m), 7.56 (4H, m), 7.52 (8H, m), 2.36 (4H, d, CH$_2$); **³¹P NMR** (CD$_2$Cl$_2$, 121 MHz): 41.8 ($^1J_{Pt-P}$ = 3622 Hz). Synthesis adapted from the synthesis for **Pd(dppe)Cl$_2$** in Reference 10.

3.4.9.7 Pt(dtb-bpy)Cl$_2$

Pt(cod)Cl$_2$ (0.350 g, 0.935 mmol), 4,4′-ditertbutyl-2,2′-bipyridine (dtb-bpy, 0.251 g, 0.935 mmol), and 8 mL methanol were stirred in a sealed tube at 75°C for 22 hours. As the suspension warmed up, the color changed to yellow-orange and eventually turned bright yellow. The tube was cooled to room temperature in a water bath and the yellow solid was filtered. After washing with diethyl ether (3 mL x 5) to remove 1,5-cyclooctadiene, the yellow product was dried under vacuum overnight (0.458 g, 92%). **¹H NMR** (CD$_2$Cl$_2$, 500 MHz): 9.52 (2H, d), 7.91 (2H, d), 7.57 (2H, dd), 1.44 (18H, s, CH$_3$); **¹³C NMR** (CD$_2$Cl$_2$, 126 MHz): 164.9, 157.2, 149.3, 124.8, 119.9, 36.2, 30.3. Synthesis adapted from Reference 11.

3.4.9.8 Ni(bc)(dppe) (3a)

1,1′-Bis-(*o*-carborane) (0.100 g, 0.349 mmol) was added to a 10 mL Schlenk flask, which was then evacuated and backfilled with N$_2$ three times. Dry THF (4 mL) was transferred to the

flask *via* cannula to give a clear solution. While stirring at room temperature, ^{n}BuLi (0.45 mL, 1.6 M, 0.72 mmol) was added drop-wise *via* syringe, giving a dark yellow solution. The reaction was then heated at 60°C for 3 hours, and the color slowly turned to a lighter yellow. After 3 hours, the flask was allowed to cool to room temperature yielding a golden-yellow solution. To a separate 25 mL Schlenk flask was added Ni(dppe)Cl$_2$ (0.184 g, 0.349 mmol), and the flask was evacuated and backfilled with N$_2$ three times. Dry THF (20 mL) was then transferred *via* cannula to give a red-orange slurry. This flask was cooled to -78 °C and stirred for 5 minutes. The dilithio-bis-carborane mixture was added dropwise (~1 mL/min) to the cold Ni(dppe)Cl$_2$ slurry, and the reaction was allowed to warm up to room temperature and react overnight, giving a deep orange solution the following day. The solvent was removed *via* rotary evaporation after 18 hours, and the orange solid was dissolved in 5-10 mL CH$_2$Cl$_2$ and passed through a pad of Celite. After removal of solvent, crude orange product (0.160 g) remained and was purified *via* column chromatography: a wide 60 mL filter frit was loaded halfway with silica in hexanes, and the crude product was dissolved in the minimum amount of 1:1 CH$_2$Cl$_2$:hexanes (R$_f$ = 0.50) and loaded on the silica. Any unreacted bis-carborane (R$_f$ = 0.90) can be removed as the initial clear/light yellow elution, and the desired product can be cleanly collected as the orange band that follows. The orange solution was concentrated to dryness to give a yellow solid (0.125 g, 49%) that was dried under vacuum overnight. **^{1}H NMR** (CD$_2$Cl$_2$, 500 MHz) δ 7.77 (br. t, 8H, Ar), 7.64 (t, 4H, Ar), 7.54 (t, 8H, Ar), 4.0-0.6 (br. m, 20H, BH), 2.0 (d, 4H, CH$_2$, $^2J_{PH}$ = 15.60 Hz); **^{11}B NMR** (CD$_2$Cl$_2$, 160 MHz) -1.96 (d, 2B), -3.83 (d, 2B), -8.35 (d, 12B), -10.62 (m, 4B); **^{13}C NMR** (CD$_2$Cl$_2$, 125 MHz) 134.62 (t, $^2J_{PC}$ = 5.2 Hz), 132.51, 129.46 (t, $^3J_{PC}$ = 5.2 Hz), 127.78 (m), 87.31 (dd, $^2J_{PC(trans)}$ = 91.8 Hz, $^2J_{PC(cis)}$ = 38.4 Hz), 84.70, 28.28 (t, $^1J_{PC}$ = 21.5 Hz); **^{31}P{^{1}H} NMR** (CD$_2$Cl$_2$, 202 MHz): 49.09. NMR chemical shifts comparable to those in

Reference 12. Single crystals for X-ray diffraction analysis were grown from slow vapor diffusion of diethyl ether into dichloromethane. Elemental analysis (including 0.5 CH_2Cl_2) found (calculated for $C_{30.5}H_{45}B_{20}ClNiP_2$): C, 46.40 (46.73); H, 5.89 (5.79).

3.4.9.9 Pd(bc)(dppe) (3b)

1,1′-Bis-(o-carborane) (0.100 g, 0.349 mmol) was added to a 10 mL Schlenk flask, which was then evacuated and backfilled with N_2 three times. Dry THF (4 mL) was transferred to the flask *via* cannula to give a clear solution. While stirring at room temperature, ^{n}BuLi (0.45 mL, 1.6 M, 0.72 mmol) was added dropwise *via* syringe, giving a dark yellow solution. The reaction mixture was then heated at 60°C for 3 hours, and the color slowly turned lighter yellow. After 3 hours, the flask was allowed to cool to room temperature yielding a golden-yellow solution. Pd(dppe)Cl$_2$ (0.202 g, 0.349 mmol) was added to a separate 25mL Schlenk flask, which was then evacuated and backfilled with N_2 three times. Dry THF (20 mL) was then transferred *via* cannula to give a white slurry. This flask was cooled to -78°C and stirred for 10 minutes. The dilithio-bis-carborane solution was added dropwise (~1 mL/min) to the cold Pd(dppe)Cl$_2$ slurry, and the reaction was allowed to warm up to room temperature and stir overnight, giving a deep orange mixture the following day. THF was removed *via* rotary evaporation after 20 hours, and the remaining orange solid was dissolved in 5-10 mL CH_2Cl_2 and passed through a pad of Celite. After removal of solvent *in vacuo*, crude orange product (0.225 g) remained and was purified *via* column chromatography. A wide 60 mL filter frit was loaded halfway with silica in hexanes, and the crude product was dissolved in minimal 1:1 CH_2Cl_2:hexanes (R_f = 0.50) and loaded on the silica. Any unreacted bis-carborane (R_f = 0.90) can be removed as the initial clear/light yellow elution, and the desired product can be cleanly collected as the orange band that follows. The orange solution was concentrated to dryness to give an orange solid (0.70 g, 25%) that was dried

under vacuum overnight. **^{1}H NMR** (CD$_2$Cl$_2$, 500 MHz) δ 7.64 (t, 4H, Ar), 7.62 (t, 8H, Ar), 7.55 (t, 8H, Ar), 3.6-0.6 (br. m, 20H, BH), 2.12 (d, 4H, CH^2, $^2J_{PH}$ = 20.4 Hz); **^{11}B NMR** (CD$_2$Cl$_2$, 160 MHz) -3.20 (m, 4B), -8.74 (m, 16B); **^{13}C NMR** (CD$_2$Cl$_2$, 125 MHz) 134.57 (t, $^2J_{PC}$ = 5.6 Hz), 132.74, 129.64 (t, $^3J_{PC}$ = 5.4 Hz), 127.13, 91.90 (dd, $^2J_{PC(trans)}$ = 138.7 Hz, $^2J_{PC(cis)}$ = 14.7 Hz), 84.80, 28.82 (t, $^1J_{PC}$ = 22.3 Hz); **^{31}P{^{1}H} NMR** (CD$_2$Cl$_2$, 202 MHz) 51.63. Single crystals for X-ray diffraction analysis were grown by cooling a concentrated solution of hot benzene to room temperature. Elemental analysis found (calculated for C$_{30}$H$_{44}$B$_{20}$PdP$_2$): C, 45.80 (45.65); H, 5.89 (5.62).

3.4.9.10 Pt(bc)(dppe) (3c)

1,1′-Bis-(*o*-carborane) (0.100 g, 0.349 mmol) was added to a 10 mL Schlenk flask, which was then evacuated and backfilled with N$_2$ three times. Dry THF (4 mL) was transferred to the flask *via* cannula to give a clear solution. While stirring at room temperature, ^{n}BuLi (0.45 mL, 1.6 M, 0.72 mmol) was added drop-wise *via* syringe, giving a dark yellow solution. The reaction was then heated at 60°C for 3 hours, and the color slowly turned lighter yellow. After 3 hours, the flask was allowed to cool to room temperature yielding a golden-yellow solution. Pt(dppe)Cl$_2$ (0.234 g, 0.349 mmol) was added to a separate 25mL Schlenk flask, which was then evacuated and backfilled with N$_2$ three times. Dry THF (15 mL) was then transferred *via* cannula to give a white slurry. This flask was cooled to -78°C and stirred for 10 minutes. The dilithio-bis-carborane solution was added dropwise (~1 mL/min) to the cold Pt(dppe)Cl$_2$ slurry, and the reaction was allowed to warm up to room temperature and stir overnight, giving a deep orange solution the following day. The orange solution was passed through a pad of Celite and washed with THF. The filtrate was then dried *via* rotary evaporation to yield a brown-orange solid. This solid was dissolved in 5-10 mL CH$_2$Cl$_2$ and passed through a pad of Celite. After removal of

solvent, crude orange product (0.225 g) remained and was purified *via* column chromatography through a pad of basic alumina. A wide 60 mL filter frit was loaded halfway with basic alumina in CH_2Cl_2, and the crude product was dissolved in minimal CH_2Cl_2 ($R_f = 0.90$) and loaded on the basic alumina. The orange filtrate (mix of product and unreacted bis-carborane) was collected, and the volume was reduced to about 1-2 mL *via* rotary evaporation. Next, 5-10 mL hexanes was added, causing a yellow solid to crash out. This solid was filtered and washed with hexanes (3 x 5 mL) and dried under vacuum for 24 hours to afford **3c** as a yellow powder (0.082 g, 27%). **^{1}H NMR** (CD_2Cl_2, 500 MHz) δ 7.70 (m, 8H, Ar), 7.63 (t, 4H, Ar), 7.55 (m, 8H, Ar), 3.5-0.7 (br. m, 20H, BH), 2.07 (d, 4H, CH_2, $^2J_{PH} = 17.7$ Hz); **^{11}B NMR** (CD_2Cl_2, 160 MHz): -3.67 (m, 4B), -8.08 (m, 16B); **^{13}C NMR** (CD_2Cl_2, 125 MHz) 134.75 (t, $^2J_{PC} = 5.4$ Hz), 132.69, 129.48 (t, $^3J_{PC} = 5.5$ Hz), 126.77 (m), 84.57, 89.12 (dd, bis-carborane C-Pt, $^2J_{PC(trans)} = 128.4$ Hz, $^2J_{PC(cis)} = 8.34$ Hz), 29.86 (m); **^{31}P{^{1}H} NMR** (CD_2Cl_2, 202 MHz): 41.44 (s, $^1J_{PtP} = 2493$ Hz). Single crystals for X-ray diffraction analysis were grown from slow vapor diffusion of diethyl ether into dichloromethane. Elemental analysis found (calculated for $C_{30}H_{44}B_{20}PtP_2$): C, 40.55 (41.04); H, 5.05 (4.80).

3.4.9.11 Pt(bc)(dtb-bpy) (4a and 4b)

2 (0.080 g, 0.279 mmol) was charged to a 10mL Schlenk flask, which was then evacuated and backfilled 3 times with N_2. Dry THF (3 mL) was added *via* cannula and the solution was stirred, followed by the addition of ^{n}BuLi (0.36 mL, 1.6 M, 0.576 mmol) at room temperature. The flask was heated at 60°C for 3 hours and then cooled to room temperature. Pt(dtb-bpy)Cl_2 (dtb-bpy = 4,4'-di-*tert*-butyl-2,2'-bipyridine, 0.149 g, 0.279 mmol) was charged to a separate 50mL Schlenk flask, which was evacuated and backfilled 3 times with N_2. Next, dry THF (20 mL) was added, and the resulting yellow slurry was cooled to -78°C. The mixture of Li_2[**bc**] was

added dropwise to the cooled slurry. The reaction mixture was allowed to warm up to room temperature and was heated to 60°C. The reaction mixture slowly turned from bright yellow to dark brown/black. After 21 hours, the solvent was moved *via* rotary evaporation to yield a yellow-brown solid. This solid was washed with CH_2Cl_2 (3 x 10 mL), yielding a gray solid (0.082 g) that was emissive under UV excitation (λ_{exc} = 365 nm). To this solid was added 5 mL hot 1,2-difluorobenzene, and this dark brown slurry was heated with a heat gun the solid completely dissolved. Next, the solution was passed through a pad of Celite, yielding a yellow-orange solution with black precipitate at the top of the Celite. This procedure was repeated two more times. The filtrate was dried *in vacuo*, and the pale orange solid was dried under vacuum overnight (0.055 g, 26%). ^1H NMR suggests a 1.0:1.4 mix of κ^2-B,C-bound (**4a**) and κ^2-C,C-bound (**4b**) isomers. Single crystals of **4a** for X-ray diffraction analysis were by cooling a concentrated solution of hot 2-MeTHF to room temperature. Attempts to reproduce this result led to products with various mixes of isomers, including both a majority κ^2-B,C-bound isomer and a majority κ^2-C,C-bound isomer, as evidenced by the ^1H NMR spectrum of the aryl region (See NMR spectra). HRMS (DART): m/z calculated for $C_{22}H_{44}B_{20}N_2Pt$ [M+H]$^+$, 748.5237 Da; found, 748.5246 Da.

4a: **^{1}H NMR** (THF-d^8, 500 MHz) δ 9.44 (d, 2H, Ar), 8.39 (d, 2H, Ar), 7.92 (dd, 2H, Ar), 3.1-1.0 (br. m, 20H, BH), 1.44 (s, 18H, ^{t}Bu); **^{13}C NMR** (THF-d^8, 125 MHz) 166.32, 157.51, 151.77, 124.54, 121.02, 82.92, 81.01, 36.06, 30.13.

4b: **^{1}H NMR** (THF-d^8, 500 MHz) δ 9.83 (d, 1H, Ar), 9.27 (d, 1H, Ar), 8.41 (d, 1H, Ar), 8.37 (d, 1H, Ar), 7.97 (dd, 1H, Ar), 7.84 (dd, 1H, Ar), 4.47 (s, 1H, CH$_{bis-carborane}$), 3.2-1.6 (br m, 20H, BH), 1.459 (9H, s, ^{t}Bu), 1.457 (9H, s, ^{t}Bu); **^{13}C NMR** (THF-d^8, 125 MHz) 165.44, 165.00,

157.99, 156.52, 154.24, 150.23, 125.15, 124.52, 121.12, 120.36, 85.17, 77.03, 70.52, 68.19, 36.53, 36.46, 30.27, 30.14.

Note: ^{11}B NMR chemical shifts for 4a and 4b overlap, so values for the mixture are reported. **^{11}B NMR** (THF-d[8], 160 MHz) -4.01 (4B), -8.79 (8B), -11.15 (8B).

3.4.9.12 Pt(tebc)(dtb-bpy) (8)

7 (0.0689 g, 0.171 mmol, **tebc**) was charged to a 10mL Schlenk flask, which was then evacuated and backfilled 3 times with N_2. Dry THF (2 mL) was added *via* cannula and the solution was stirred, followed by the slow addition of [n]BuLi (0.22 mL, 1.6 M, 0.351 mmol) at room temperature. The flask was heated at 60°C for 3 hours and then cooled to room temperature. Pt(dtb-bpy)Cl$_2$ (dtb-bpy = 4,4'-di-*tert*-butyl-2,2'-bipyridine, 0.0914 g, 0.171 mmol) was charged to a separate 25mL Schlenk flask, which was evacuated and backfilled 3 times with N_2. Next, dry THF (15 mL) was added, affording a yellow slurry, which was cooled to -78°C. The mixture containing [Li$_2$·(**tebc**)] was added dropwise to the cooled slurry. The reaction mixture was allowed to warm up to room temperature and was then heated at 60°C for 60 hours. The reaction slowly turned from bright yellow to yellow-brown. After 60 hours, the solvent was moved *via* rotary evaporation to yield a yellow-brown solid. This solid was dissolved in diethyl ether and passed through a pad of Celite, and the filtrate was then dried *in vacuo*. Next, the resulting solid was washed with cold pentane (5 x 2 mL), yielding a pale orange solid. The solid was dissolved in CH$_2$Cl$_2$ and passed through a silica plug. The filtrate was dried *in vacuo*, and the resulting solid was dried under vacuum overnight (0.063 g, 43%). **^{1}H NMR** (CD$_2$Cl$_2$, 500 MHz) δ 9.56 (d, 1H, Ar), 9.36 (d, 1H, Ar), 8.08 (d, 1H, Ar), 8.02 (d, 1H, Ar), 7.68 (dd, 1H, Ar), 7.47 (dd, 1H, Ar), 3.87 (s, 1H, CH$_{bis-carborane}$), 3.3-1.2 (16H, br. m, BH), 1.45 (9H, s, [t]Bu), 1.43 (9H, s, [t]Bu), 1.02-0.82 (m, 12H, CH$_2$CH_3), 0.56-0.79 (m, 8H, CH$_2$); **^{11}B NMR** (CD$_2$Cl$_2$, 160

MHz) 7.74 (m, 4B), -8.46 (s, 8B), -11.25 (s, 4B), -13.81 (s, 4B); ^{13}C **NMR** (CD_2Cl_2, 125 MHz) 164.12 (s, C^2 dtb-bpy, C—Pt_{trans}), 163.58, 157.22, 155.85, 155.19, 149.79, 123.99, 123.77, 120.02, 119.17, 76.63, 73.20, 59.56, 55.39, 35.98, 35.90, 30.36, 30.23 (d, *tert*-butyl CH_3, $J =$ 16.2 Hz), 13.95, 13.71, 13.57, 13.51, (ethyl CH_3), 9.11 (br. m, ethyl CH_2). Single crystals for X-ray diffraction analysis were grown the slow evaporation of diethyl ether over the course of one week. HRMS (Orbitrap): m/z calculated for $C_{30}H_{64}B_{20}N_2Pt$ [M$^-$], 863.6724 Da; found, 863.0652 Da.

3.4.9.13 [NEt$_4$]$_2$[Pd(bc)$_2$]

2 (0.100 g, 0.349 mmol) was added to a 25 mL Schlenk flask, which was then evacuated and backfilled with N_2 three times. Dry THF (4 mL) was transferred to the flask *via* cannula, generating a clear solution. While stirring at room temperature, ^{n}BuLi (0.45 mL, 1.6 M, 0.72 mmol) was added dropwise *via* syringe to give a dark yellow solution. The reaction was then heated to 60°C for 3 hours, and the color slowly turned lighter yellow. After 3 hours, the flask was cooled to room temperature, and under positive N_2 flow, $PdCl_2$ (0.0309 g, 0.175 mmol) was added. The temperature was increased to 60°C and the mixture was allowed to stir for 21 hours. The reaction was cooled to room temperature, passed through a pad of Celite, and the filtrate was dried *in vacuo*. The resulting brown solid was then dissolved in H_2O (10 mL). To this solution was added a solution of tetraethylammonium bromide (NEt$_4$Br, 0.0736 g, 0.349 mmol) dissolved in 2 mL H_2O, and brown solid immediately precipitated. The solid was filtered and washed with H_2O (3 x 10 mL) was then dissolved in CH_2Cl_2 and dried over Na_2SO_4. The mixture was filtered and the solvent removed *via* rotary evaporation. Next, the solid was dissolved in minimal CH_2Cl_2 and loaded on silica. The plug was flushed with CH_2Cl_2 (100 mL) to remove side products, and then flushed with acetone (50 mL) to collect the product. Solvent was removed *via* rotary

evaporation, and the brown solid was vacuum dried (0.059 g, 25%). *Note: We believe B—H activation and/or deboronation may be occurring under the given reaction conditions for [NEt4]2[Pd(bc)2]; however, the ^{11}B NMR spectrum for [NEt4]2[Pd(bc)2] isolated under these conditions are in agreement with the ^{11}B NMR spectrum for the side product isolated during the synthesis of 3b (see Figure B7 below).* **^{1}H NMR** (CD$_2$Cl$_2$, 500 MHz) δ 3.4-1.0 (br. m, 20H, BH), 3.21 (q, 16H, CH$_2$), 1.35 (tt, 24H, CH$_3$); **^{11}B NMR** (CD$_2$Cl$_2$, 160 MHz) -2.66 (m, 9B), -9.31 (m, 26B),-16.75 (2B), -22.07 (2B), -32.64 (0.5B), -35.11 (0.5B); **^{13}C NMR** (CD$_2$Cl$_2$, 125 MHz) 125.77, 82.77, 82.39, 72.30, 65.49, 65.22, 63.25, 34.46, 30.44, 30.05, 7.87. Elemental analysis found (calculated for C$_{24}$H$_{80}$B$_{40}$N$_2$Pd): C, 32.68 (30.81); H, 8.58 (8.62).

3.4.9.14 [NEt4]2[Pt(bc)2]

2 (0.100 g, 0.349 mmol) was added to a 25 mL Schlenk flask, which was then evacuated and backfilled with N$_2$ three times. Dry THF (4 mL) was transferred to the flask *via* cannula, generating a clear solution. While stirring at room temperature, [n]BuLi (0.45 mL, 1.6 M, 0.72 mmol) was added dropwise *via* syringe to give a dark yellow solution. The reaction mixture was then heated at 60°C for 3 hours, and the color slowly turned lighter yellow. After 3 hours, the flask was cooled to -78°C, and under positive N$_2$ flow, Pt(cod)Cl$_2$ (cod = 1,5-cyclooctadiene, 0.065 g, 0.175 mmol) was added. The temperature was increased to 60°C and the resulting mixture was allowed to stir for 21 hours. The resulting dark brown mixture was allowed to cool to room temperature and was passed through a pad of Celite. The filtrate was dried *in vacuo*. The resulting solid was then dissolved in H$_2$O (10 mL). To this solution was added a solution of tetraethylammonium bromide (NEt$_4$Br, 0.0736 g, 0.349 mmol) dissolved in 2 mL H$_2$O, and dark green solid immediately precipitated. The solid was filtered and washed with H$_2$O (3 x 10 mL) and was then dissolved in CH$_2$Cl$_2$ and dried over Na$_2$SO$_4$. The dark brown solution was filtered

and the solvent removed *via* rotary evaporation. Next, the solid was dissolved in minimal CH_2Cl_2

and loaded on silica. The plug was flushed with CH_2Cl_2 (100 mL) to remove side products, and

then flushed with acetone (50 mL) to collect the product. Solvent was removed *via* rotary

evaporation, and the resulting brown solid was vacuum dried (0.182 g, 68%). *Note: We believe*

B—H activation and/or deboronation may be occurring under the given reaction conditions for

***[NEt$_4$]$_2$[Pt(bc)$_2$]**; however, the ^{11}B NMR spectrum for **[NEt$_4$]$_2$[Pt(bc)$_2$]** isolated under these*

conditions are in agreement with the ^{11}B NMR spectrum for the side product isolated during the

*synthesis of **3c** (see Figure B7 below).* **^{1}H NMR** (CD_2Cl_2, 500 MHz): 3.3-1.0 (br. m, 20H, BH),

3.21 (q, 16H, CH_2), 1.35 (tt, 24H, CH_3); **^{11}B NMR** (CD_2Cl_2, 160 MHz) -2.84 (m, 8B), -9.45 (m,

25H), -16.94 (d, 4B), -22.25 (d, 2B), -32.77 (d, 0.5B), -35.21 (d, 0.5B); **^{13}C NMR** (CD_2Cl_2, 125

MHz) 72.31, 71.22, 65.43, 63.26, 29.88, 22.72, 14.21, 7.86. Elemental analysis found (calculated

for $C_{24}H_{80}B_{40}N_2Pt$): C, 31.37 (28.14); H, 7.56 (7.87).

3.4.10 Supplementary Figures and Tables
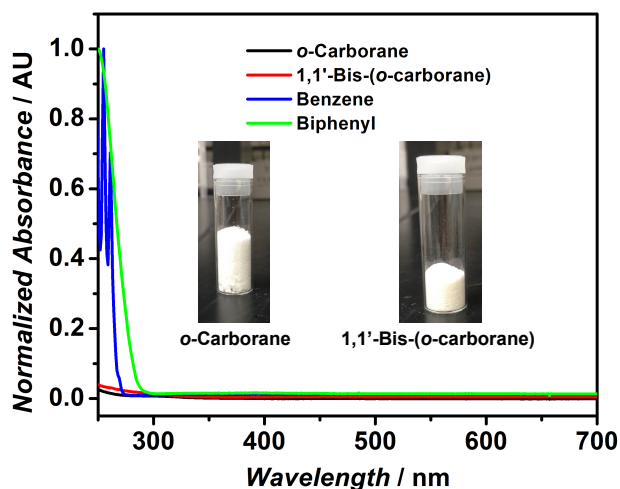
Figure B1 UV-Vis absorption spectrum of **1** and **2**. Solutions were made to 0.002 M concentration.
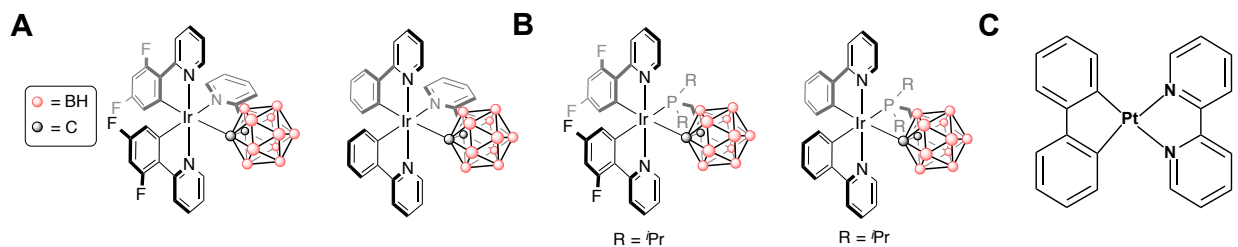
Figure B2 Structures of luminescent compounds mentioned in Chapter 3. (A) Ir(III) compounds containing a κ^2-C,N-bound 1-(2-pyridyl)-*o*-carboranyl ligand (reference 13, Appendix B); (B) Ir(III) compounds containing a κ^2-C,P-bound 1-(^{i}Pr$_2$PCH$_2$)-*o*-carboranyl (reference 14, Appendix B); (C) Pt(bph)(bpy) where bph = biphenyl and bpy = 2,2′-bipyridine (reference 15, Appendix B).
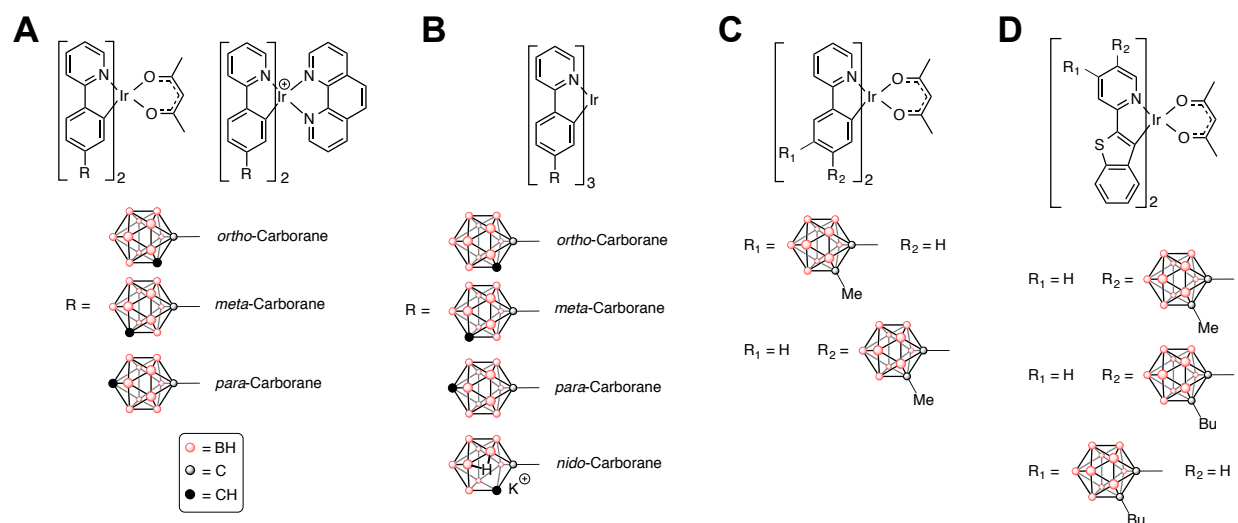
Figure B3 Structures of Ir(III) compounds that contain *ortho*-, *meta*-, *para*, and *nido*-carborane as substituents. (A) Reference 16; (B) Reference 17; (C) Reference 18; (D) Reference 19.

	3a	3b	3c
Ni(bc)(dppe)	Pd(bc)(dppe)	Pt(bc)(dppe)	
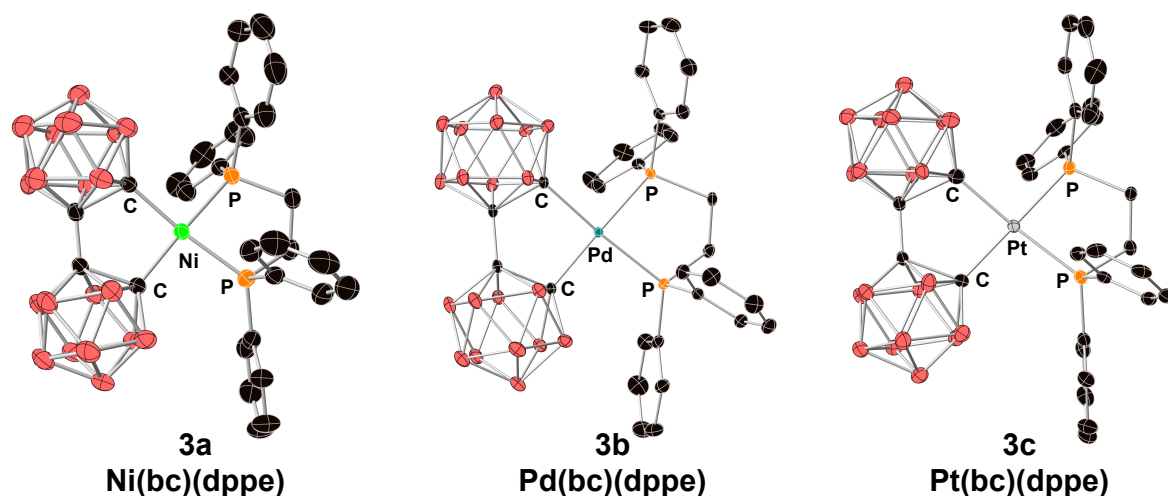
Figure B4 Thermal ellipsoid plots of **3a-3c** at 50% probability.

Table B1 Selected bond distances and angles for **3a–3c**.

Parameter	3a	3b	3c
M-C1 (Å)	2.007	2.097	2.090
M-C4 (Å)	1.995	2.103	2.093
C1-C2 (Å)	1.694	1.688	1.744
C2-C3 (Å)	1.514	1.531	1.514
C3-C4 (Å)	1.694	1.690	1.728
M-P1 (Å)	2.253	2.312	2.297
M-P2 (Å)	2.243	2.304	2.310
C1-M-C4 (°)	90.82	88.20	86.88
M-C1-C2 (°)	111.25	111.60	113.48
C1-C2-C3 (°)	113.04	114.43	112.52
C2-C3-C4 (°)	113.40	114.18	113.69
C3-C4-M (°)	111.43	111.51	113.36
C1-M-P2 (°)	171.46	174.30	173.20
C4-M-P1 (°)	172.40	174.71	173.05
M-M (Å)	10.976	12.176	8.685
C1-C4 (Å)	2.850	2.923	2.876
C1-C2-C3-C4 dihedral	-0.2	-2.91	0.59
C1-C2-C3-C4-M sum of angles (°)	539.94	539.92	539.93

Table B2 Selected bond distances and angles for **3a–3c** and the average bond distances and angles of corresponding M(bph)(P^P) complexes.

Parameter	3a	Avg. Ni(bph)(P^P)	3b	Avg. Pd(bph)(P^P)	3c	Avg. Pt(bph)(P^P)
M-C1 (Å)	2.007	1.960	2.097	2.050	2.090	2.050
M-C4 (Å)	1.995	1.940	2.103	2.050	2.093	2.030
C1-M-C4 (°)	90.82	83.25	88.20	80.82	86.88	80.66
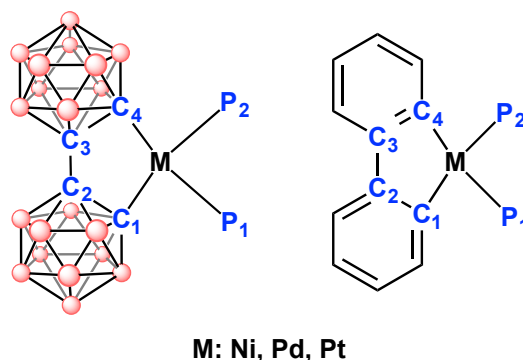
M: Ni, Pd, Pt

Figure B5 Numbering scheme for values presented in Table B1 and Table B2. Left: M = Ni, **3a**; M = Pd, **3b**; M = Pt, **3c**. Right: M(bph)(P^P), where M = Ni, Pd, Pt and (P^P) = chelated diphosphine ligand.

To demonstrate that the bc framework is structurally similar to the biphenyl (bph) framework, we compared bond distances, angles, and molecular geometries of M(bc)(dppe) to those of a series of cyclometallated M(bph)(P^P) in reported X-ray crystal structures.[20] X-ray quality crystals of **3a-3c** were grown using slow evaporation of diethyl ether, vapor diffusion of diethyl ether into dichloromethane, or cooling of a concentrated solution of hot benzene. For **3a-3c**, the M—C bond is about 0.05 Å longer than the average M—C bond in corresponding biphenyl complexes. Of the three complexes **3a-3c**, the Ni—C bond (**3a**) is the shortest M—C bond at 2.00 Å, and both Pd—C (**3b**) and Pt—C (**3c**) bond lengths are about 2.09 Å. These observations are consistent with Ni possessing the smallest atomic radius and Pd and Pt exhibit similar atomic radii due to the lanthanide contraction for Pt.[21]

The C1—M—C4 bond angles decrease as the size of the metal atom increases, which compares well with analogous Group 10 bph complexes. However, the trend is more pronounced

in the **bc** series with this angle being 6-8° larger than the average C1—M—C4 angle in the biphenyl complexes. The C1—C2—C3—C4 dihedral angles of 0.20°, 2.91°, and 0.59° for **3a**, **3b**, and **3c**, respectively, suggest the chelation of **2** leads to a minimally distorted square planar structure. The C1—C4 distances between the two metal-bound carbons fall within a range of 0.07 Å of each other (2.850 Å to 2.923 Å), indicating the larger C1—M—C4 angle is likely a structural characteristic of **2**. For comparison, the average corresponding C1—C4 distance in M(bph)(P^P) complexes is about 0.2 Å shorter at 2.662 Å, further rationalizing the more acute C1—M—C4 angles seen in those bph complexes. Furthermore, the **bc** C1—M—C4 bond angles are larger than all reported C1—M—C4 bond angles for M(bph)(P^P) complexes. Compounds **3a-3c** have C—M—P$_{trans}$ angles of 171-174°, making them slightly distorted square planar complexes. These values are comparable to those of the reported cyclometallated M(bph)(P^P) compounds, indicating that **bc** does not influence the intramolecular geometry much differently than biphenyl.
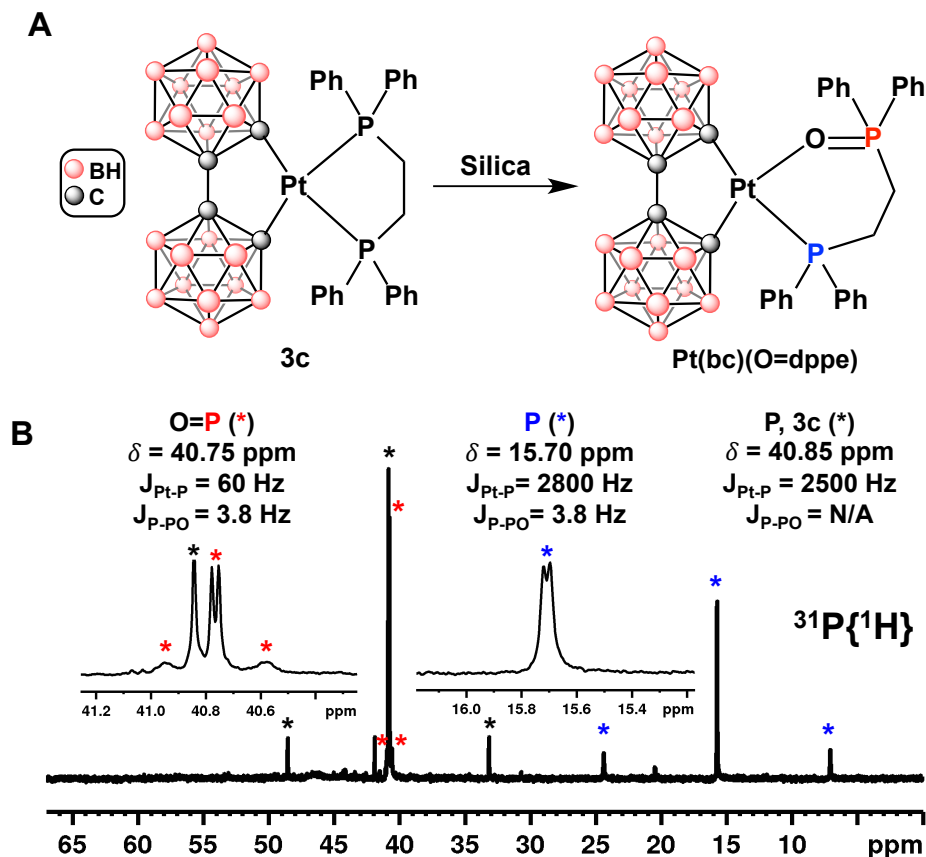
Figure B6 (A) Reaction scheme for the oxidation of **3c** on silica to form **Pt(bc)(O=dppe)**. (B) $^{31}P\{^{1}H\}$ NMR spectrum of the product **Pt(bc)(O=dppe)** isolated after passing **3c** through a short plug of silica eluted with CH_2Cl_2. Insets show expanded regions of the ^{31}P NMR spectrum corresponding to each of the phosphorous atoms in the dppe ligand. Asterisks correspond to the ^{31}P peak and Pt—P satellites for each phosphorous: black = both P atoms in **3c**; red = O=P in **Pt(bc)(O=dppe)**; blue = P in **Pt(bc)(O=dppe)**.

The purification of **3c** proved troublesome as one of the P—Pt bonds easily underwent oxidation on silica, forming the monooxidized dppe species as evidenced by the formation of 2 doublets with unique $^{1}J_{Pt-P}$ values in the $^{31}P\{^{1}H\}$ NMR spectrum. For the oxidized P (O=P, red in Figure 3A), $\delta = 40.75$ ppm with $^{2}J_{Pt—P} = 60$ Hz and $^{3}J_{P—PO} = 3.8$ Hz. For the unoxidized P (P, blue in Figure 3A), $\delta = 15.70$ ppm with $^{1}J_{Pt—P} = 2800$ Hz and $^{3}J_{P—PO} = 3.8$ Hz. These chemical shifts and coupling constants are similar to those for compounds **2a** and **2b** in Reference 22. Purifying the crude reaction mixture for **3c** *via* column chromatography with basic alumina yielded the unoxidized, isolated compound at 27% yield.
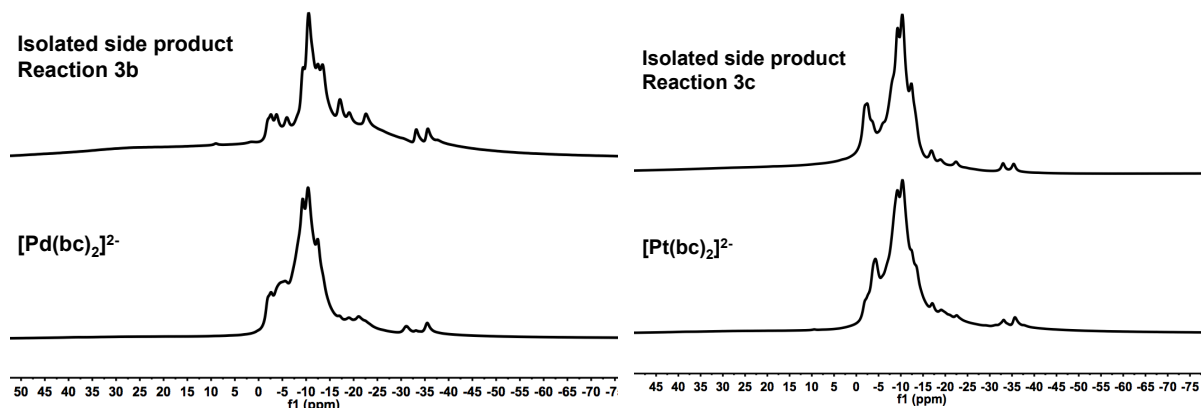
Figure B7 Left: Stacked ^{11}B{^{1}H} NMR spectra for the $[Pd(bc)_2]^{2-}$ side product isolated during the synthesis of **3b** (top) and independently synthesized $[Pd(bc)_2]^{2-}$ (see experimental). Right: Stacked ^{11}B{^{1}H} NMR spectra for the $[Pt(bc)_2]^{2-}$ side product isolated during the synthesis of **3c** (top) and independently synthesized $[Pt(bc)_2]^{2-}$ (see experimental).

For each reaction, the other major by-product is $[M(bc)_2]^{2-}$ (where M = Ni, Pd, Pt), which is isolated *via* silica column chromatography. The formation of this di-substituted complex is likely due to the low concentration of M(dppe)Cl$_2$ relative to newly generated and more soluble M(bc)(dppe) under the reaction conditions, making M(bc)(dppe) more prone to a second nucleophilic attack from the **Li$_2$-[bc]**. The ^{11}B NMR of the isolated reaction product for **3b** and **3c** matched the ^{11}B NMR of the independently synthesized $[Pd(bc)_2]^{2-}$ and $[Pt(bc)_2]^{2-}$ complexes (Figure B5), supporting our hypothesis.

We believe B—H activation and/or deboronation may be occurring under the given reaction conditions for $[Pd(bc)_2]^{2-}$ and $[Pt(bc)_2]^{2-}$, and that the reaction product contains admixtures of ***closo-nido*-[bc]** and/or its metalation products. Kazakov and coworkers have reported the partial deboronation of **2** in the presence of water,[23] and their reported ^{11}B NMR chemical shifts are similar to those observed in for $[Pd(bc)_2]^{2-}$ and $[Pt(bc)_2]^{2-}$ (Figure B7). However, the ^{11}B NMR spectra for $[Pd(bc)_2]^{2-}$ and $[Pt(bc)_2]^{2-}$ isolated under these conditions are

in agreement with the ^{11}B NMR spectra for the side product isolated during the synthesis of **3b** and **3c**.

Additionally, ^{31}P NMR shows the *in-situ* formation of mono-oxidized dppe, $Ph_2P(CH_2)_2P(O)Ph_2$ (**O=dppe**) for the synthesis of **3a-3c**, suggesting the ligand is displaced by an extra equivalent of **Li$_2$-[bc]** as the metal center is substituted twice (Figure B6). The [31]P{[1]H} chemical shifts for **O=dppe** are similar to those for compound **2** in Reference 24. Interestingly, we still observe free **O=dppe** despite stringent air-free conditions.
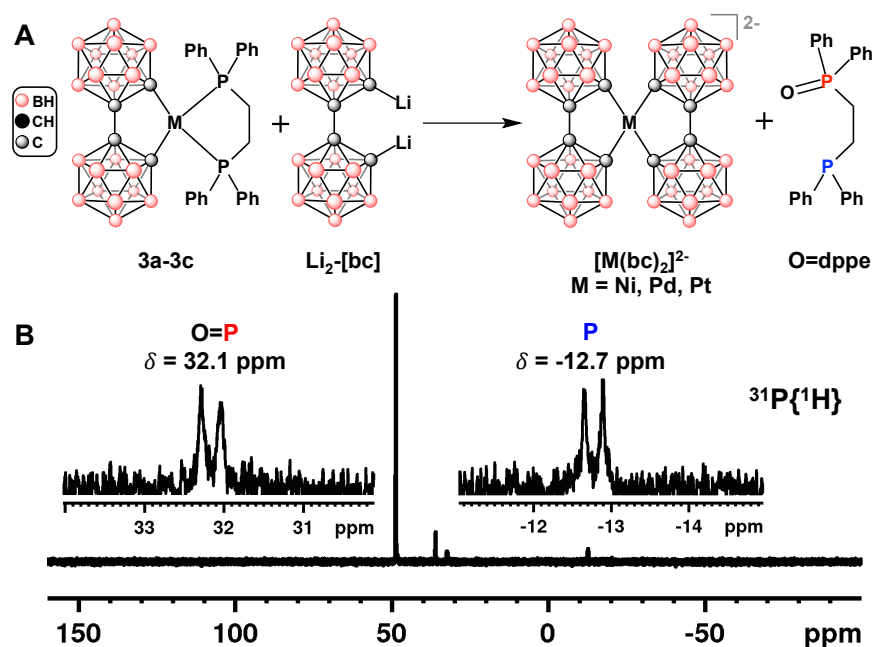
Figure B8 (A) Reaction scheme for the formation of [**M(bc)$_2$**]$^{2-}$ (M = Ni, Pd, Pt) and **O=dppe**. (B) Representative *in-situ* ^{31}P{^{1}H} NMR spectrum during the synthesis of **3a** shows the formation of free **O=dppe** (δ = 32.1 ppm, O=P; δ = -12.7 ppm, P), which results from the reaction of **Li$_2$-[bc]** with **3a** (δ = 49.09 ppm) to form [**Ni(bc)$_2$**]$^{2-}$. Interestingly, **O=dppe** formed even under rigorous oxygen-free conditions.
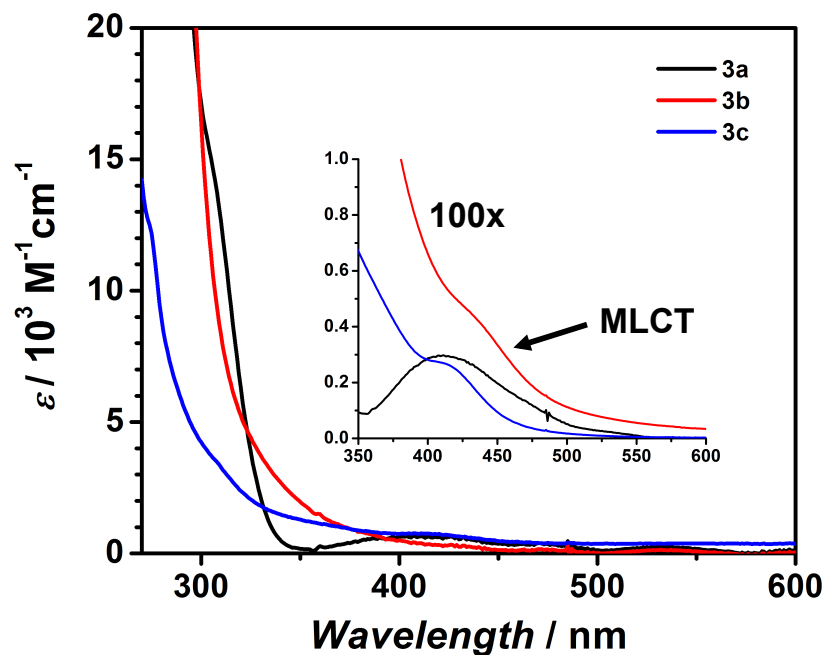
Figure B9 UV-Vis absorption spectrum for **3a** (black), **3b** (red), and **3c** (blue). Inset: Zoomed in region depicting MLCT transitions.
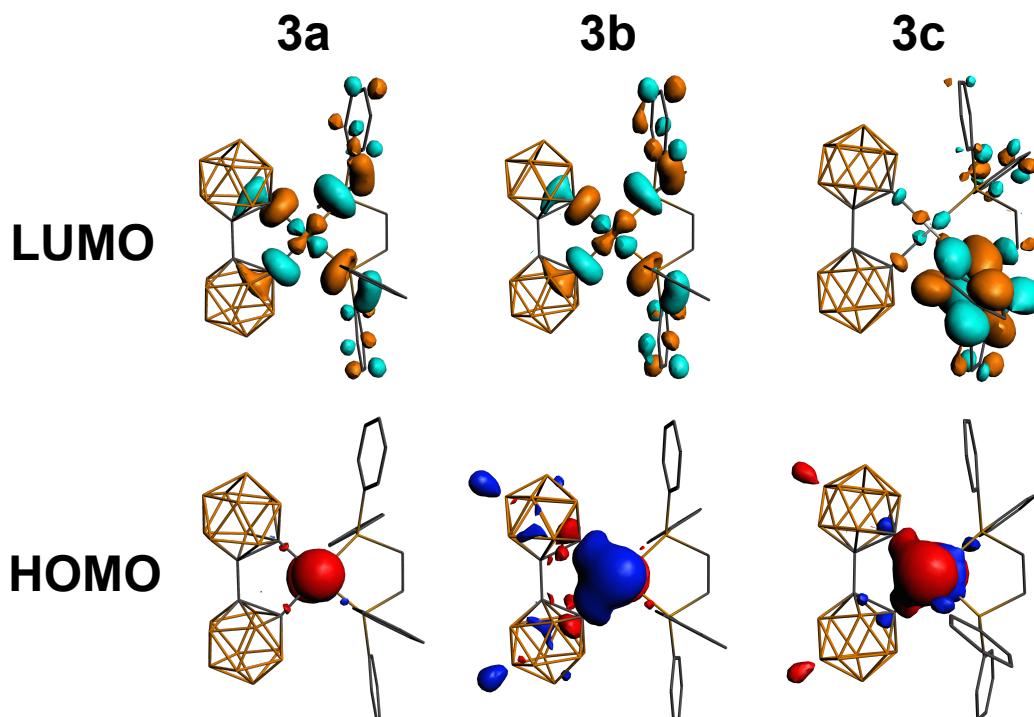
Figure B10 HOMO and LUMO images derived from DFT calculations of **3a** (left), **3b** (middle), and **3c** (right). Involvement of the **bc** ligand in HOMO-LUMO transitions is negligible, indicating the **bc** ligand is photophysically innocent.
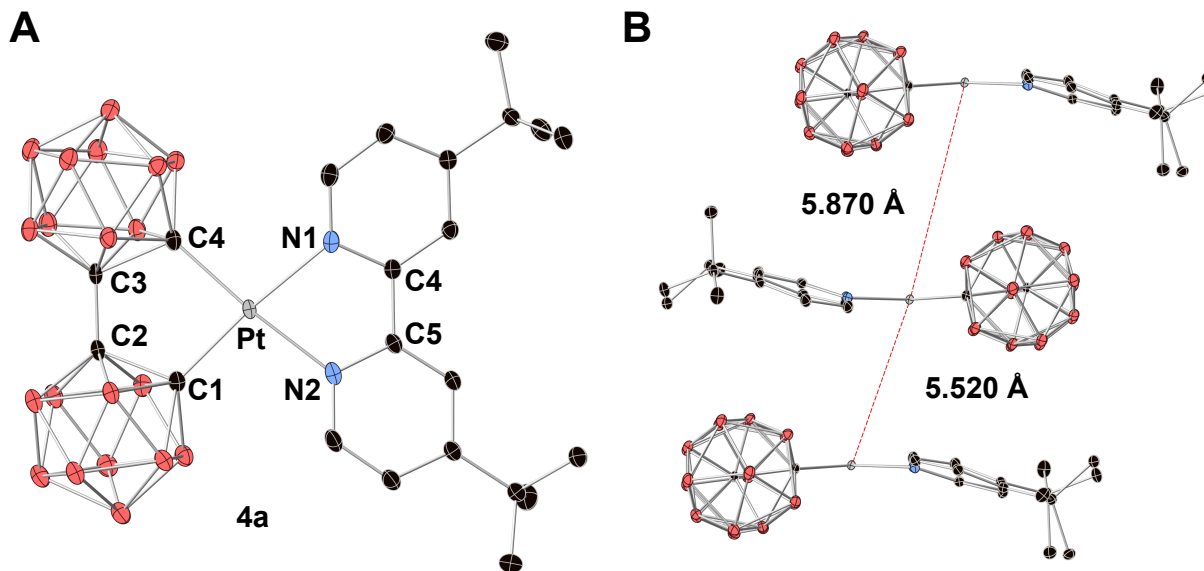
Figure B11 A) Thermal ellipsoid plot of **4a** (50% probability). H atoms were omitted for clarity. B) Stacking of **4a** Pt(II)···Pt(II) distances of 5.870 Å and 5.520 Å.

Table B3 Selected bond distances and angles for **4a**.

Parameter	4a
Pt-C1 (Å)	2.043
Pt-C4 (Å)	2.045
C1-C2 (Å)	1.708
C2-C3 (Å)	1.516
C3-C4 (Å)	1.71
Pt-N1 (Å)	2.109
Pt-N2 (Å)	2.105
C1-Pt-C4 (°)	86.54
Pt-C1-C2 (°)	114.67
C1-C2-C3 (°)	112.04
C2-C3-C4 (°)	112.15
C3-C4-Pt (°)	114.43
C1-Pt-N1 (°)	174.27
C4-Pt-N2 (°)	173.08
Pt···Pt (Å)	5.87
C1-C4 (Å)	2.802
C1-C2-C3-C4 dihedral (°)	1.22
N1-C4-C5-N2 dihedral (°)	1.27

Table B4 Selected bond distances and angles for **4a** and the selected average bond distances and angles of Pt(bph)(N^N) complexes.

Parameter	4a	Pt(bph)(N^N)
Pt-C1 (Å)	2.043	2.011
Pt-C4 (Å)	2.045	1.996
Pt-N1 (Å)	2.091	2.106
Pt-N2 (Å)	2.105	2.126
C1-Pt-C4 (°)	86.54	80.76
C1-Pt-N1 (°)	174.27	151.44
C4-Pt-N2 (°)	173.08	151.33

For **4a**, both Pt—C bond lengths are almost identical at 2.043 Å and 2.045 Å, and they are only 0.04 Å longer than the average Pt—C bond found in all Pt(bph)(N^N) crystal structures available in the Cambridge Structural Database. At 2.105 Å and 2.091 Å, Pt—N bonds in this molecule are roughly the same as the average Pt—N bond in Pt(bph)(N^N) compounds, with the difference in length of about 0.02-0.03 Å. The C—Pt—C angle in the **bc** analogue is about 6° larger than the average corresponding angle in all N^N chelated biphenyl analogues (86.54° versus 80.76°), which is characteristic of **bc**-chelated metal ions reported. This C—M—C angle for **4a** is also consistent with the C—M—C angle seen in **3a-3c** (Table S2). Based on this evidence, the intramolecular geometry of the synthesized **bc** complex is roughly equivalent to that of its biphenyl analogues.
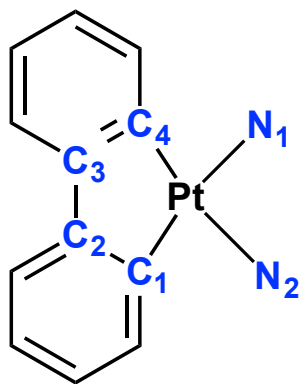
Figure B12 Numbering scheme for **Pt(bph)(N^N)** complexes listed in Table B3 and Table B4.
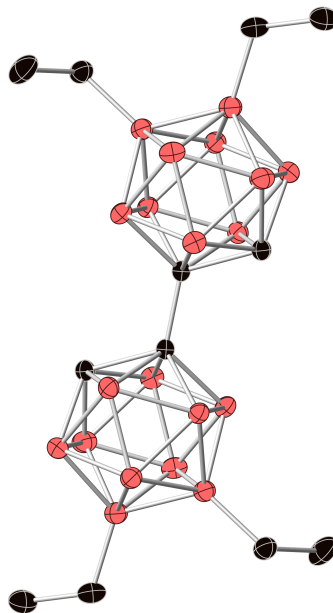
Figure B13 Thermal ellipsoid plot of **7** (50% probability). Salmon = B; black = C. H atoms were omitted for clarity.
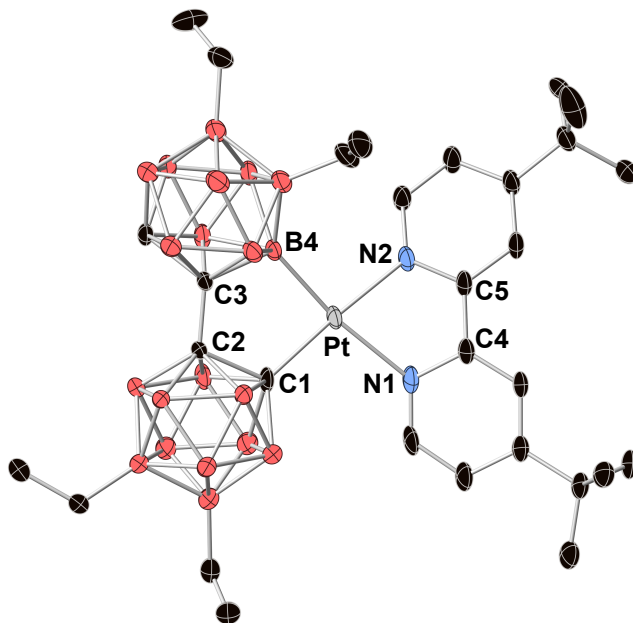
Figure B14 Thermal ellipsoid plot of **8** (50% probability). H atoms were omitted for clarity. Labels indicate the numbering scheme used for Table B5.

Table B5 Selected bond angles and distances for **8**.

Parameter	8
Pt-C1 (Å)	2.036
Pt-B4 (Å)	2.073
C1-C2 (Å)	1.704
C2-C3 (Å)	1.517
C3-B4 (Å)	1.725
Pt-N1 (Å)	2.175
Pt-N2 (Å)	2.053
C1-Pt-B4 (°)	87.02
Pt-C1-C2 (°)	115.78
C1-C2-C3 (°)	110.73
C2-C3-B4 (°)	114.11
C3-B4-Pt (°)	112.04
C1-Pt-N2 (°)	176.55
B4-Pt-N1 (°)	168.82
Pt···Pt (Å)	7.979
C1-B4 (Å)	2.829
C1-C2-C3-B4 dihedral (°)	6.1
N1-C4-C5-N2 dihedral (°)	4.43
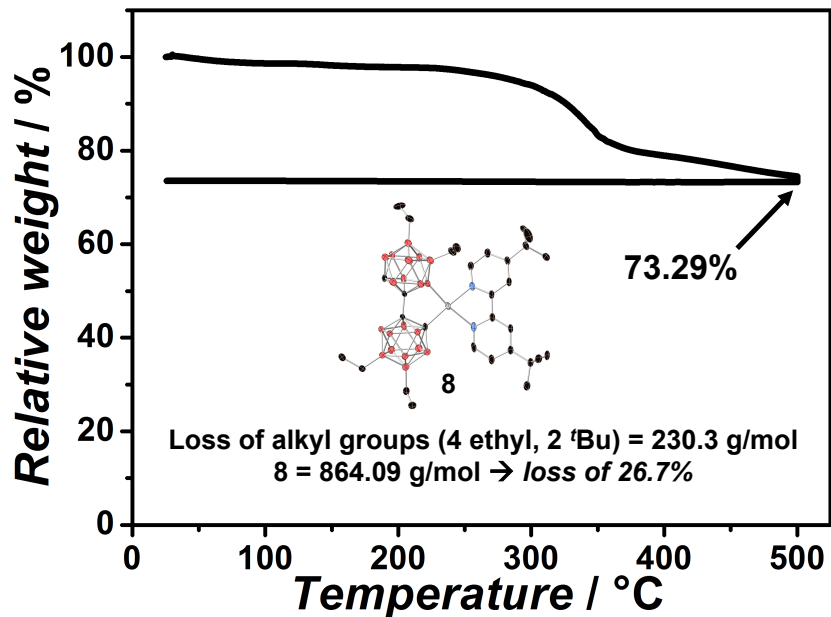
Figure B15 Thermogravimetric analysis (TGA) of compound **8** up to 500°C. The **bc** framework remains intact, and the loss in mass corresponds to the cleavage of alkyl groups from both ligands.

3.5 References

1. a) H. Yersin, Ed. *Highely Efficient OLEDs with Phosphorescent Materials*; Wiley-VCH: Weinheim, 2008; b) P.-T. Chou, Y. Chi, Chem. Eur. J., 2007, **13**, 380-395; c) Y. Chi, P.-T. Chou, *Chem. Soc. Rev.*, 2010, **39**, 638-655.
2. For selected examples of phosphorescent cyclometallated Pt(II) complexes, see: a) J. Brooks, Y. Babayan, S. Lamansky, P. I. Djurovich, I. Tsyba, R. Bau, M. E. Thompson, Inorg. Chem., 2002, **41**, 3055-3066; b) J. Kavitha, S.-Y. Chang, Y. Chi, J.-K. Yu, Y.-H. Hu, P.-T. Chou, S.-M. Peng, G.-H. Lee, Y.-T. Tao, C.-H. Chien, A. J. Carty, Adv. Funct. Mater., 2005, **15**, 223-229; c) S.-Y. Chang, J. Kavitha, S.-W. Li, C.-S. Hsu, Y. Chi, Y.-S. Yeh, P.-T. Chou, G.-H. Lee, A. J. Carty, Y.-T. Tao, C.-H. Chien, Inorg. Chem., 2006, **45**, 137-146; d) S.-Y. Chang, Y.-M. Cheng, Y. Chi, Y.-C. Lin, C.-M.-Jiang, G.-H. Lee, P.-T. Chou, Dalton Trans., 2008, 6901-6911; e) Z. M. Hudson, C. Sun, M. G. Helander, H. Amarne, Z.-H. Lu, S. Wang, Adv. Funct. Mater., 2010, **20**, 3426-3439; f) X.-C. Hang, T. Fleetham, E. Turner, J. Brooks, J. Li, Angew. Chem., Int. Ed., 2013, **52**, 6753-6756. g) Y. Unger, D. Meyer, O. Molt, C. Schildknecht, I. Münster, G. Wagenblast, T. Strassner, Angew. Chem. Int. Ed. 2010, **49**, 10214 –10216; h) M. Tenne, S. Metz, G. Wagenblast, I. Münster, T. Strassner, Organometallics, 2015, **34**, 4433-4440.
3. a) D. Bandyopadhyay, P. Bandyopadhyay, A. Chakravorty, F. A. Cotton, L. R. Falvello, Inorg. Chem., 1983, **22**, 1315-1321; b) L. Chassot, E. Müller, A. von Zelewsky, Inorg. Chem., 1984, **23**, 4249-4253; c) M. Ghedini, D. Pucci, A. Crispini, G. Barberio, Organometallics, 1999, **18**, 2116-2124; d) K. E. Dungey, B. E. Thompson, N. A. P. Kane-Maguire, L. L. Wright, Inorg. Chem., 2000, **39**, 5192-5196.
4. a) D. P. Rillema, A. J. Cruz, C. Moore, K. Siam, A. Jehan, D. Base, T. Nguyen, W. Huang, Inorg. Chem., 2013, **52**, 596-607; b) D. P. Rillema, S. R. Stoyanov, A. J. Cruz, H. Nguyen, C. Moore, W. Huang, K. Siam, A. Jehan, V. KomReddy, Dalton Trans., 2015, **44**, 17075-17090.
5. a) M. Scholz, E. Hey-Hawkins, Chem. Rev., 2011, **111**, 7035-7062; b) J. M. Oliva, P. v. R. Schleyer, G. Aullón, J. I. Burgos, A. Fernández-Barbero, I. Alkorta, Phys. Chem. Chem. Phys., 2010, **12**, 5101-5108.
6. For select examples, see: a) Y. Quan, Z. Xie, Angew. Chem., 2016, **128**, 1317-1320; b) R. Cheng, J. Zhang, J. Zhang, Z. Qiu, Z. Xie, Angew. Chem., 2016, **128**, 1783-1786; c) C. Tang, Z. Xie, Angew. Chem., Int. Ed., 2015, **54**, 7662-7665; d) H. Lyu, Y. Quan, Z. Xie, Angew. Chem., 2015, **127**, 10769-10772; e) A. M. Spokoyny, Pure Appl. Chem., 2013, **85**, 903-919; f) A. M. Spokoyny, C. D. Lewis, G. Teverovskiy, S. L. Buchwald, Organometallics, 2012, **31**, 8478-8481; g) C. A. Lugo, C. E. Moore, A. L. Rheingold, V. Lavallo, Inorg. Chem., 2015, **54**, 2094-2096; h) A. R. Popescu, F. Teixidor, C. Viñas, Coord. Chem. Rev., 2014, **269**, 54-84; i) B. Xu, Y.-P. Wang, Z.-J. Yao, G.-X. Jin, Dalton Trans., 2015, **44**, 1530-1533; j) J. Kahlert, L. Böhling, A. Brockhinke, H.-G. Stammler, B. Neumann, L. M. Rendina, P. J. Low, L. Weber, M. A. Fox, Dalton Trans., 2015, **44**, 9766-9781; k) Z. Zheng, W. Jiang, A. A. Zinn, C. B. Knobler, M. F. Hawthorne, Inorg. Chem., 1995, **34**, 2095-2100; l) P. A. Jelliss, J. Mason, J. M. Nazzoli, J. H. Orlando, A. Vinson, N. P. Rath, M. J. Shaw, Inorg. Chem., 2006, **45**, 370-385; m) S. W. Buckner, M. J. Fischer, P. A. Jelliss, R. Luo, S. D. Minteer, N. P. Rath, A. Siemiarczuk, Inorg. Chem., 2006, **45**, 7339-7347.

7. a) H. J. Bae, H. Kim, K. M. Lee, T. Kim, M. Eo, Y. S. Lee, Y. Do, M. H. Lee, Dalton Trans., 2013, **42**, 8549-8552; b) T. Kim, J. Lee, S. U. Lee, M. H. Lee, Organometallics, 2015, **34**, 3455–3458; c) A. M. Prokhorov, P. A. Slepukhin, V. L. Rusinov, V. N. Kalinin, D. N. Kozhevnikov, Chem. Commun., 2011, **47**, 7713-7715; d) A. M. Prokhorov, T. Hofbeck, R. Czerwieniec, A. F. Suleymanova, D. N. Kozhevnikov, H. Yersin, J. Am. Chem. Soc., 2014, **136**, 9637-9642.

8. a) C. Shi, H. Sun, Q. Jiang, J. Wang, W. Huang, H. Yan, Chem. Commun., 2013, **49**, 4746-4748; b) C. Shi, H. Sun, X. Tang, W. Lv, H. Yan, Q. Zhao, J. Wang, W. Huang, Angew. Chem., Int. Ed., 2013, **52**, 13434-13438; c) T. Kim, H. Kim, K. M. Lee, Y. S. Lee, M. H. Lee, Inorg. Chem., 2013, **52**, 160-168; d) H. J. Bae, J. Chung, H. Kim, J. Park, K. M. Lee, T.-W. Koh, Y. S. Lee, S. Yoo, Y. Do, M. H. Lee, Inorg. Chem., 2014, **53**, 128-138.

9. For recent, comprehensive reviews on boron cluster-based luminescent materials, see: a) X. Li, H. Yan, Q. Zhao, Chem. Eur. J., 2016, **22**, 1888-1898; b) S. Mukherjee, P. Thilagar, Chem. Commun., 2016, **52**, 1070-1093.

10. a) R. A. Wiesboeck, M. F. Hawthorne, J. Am. Chem. Soc., 1964, **86**, 1642-1643; b) D. A. Owen, M. F. Hawthorne, J. Am. Chem. Soc., 1970, **92**, 3194-3196; c) D. A. Owen, M. F. Hawthorne, J. Am. Chem. Soc., 1971, **93**, 873-880; d) First example of oxidative coupling of two *o*-carboranes: L. I. Zakharkin, A. I. Kovredov, Bull. Acad. Sci. USSR, Div. Chem. Sci., 1973, **22**, 1396; e) X. Yang, W. Jiang, C. B. Knobler, M. F. Hawthorne, J. Am. Chem. Soc., 1992, **114**, 9719-9721; f) Bis-carboranes that feature both C—C and B—C bonds: X. Yang, W. Jiang, C. B. Knobler, M. D. Mortimer, M. F. Hawthorne, Inorg. Chim. Acta, 1995, **240**, 371-378; g) D. E. Harwell, M. D. Mortimer, C. B. Knobler, F. A. L. Anet, M. F. Hawthorne, J. Am. Chem. Soc., 1996, **118**, 2679-2685; h) D. E. Harwell, J. McMillan, C. B. Knobler, M. F. Hawthorne, Inorg. Chem., 1997, **36**, 5951-5955; i) Only report of functionalized **2**: A. Herzog, A. Maderna, G. N. Harakas, C. B. Knobler, M. F. Hawthorne, Chem. Eur. J., 1999, **5**, 1212-1217; j) Optimized synthesis of **2**: S. Ren, Z. Xie, Organometallics, 2008, **27**, 5167–5168.

11. a) M. J. Martin, W. Y. Man, G. M. Rosair, A. J. Welch, J. Organomet. Chem., 2015, **798**, 36-40; b) Z.-J. Yao, Y.-Y. Zhang, G.-X. Jin, J. Organomet. Chem., 2015, **798**, 274-277; c) L. E. Riley, A. P. Y. Chan, J. Taylor, W. Y. Man, D. Ellis, G. M. Rosair, A. J. Welch, I. B. Sivaev, Dalton Trans., 2016, **45**, 1127-1137.

12. a) C. Cornioley-Deuschel, A. von Zelewsky, Inorg. Chem., 1987, **26**, 3354-3358; b) M. Maestri, D, Sandrini, V. Balzani, A. von Zelewsky, C. Deuschel-Cornioley, P. Jolliet, Helv. Chim. Acta, 1988, **71**, 1053-1059; c) C. B. Blanton, Z. Murtaza, R. J. Shaver, D. P. Rillema, Inorg. Chem., 1992, **31**, 3230-3235; d) J. A. Zuleta, C. A. Chesta, R. Eisenberg, J. Am. Chem. Soc., 1989, **111**, 8916-8917; e) J. M. Bevilacqua, R. Eisenberg, Inorg. Chem., 1994, **33**, 2913-2923; f) S. D. Cummings, R. Eisenberg, J. Am. Chem. Soc., 1996, **118**, 1949-1960; g) W. Paw, S. D. Cummings, M. A. Mansour, W. B. Connick, D. K. Geiger, R. Eisenberg, Coord. Chem. Rev., 1998, **171**, 125-150; h) M. Hissler, J. E. McGarrah, W. B. Connick, D. K. Geiger, S. D. Cummings, R. Eisenberg, Coord. Chem. Rev., 2000, **208**, 115-137.

13. These results are consistent with the decrease in the $^1J_{\text{Pt-P}}$ value for other Pt(P^P)Cl$_2$ to Pt(P^P)L$_2$ complexes, where P^P = chelating diphosphine and L = strong-field ligand. a) P. E. Garrou, Chem. Rev., 1981, **81**, 229-266; b) B. L. Edelbach, D. A. Vicic, R. J. Lachicotte, W. D. Jones, Organometallics, 1998, **17**, 4784-4794; c) P. Sgarbossa, A. Scarso, R. A. Michelin, G. Strukul, Organometallics, 2007, **26**, 2714-2719.

14. For selected examples of molecules featuring carborane-based B—M bonds, see: a) A. M. Spokoyny, M. G. Reuter, C. L. Stern, M. A. Ratner, T. Seideman, C. A. Mirkin, J. Am. Chem. Soc., 2009, **131**, 9482-9483; b) Z.-J. Yao, W.-Y. Yu, Y.-J. Lin, S.-L. Huang, Z.-H. Li, G.-X. Jin, J. Am. Chem. Soc., 2014, **136**, 2825-2832; c) N. Fey, M. F. Haddow, R. Mistry, N. C. Norman, A. G. Orpen, T. J. Reynolds, P. G. Pringle, Organometallics, 2012*, **31**, 2907-2913; d) M. E. El-Zaria, H. Arii, H. Nakamura, Inorg. Chem., 2011, **50**, 4149-4161; e) B. J. Eleazer, M. D. Smith, D. V. Peryshkov, Organometallics, 2016, *In Press*. **DOI:** 10.1021/acs.organomet.5b00807.

15. a) P.-I. Kvam, M. V. Puzyk, K. P. Balashev, J. Songstad, Acta Chem. Scand., 1995, **49**, 335-343; b) N. G. Connelly, W. E. Geiger, Chem. Rev. 1996, **96**, 877-910.

16. a) Y. Zhang, S. Lee, S. R. Forrest, Nature Commun., 2014, **5**, 1-7; b) S. Scholz, R. Meerheim, K. Walzer, K. Leo, Proc. SPIE 6999, 2008, 69991B; (c) V. Sivasubramaniam, F. Brodkorb, S. Hanning, H. P. Loebl, V. van Elsbergen, H. Boerner, U. Scerf, M. Kreyenschmidt, J. Fluorine Chem., 2009, **130**, 640-649; (d) I. R. de Moraes, S. Scholz, B. Lüssem, K. Leo, Org. Electron., 2011, **12**, 341-347; e) R. Seifert, I. R. de Moraes, S. Scholz, M. C. Gather, B. Lüssem, K. Leo, Org. Electron., 2013, **14**, 115-123.

17. M. F. Hawthorne, J. Chem. Educ., 2009, **86**, 1131.

CHAPTER 4 – FINE-TUNING ELECTRONIC PROPERTIES OF LUMINESCENT PT(II) COMPLEXES *VIA* VERTEX-DIFFERENTIATED COORDINATION OF STERICALLY INVARIANT CARBORANE-BASED LIGANDS

4.1 Introduction

Luminescent Pt(II) complexes have been employed in a variety of applications ranging from photocatalysis,[1] organic light-emitting diodes (OLEDs),[2] biological labeling reagents,[3] and singlet oxygen sensitizers,[4] among others. The optical properties of cyclometalated Pt(II) complexes are determined by the characteristics of their ground and lowest energy excited states, so these properties can be tuned by modifying the electronic nature of the cyclometalating ligands. In typical mixed-ligand complexes, (L)(L′)Pt(II), the highest occupied molecular orbital (HOMO) is generally localized on the metal center and one ligand (Pt(II) and L), and the lowest unoccupied molecular orbital (LUMO) is located on the remaining ligand (L′).[2,5] For example, complexes of the type Pt(bph)(bpy) (bph = biphenyl, bpy = 2,2′-bipyridine; **1**) feature a HOMO that is distributed across both the Pt(II) center and the bph moiety with the LUMO almost entirely localized on the bpy ligand.[5a,b] As a result, the electronic properties of the Pt(II) complex can be modified through ligand functionalization.

Specifically, the introduction of functional groups R and R′ on the bph and bpy ligands, respectively, will drastically influence the luminescent and electrochemical properties of resulting Pt(II) complexes (**2**, Figure 4.1). Rilemma and coworkers demonstrated that the emission wavelength, reduction potential, and HOMO–LUMO gap of **1** could be rationally tuned according to the Hammett constant of a functional group at the 4 and 4′ positions of the bpy ligand.[5b] Similarly, functionalization of the aryl moiety in related Pt(II) complexes has been shown to influence the oxidation potential and shift the wavelength of emission through

modulation of the HOMO energy.[2a-b,4a] While one can leverage this control to design molecules that emit throughout the visible spectrum and to engineer molecules with the desired HOMO and LUMO energies, there still exist several challenges.
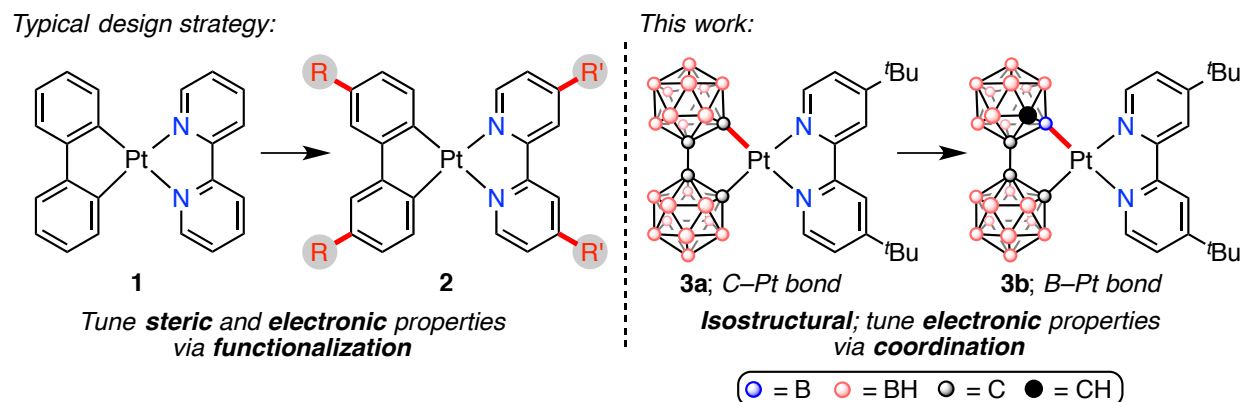
Figure 4.1 Common strategy for tuning electronic properties of cyclometalated Pt(II) complexes through ligand modification (left), and strategy presented in this work to modify electronic properties *via* coordination mode of **bc** ligand (right).

Modifying the cyclometalating ligand can drastically affect other excited state properties of the metal complex, such as the lifetime and quantum yield, which, in some cases, may be difficult to predict *a priori*. For example, the quantum yields (ϕ) and excited state lifetimes (τ) of a series of Pt(II) complexes bearing N-heterocyclic carbene (NHC) and β-diketonate cyclometalating ligands were found to vary widely depending on the functional group on the aryl fragment of the NHC ligand, ranging from $\phi = 0.11$ and $\tau = 91$ μs to $\phi = 0.90$ and $\tau = 23$ μs.[6a] Moreover, functional groups used to tune spectroscopic properties may not be compatible with the environment or the application they will be used in. For instance, fluoride groups are commonly used to blue-shift the emission of metal complexes for use in blue OLED devices; however, the aryl C–F bond has been shown to be electrochemically unstable during OLED device operation, leading to rapid decomposition of the emissive molecule and short OLED device lifetimes.[7] Lastly, square planar Pt(II) complexes are prone to aggregation at high

concentrations due to their flat geometry;[8] as such, ligand functionalization may considerably alter the overall steric profile of the metal complex and potentially enable self-quenching pathways or the formation of excimers, which can adversely affect the emission spectrum of the Pt(II) complex. The ability to tune the optical properties of a metal complex in a predictable manner without modifying other excited state properties or introducing significant steric bulk would be a potentially useful method to circumvent these complications.

Carboranes[9] are chemically and thermally robust icosahedral boron-rich clusters with unique electronic properties and have recently been incorporated into cyclometalating ligands used in many luminescent transition metal complexes.[10] In contrast to aryl-based ligand frameworks that are typically limited to forming carbon-metal bonds, carboranes can covalently bond with a metal center through both carbon[11] and boron[12] vertices, or interact with a metal center noncovalently upon deboronation and formation of the formally anionic *nido*-carboranyl species.[13] Notably, the electronic character of the carborane ligand varies from electron-withdrawing when C-bound to electron-releasing when B-bound, especially at the boron vertices furthest away from the carbons,[14] providing a unique platform for isosteric tuning of electronic properties. We considered this strategy in the context of 1,1′-bis(*o*-carborane) (**H₂-bc**),[15] a carborane-based analogue of biphenyl, to determine whether the emission wavelength and electrochemical properties of a metal complex could be tuned by modifying the coordination mode of the carborane moiety to the metal center. Importantly, as this approach effects a subtle change in the ligand field observed by the metal without the introduction of functional groups, there should be little change in the steric profile of the metal complex and minimal influence on other excited state properties.

4.2 Results and Discussion

4.2.1 Synthesis

We previously reported the synthesis of a luminescent Pt(II) complex **3**, which was generated though the addition of a solution of the dilithio salt of **bc** (Li$_2$[**bc**]) to a slurry of Pt(dtb-bpy)Cl$_2$ (dtb-bpy = 4,4′-di-*tert*-butyl-2,2′-bipyridine) in THF (Figure 4.2A).[12f] Based on ^{1}H NMR data of the isolated product, a mixture of species was present: a symmetric isomer in which **bc** coordinates to the Pt(II) center in a κ^2-C,C-bound mode (**3a**), and an asymmertric isomer with **bc** coordinated in a κ^2-B,C-bound mode (**3b**; Figures 4.2A and C1, Appendix C). When this reaction was repeated, the ratio of isomers in the isolated product ranged from >90% **3a** to >90% **3b** (Figure C1, Appendix C). Additionally, the ratio of **3a** to **3b** produced was inconsistent when different sources of ^{n}BuLi were used to deprotonate **H$_2$-bc** (Table C1, Appendix C). Due to the high level of variation in isomer distribution using lithium-based reagents, we sought to mitigate sources of experimental error that may potentially occur during the deprotonation step by attempting to isolate the Li$_2$[**bc**] salt.
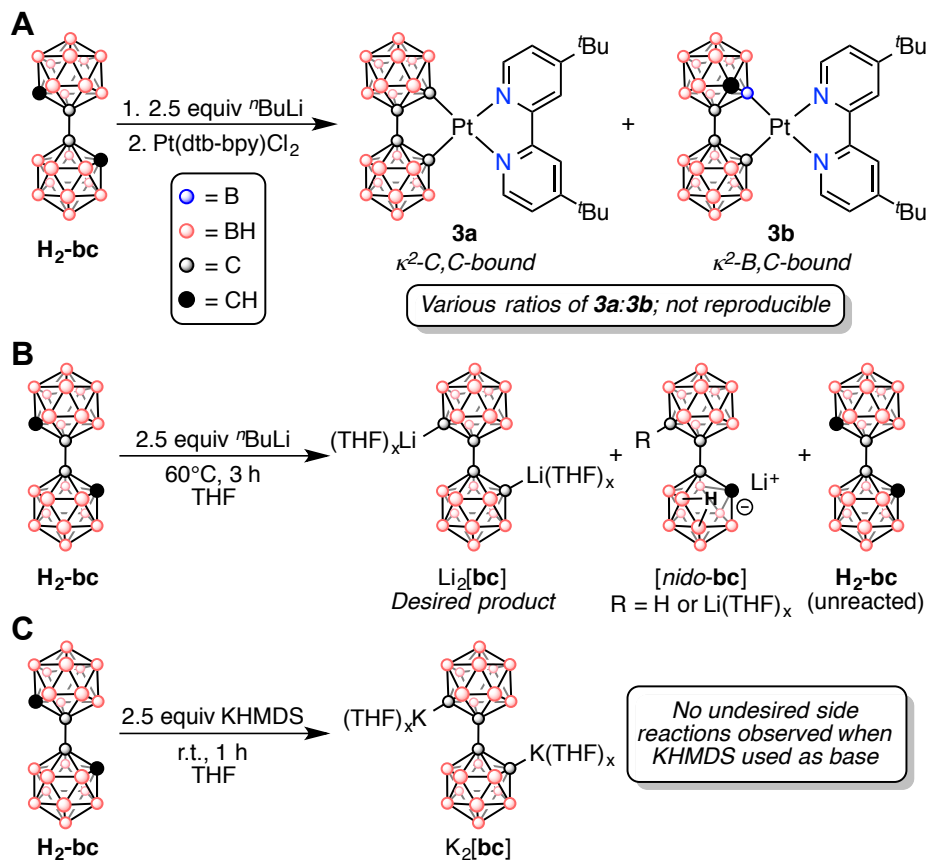
Figure 4.2 (A) A mixture of **3a** and **3b** is generated in various ratios. (B) Deprotonation of **H₂-bc** with *ⁿ*BuLi results in the formation of [*nido*-**bc**] side products and unreacted **H₂-bc**. (C) The use of KHMDS to deprotonate **H₂-bc** yields the K₂[**bc**] salt with no observed deboronation products.

Following the lithiation conditions previously employed,[12f] 2.5 equivalents of *ⁿ*BuLi were added to a solution of **H₂-bc** in THF and heated to 60 °C for 3 hours. After the solvent was removed *in vacuo*, the crude product was washed with *n*-pentane and a white solid was isolated. In addition to the desired Li₂[**bc**] product, both [*nido*-**bc**], a known decomposition product of **H₂-bc** in the presence of strong bases or nucleophiles,[16] and unreacted **H₂-bc** were observed in the isolated solid *via* ¹H and ¹¹B NMR spectroscopy (Figures 4.2B and C2, Appendix C). While it is conceivable the alkyl lithium nucleophile is responsible for deboronation, one cannot rule out a previously observed "self-attack" of the lithio-*o*-carborane, Li[**H-oCB**], resulting in the formation of a *nido*-carboranyl species.[16e] The lithiation time was further varied from 1-3 hours

in an effort to minimize the formation of side products during the deprotonation of **H$_2$-bc**; however, none of these conditions offered any systematic control over the ratio of **3a** to **3b** produced (Table C2, Appendix C). Based on these observations, we concluded ^{n}BuLi was not a suitable base for use in the deprotonation of **H$_2$-bc**. We hypothesized the use of potassium bis(trimethylsilyl)amide (KHMDS), a less basic and non-nucleophilic alternative to ^{n}BuLi, might result in fewer side products generated during the course of the reaction. Indeed, full conversion to a single new species was observed by ^{11}B NMR spectroscopy after 2.5 equivalents of KHMDS were added to a THF solution of **H$_2$-bc** and stirred at room temperature for 1 hour (Figures 4.2C and C3, Appendix C). Importantly, no deboronation products were observed *via* ^{1}H or ^{11}B NMR spectroscopy (Figure C3B, Appendix C), suggesting KHMDS might be a suitable alternative to ^{n}BuLi.
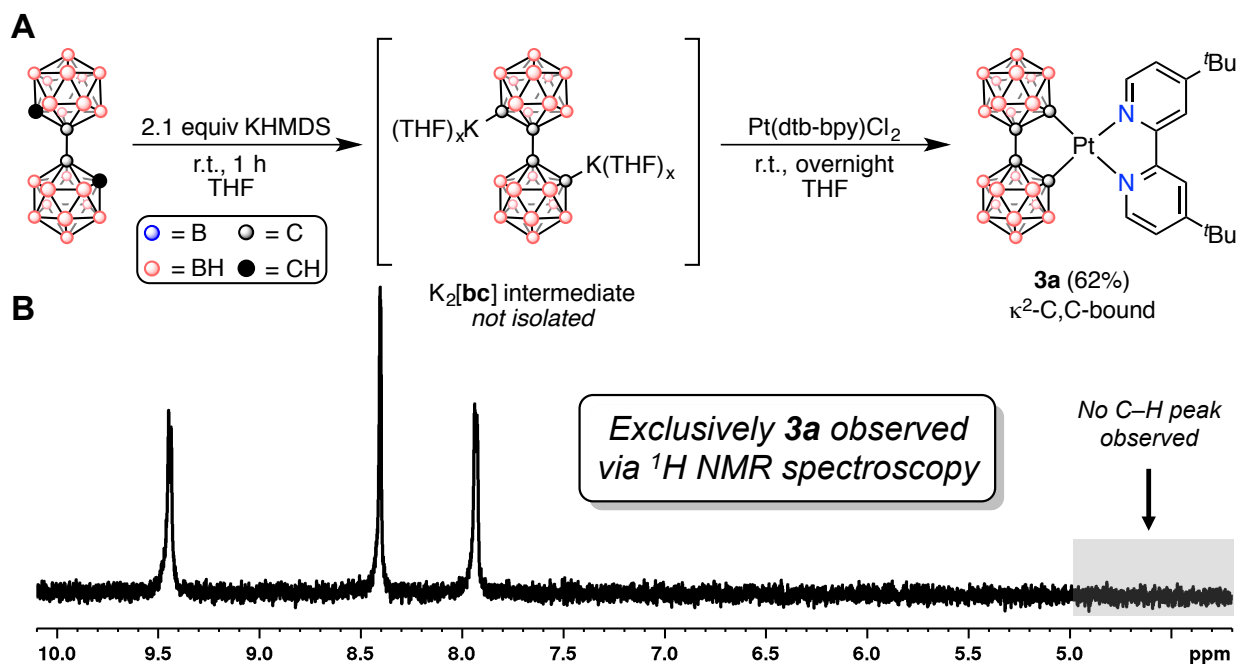
Figure 4.3 (A) Synthesis of **3a** *via* K$_2$[**bc**]. (B) ^{1}H NMR spectrum (THF-d$_8$) of the product from (A) suggests exclusively **3a** was formed.

We were then interested in probing the reactivity of the $K_2[\mathbf{bc}]$ salt in the synthesis of **3**. A solution of $K_2[\mathbf{bc}]$ was added to a slurry of Pt(dtb-bpy)Cl$_2$ in THF and the reaction mixture was stirred overnight at room temperature (Figure 4.3A). Based on ^{1}H NMR spectroscopy of the isolated product, only **3a**, the κ^2-C,C-bound isomer, was observed (Figure 4.3B, 62% yield). The use of $K_2[\mathbf{bc}]$ generated by deprotonation of **H$_2$-bc** with KHMDS provides a previously unavailable route to exclusively synthesize **3a**.

Next, we focused on understanding how the formation of **3b** occurs. A series of control experiments in which side products potentially generated during the lithiation of **H$_2$-bc** are introduced as additives, as well as experiments employing formally cationic Pt(II) starting materials, are detailed in Appendix C (Tables C3-C4). Overall, these experiments resulted in the formation of primarily the κ^2-C,C-bound isomer (85-99% **3a**). Since the side products that form upon reaction with ^{n}BuLi had little influence over the formation of **3b**, we suspected undesired reactions might be occurring as a result of unreacted ^{n}BuLi still present in solution. In previous reactions in which ^{n}BuLi was used for the deprotonation of **H$_2$-bc**, the Li$_2[\mathbf{bc}]$ reaction mixture was typically added to a slurry of Pt(dtb-bpy)Cl$_2$ in THF. Due to the presence of unreacted **H$_2$-bc** in the isolated lithation product of **H$_2$-bc** (Figures 4.2B and C2, Appendix C), we hypothesized unreacted ^{n}BuLi still present in the reaction mixture could react with Pt(dtb-bpy)Cl$_2$ to form an alkyl Pt(II) intermediate that exhibits different reactivity compared to the Pt(dtb-bpy)Cl$_2$ precursor.

Therefore, we performed an experiment in which 1 equivalent of ^{n}BuLi was added to a slurry of Pt(dtb-bpy)Cl$_2$ in THF at -30 °C, followed by the addition of a THF solution of the monopotassio **bc** salt, K[**H-bc**] (Figure C4, Appendix C). An immediate color change was observed upon the addition of ^{n}BuLi to the slurry of Pt(dtb-bpy)Cl$_2$, as well as the formation of a

black solid, presumably Pt metal. After K[**H-bc**] was added, the reaction mixture was allowed to warm to room temperature and proceed overnight. ^{1}H NMR spectroscopy of the crude product showed a mixture of isomers containing 90% **3b** (Figure C4B, Appendix C). Encouraged by this result, we screened several alkyl lithium and Grignard reagents, with the results summarized in Table C5 (Appendix C). It was found that the use of MeLi resulted in the greatest ratio of **3b** (>95%, Table C5, entry 5, Appendix C). This reaction was repeated on the NMR scale and monitored by ^{1}H NMR spectroscopy *in situ* in order to gain a better mechanistic understanding into the formation of **3b** (Figure C5-C6, Appendix C). Following the addition of MeLi to Pt(dtb-bpy)Cl$_2$ in THF-d$_8$, Pt(dtb-bpy)Me$_2$ is the major product observed, with unreacted Pt(dtb-bpy)Cl$_2$ and free dtb-bpy also present in the reaction mixture (Figure C5B, Appendix C). The appearance of free dtb-bpy suggests the formation of Pt(0), which is consistent with reports that alkyl Pt(II) complexes undergo reductive elimination to form Pt(0) species.[17] Following the addition of K[**H-bc**], a mixture of products containing a 19:1 ratio of **3b:3a** was observed *via* ^{1}H NMR spectroscopy (Figure C6C, Appendix C)**.** This signifies that upon using K[**H-bc**] under these conditions, one can selectively bias the reaction towards the formation of **3b**. Upon scale-up of this reaction, **3b** could be isolated in 12% yield and subjected to a full characterization by ^{1}H, ^{13}C{^{1}H}, and ^{11}B NMR spectroscopy and single crystal X-ray crystallographic studies (Figure 4.4 and Appendix C).
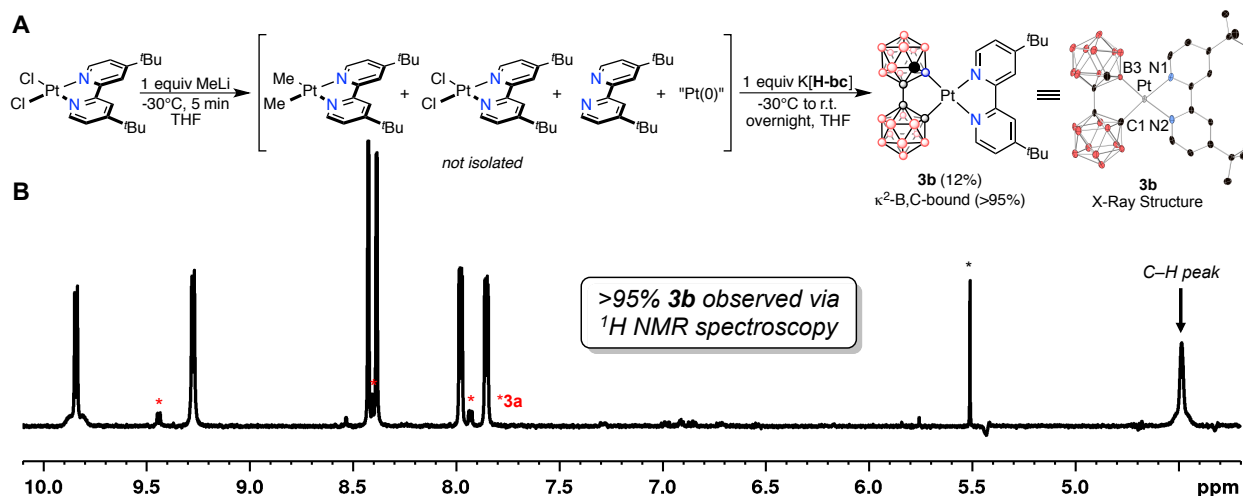
Figure 4.4 Scheme for the synthesis of **3b** (>95%). Right: X-ray crystal structure of **3b** drawn with 50% ellipsoid probability (CCDC 1851573). H atoms and solvent molecules are omitted for clarity. (B) ^{1}H NMR spectrum (THF-d$_8$) obtained on the isolated product from (A) suggests a mixture containing >95% **3b**. *Residual CH$_2$Cl$_2$.

Crystals of **3b** suitable for X-ray analysis were grown by slow evaporation of a concentrated solution of 2-MeTHF over the course of one week, and the diffraction study confirmed the NMR spectroscopic analysis and the presence of the asymmetric isomer with one Pt–C(1) bond and one Pt–B(3) bond (Figures 4.4A and C7, and Table C6, Appendix C). Similar to **3a**,[12f] the bulky **bc** ligand forces **3b** to pack "head-to-tail" with Pt(II)···Pt(II) distances ranging from 5.495(4) Å to 5.909(5) Å (Figure C8, Appendix C), which exceed the expected range where intermolecular Pt(II)···Pt(II) interactions responsible for deleterious non-radiative emission quenching can occur (3.15–3.76 Å).[18] The boryl carborane–Pt(II) bond in **3b** forms through B(3), which is adjacent to C and relatively electron-poor compared to B(4), which is separated from C by one atom. At 2.037(2) Å, the Pt–B(3) bond is comparable in length to the 2.035(3) Å Pt–C(1) bond, and the greater *trans* influence of the carborane-based boryl group is evidenced in the slight elongation of the Pt–N(2) bond versus the Pt–N(1) bond (2.130(3) Å and 2.115(1) Å, respectively; Figure C7, Appendix C).[12,19] In a similar Pt(II) complex in which the boryl carborane–Pt(II) bond forms though the more electron-rich B(4), the *trans* influence is more

124

pronounced with the Pt–N bond *trans* to B(4) 0.1219 Å longer than the Pt–N bond *trans* to

C(1).[12f] Furthermore, a **bc**-based Ru(II) complex that contains one Ru–C(1) bond and one Ru–

B(3) bond also exhibits a subdued *trans* influence that is comparable to that of **3b**, as there is a

difference of 0.0360 Å between Ru–L bonds *trans* to B(3) and C(1).[12g]

These structural data highlight the unique vertex-differentiated electronic influence of

boron clusters. Importantly, a structural overlay of **3a** and **3b** reveals only subtle differences in

molecular structure (Figure C7C, Appendix C), suggesting electronic properties of the metal

complex can be potentially tuned by varying the coordination mode of the carborane-based

ligand while preserving the overall steric profile of the complex.

Although the conditions presented in Figure 4.4 selectively produce the **3b** isomer

amenable towards isolation, we were interested in further mechanistic studies in an attempt to

improve the isolated yield. First, control experiments were performed to determine the role of

alkyl Pt(II) complexes in the formation of **3b**. The addition of a THF solution of K[**H-bc**] to a

slurry of either Pt(dtb-bpy)MeCl or Pt(dtb-bpy)Me$_2$ in THF did not result in the formation of any

emissive product, and neither **3a** nor **3b** were observed by ^{1}H NMR spectroscopy (Figure C9,

Appendix C). We therefore concluded that the formation of **3b** likely does not proceed directly

from an alkyl Pt(II) intermediate. We then turned our attention to the Pt(0) intermediates formed

in the reaction mixture as many reports detail the B–H activation of carboranes with low valent

transition metals.[12c,20] Introducing an additive to stabilize the Pt(0) species generated *in situ* may

potentially improve the yield of **3b**; indeed, we observed the addition of 1,5-cyclooctadiene to

the reaction mixture facilitated the formation of **3b**, implicating the involvement of a Pt(0)

species during the formation of **3b** (Table C7 and subsequent discussion, Appendix C). The use

of Pt$_2$(dba)$_3$ as a Pt(0) precursor resulted in the formation of trace amounts of **3b**, with no **3a**

observable by ^{1}H NMR spectroscopy (Figure C10, Appendix C). Based on these results, alternative Pt(0) starting materials could potentially further improve the yield of **3b**, although a more detailed investigation into the development of such precursors is needed. With a reliable route to generate predominantly **3b** (>95%), we were interested in elucidating the differences in spectroscopic and electronic properties between **3a** and **3b**.

4.2.2 Electrochemistry and Computational Analysis

Cyclic voltammetry (CV) measurements were conducted on **3a** and **3b** to gain insight into their ground state electronic properties. CV plots are presented in Figure 4.5A with corresponding data summarized in Table 4.1. Both complexes exhibit a reversible, one-electron reduction from -1.85 V (**3a**) to -1.98 V (**3b**) versus the ferrocenium/ferrocene redox couple (Fc$^+$/Fc).
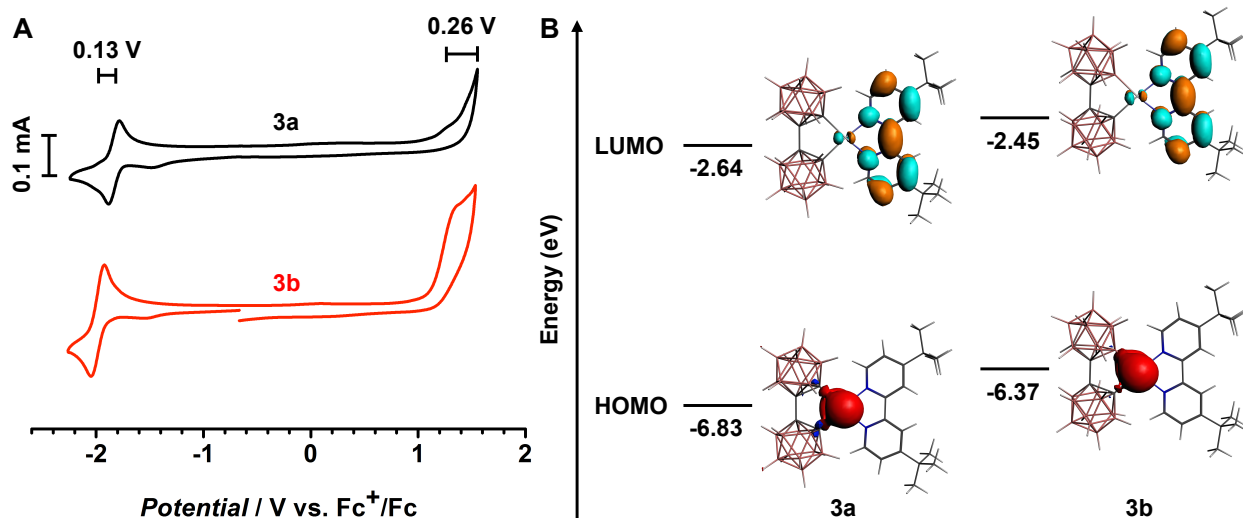
Figure 4.5 (A) Stacked cyclic voltammograms of **3a** and **3b** with scale bar of 0.1 mA. Recorded in anhydrous 1,2-difluorobenzene with 0.1 M [N^{n}Bu$_4$][PF$_6$] and referenced to the ferrocenium/ferrocene redox couple (Fc$^+$/Fc; scan rate = 0.1 V/s). Scale bars above indicate shift in redox potentials between **3a** and **3b**. (B) Frontier molecular orbital diagrams of **3a** and **3b**. HOMO and LUMO diagrams were calculated from the geometry-optimized singlet ground states (B3LYP:TZ2P level of theory).

Table 4.1 Electrochemical data for **3a** and **3b**.[a]

	$E_{1/2}{}^{red}$ (V)	E^{ox} (V)	ΔE^{redox} (V)[b]
3a	-1.85	> 1.55[c]	> 3.40
3b	-1.98	1.29[d]	3.27

[a]Values reported relative to the ferrocenium/ferrocene redox couple (Fc$^+$/Fc) at 0.5 mM, scan rate = 0.1 V/s. [b]$\Delta E^{redox} = E^{ox} - E_{1/2}{}^{red}$. [c]No oxidation peak observed within the solvent window. [d]Irreversible.

An irreversible oxidation for **3b** can be discerned in the envelope of the solvent oxidation wave, and a distinct oxidation process (E^{ox} = 1.29 V versus Fc$^+$/Fc) can be identified using differential pulsed voltammetry (DPV; Figure S12). In contrast, no oxidation process was observed for **3a** within the electrochemical window of 1,2-difluorobenzene by CV or DPV analyses (Figure C12, Appendix C). Therefore, we suggest the oxidation for **3a** occurs at a potential greater than 1.55 V versus Fc$^+$/Fc. These data are consistent with a one-electron reduction centered on the dtb-bpy ligand and an oxidation that occurs predominately at the Pt(II) metal center.[5a-c,6,18] Furthermore, this electrochemical behavior suggests a dtb-bpy-localized LUMO state and a HOMO with substantial metal character, as seen in DFT calculations for **3a** and **3b** (*vide infra*). The cathodic shift in redox potentials observed for **3b** relative to those for **3a** can be rationalized by the influence of the coordination mode of **bc** to the Pt(II) center. The **bc** ligand has been shown to be a stronger σ-donor when bonded to a metal center through boron rather than carbon,[12g] which is consistent with the stronger σ-donating properties of boryl moieties versus carbanion species.[21] As a result, **3b** will have a more electron-rich Pt(II) center that is easier to oxidize (cathodically shifted oxidation potential) compared to the metal center of **3a**. Correspondingly, it should be more difficult to reduce a relatively electron-rich system, which is consistent with the lower reduction potential observed for **3b** compared to that of **3a**. The electronic structures of **3a** and **3b** were calculated using density functional theory (DFT) to provide further insights into the observed electrochemical properties. The ground-state

geometries of **3a** and **3b** based on the crystal structure of **3a** were optimized at the BP:TZP level, and single-point calculations were carried out at the B3LYP:TZ2P level of theory with the COSMO solvation model for THF. For both isomers, the HOMO is almost entirely localized on the Pt(II) center with negligible contribution from the **bc** ligand, and the LUMO is predominantly centered on the dtb-bpy ligand with slight metal character (Figure 4.5B). The optimized triplet-state geometries reveal a significant tetrahedral distortion, and the triplet spin-density is distributed across the metal center and dtb-bpy ligand for both **3a** and **3b** (Figure C13, Appendix C). This frontier orbital diagram is comparable to those obtained for previously reported metal complexes featuring **bc**-based ligands.[12f]

Once again, the greater σ-donating ability of the boryl group relative to a carbanion is evidenced by the slightly higher HOMO energy for **3b** versus that of **3a** (-6.37 eV and -6.83 eV, respectively) due to the stronger ligand field imposed by the boryl anion. Additionally, more electron density located on the metal center should result in a greater degree of π-backbonding to the dtb-bpy ligand, leading to a destabilization of the LUMO energy. Indeed, a slight increase in LUMO energy is observed for **3b** relative to **3a** (-2.45 eV and -2.64 eV, respectively). Lastly, the calculated HOMO-LUMO gap for **3b** (3.92 eV) is slightly smaller than that of **3a** (4.19 eV), which is consistent with electrochemical and UV-Vis absorption data (Figures 4.5A and 4.6A, respectively).

4.2.3 Photophysical Data

In order to ascertain the influence of the coordination mode of **bc** on the luminescent properties of the resulting Pt(II) complexes, we carried out a series of photophysical measurements on **3a** and **3b**. The absorption and emission spectra are presented in Figure 4.6 with corresponding data in Table 4.2. Both **3a** and **3b** exhibit strong absorbance bands from 310–

325 nm attributed to the spin-allowed $^1\pi$-π^* transitions (^{1}LC) on the dtb-bpy ligand. The broad, lower intensity absorbance bands from 350–390 nm can be attributed to spin-allowed and spin-forbidden metal-to-ligand charge transfer transitions (^{1}MLCT and ^{3}MLCT, respectively). Notably, the ^{1}MLCT and ^{3}MLCT bands for **3b** (357 nm, 387 nm) are bathchromically shifted by up to 14 nm compared to the analogous bands for **3a** (349 nm, 373 nm). Furthermore, the energy of the ^{1}MLCT and ^{3}MLCT transitions for **3a** and **3b** are comparable to redox gaps measured by solution electrochemistry (**3a**: λ_{MLCT} = 373 nm, 3.32 eV; ΔE^{redox} > 3.40 V; **3b**: λ_{MLCT} = 387 nm, 3.20 eV; ΔE^{redox} = 3.27 V).
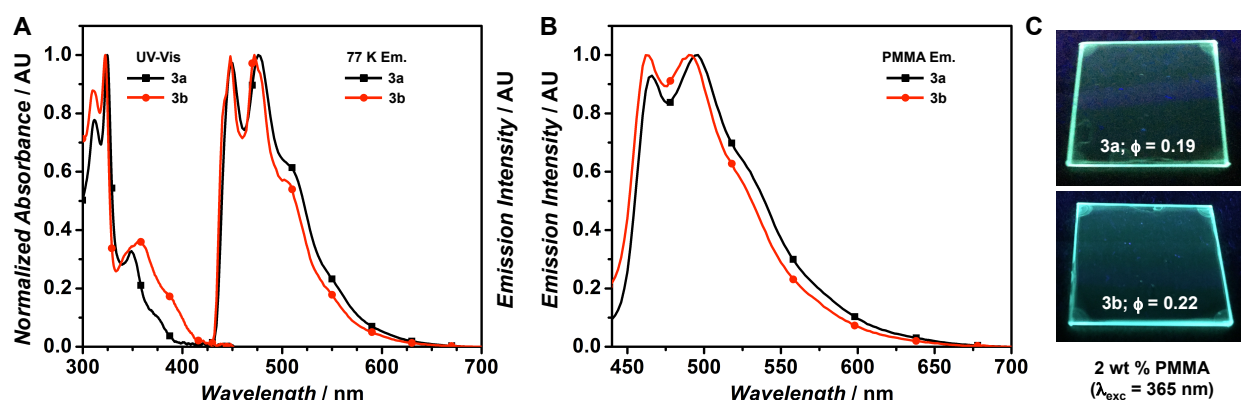
Figure 4.6 (A) UV-Vis absorption (left) and 77 K emission (right) emission spectra for **3a** and **3b** obtained from solutions of 2-MeTHF. (B) Emission spectra of 2 wt % PMMA films of **3a** and **3b** (λ_{exc} = 365 nm). (C) Pictures of 2 wt % PMMA films of **3a** and **3b** when irradiated with UV light (λ_{exc} = 365 nm).

Neither complex displays observable emission in a deaerated solution of 2-MeTHF at room temperature, but both complexes are brightly luminescent when cooled to 77 K and when doped in PMMA films (Figure 4.6). In addition, **3a** and **3b** both exhibit blue-green emission as neat solids (Figure C14, Appendix C). Interestingly, the emission spectra for the neat solid and doped PMMA film are almost identical for each isomer (Figure C14 and Table C8, Appendix C), suggesting the steric bulk of the **bc** ligand precludes any intermolecular interactions that might

affect luminescence. This observation is consistent with the solid-state packing determined from the single crystal X-ray structures for both **3a** and **3b** (*vide supra*; Figure C8, Appendix C).[12f]

Table 4.2 Photophysical Data for **3a** and **3b**.

	Absorbance $\lambda_{max}{}^a$ (nm)	Emission $\lambda_{max}{}^b$ (nm)	$\phi_{PL}{}^{b,c}$	$\tau^{b,d}$ (µs)	$k_r{}^e$ (10^4 s^{-1})	$k_{nr}{}^e$ (10^4 s^{-1})
3a	310, 323, 349, 373	465, 495, 528^f (449, 477, 511^f)	0.19	9.41 (18.1)	2.02	8.61
3b	312, 325, 357, 387	462, 490, 521^f (448, 472, 504^f)	0.22	9.04 (22.8)	2.43	8.63

[a]UV-Vis absorption spectra were obtained in 2-MeTHF (1 x 10^{-5} M). [b]Emission maxima, quantum yields, and excited state lifetimes were measured in 2 wt % PMMA films. Emission spectra, quantum yields, and excited state lifetimes recorded in 2-MeTHF at 77 K are marked with parentheses. [c]Quantum yields were measured using an integrating sphere under N$_2$. Error in quantum yield measurement is ±10%. [d]Excited state lifetime values in PMMA films are obtained from the weighted average of a biexponential decay, and values in 2-MeTHF at 77 K are obtained from a single exponential decay. Error in the excited state lifetime measurement is ±5%. [e]Calculated for PMMA films according to the equations $k_r = \phi/\tau$ and $k_{nr} = (1-\phi)/\tau$, where k_r is the radiative rate constant, k_{nr} is the nonradiative rate constant, ϕ is the quantum yield, and τ is the excited state lifetime. [f]Shoulder.

Low temperature emission spectra for **3a** and **3b** both display well-defined vibronic features consistent with emission from a ligand-centered triplet state (^{3}LC; Figure 4.6A). While the E_{0-0} energies are nearly indistinguishable between both isomers, the lower energy vibronic bands for **3b** are slightly blue-shifted (~5 nm) relative to those of **3a** (Table 1). At 77 K, the excited state lifetimes (τ) for both isomers are comparable at 18.1 µs and 22.8 µs (**3a** and **3b**, respectively; Table 4.1). PMMA films of **3a** and **3b** both exhibit broadened and red-shifted vibronic manifolds relative to the corresponding spectra obtained at 77 K (Figure 4.5B). Similar to the low temperature emission spectra for both isomers, emission from the PMMA film of **3b** is hypsochromically shifted compared to emission from the PMMA film of **3a**. Quantum yields (φ) and excited state lifetimes for doped PMMA matrices of these complexes are quite similar (**3a**: ϕ = 0.19, τ = 9.41 µs; **3b**: ϕ = 0.22, τ = 9.04 µs; Table 2). From ϕ and τ, the radiative (k_r) and

non-radiative (k_{nr}) rate constants can be determined. While k_{nr} values for both **3a** and **3b** are nearly identical (8.61 x 10^4 s^{-1} and 8.63 x 10^4 s^{-1}, respectively), the k_r value observed for **3b** (2.43 x 10^4 s^{-1}) is slightly larger than that of **3a** (2.04 x 10^4 s^{-1}). Overall, these data suggest similar emission processes for both isomers, which is consistent with the calculated triplet spin densities for **3a** and **3b** that show minimal contribution from the **bc** ligand (Figure C13, Appendix C).

4.3 Conclusions

We have demonstrated the emission wavelength and redox potentials of a luminescent Pt(II) complex can be tuned by modifying the coordination of the **bc** ligand to the metal center. The κ^2-C,C-bound isomer, **3a**, is generated through a salt metathesis reaction, whereas the κ^2-B,C-bound isomer, **3b**, appears to form through a Pt(0) intermediate. The greater σ-donating ability of the boryl moiety versus that of the carbanion species is apparent based on electrochemical measurements, which show a cathodic shift in redox potentials that is consistent with a more electron-rich system. This observation is corroborated by DFT computations and UV-Vis data as both suggest a stronger ligand field when **bc** is bound to the Pt(II) center through boron rather than carbon. Although the photophysical properties of both isomers are comparable, there is a subtle blue-shift in the emission spectrum for **3b** relative to **3a**. Therefore, leveraging the sterically invariant nature of the **bc** ligand scaffold can potentially provide a route to fine-tune the emission profile of the resulting Pt(II) complex without dramatically influencing other photophysical properties such as quantum yield and excited state lifetimes.

Notably, this method to tune the electronic properties of a metal complex does not involve the functionalization of the cyclometalating aryl-based ligands, which have previously been shown to have poorly programmable effects on the photophysical properties of the resulting

metal complexes.[6-8] The carborane-based ligand scaffold is uniquely poised to address this issue as carboranes can form stable bonds with metal centers through both carbon and boron vertices. With increasing access to functionalization methods for carboranes,[22] there is an expanding range of potential ligands available for use in metal complexes.

4.4 Appendix C

4.4.1 General Considerations

All experiments were set up in a nitrogen-filled glovebox or performed under an atmosphere of nitrogen using standard Schlenk and cannula techniques. All work-up and characterization was performed under ambient conditions. The "ambient conditions" for this manuscript refer to room temperature (20 - 25 °C) and uncontrolled laboratory air. Tetrahydrofuran (THF) used for reactions was sparged through argon and passed through activated alumina before use. 1,2-Difluorobenzene used for cyclic voltammetry was distilled over calcium hydride and vacuum-transferred into a receiving flask, brought in the glovebox, and stored over molecular sieves. Tetrabutylammonium hexafluorophosphate was recrystallized from a hot concentrated solution of ethanol twice and dried under vacuum prior to use for cyclic voltammetry measurements.

4.4.2 Materials

Deuterated solvents were purchased from Cambridge Isotope Laboratories and stored over 3Å molecular sieves prior to use. 1,1′-Bis(o-carborane) (**H₂-bc**) and Pt(dtb-bpy)Cl₂ were synthesized according to our previously reported procedures.[12f] K₂[PtCl₆], 4,4′-di-*tert*-butyl-2,2′-bipyridine (dtb-bpy), calcium hydride, potassium bis(trimethylsilyl)amide (KHMDS), *n*-butyllithium (2.5 M in hexanes), ethylmagnesium bromide (3 M in diethyl ether),

benzylmagnesium bromide (3 M in 2-MeTHF), methyllithium (3.0 M in diethoxymethane), methyllithium (1.6 M in diethyl ether), sodium tetrakis [3,5-bis(trifluoromethyl)phenyl]borate, 1,5-cyclooctadiene, triphenylphosphine, and silver tetrafluoroborate were purchased from Sigma-Aldrich. $Pt_2(dba)_3$ was purchased from Strem Chemicals. 1,2-Difluorobenzene and tetrabutylammonium hexafluorophosphate were purchased from Oakwood Chemical. Poly(methyl methacrylate) (PMMA, 35 kDa) was purchased from Acros Organics. *o*-Carborane $(1,2-C_2B_{10}H_{12})$ was purchased from Boron Specialties (USA) and was purified prior to use in the following procedure: a round-bottomed flask was charged with *o*-carborane (15 g, 10.4 mmol) and MeOH (150 mL). Concentrated HCl (50 mL) was added slowly to the reaction vessel, and the resulting mixture was heated to 50 °C and stirred overnight. The solution was then cooled, H_2O (200 mL) was added, and the resulting white solid was isolated by vacuum filtration, washed with water, and air-dried. The solid was then dissolved in CH_2Cl_2, dried with $MgSO_4$, and filtered through Celite. The solution was dried *in vacuo* to afford a white powder. The powder was then sublimed at 60 °C under dynamic vacuum. After sublimation away from the yellow residue, the white sublimate was dissolved in 1,2-dichloroethane. Activated carbon/charcoal (ca. 3–5 g) was added, and the mixture was stirred for 6 hours at about 75°C. The suspension was then filtered, and the filtrate was concentrated under vacuum. The resulting white solid was again sublimed at 60 °C to afford purified *o*-carborane. All reagents were used as received unless otherwise indicated.

4.4.3 Instruments

^1H and $^{13}C\{^1H\}$ NMR spectra were obtained on a Bruker AV500 spectrometer; ^{11}B NMR spectra were obtained on a Bruker DRX500 spectrometer. Bruker Topspin software was used to process the NMR data. ^1H and $^{13}C\{^1H\}$ NMR spectra were referenced to residual solvent

resonances in deuterated solvents (THF-d$_8$: ^{1}H, 3.580 ppm; ^{13}C, 67.210 ppm; Note: due to high humidity H$_2$O resonances are often present). ^{11}B NMR spectra were referenced to BF$_3$·Et$_2$O (0 ppm) standard. UV−Vis spectra were recorded on a Hewlett-Packard 4853 diode array spectrometer. Phosphorescence lifetime measurements for **3a** and **3b** were performed by a time-correlated single-photon counting method using an IBH fluorocube lifetime instrument equipped with a 405 nm LED excitation source. Quantum yield measurements were carried out using a Hamamatsu C9920 system equipped with a xenon lamp, calibrated integrating sphere, and model C10027 photonic multichannel analyzer. Steady-state emission measurements of **3a** and **3b** as solids, in thin films, and in frozen solutions at 77 K were performed using a Photon Technology International QuantaMaster spectrofluorimeter.

4.4.4 Preparation of PMMA Thin Films

A solution of PMMA (0.100 g, 35 kDa) in 1,2-difluorobenzene (1 mL) was thermally sonicated for 1 hour at 40°C, or until PMMA was completely dissolved. Next, **3a** or **3b** (0.002 g, 2 wt. %) was added to the solution and sonicated for an additional 5-10 minutes. The solution of **3a**/PMMA or **3b**/PMMA was spin coated on a quartz substrate (800-1,000 RPM, 30 seconds), and this was repeated (~4-6 times) until the film was thick enough emit light under $\lambda = 365$ nm excitation in a dark room under ambient conditions.

4.4.5 X-Ray Data Collection and Processing Parameters

For **3b** a single crystal was mounted on a nylon loop using perfluoropolyether oil and cooled rapidly to 100 K with a stream of cold dinitrogen. Diffraction data were measured using a Bruker APEX-II CCD diffractometer using Mo-$K\alpha$ radiation. The cell refinement and data reduction were carried out using Bruker SAINT and the structure was solved with SHELXS-97. All subsequent crystallographic calculations were performed using SHELXL-2013. Solvent

molecules with significant disorder were rendered using the SQUEEZE method.

4.4.6 Cyclic Voltammetry

Cyclic voltammetry was performed on **3a** and **3b** and using a CH Instruments Model 600D potentiostat with a glassy carbon disc working electrode, platinum wire counter electrode, and Ag/AgCl wire reference in a saturated solution of KCl in MeCN. All experiments were conducted in 0.1M $[N^nBu_4]PF_6$/1,2-difluorobenzene with 0.5 mM analyte concentrations. 1,2-difluorobenzene solutions were degassed by sparging with N_2 for 10 minutes, and the cyclic voltammetry was performed under constant flow of N_2 gas. A scan rate of 100 mV/s was used with ferrocene as an internal standard.

4.4.7 DFT Calculation Details

Optimized geometries for **3a** and **3b** were calculated from crystallographic data of **3a** and optimized with DFT calculations using standard triple-ξ polarization (TZP) basis sets available in the Amsterdam Density Functional 2014.04 Rev. 44409 (ADF)[1] software suite, with Becke[2] and Perdew[3] (BP) Slater-type orbitals (STOs) on a 6 core Apple computer. The local density approximation (LDA) was made with BP and exchange and correlation corrections available by default in the ADF 2014.04 suite. Single point calculations were performed using the B3LYP[4,5] level of theory and a TZ2P basis set. The COSMO solvation model (THF) was used for both geometry optimizations and single point calculations. All-electron basis sets were used for all atoms (cores remained un-frozen). Electron spins were restricted for S_0 calculations, and electron spins were unrestricted for T_1 calculations. Relativistic correlations were made using Zero-Order Relativistic Approximation (ZORA)[6-8] for Pt.

4.4.8 Synthetic Procedures

4.4.8.1 Pt(bc)(dtb-bpy), κ^2-C,C-bound (3a)

Inside a N_2 filled glove box, **bc** (0.0400 g, 0.140 mmol), potassium bis(trimethylsilyl)amide (KHMDS, 0.0585 g, 0.293 mmol, 2.1 equiv), and 3 mL THF were added to a 20 mL vial, which was then stirred at room temperature for 1 hour. In a 50 mL round bottom flask, Pt(dtb-bpy)Cl$_2$ (0.0750 g, 0.140 mmol, 1 equiv) and 15 mL THF were combined to yield a yellow slurry. The solution of K$_2$[**bc**] was added to the slurry of Pt(dtb-bpy)Cl$_2$ dropwise and allowed to react at room temperature overnight. After 18 hours, the darker yellow reaction mixture was removed from the glovebox, and the solvent was removed *via* rotary evaporation. CH$_2$Cl$_2$ (~20 mL) was added and this slurry was filtered through Celite, yielding a dark orange filtrate (which was discarded) and a gray solid stuck on the Celite that was emissive under UV excitation from a hand-held TLC lamp (λ_{exc} = 365 nm). 1,2-Difluorobenzene (~25 mL) was heated to boiling and passed through the Celite in portions (5 x 5 mL) to wash though the gray solid. The tan filtrate was dried *via* rotary evaporation, yielding a tan solid. The solid was then washed with portions of THF (3 x 3 mL) and filtered, and the gray-white solid was vacuum dried (0.063 g, 62%). ^{1}H NMR data suggests exclusively κ^2-C,C-bound isomer (**3a**). **^{1}H NMR** (THF-d^8, 500 MHz) δ 9.44 (d, 2H, Ar), 8.40 (d, 2H, Ar), 7.93 (dd, 2H, Ar), 3.1-1.0 (br. m, 20H, BH), 1.46 (s, 18H, ^{t}Bu); **^{11}B NMR** (THF-d$_8$, 160 MHz) δ -0.21 to -2.73 (8B), -7.15 (12B); **^{13}C{^{1}H} NMR** (THF-d^8, 125 MHz) δ 166.17, 157.32, 151.55, 124.33, 121.95, 36.43, 29.95. *Note: C$_{bis-carborane}$ are not observed due to limited solubility of 3a.*

4.4.8.2 Pt(bc)(dtb-bpy), κ^2-B,C-bound (3b)

Inside a N_2 filled glove box, **bc** (0.010 g, 0.035 mmol), potassium bis(trimethylsilyl)amide (KHMDS, 0.070 g, 0.035 mmol, 1 equiv), and 1 mL THF were added to

a 20 mL vial, which was then allowed to react at room temperature for 1 hour. In a separate 20 mL vial, Pt(dtb-bpy)Cl$_2$ (0.018 g, 0.035 mmol, 1 equiv) and 5 mL THF were combined in a 20 mL vial, which was stored at -30 °C for 1 hour. The Pt(dtb-bpy)Cl$_2$ slurry was removed from the freezer and MeLi was added (12 mL, 3 M in diethoxymethane, 0.035 mmol, 1 equiv), and this reaction mixture was allowed to stir for about one minute. Next, the K[**H-bc**] reaction mixture was added dropwise to the Pt(II) reaction mixture, which was then allowed to warm up to room temperature and react overnight. After 18 hours, the deep red reaction mixture was removed from the glovebox, and the solvent was removed *in vacuo*. CH$_2$Cl$_2$ (3-5 mL) was added and this slurry was filtered through Celite, yielding a dark orange filtrate (which was discarded) and a gray solid stuck on the Celite that was emissive under UV excitation from a hand-held TLC lamp (λ_{exc} = 365 nm). 1,2-Difluorobenzene (~10 mL) was heated to boiling and passed through the Celite in portions (5 x 2 mL) to wash though the gray solid. The clear filtrate was dried *in vacuo*, yielding a tan solid. The solid was washed with portions of THF (3 x 1 mL) and filtered, and the gray-white solid was vacuum dried (0.003 g, 12%). ^{1}H NMR data suggests >95% κ^2-B,C-bound isomer (**3b**). **^{1}H NMR** (THF-d^8, 500 MHz) δ 9.84 (d, 1H, Ar), 9.27 (d, 1H, Ar), 8.42 (d, 1H, Ar), 8.37 (d, 1H, Ar), 7.98 (dd, 1H, Ar), 7.85 (dd, 1H, Ar), 4.48 (s, 1H, CH$_{bis-carborane}$), 3.2-1.6 (br m, 20H, BH), 1.464 (9H, s, ^{t}Bu), 1.459 (9H, s, ^{t}Bu); **^{11}B NMR** (THF-d$_8$, 160 MHz) δ -6.29 (6B), -11.02 (6B), -13.48 (8B); **^{13}C{^{1}H} NMR** (THF-d^8, 125 MHz) δ 165.26, 164.82, 157.80, 156.34, 154.06, 150.06, 124.98, 124.34, 120.93, 120.17, 36.34, 36.28, 30.09, 29.97. *Note: C$_{bis-carborane}$ are not observed due to limited solubility of **3b***. X-ray quality crystals of **3b** were grown from the slow evaporation of a concentrated solution of 2-MeTHF over the course of one week. One molecule of 2-MeTHF was rendered using the SQUEEZE method due to disorder.

4.4.9 Supplementary Figures and Tables
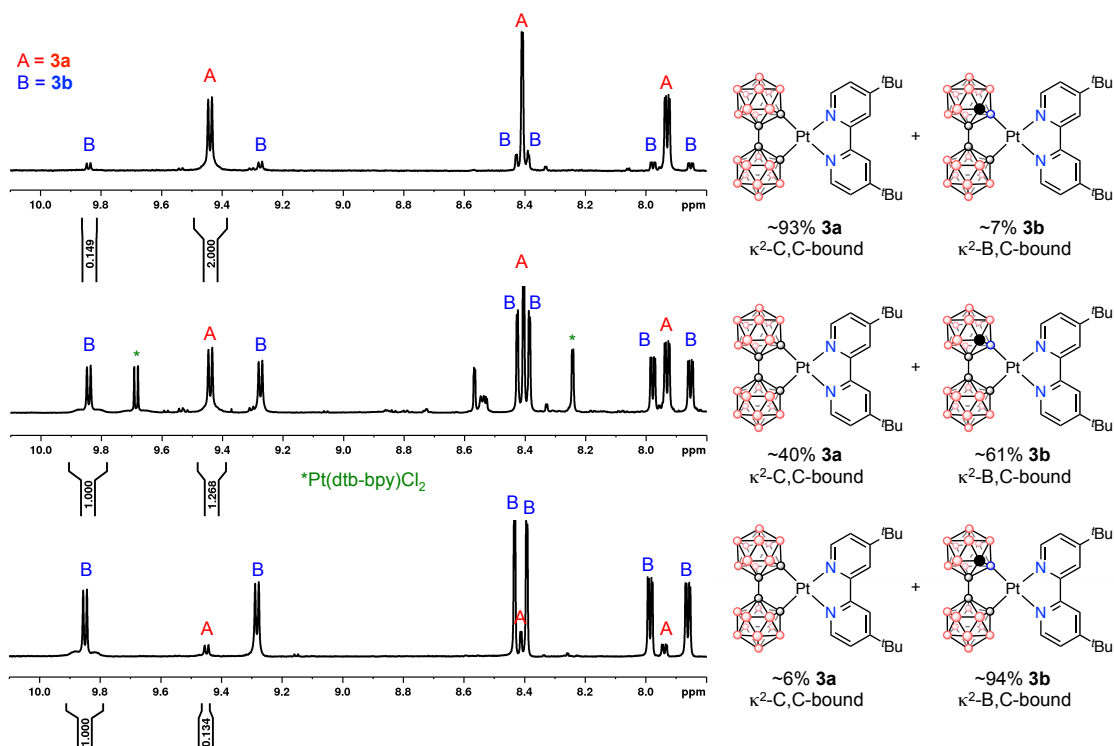
Figure C1 ^{1}H NMR spectra (THF-d$_8$) for isolated mixtures of **3a** and **3b** highlighting the large distribution of isomers.

Table C1 Isomer distribution of **3a** and **3b** depending on batch of ^{n}BuLi.^{a,b}
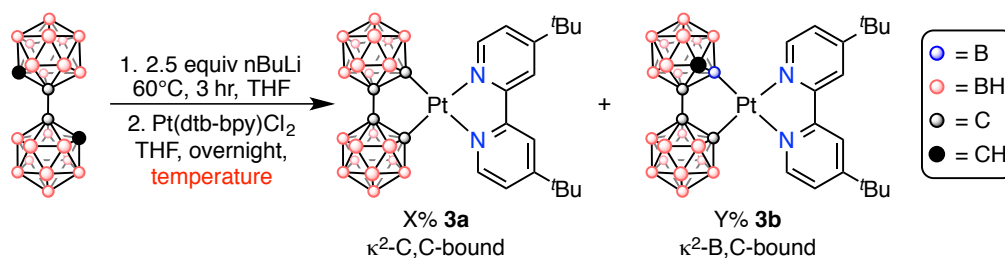
Bottle of ^{n}BuLi	Temperature	X% (% **3a**)	Y% (% **3b**)	Isolated Yield %
A	-80°C to 60°C	95	5	42
A	60°C	5	95	30
B	-80°C to 60°C	60	40	21
B	60°C	40	60	27
C	-80°C to 60°C	70	30	20
C	60°C	40	60	11

^{a}Determined by ^{1}H NMR spectroscopy. ^{b}Initial experiments suggested that the ratio of **3a** to **3b** was dependent on the temperature at which the Li$_2$[**bc**] reaction mixture was added to the slurry of Pt(dtb-bpy)Cl$_2$ in THF (^{n}BuLi Bottle A, entries 1 and 2). These results were not reproducible when the experiment was repeated with different bottles of ^{n}BuLi (^{n}BuLi Bottles B and C, entries 3-6).
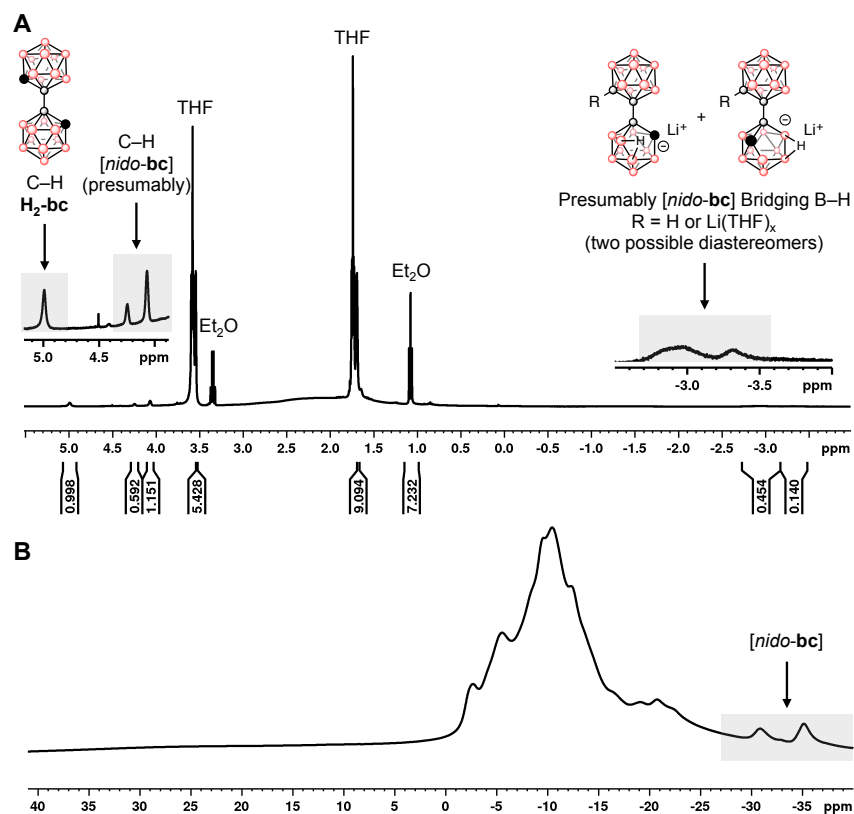
Figure C2 (A) ^{1}H NMR spectrum and (B) ^{11}B NMR spectrum of the product isolated using the lithiation conditions employed in the synthesis of **3a**/**3b**. NMR spectra were obtained in THF-d$_8$. In addition to the desired Li$_2$[**bc**] product, [*nido*-**bc**] and unreacted **H$_2$-bc** are also observed.

Table C2 Effect of **bc** lithiation time on isomer distribution of **3a** and **3b**.[a,b,c]
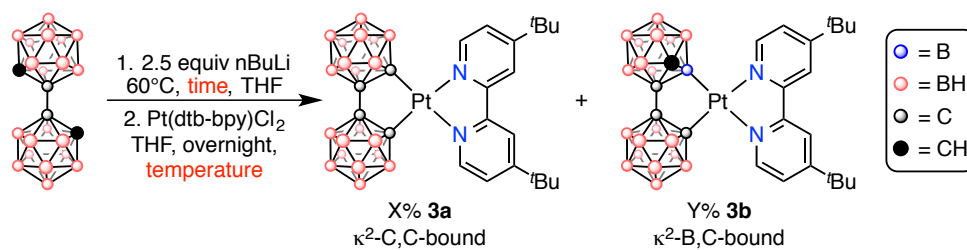
Time (hours)	Temperature	X% (% **3a**)	Y% (% **3b**)	Isolated Yield %[d]
1.5	-80°C to 60°C	5	95	20
3	-80°C to 60°C	60	40	21
1	60°C	50	50	30
2	60°C	20	80	38
3	60°C	40	60	27

[a]Determined by ^{1}H NMR spectroscopy. [b]One bottle of ^{n}BuLi was used for these experiments (^{n}BuLi Bottle B from Table C1). [c]Reactions were performed according to the general method for the synthesis of **3a**/**3b** using ^{n}BuLi. [d]Isolated yield for product mixture containing both **3a**/**3b**.
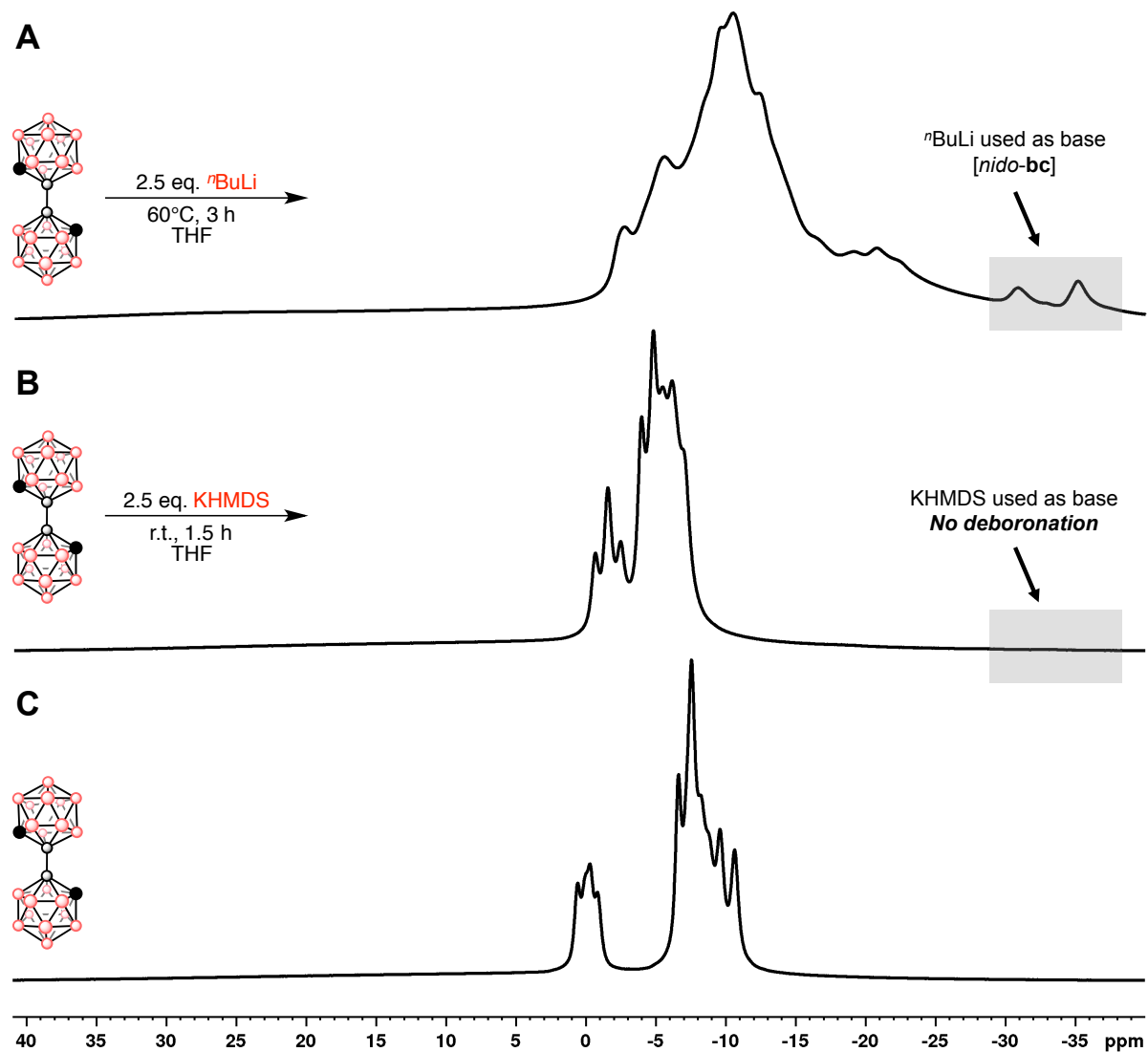
Figure C3 ^{11}B NMR spectra of (A) reaction mixture following deprotonation of **H₂-bc** with 2.5 equivalents of *n*BuLi (THF-d₈); (B) reaction mixture following deprotonation of **H₂-bc** with 2.5 equivalents of KHMDS (THF); (C) **H₂-bc** starting material (THF).

Table C3 Effect of additives on the product distribution of **3a/3b**.[a]
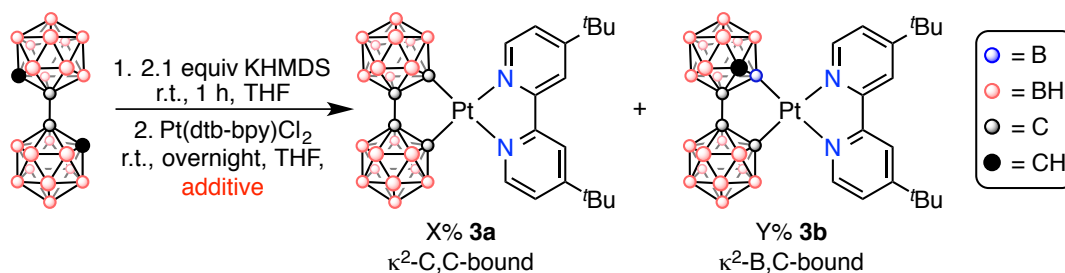
Additive	X% (% **3a**)	Y% (% **3b**)	Isolated Yield %
LiOH	95	5	–[b]
[K][*nido*-**bc**]	>99	<1	–[b]
[N^{n}Bu$_4$][*nido*-**bc**]	>99	<1	–[b]
AgBF$_4$	90	10	<5[c]

[a]Determined by ^{1}H NMR spectroscopy. [b]Purified products not isolated, ratios of isomers determined from ^{1}H NMR data of the crude reaction mixtures. [c]Majority of the mass balance is a black solid, presumably Pt metal. [K][*nido*-**bc**] and [N^{n}Bu$_4$][*nido*-**bc**] were synthesized according to previously reported procedures.[9]

Table C4 Cationic Pt(II) starting material.[a]
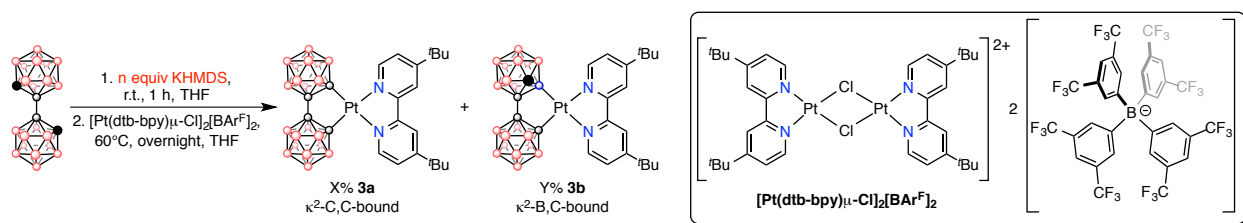
Equiv KHMDS	X% (% **3a**)	Y% (% **3b**)	Isolated Yield %
1	85	15	31
0[b]	–	–	–

[a]Determined by ^{1}H NMR spectroscopy. [b]No emissive product formed during the course of this reaction. The synthesis of [Pt(dtb-bpy)*m*-Cl]$_2$[BAr^F]$_2$ was adapted from a previously reported procedure.[10]

Initially, we examined the use of side products as additives in the reaction mixture to determine how the formation of **3b** was occurring. The use of LiOH, a potential contaminant in ^{n}BuLi, resulted in the formation of almost entirely **3a** (>95%, Table C3, entry 1). Similarly, the introduction of [*nido*-**bc**] to the reaction mixture, a side product observed during the course of the deprotonation of **H$_2$-bc**, resulted in the formation of >99% **3a** isomer (Table C3, entries 2 and 3).

We then investigated the use of formally cationic Pt(II) precursors. The use of AgBF$_4$ as an additive to generate [Pt(dtb-bpy)μ-Cl]$_2$[BF$_4$]$_2$ *in situ* resulted in the formation of a mixture of isomers containing 10% **3b** (Table C3, entry 4). A significant amount of a black solid, presumably Pt metal, formed upon the addition of AgBF$_4$ to the reaction mixture, resulting in an isolated yield of <5%. To circumvent this issue, we synthesized [Pt(dtb-bpy)μ-Cl]$_2$[BAr^F]$_2$ for use as a well-defined cationic Pt(II) starting material. Reactions between this Pt(II) precursor and K[**H-bc**] resulted in an isomer distribution of 85:15 **3a**:**3b** with a slightly improved isolated yield of 31% (Table C4, entry 1). No emissive product was observed when **H$_2$-bc** was used under similar conditions (Table C4, entry 2).
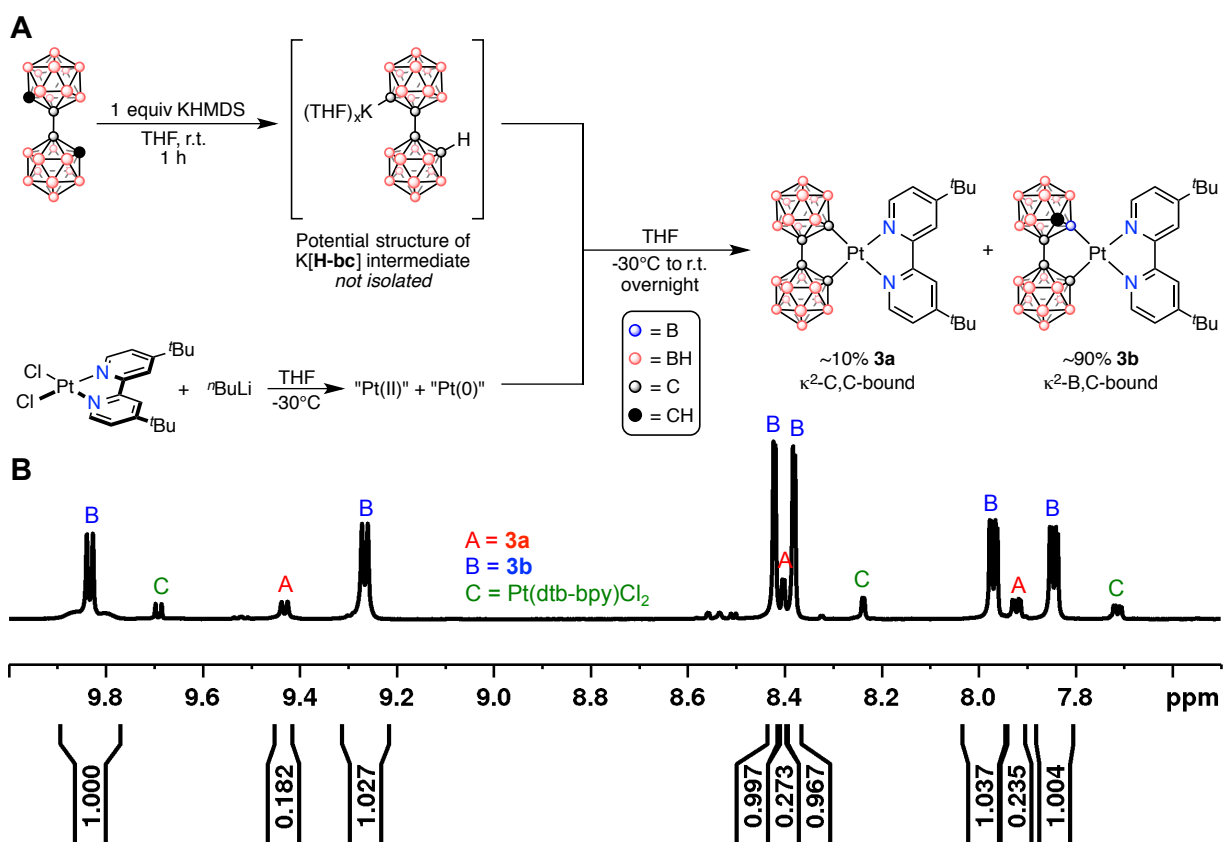
Figure C4 (A) Reaction scheme for addition of K[**H-bc**] to a reaction mixture containing Pt(dtb-bpy)Cl$_2$ and 1 equivalent ^{n}BuLi. (B) ^{1}H NMR spectrum (THF-d$_8$) of product (not purified).

Based on the small amount of unreacted **H₂-bc** observed in the product isolated after the lithiation of **H₂-bc** (Fig C2), we hypothesized unreacted ^{n}BuLi might be present in the reaction mixture. Upon addition of the Li₂[**bc**] reaction mixture to the Pt(II) precursor, any remaining ^{n}BuLi may potentially react with Pt(dtb-bpy)Cl₂ to form an alkyl Pt(II) complex as a precursor to **3b**. To test this, we performed a reaction in which 1 equivalent ^{n}BuLi was added to a cold slurry of Pt(dtb-bpy)Cl₂, then a solution of K[**H-bc**] was added to this reaction mixture (Fig C4A). Neither K[**H-bc**] nor the product of the reaction between Pt(dtb-bpy)Cl₂ and ^{n}BuLi were isolated in this experiment. The crude product was subjected to ^{1}H NMR spectroscopy (THF-d₈), and the mixture of isomers was found to contain ~90% **3b** (Figure C4B). Encouraged by this result, we performed a screen of alkyl lithium reagents and Grignard reagents to determine which reagent resulted in the largest amount of **3b** (Table C5).

Table C5 Optimization of **3b** formation.^{a}
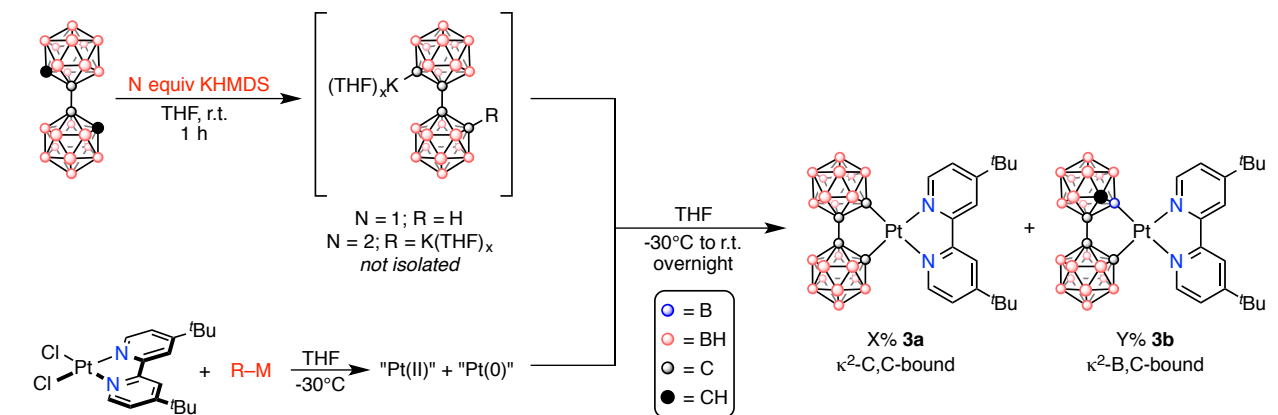
N equiv KHMDS	R–M	X% (% **3a**)	Y% (% **3b**)
1	2.5 M *n*-butyllithium in hexanes	10	90
2	2.5 M *n*-butyllithium in hexanes	35	65
1	3 M Ethylmagnesium bromide in diethyl ether	$-^b$	$-^b$
1	3 M Benzylmagnesium bromide in 2-MeTHF	80	20
1	3 M Methyllithium in diethoxymethane	>95	<5

^{a}Ratios of **3a** to **3b** determined by ^{1}H NMR spectroscopy. ^{b}Complex mixture and decomposition, no emissive product observed.

Initially, we studied how the deprotonation of **H$_2$-bc** affected the distribution of isomers. When 1 equivalent of KHMDS was used to deprotonate **H$_2$-bc**, the mixture of isomers was 90% **3b** (Table C5, entry 1), whereas when 2 equivalents of KHMDS were used, the relative amount of **3b** dropped to 65% (Table C5, entry 2). Based on these results, we moved forward with 1 equivalent of KHMDS in subsequent reactions.

The use of an alkyl Grignard reagent in place of ^{n}BuLi (EtMgBr, Table C5, entry 3) resulted in a complex mixture of products and the formation of a black solid, presumably Pt metal. No emissive product was observed under these reaction conditions. We probed the importance of an available β-proton in the Grignard reagent by using benzylmagnesium bromide (no β-proton; Table C5, entry 4). This reaction resulted in a mixture of isomers containing 20% **3b**. Finally, we performed this reaction with the addition of 1 equivalent of methyllithium in diethoxymethane (Table C5, entry 5). Under these reaction conditions, the mixture of isomers was at least 95% **3b** (repeated 3 times).
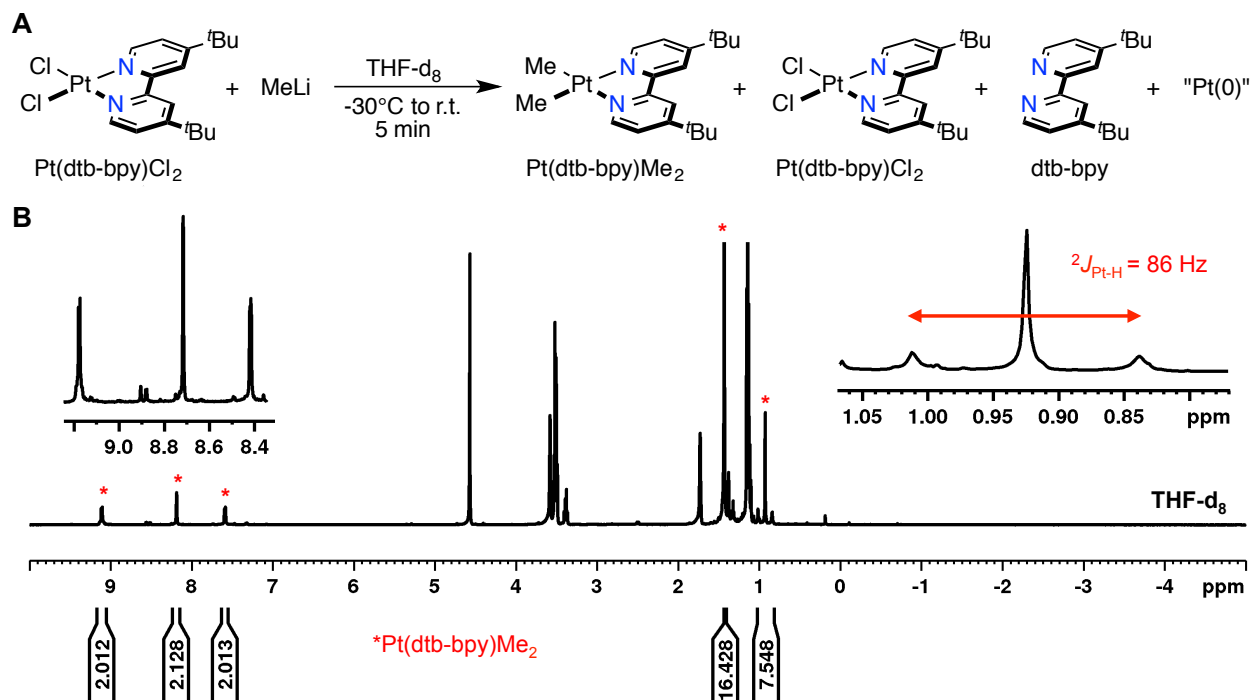
Figure C5 (A) NMR-scale reaction in which the addition of 1 equivalent of MeLi to Pt(dtb-bpy)Cl$_2$ offers both Pt(II) and Pt(0) products. (B) ^{1}H NMR spectrum (THF-d$_8$) of the reaction from (A) showing the major product is Pt(dtb-bpy)Me$_2$ (^{1}H NMR data are consistent with those from reference 11).

In order to determine the fate of Pt(dtb-bpy)Cl$_2$ upon the addition of an alkyl lithium reagent, we conducted an NMR-scale reaction in which 1 equivalent of MeLi (3 M solution in diethoxymethane) was added to Pt(dtb-bpy)Cl$_2$ in THF-d$_8$ (Figures C5 and C6A). Based on ^{1}H NMR spectroscopy, the major product formed from this reaction is Pt(dtb-bpy)Me$_2$. Unreacted Pt(dtb-bpy)Cl$_2$ and a small amount of free dtb-bpy are also present in the reaction mixture (*Reaction Mixture A*, Figure C6A), suggesting the reduction of Pt(II) occurs under these conditions. To this reaction mixture was added 1 equivalent of MeLi (2nd equivalent of MeLi overall) to yield *Reaction Mixture B* (Figure C6B). The amount of free dtb-bpy in the reaction mixture increased, and new unidentified side products were also observed via ^{1}H NMR spectroscopy. Next, a solution of K[**H-bc**] was added to this reaction mixture, which was then allowed to react overnight (*Reaction Mixture C*, Figure C6C). A mixture of isomers containing

95% **3b** was observed via ^{1}H NMR spectroscopy. The major species in this reaction mixture is unreacted Pt(dtb-bpy)Me$_2$.
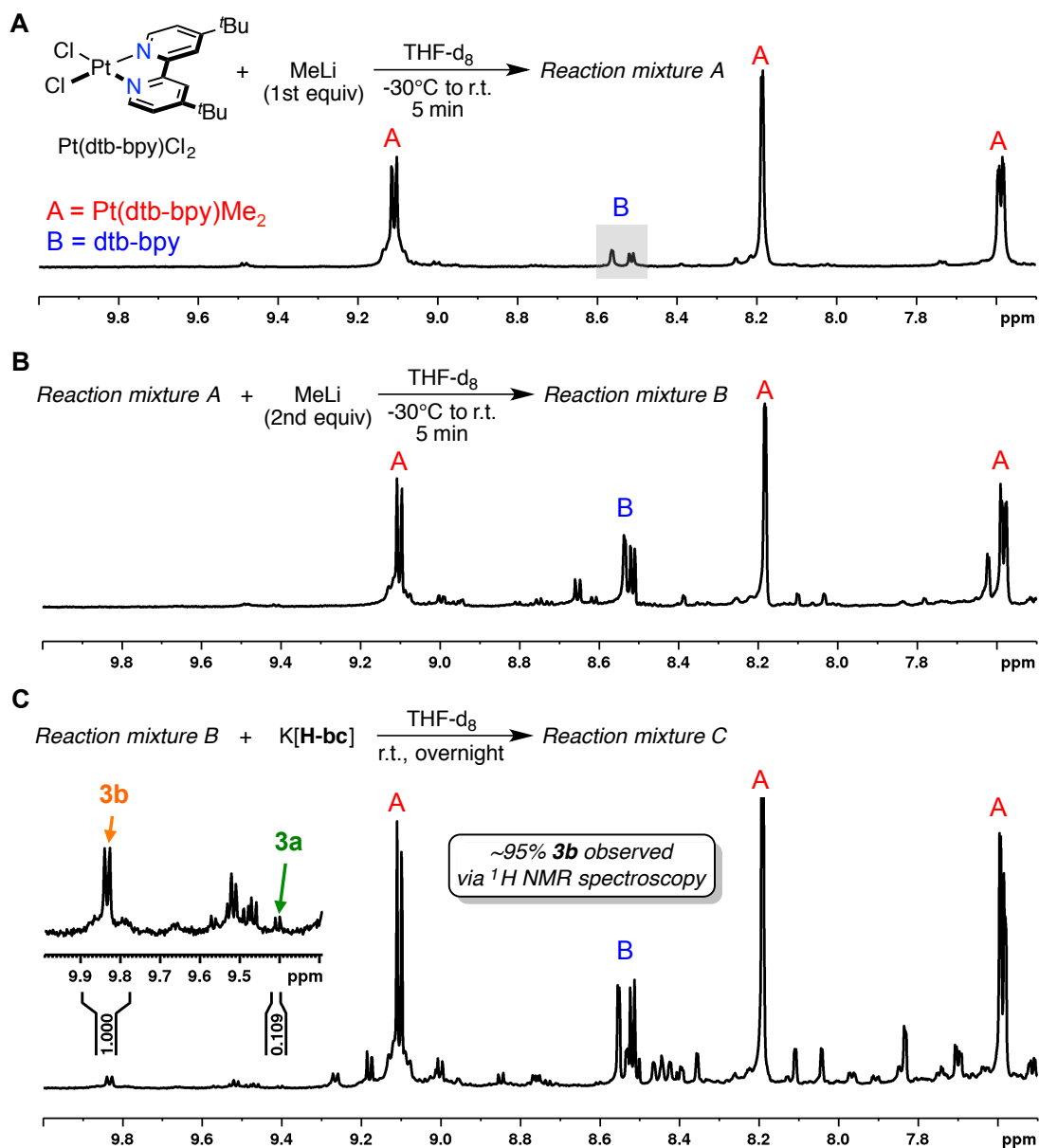
Figure C6 Sequential addition of reagents to an NMR-scale reaction (monitored by ^{1}H NMR spectroscopy, THF-d8). (A) The addition of 1 equivalent of MeLi to Pt(dtb-bpy)Cl$_2$ yielding *Reaction Mixture A*; (B) the addition of 1 equivalent of MeLi (2nd equivalent of MeLi overall) to *Reaction Mixture A* to yield *Reaction Mixture B*; (C) the addition of K[**H-bc**] to *Reaction Mixture B* to yield *Reaction Mixture C*, which contains a 95:5 **3b**:**3a** ratio of isomers as a minor product. The major species observed by ^{1}H NMR spectroscopy in *Reaction Mixture C* is unreacted Pt(dtb-bpy)Me$_2$.

146
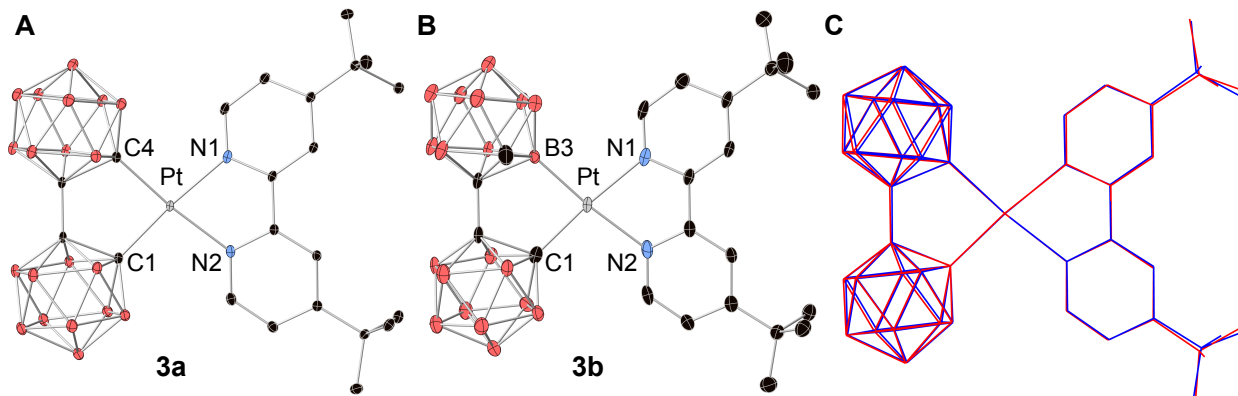
Figure C7 Thermal ellipsoid plots of (A) **3a** and (B) **3b** (50% probability). H atoms were omitted for clarity. See reference 12 for CIF data for **3a**. (C) Structural overlay of **3a** (red) and **3b** (blue).

Table C6 Selected bond distances for **3a** and **3b**.[a]

3a		**3b**	
Parameter	Distance (Å)	Parameter	Distance (Å)
Pt–C4	2.045(2)	Pt–B3	2.037(2)
Pt–C1	2.043(0)	Pt–C1	2.035(3)
Pt–N1	2.091(5)	Pt–N1	2.115(1)
Pt–N2	2.104(7)	Pt–N2	2.130(3)

[a]Values from reference 12.
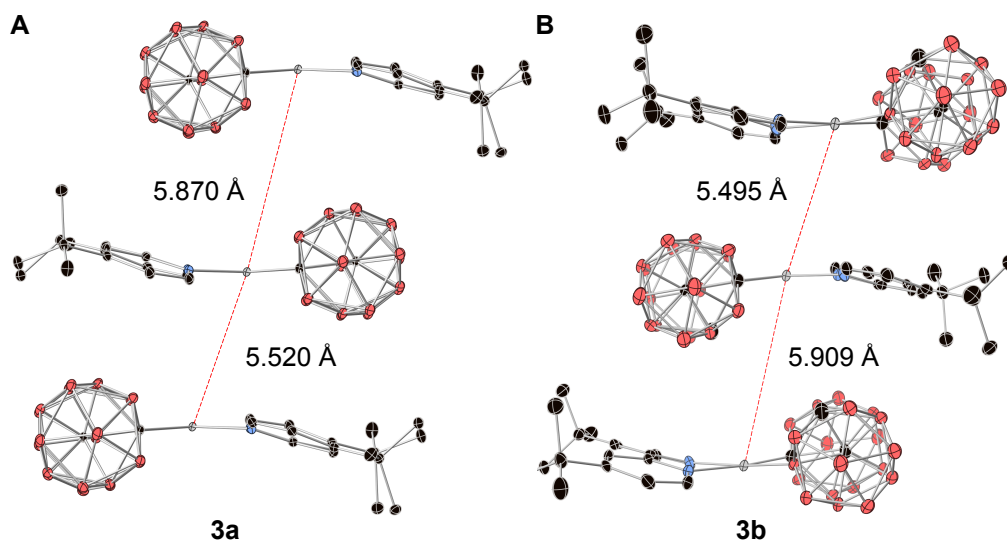
Figure C8 Intermolecular stacking of (A) **3a** and (B) **3b** with Pt(II)···Pt(II) distances highlighted. See reference 12 for CIF data for **3a**.
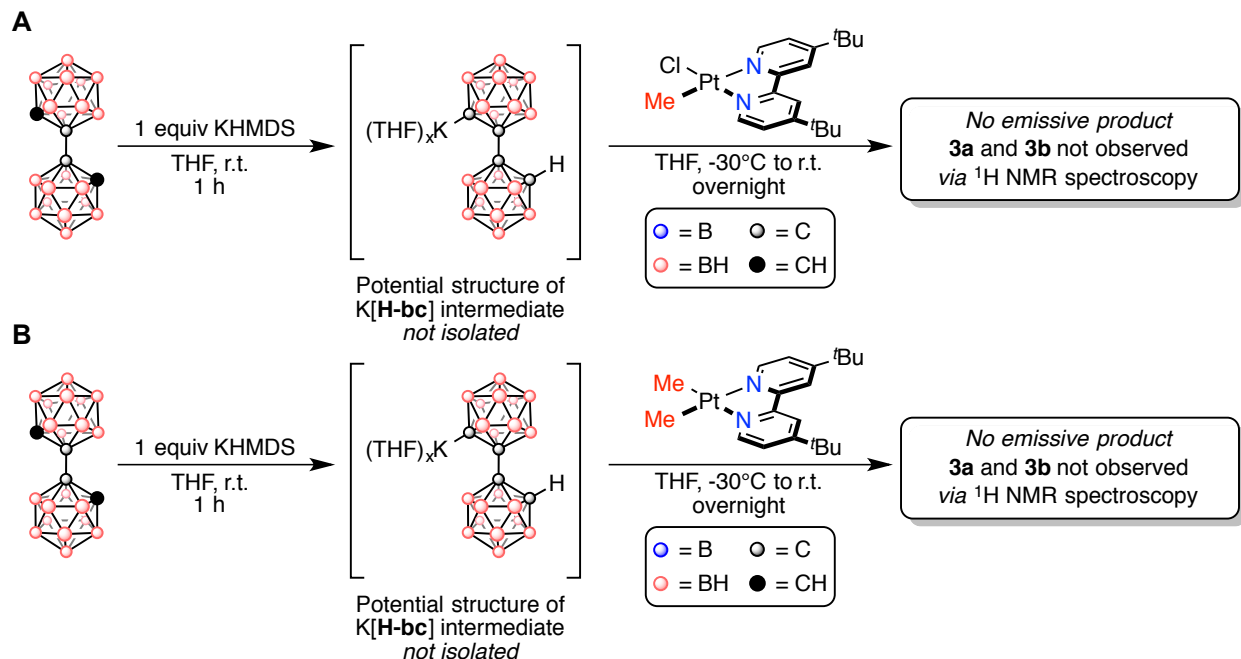
Figure C9 Control reactions with the addition of K[**H-bc**] to both Pt(dtb-bpy)MeCl (A) and Pt(dtb-bpy)Me$_2$ (B) yielded no emissive products and no **3a** or **3b** observable by ^{1}H NMR spectroscopy. These reaction conditions are identical to those employed for the successful synthesis of **3b**. Pt(dtb-bpy)Me$_2$[11] and Pt(dtb-bpy)MeCl[13] were synthesized according to previously reported procedures.

In order to gain mechanistic insight, a set of control reactions was performed in which the starting Pt(II) precursor was Pt(dtb-bpy)MeCl (a potential product after the addition of MeLi to Pt(dtb-bpy)Cl$_2$; Figure C7A) and Pt(dtb-bpy)Me$_2$ (product observed *via* ^{1}H NMR spectroscopy after the addition of MeLi to Pt(dtb-bpy)Cl$_2$; Figure C7B). No emissive product was formed in either reaction, and neither **3a** nor **3b** was observed *via* ^{1}H NMR spectroscopy. Based on these results, it seems unlikely that the formation of **3b** occurs through a Pt(II) intermediate.

Table C7 Effects of MeLi solution and additives on formation of **3b**.[a]
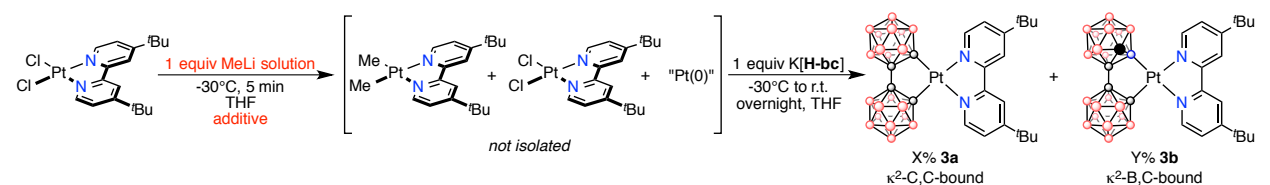
MeLi solution	Additive	X% (% **3a**)	Y% (% **3b**)	Isolated Yield (%)
Diethoxymethane	–	5	95	12%
Diethyl ether	–	–[b]	–[b]	–[b]
Diethyl ether	1,5-cyclooctadiene (5 equiv)	–[b]	–[b]	–[b]
Diethyl ether	1,5-cyclooctadiene (20 equiv)	70	30	38%

[a]Ratios of **3a** to **3b** determined by ^{1}H NMR spectroscopy. [b]Complex mixture and decomposition, no emissive product observed.

Significant differences in reactivity were observed based on the solution of MeLi used. When a solution of MeLi in diethoxymethane was employed, a mixture of isomers containing 95% **3b** was isolated in 12% yield (Table C6, entry 1). If a diethyl ether solution of MeLi was used, however, no emissive product formed and no **3a** or **3b** was observed *via* ^{1}H NMR spectroscopy (Table C6, entry 2). We hypothesized the formation of **3b** occurred through a Pt(0) intermediate, and varying the solvent affected the stability of the Pt(0) intermediate that formed. Therefore, we introduced 1,5-cyclooctadiene (COD) as an additive that would potentially stabilize any Pt(0) intermediate and prevent the formation of Pt metal. While there was no observable **3b** product with the addition of 5 equivalents of COD (Table C6, entry 3), the addition of 20 equivalents of COD resulted in a mixture of isomers that contained 30% **3b** (Table C6, entry 4). Although the ratio of **3b**:**3a** is lower under these conditions than when a diethoxymethane solution of MeLi is used with no additives (95:5, Table C6, entry 1), this evidence indirectly suggests that **3b** is formed *via* a Pt(0) intermediate.

We then used Pt$_2$dba$_3$ as a Pt(0) starting material in order to potentially improve the yield of **3b** (Figure C8). In this reaction, Pt$_2$(dba)$_3$ was combined with a slight excess of dtb-bpy in THF-d8 at room temperature. Next, a solution of K[**H-bc**] in THF-d$_8$ was added to this reaction

149

mixture and reaction progress was monitored *via* ^{1}H NMR spectroscopy. After heating overnight at 65 °C, ^{1}H NMR spectroscopy revealed the formation of trace amounts of **3b** (Figure C8B). No **3a** was observed in this reaction mixture. The addition of 20 equivalents of either 1,5-cyclooctadiene (Figure C9A) or PPh$_3$ (Figure C9B) to potentially improve the stability of any Pt(0) intermediate that might form resulted in the formation of a complex mixture of products with no **3a** or **3b** observable by ^{1}H NMR spectroscopy. Pt$_2$(dba)$_3$ does not seem to be a suitable Pt(0) starting material under these conditions, and a more thorough optimization is necessary.
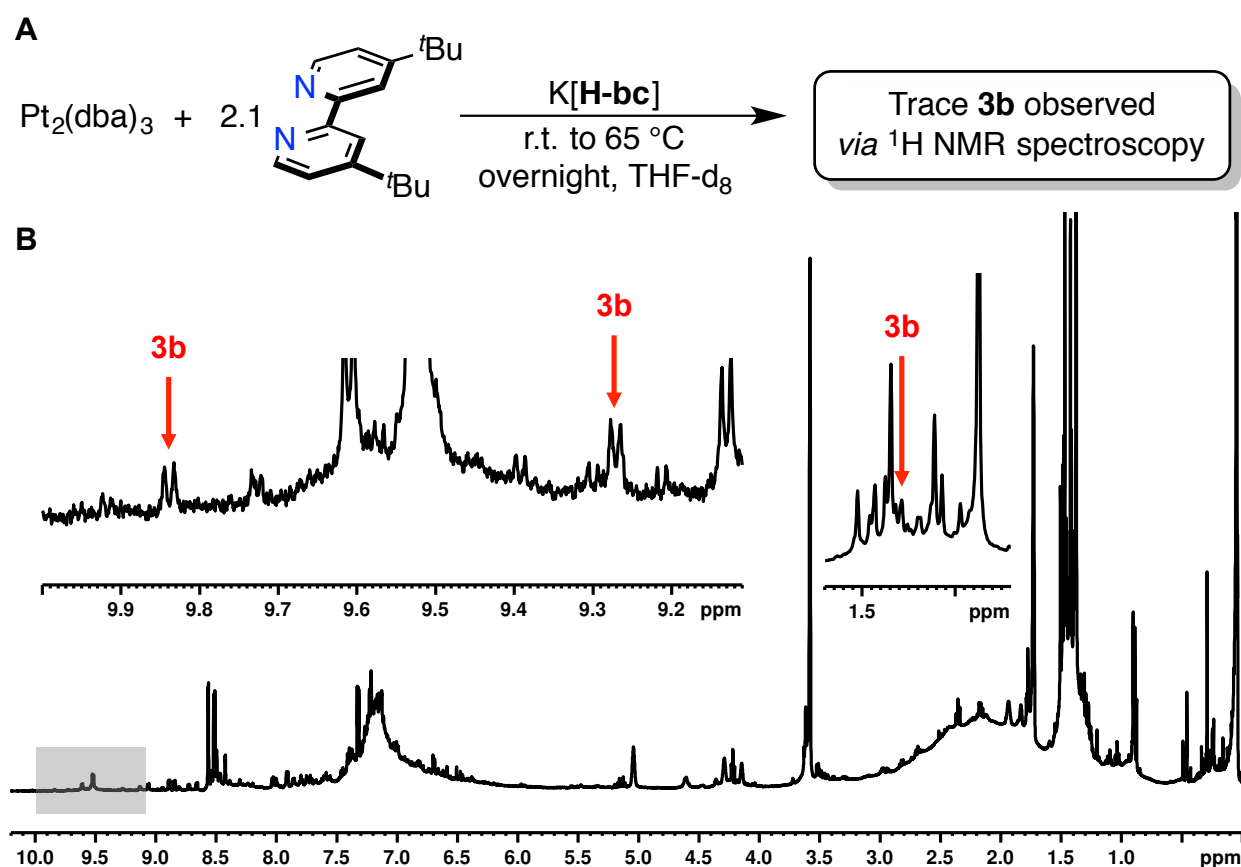
Figure C10 (A) NMR-scale reaction using Pt$_2$(dba)$_3$ as a Pt(0) precursor yields trace amounts of **3b**. (B) ^{1}H NMR spectrum (THF-d$_8$) for the reaction presented in (A), with highlighted regions showing resonances corresponding to **3b**.
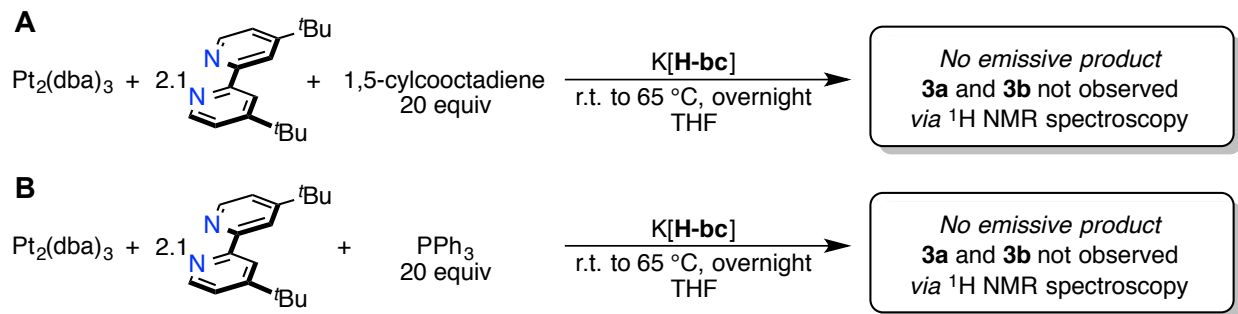
Figure C11 Reactions with Pt$_2$(dba)$_3$, dtb-bpy, and K[**H-bc**] and 20 equivalents of 1,5-cyclooctadiene (A) or PPh$_3$ (B). Under these reaction conditions, no emissive product formed and neither **3a** nor **3b** were observed *via* ^{1}H NMR spectroscopy.
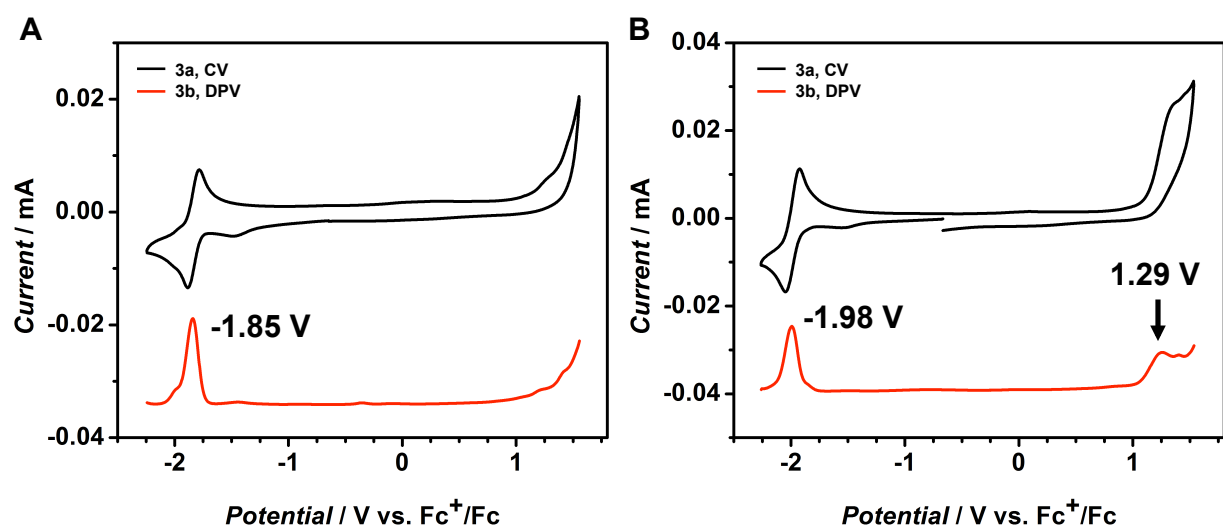
Figure C12 Stacked plots of cyclic voltammetry (CV, black trace) and differential pulsed voltammetry (DPV, red trace) measurements of **3a** (A) and **3b** (B). Experiments were performed in anhydrous 1,2-difluorobenzene with 0.1 M [N^{n}Bu$_4$][PF$_6$] and referenced to the ferrocenium/ferrocene redox couple (Fc$^+$/Fc). CV measurements were conducted with a scan rate of 0.1 V/s.
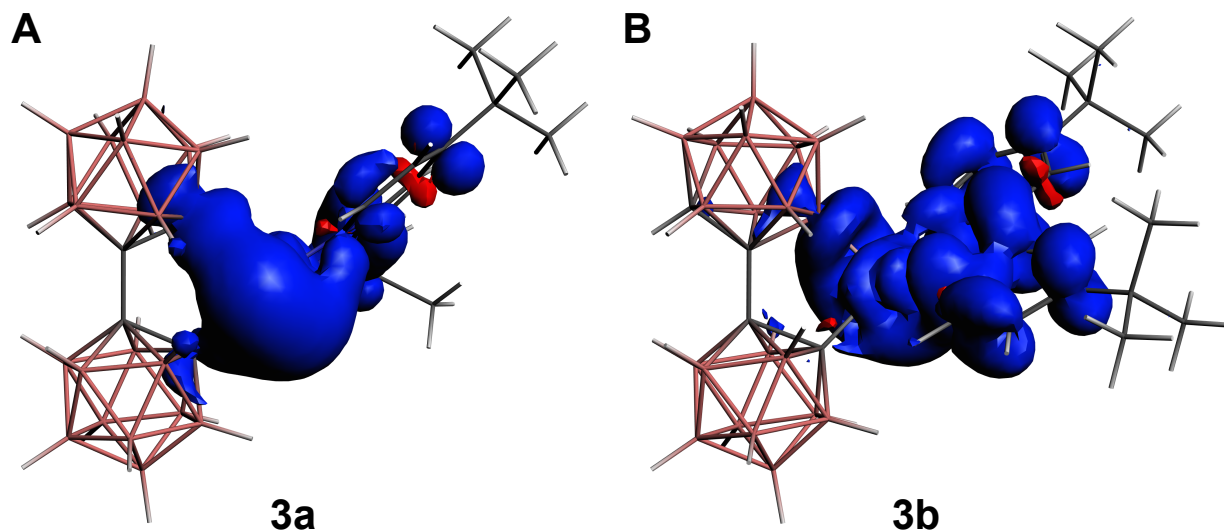
Figure C13 Triplet spin-density plots for **3a** (A) and **3b** (B). Optimized triplet geometries were obtained from the crystal structure of **3a** at the BP:TZP level, and single-point calculations were carried out at the B3LYP:TZ2P level of theory with the COSMO solvation model for THF.
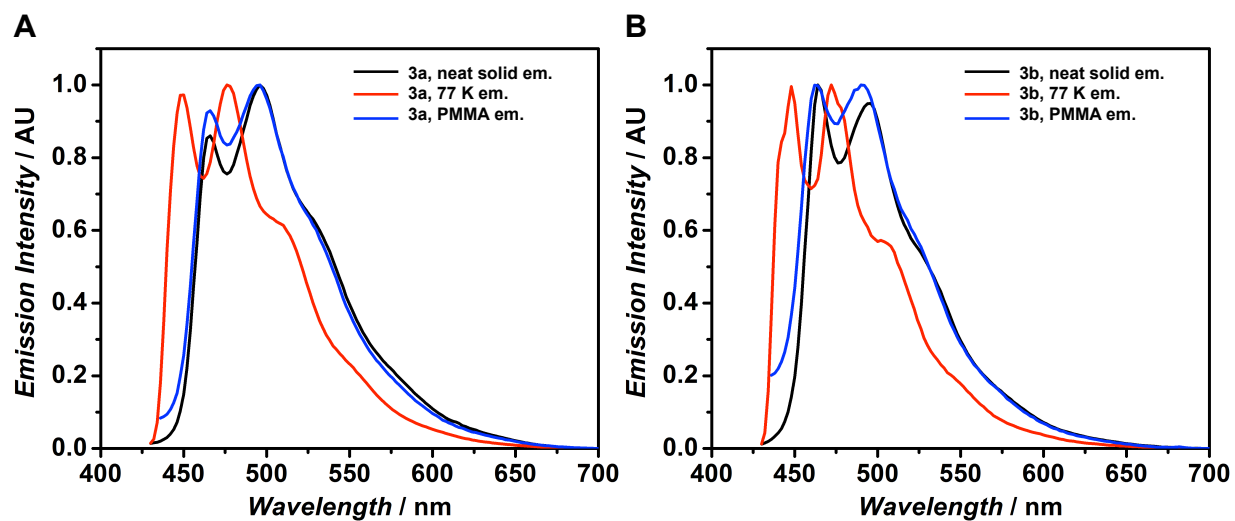
Figure C14 Emission spectra for neat solids (black trace), frozen solutions at 77 K (red trace), and PMMA films (blue trace) of **3a** (A) and **3b** (B).

Table C8 Emission and selected excited state lifetime data for **3a** and **3b**.

	Neat Solid	PMMA[a]	77 K[b]	τ^d
3a	466, 496, 528[c]	466, 495, 528[c]	449, 477	9.41 µs (2.90 µs, 23.38%; 8.14 µs, 79.07%)
3b	463, 495, 523[c]	462, 490, 521[c]	448, 472	9.04 µs (2.49 µs, 18.23%; 10.50 µs, 81.77%)

[a]2 wt % **3a** or **3b** in PMMA. [b]Obtained in 2-MeTHF. [c]Shoulder. [d]Excited state lifetime values for PMMA films (error in the measurement is ±5%). Values obtained as a weighted average of a biexponential decay. Individual lifetime components and their relative amplitudes are in parentheses.

4.4.10 References For Appendix C

1. C. F. Guerra, J. G. Snijders, G. te Velde, E. J. Baerends, *Theo. Chem. Acc.* **1998**, *99*, 391-403; G. te Velde, F. M. Bickelhaupt, E. J. Baerends C. F. Guerra, S. J. A. Van Gisbergen, J. G. Snijders, T. Ziegler, *J. Comput. Chem.* **2001**, *22*, 931-967; ADF 2014/GUI 2014, SCM, Amsterdam, The Netherlands, http://www.scm.com, E.J. Baerends, T. Ziegler, J. Autschbach, D. Bashford, A. Bérces, F.M. Bickelhaupt, C. Bo, P.M. Boerrigter, L. Cavallo, D.P. Chong, L. Deng, R.M. Dickson, D.E. Ellis, M. van Faassen, L. Fan, T.H. Fischer, C. Fonseca Guerra, M. Franchini, A. Ghysels, A. Giammona, S.J.A. van Gisbergen, A.W. Götz, J.A. Groeneveld, O.V. Gritsenko, M. Grüning, S. Gusarov, F.E. Harris, P. van den Hoek, C.R. Jacob, H. Jacobsen, L. Jensen, J.W. Kaminski, G. van Kessel, F. Kootstra, A. Kovalenko, M.V. Krykunov, E. van Lenthe, D.A. McCormack, A. Michalak, M. Mitoraj, S.M. Morton, J. Neugebauer, V.P. Nicu, L. Noodleman, V.P. Osinga, S. Patchkovskii, M. Pavanello, P.H.T. Philipsen, D. Post, C.C. Pye, W. Ravenek, J.I. Rodríguez, P. Ros, P.R.T. Schipper, H. van Schoot, G. Schreckenbach, J.S. Seldenthuis, M. Seth, J.G. Snijders, M. Solà, M. Swart, D. Swerhone, G. te Velde, P. Vernooijs, L. Versluis, L. Visscher, O. Visser, F. Wang, T.A. Wesolowski, E.M. van Wezenbeek, G. Wiesenekker, S.K. Wolff, T.K. Woo, A.L. Yakovlev.
2. A. D. Becke, *Phys. Rev. A* **1988**, *38*, 3098-3100.
3. J. P. Perdew, *Phys. Rev. B* **1986**, *33*, 8822-8824.
4. A. D. Becke, *J. Chem. Phys.* **1993**, *98*, 5648-5652.
5. C. Lee, W. Yang, R. G. Parr, *Phys. Rev. B* **1988**, *37*, 785.
6. E. van Lenthe, E. J. Baerends, J. G. Snijders, *J. Chem. Phys.* **1993**, *99*, 4597-4610.
7. E. van Lenthe, E. J. Baerends, J. G. Snijders, *J. Chem. Phys.* **1994**, *101*, 9783-9792.
8. E. van Lenthe, A. Ehlers, E. J. Baerends, *J. Chem. Phys.* **1999**, *110*, 8943-8953.
9. G. S. Kazakov, I. B. Sivaev, K. Y. Suponitsky, A. D. Kirilin, V. I. Bregadze, A. J. Welch, *J. Organomet. Chem.* **2016**, *805*, 1-5.
10. J. L. McBee, A. T. Bell, T. D. Tilley, *J. Am. Chem. Soc.* **2008**, *130*, 16562-16571.
11. S. Achar, J. D. Scott, J. J. Vittal, R. J. Puddephatt, *Organometallics* **1993**, *12*, 4592-4598.
12. K. O. Kirlikovali, J. C. Axtell, A. Gonzalez, A. C. Phung, S. I. Khan, A. M. Spokoyny, *Chem. Sci.* **2016**, *7*, 5132-5138.
13. L. R. Rendina, J. J. Vittal, R. J. Puddephatt, *Organometallics* **1995**, *14*, 1030-1038.

4.5 References

1. (a) Sun, C.-Y.; To, W.-P.; Hung, F.-F.; Wang, X.-L.; Su, Z.-M.; Che, C.-M. Metal–Organic Framework Composites with Luminescent Pincer Platinum(II) Complexes: ^{3}MMLCT Emission and Photoinduced Dehydrogenation Catalysis. *Chem. Sci.* **2018**, *9*, 2357-2364. (b) Lin, S.; Kitamoto, K.; Ozawa, H.; Sakai, K. Improved Photocatalytic Hydrogen Evolution Driven by Chloro(terpyridine)platinum(II) Derivatives Tethered to a Single Pendant Viologen Acceptor. *Dalton Trans.* **2016**, *45*, 10643-10654. (c) Wang, X.; Goeb, S.; Ji, Z.; Pogulaichenko, N. A.; Castellano, F. N. Homogenous Photocatalytic Hydrogen Production Using p-Conjugated Platinum(II) Arylacetylide Sensitizers. *Inorg. Chem.* **2011**, *50*, 705-707. (d) Mori, K.; Ogawa, S.; Martis, M.; Yamashita, H. Intercalation of Pt(II) Terpyridine Complexes into Layered $K_4Nb_6O_{17}$ and Visible-Light-Driven Photocatalytic Production of H_2. *J. Phys. Chem. C* **2012**, *116*, 18873-18877. (e) Du, P.; Schneider, J.; Jarosz, P.; Eisenberg, R. Photocatalytic Generation of Hydrogen from Water Using a Platinum(II) Terpyridyl Acetylide Chromophore. *J. Am. Chem. Soc.* **2006**, *128*, 7726-7727.

2. (a) Kalinowski, J.; Fattori, V.; Cocchi, M.; Williams, J. A. G. Light-Emitting Devices Based on Organometallic Platinum Complexes as Emitters. *Coord. Chem. Rev.* **2011**, *255*, 2401-2425. (b) Williams, J. A. G.; Develay, S.; Rochester, D. L.; Murphy, L. Optimising the Luminescence of Platinum(II) complexes and their Application in Organic Light Emitting Devices (OLEDs). *Coord. Chem. Rev.* **2008**, *252*, 2596-2611. (c) Chi, Y.; Chou, P.-T. Transition-Metal Phosphors with Cyclometalating Ligands: Fundamentals and Applications. *Chem. Soc. Rev.* **2010**, *39*, 638-655. (d) Fleetham, T.; Li, G.; Li, J. Phosphorescent Pt(II) and Pd(II) Complexes for Efficient, High-Color-Quality, and Stable OLEDs. *Adv. Mater.* **2017**, *29*, 1601861. (e) H. Yersin, *Highly Efficient OLEDs with Phosphorescent Materials*, Wiley-VCH, Weinheim, **2008**. (f) Chou, P.-T.; Chi, Y. Phosphorescent Dyes for Organic Light-Emitting Diodes. *Chem. Eur. J.* **2007**, *13*, 380-395.

3. (a) Li, K.; Tong, G. S. M.; Wan, Q.; Cheng, G.; Tong, W.-Y.; Ang, W.-H.; Kwong, W.-L.; Che, C.-M. Highly Phosphorescent Platinum(II) Emitters: Photophysics, Materials and Biological Applications. *Chem. Sci.* **2016**, *7*, 1653-1673. (b) Mauro, M.; Aliprandi, A.; Septiadi, D.; Kehr, N. S.; De Cola, L. When Self-Assembly Meets Biology: Luminescent Platinum Complexes for Imaging Applications. *Chem. Soc. Rev.* **2014**, *43*, 4144-4166. (c) Fereidoonnezhad, M.; Kaboudin, B.; Mirzaee, T.; Aghakhanpour, R. B.; Haghighi, M. G.; Faghih, Z.; Faghih, Z.; Ahmadipour, Z.; Notash, B.; Shahsavari, H. R. Cyclometalated Platinum(II) Complexes Bearing Bidentate *O,O′*-Di(alkyl)dithiophosphate Ligands: Photoluminescence and Cytotoxic Properties. *Organometallics* **2017**, *36*, 1707-1717. (d) Zhang, Y.; Luo, Q.; Zheng, W.; Wang, Z.; Lin, Y.; Zhang, E.; Lü, S.; Xiang, J.; Zhao, Y.; Wang, F. Luminescent Cyclometallated Platinum(II) Complexes: Highly Promising EGFR/DNA Probes and Dual-Targeting Anticancer Agents. *Inorg. Chem. Front.* **2018**, *5*, 413-424.

4. (a) Djurovich, P. I.; Murphy, D.; Thompson, M. E.; Hernandez, B.; Gao, R.; Hunt, P. L.; Selke, M. Cyclometalated Iridium and Platinum Complexes as Singlet Oxygen Photosensitizers: Quantum Yields, Quenching Rates and Correlation with Electronic Structures. *Dalton Trans.* **2007**, 3764-3770. (b) Wu, W.; Yang, P. Ma, L.; Lalevée, J.; Zhao, J. Visible-Light Harvesting Pt^{II} Complexes as Singlet Oxygen Photosensitizers for Photooxidation of 1,5-Dihydroxynaphthalene. *Eur. J. Inorg. Chem.* **2013**, 228-231. (c) Lai, S.-W.; Liu, Y.; Zhang, D.; Wang, B. Lok, C.-N.; Che, C.-M.; Selke, M. Efficient Singlet

Oxygen Generation by Luminescent 2-(2′-Thienyl)Pyridyl Cyclometalated Platinum(II) Complexes and Their Calixarene Derivatives. *Photochemistry and Photobiology* **2010**, *86*, 1414-1420. (d) Ashen-Garry, D.; Selke, M. Singlet Oxygen Generation by Cyclometalated Complexes and Applications. *Photochemistry and Photobiology* **2014**, *90*, 257-274.

5. (a) Rillema, D. P.; Cruz, A. J.; Moore, C.; Siam, K.; Jehan, A.; Base, D.; Nguyen, T.; Huang, W. *Inorg. Chem.* **2013**, *52*, 596-607. (b) Rillema, D. P.; Stoyanov, S. R.; Cruz, A. J.; Nguyen, H.; Moore, C.; Huang, W.; Siam, K.; Jehan, A.; KomReddy, V. *Dalton Trans.* **2015**, *44*, 17075-17090. (c) Brooks, J.; Babayan, Y.; Lamansky, S.; Djurovich, P. I.; Tsyba, I.; Bau, R.; Thompson, M. E. *Inorg. Chem.* **2002**, *41*, 3055-3066. (d) Tong, G. S.-M.; Che, C.-M. Emissive of Nonemissive? A Theoretical Analysis of the Phosphorescence Efficiencies of Cyclometalated Platinum(II) Complexes. *Chem. Eur. J.* **2009**, *15*, 7225-7237. (e) Hebenbrock, M.; Stegemann, L.; Kösters, J.; Doltsinis, N. L.; Müller, J.; Strassert, C. A. Phosphorescent Pt(II) Complexes Bearing a Monoanionic C^N^N Luminophore and Tunable Ancillary Ligands. *Dalton Trans.* **2017**, *46*, 3160-3169.

6. (a) Unger, Y.; Meyer, D.; Molt, O.; Schildknecht, C.; Münster, I.; Wagenblast, G.; Strassner, T. Green-Blue Emitters: NHC-Based Cyclometalated [Pt(C^C*)(acac)] Complexes. *Angew. Chem. Int. Ed.* **2010**, *49*, 10214-20216. (b) Strassner, T. Phosphorescent Platinum(II) Complexes with C^C* Cyclometalated NHC Ligands. *Acc. Chem. Res.* **2016**, *49*, 2680-2689.

7. (a) Sivasubramaniam, V.; Brodkorb, F.; Hanning, S.; Loebl, H. P.; van Elsbergen, V.; Boerner, H.; Scerf, U.; Kreyenschmidt, M. Fluorine Cleavage of the Light Blue Heteroleptic Triplet Emitter FIrpic. *J. Fluorine Chem.* **2009**, *130*, 640-649. (b) Seifert, R.; de Moraes, I. R.; Scholz, S.; Gather, M. C.; Lüssem, B.; Leo, K. Chemical Degradation Mechanisms of Highly Efficient Blue Phosphorescent Emitters Used for Organic Light Emitting Diodes. *Org. Electron.* **2013**, *14*, 115-123.

8. (a) Ma, B.; Djurovich, P. I.; Thompson, M. E. Excimer and Electron Transfer Quenching Studies of a Cyclometalated Platinum Complex. *Coord. Chem. Rev.* **2005**, *249*, 1501-1510. (b) Kunkely, H.; Volger, A. Photoluminescence of [Pt^{II}(4,7-diphenyl-1,10-phenanthroline)(CN)$_2$] in Solution. *J. Am. Chem. Soc.* **1990**, *112*, 5625-5627. (c) W. K.-T.; Che, C.-M.; Cho, K.-C. Inorganic Excimer. Spectroscopy, Photoredox Properties and Excimeric Emission of Dicyano(4,4′-di-*tert*-buytl-2,2′-bipyridine)platinum(II). *J. Chem. Soc., Dalton. Trans.* **1991**, 1077-1080. (d) Chan, C.-W.; Che, C.-M.; Cheng, M.-C.; Wang, Y. Spectroscopy, Photophysical Properties, and X-ray Crystal Structure of Platinum(II) Complexes of Quarterpyridine. *Inorg. Chem.* **1992**, *31*, 4874-4878. (e) Che, C.-M.; Wan, K.-T.; He, L.-Y.; Poon, C.-K.; Yan, V. W.-W. Novel Luminescent Platinum(II) Complexes. Photophysics and Photochemistry of Pt(5,5′-Me$_2$bpy)(CN)$_2$ (5,5′-Me$_2$bpy=5,5′-Dimethyl-2,2′-bipyridine). *J. Chem. Soc., Dalton Trans.* **1989**, 943-944.

9. (a) Heying, T. L.; Ager, J. W., Jr.; Clark, S. L.; Mangold, D. J.; Goldstein, H. L.; Hillman, M.; Polak, R. J.; Szymanski, J. W. A New Series of Organoboranes. I. Carboranes from the Reaction of Decaborane with Acetylenic Compounds. *Inorg. Chem.* **1963**, *2*, 1089-1092. (b) Fein, M. M.; Grafstein, D.; Paustian, J. E.; Bobinski, J.; Lichstein, B. M.; Mayes, N.; Schwartz, N. N.; Cohen, M. S. Carboranes. II. The Preparation of 1- and 1,2-Susbtituted Carboranes. *Inorg. Chem.* **1963**, *2*, 1115-1119. (c) Fein, M. M.; Bobinski, J.; Mayes, N.; Schwartz, N.; Cohen, M. S. Carboranes. I. The Preparation and Chemistry of 1-Isopropenylcarborane and its Derivatives (a New Family of Stable Clovoboranes). *Inorg. Chem.* **1963**, *2*, 1111-1115. (d) Zakharkin, L. I.; Stanki, V. I.; Brattsev, V. A.; Chapovskii, Y. A.; Klimova, A. I.; Okhlobystin, O. Y.; Ponomarenko, A. A. Dolk. The Synthesis and

Properties of a New Class of Organoboron Compounds $B_{10}C_2H_{12}$ (baren) and its Derivatives. *Akad. Nauk. SSSR* **1964**, *155*, 1119-1122. (e) Hawthorne, M. F.; Andrews, T. D.; Garrett, P. M.; Olsen, F. P.; Reintjes, M.; Tebbe, F. N.; Warren, L. F.; Wegner, P. A.; Young, D. C. Icosahedral Carboranes and Intermediates Leading to the Preparation of Carbametallic Boron Hydride Derivatives. *Inorg. Synth.* **1967**, *10*, 91. (f) Grimes, R. N. *Carboranes*, 3rd ed; Academic Press: 2016.

10. For recent, comprehensive reviews on boron-cluster-based luminescent metal complexes, see: (a) Li, X.; Yan, H.; Zhao, Q. Carboranes as a Tool to Tune Phosphorescence. *Chem. Eur. J.* **2016**, *22*, 1888-1898. (b) Mukherjee, S.; Thilagar, P. Boron Clusters in Luminescent Materials. *Chem. Commun.* **2016**, *52*, 1070-1093. (c) Xu, W.-J.; Qin, Y.-Y.; Wei, L.-W.; Zhang, K. Y.; Liu, S.-J.; Zhao, Q. Boron-Functionalized Phosphorescent Iridium(III) Complexes. *Eur. J. Inorg. Chem.* **2017**, 4393-4405.

11. For selected examples, see: (a) Islam, M. J.; Smith, M. D.; Peryshkov, D. V. Sterically Encumbered Dianionic Dicarboranyl Pincer Ligand $(C_5H_3N)(C_2B_{10}H_{11})_2$ and its CNC Nickel(II) Complex. *J. Organomet. Chem.* **2017**, DOI: 10.1016/j.jorganchem.2017.11.004. (b) Bae, H. J.; Kim, H.; Lee, K. M.; Kim, T.; Eo, M.; Lee, Y. S.; Do, Y.; Lee, M. H. Heteroleptic Tris-Cyclometalated Iridium(III) Complexes Supported by an *o*-Carboranyl-Pyridine Ligand. *Dalton Trans*. **2013**, *42*, 8549-8552. (c) Kim, T.; Lee, J.; Lee, S. U.; Lee, M. H. *o*-Carboranyl–Phosphine as a New Class of Strong-Field Ancillary Ligand in Cyclometalated Iridium(III) Complexes: Toward Blue Phosphorescence. *Organometallics* **2015**, *34*, 3455-3458. (d) Prokhorov, A. M.; Hofbeck, T.; Czerwieniec, R.; Suleymanova, A. F.; Kozhevnikov, D. N.; Yersin, H. Brightly Luminescent Pt(II) Pincer Complexes with a Sterically Demanding Carboranyl-Phenylpyridine Ligand: A New Material Class for Diverse Optoelectronic Applications. *J. Am. Chem. Soc*. **2014**, *136*, 9637-9642. (e) Harwell, D. E.; McMillan, J.; Knobler, C. B.; Hawthorne, M. F. Structural Characterization of Representative d^7, d^8, and d^9 Transition Metal Complexes of Bis(*o*-carborane). *Inorg. Chem.* **1997**, *36*, 5951-5955. (f) Martin, M. J.; Man, W. Y.; Rosair, G. M.; Welch, A. J. 1,1′-Bis(*ortho*-carborane) as a k^2 Co-Ligand. *J. Organomet. Chem.* **2015**, *798*, 36-40. (g) Yao, Z.-J.; Zhang, Y.-Y.; Jin, G.-X. *Pseudo*-aromatic Bis-*o*-carborane Iridium and Rhodium Complexes. *J. Organomet. Chem.* **2015**, *798*, 274-277.

12. For selected examples, see: (a) Eleazer, B. J.; Peryshkov, D. V. Coordination Chemistry of Carborane Clusters: Metal-Boron Bonds in Carborane, Carboranyl, and Carboryne Complexes. *Comments Inorg. Chem.* **2018**, DOI: 10.1080/02603594.2018.1465939. (b) Eleazer, B. J.; Smith, M. D.; Popov, A. A.; Peryshkov, D. V. Expansion of the (BB)>Ru Metallacycle with Coinage Metal Cations: Formation of B–M–Ru–B (M = Cu, Ag, Au) Dimetalacyclodiboryls. *Chem. Sci.* **2018**, *9*, 2601-2608. (c) Eleazer, B. J.; Smith, M. D.; Popov, A. A.; Peryshkov, D. V. (BB)-Carboryne Complex of Ruthenium: Synthesis by Double B–H Activation at a Single Metal Center. *J. Am. Chem. Soc.* **2016**, *138*, 10531-10538. (d) Prokhorov, A. M.; Slepukhin, P. A.; Rusinov, V. L.; Kalinin, V. N.; Kozhevnikov, D. N. 2,2′-Bipyridinyl Carboranes as B,N,N-Ligands in Cyclometallated Complexes of Platinum(II). *Chem. Commun.* **2011**, *47*, 7713-7715. (e) Saleh, L. M. A.; Dziedzic, R. M.; Khan, S. I.; Spokoyny, A. M. Forging Unsupported Metal–Boryl Bonds with Icosahedral Carboranes. **2016**, *22*, 8466-8470. (f) Kirlikovali, K. O.; Axtell, J. C.; Gonzalez, A.; Phung, A. C.; Khan, S. I.; Spokoyny, A. M. Luminescent Metal Complexes Featuring Photophysically Innocent Boron Cluster Ligands. *Chem. Sci*. **2016**, *7*, 5132-5138. (g) Riley, L. E.; Chan, A. P. Y.; Taylor, J.; Man, W. Y.; Ellis, D.; Rosair, G. M.; Welch, A. J.; Sivaev,

I. B. Unprecedented Flexibility of the 1,1′-Bis(*o*-carborane) Ligand: Catalytically-Active Species Stabilised by B-Agostic B–H→Ru Interactions. *Dalton Trans.* **2016**, *45*, 1127-1137.

13. For selected examples, see: (a) Hawthorne, M. F.; Young, D. C.; Wegner, P. A. Carbametallic Boron Hydride Derivatives. I. Apparent Analogs of Ferrocene and Ferrocenium Ion. *J. Am. Chem. Soc.* **1965**, *87*, 1818-1819. (b) Axtell, J. C.; Kirlikovali, K. O.; Djurovich, P. I.; Jung, D.; Nguyen, V. T.; Munekiyo, B. Royappa, A. T.; Rheingold, A. L.; Spokoyny, A. M. Blue Phosphorescent Zwitterionic Iridium(III) Complexes Featuring Weakly-Coordinating Anionic *nido*-Carborane-Based Ligands. *J. Am. Chem. Soc.* **2016**, *138*, 15758-15765. (c) Thiripuranathar, G.; Chan, A. P. Y.; Mandal,D.; Man, W. Y.; Argentari, M.; Rosair, G. M.; Welch, A. J. Double Deboronation and Homometalation of 1,1′-Bis(*ortho*-carborane). *Dalton Trans.* **2017**, *46*, 1811-1821. (d) Rojo, I.; Teixidor, F.; Viñas, C.; Kivekäs, R.; Sillanpää, R. Relevance of the Electronegativity of Boron in h^5-Coordinating Ligands: Regioselective Monoalkylation and Monoarylation in Cobaltabisdicarbollide [3,3′-Co(1,2-C$_2$B$_9$H$_{11}$)$_2$]$_2$ Clusters. *Chem. Eur. J.* **2003**, *9*, 4311-4323. (e) Li, T. C.; Spokoyny, A. M.; She, C.; Farha, O. K.; Mirkin, C. A.; Marks, T. J.; Hupp, J. T. *J. Am. Chem. Soc.* **2010**, *132*, 4580-4582.

14. (a) Spokoyny, A. M.; Machan, C. W.; Clingerman, D. J.; Rosen, M. S.; Wiester, M. J.; Kennedy, R. D.; Stern, C. L.; Sarjeant, A. A.; Mirkin, C. A. A Coordination Chemistry Dichotomy for Icosahedral Carborane-Based Ligands. *Nat. Chem.* **2011**, *3*, 590-596. (b) Spokoyny, A. M.; Lewis, C. D.; Teverovskiy, G.; Buchwald, S. L. Extremely Electron-Rich, Boron-Functionalized, Icosahedral Carborane-Based Phosphinoboranes. *Organometallics* **2012**, *31*, 8478-8481. (c) Weller, A. Ligand Design: The Two Faces of Carboranes. *Nat. Chem.* **2011**, *3*, 577-578.

15. (a) Wiesboeck, R. A.; Hawthorne, M. F. Dicarbaundecaborane (13) and Derivatives. *J. Am. Chem. Soc.* **1964**, *86*, 1642-1643. (b) Owen, D. A.; Hawthorne, M. F. Novel Chelated Biscarborane Transition Metal Complexes Formed through Carbon–Metal *s* Bonds. *J. Am. Chem. Soc.* **1970**, *92*, 3194-3196. (c) Axtell, J. C.; Kirlikovali, K. O.; Dziedzic, R. M.; Gembicky, M.; Rheingold, A. L.; Spokoyny, A. M. Magnesium Reagents Featuring a 1,1′-Bis(*o*-carborane) Ligand Platform. *Eur. J. Inorg. Chem.* **2017**, *38-39*, 4411-4416. (d) Owen, D. A.; Hawthorne, M. F. Chelated Biscarborane Transition Metal Derivatives Formed through Carbon-Metal *s* Bonds. *J. Am. Chem. Soc.* **1971**, *93*, 873-880. (e) Ren, S.; Xie, Z. A Facile and Practical Synthetic Route to 1,1′-Bis(*o*-carborane). *Organometallics* **2008**, *27*, 5167-5168.

16. (a) Wiesboeck, R. A.; Hawthorne, M. F. Dicarbaundecaborane(13) and Derivatives. *J. Am. Chem. Soc.* **1964**, *86*, 1642-1643. (b) Hawthorne, M. F.; Young, D. C.; Garrett, P. M.; Owen, D. A.; Schwerin, S. G.; Tebbe, F. N.; Wegner, P. A. The Preparation and Characterization of the (3)-1,2- and (3)-1,7-Dicarbadodecahydroundecaborate(-1) Ions. *J. Am. Chem. Soc.* **1968**, *90*, 862-868. (c) Hawthorne, M. F.; Owen, D. A.; Wiggins, J. W. The Degradation of Biscarborane. *Inorg. Chem.* **1971**, *10*, 1304-1306. (d) Kazakov, G. S.; Sivaev, I. B.; Suponitsky, K. Y.; Kirilin, A. D.; Bregadze, V. I.; Welch, A. J. Facile Synthesis of *closo-nido* Bis(carborane) and its Highly Regioselective Halogenation. *J. Organomet. Chem.* **2016**, *805*, 1-5. (e) Popescu, A.-R.; Musteti, A. D.; Ferrer-Ugalde, A.; Viñas, C.; Núñez, R.; Teixidor, F. Influential Role of Ethereal Solvent on Organolithium Compounds: The Case of Carboranyllithium. *Chem. Eur. J.* **2012**, *18*, 3174-3184.

17. (a) DiCosimo, R.; Whitesides, G. M. Reductive Elimination of a Carbon–Carbon Bond from Bis(trialkylphosphine)-3,3-dimethylplatinacyclobutanes Produces

Bis(trialkylphosphine)platinum(0) and 1,1-Dimethylcyclopropane. *J. Am. Chem. Soc.* **1982**, *104*, 3601-3607. (b) Young, G. B.; Whitesides, G. M. Oxidative Addition and Reductive Elimination Reactions Involving Platinum Metallacycles. *J. Am. Chem. Soc.* **1978**, *100*, 5808-5815. (c) Spencer, J. L.; Ittel, S. D.; Cushing, M. A. Olefin Complexes of Platinum. *Inorg. Synth.* **1979**, *19*, 213-218. (d) Crascall, L. E.; Spencer, J. L.; Doyle, R. A.; Angelici, R. J. Olefin Complexes of Platinum. *Inorg. Synth.* **1990**, *28*, 126-132. (e) Reger, D. L.; Ding, Y. Preparation and Reactivity of the Platinum(0) Anion [(Me$_2$NCS$_2$)Pt(PEt$_3$)]$^-$. *Organometallics* **1994**, *13*, 1047-1048.

18. (a) Bandyopadhyay, D.; Bandyopadhyay, P., Chakravorty, A.; Cotton, F. A., Falvello, L. R. Isomeric Bis[(phenylazo)acetaldoximato]platinum(II) Compounds. *Inorg. Chem.* **1983**, *22*, 1315-1321. (b) Chassot, L.; Müller, E.; von Zelewsky, A. *cis*-Bis(2-phenylpyridine)platinum(II) (CBPPP): A Simple Molecular Platinum Compound. *Inorg. Chem.* **1984**, *23*, 4249-4253. (c) Dungey, K. E.; Thompson, B. D.; Kane-Maguire, N. A. P.; Wright, L. L. Photobehavior of (*a*-Diimine)dimesitylplatinum(II) Complexes. *Inorg. Chem.* **2000**, *39*, 5192-5196. (d) Cornioley-Deuschel, C.; von Zelewsky, A. Complexes of Platinum(II) and Palladium(II) with the 2,2′-Biphenyldiyl Dianion as a *s*-Bonded Chelate Ligand. *Inorg. Chem.* **1987**, *26*, 3354-3358. (e) Blanton, C. B.; Murtaza, Z.; Shaver, R. J.; Rillema, D. P. Excited-State Properties of Platinum(II) Complexes Containing Biphenyl as a Ligand: Complexes of the Type [(bph)PtL$_2$], where L = Monodentate or Saturated Bidentate Ligands. *Inorg. Chem.* **1992**, *31*, 3230-3235. (f) Kvam, P.-I.; Puzyk, M. V.; Balashev, K. P.; Songstad, J. Spectroscopic and Electrochemical Properties of Some Mixed-Ligand Cyclometalated Platinum(II) Complexes Derived from 2-Phenylpyridine. *Acta Chem. Scand.* **1995**, *49*, 335-343.

19. (a) Segawa, Y.; Yamashita, M.; Nozaki, K. Syntheses of PBP Pincer Iridium Complexes: A Supporting Boryl Ligand. *J. Am. Chem. Soc.* **2009**, *131*, 9201-9203. (b) Spokoyny, A. M.; Reuter, M. G.; Stern, C. L.; Ratner, M. A.; Seideman, T.; Mirkin, C. A. Carborane-Based Pincers: Synthesis and Structure of SeBSe and SBS Pd(II) Complexes. *J. Am. Chem. Soc.* **2009**, *131*, 9482-9483. (c) El-Zaria, M. E.; Arii, H.; Nakamura, H. *m*-Carborane-Based Chiral NBN Pincer-Metal Complexes: Synthesis, Structure, and Application in Asymmetric Catlaysis. *Inorg. Chem.* **2011**, *50*, 4149-4161. (d) Shih, W. C.; Gu, W.; MacInnis, M. C.; Timpa, S. D.; Bhuvanesh, N.; Zhou, J.; Ozerov, O. V. Facile Insertion of Rh and Ir into a Boron–Phenyl Bond, Leading to Boryl/Bis(phosphine) PBP Pincer Complexes. *J. Am. Chem. Soc*. **2016**, *138*, 2086-2089.

20. (a) Hoel, E. L.; Hawthorne, M. F. Preparation of *B-s*-Carboranyl Iridium Complexes by Oxidative Addition of Terminal Boron–Hydrogen Bonds to Iridium(I) Species. *J. Am. Chem. Soc.* **1975**, *97*, 6388-6395. (b) Lee, Y.-J.; Lee, J.-D.; Kim, S.-J.; Ko, J.; Suh, I.-H.; Cheong, M.; Kang, S. O. Steric Influence on the Reactivity of Silyl-*o*-carboranes: Oxidative-Addition Reactions Involving Si–H and B–H Activation. *Organometallics* **2004**, *23*, 135-143. (c) Fey, N.; Haddow, M. F.; Mistry, R.; Norman, N. C.; Orpen, A. G.; Reynolds, T. J.; Pringly, P. G. Regioselective B–Cyclometallation of a Bulky *o*-Carboranyl Phosphine and the Unexpected Formation of a Dirhodium(II) Complex. *Organometallics* **2012**, *31*, 2907-2913.

21. (a) Dang, L.; Lin, Z.; Marder, T. B. Boryl Ligands and their Roles in Metal-Catalysed Borylation Reactions. *Chem. Commun.* **2009**, 3987-3995. (b) Braunschweig, H. Transition Metal Comlpexes of Boron. *Angew. Chem. Int. Ed.* **1998**, *37*, 1786-1801. (c) Zhu, J.; Lin, Z.; Marder, T. B. Trans Influence of Boryl Ligands and Comparison with C, Si, and Sn Ligands. *Inorg. Chem.* **2005**, *44*, 9384-9390.

22. Duttwyler, S. Recent Advances in B–H Functionalization of Icosahedral Carboranes and Boranes by Transition Metal Catalysis. *Pure Appl. Chem.* **2018**, *90*, 733-744. (b) Quan, Y.; Qiu, Z.; Xie, Z. Transition-Metal-Catalyzed Selective Cage B–H Functionalization of *o*-Carboranes. *Chem. Eur. J.* **2018**, *24*, 2795-2805. (c) Dziedzic, R. M.; Martin, J. L.; Axtell, J. C.; Saleh, L. M. A.; Ong, T.-C.; Yang, Y.-F.; Messina, M. S.; Rheingold, A. L.; Houk, K. N.; Spokoyny, A. M. Cage-Walking: Vertex Differentiation by Palladium-Catalyzed Isomerization of B(9)-Bromo-*meta*-Carborane. *J. Am. Chem. Soc.* **2017**, *139*, 7729-7732. (d) Dziedzic, R. M.; Saleh, L. M. A.; Axtell, J. C.; Martin, J. L.; Stevens, S. L.; Royappa, A. T.; Rheingold, A. L.; Spokoyny, A. M. B–N, B–O, and B–CN Bond Formation via Palladium-Catalyzed Cross-Coupling of B-Bromo-Carboranes. *J. Am. Chem. Soc.* **2016**, *138*, 9081-9084. (e) Cheng, R.; Li, B.; Wu, J.; Zhang, J.; Qiu, Z.; Tang, W.; You, S.-L.; Tang, Y.; Xie, Z. Enantioselective Synthesis of Chiral-at-Cage *o*-Carboranes via Pd-Catalyzed Asymmetric B–H Substitution. *J. Am. Chem. Soc.* **2018**, *140*, 4508-4511. (f) Cheng, R.; Qiu, Z.; Xie, Z. Iridium-Catalysed Regioselective Borylation of Carboranes via Direct B–H Activation. *Nat. Commun.* **2017**, *8*, 14827-14833.

Chapter 5 – TOWARDS TETRADENTATE LUMINESCENT PT(II) COMPLEXES FEATURING CARBORANE-BASED LIGANDS

5.1 Introduction

In Chapters 3 and 4, we introduced a sterically encumbering and photophysically innocent dianionic ligand scaffold based on 1,1′-bis(*o*-carborane) (**bc**) for use in phosphorescent Pt(II) complexes (**Pt-BC**, Figure 5.1A).[1a] Additionally, we demonstrated the ability to fine-tune electronic properties, such as the emission wavelength and redox properties, of the resulting Pt(II) complex by virtue of the vertex-differentiated coordination chemistry of this robust ligand scaffold.[1b] One key limitation with these carborane-based Pt(II) emitters that is preventing their implementation in organic light-emitting diode (OLED) applications is the low quantum yields observed ($\phi < 0.22$ in 2 wt. % PMMA films).[1] Notably, the low quantum yields for these emitters are consistent with low quantum yields observed for similar Pt(II) complexes featuring two bidentate cyclometalating ligands.[2] In order to provide further insight into the photophysical properties and the nature of the low quantum yields for these **bc**-based Pt(II) complexes, the electronic structure of **Pt-BC** was calculated using density functional theory (DFT) as a representative example for this class of molecules (Figure 5.1A). The optimized geometry for the singlet (S_0) ground state for **Pt-BC** is a slightly distorted square planar structure, which is in agreement with the reported crystal X-ray structure for this compound.[1a] In contrast, the triplet (T_1) excited state optimized geometry exhibits a significant distortion to an almost tetrahedral structure. Rather than relaxing back to the S_0 ground state *via* radiative decay, the complex must relax non-radiatively and twist to the favored square planar geometry. This non-radiative decay process is consistent with the relatively low quantum yield observed for **Pt-BC** ($\phi = 0.19$).[1b] In

order to mitigate the potential for this excited state distortion to occur, we envisaged designing a more rigid carborane-based ligand framework that would potentially result in Pt(II) complexes with greater quantum efficiencies.
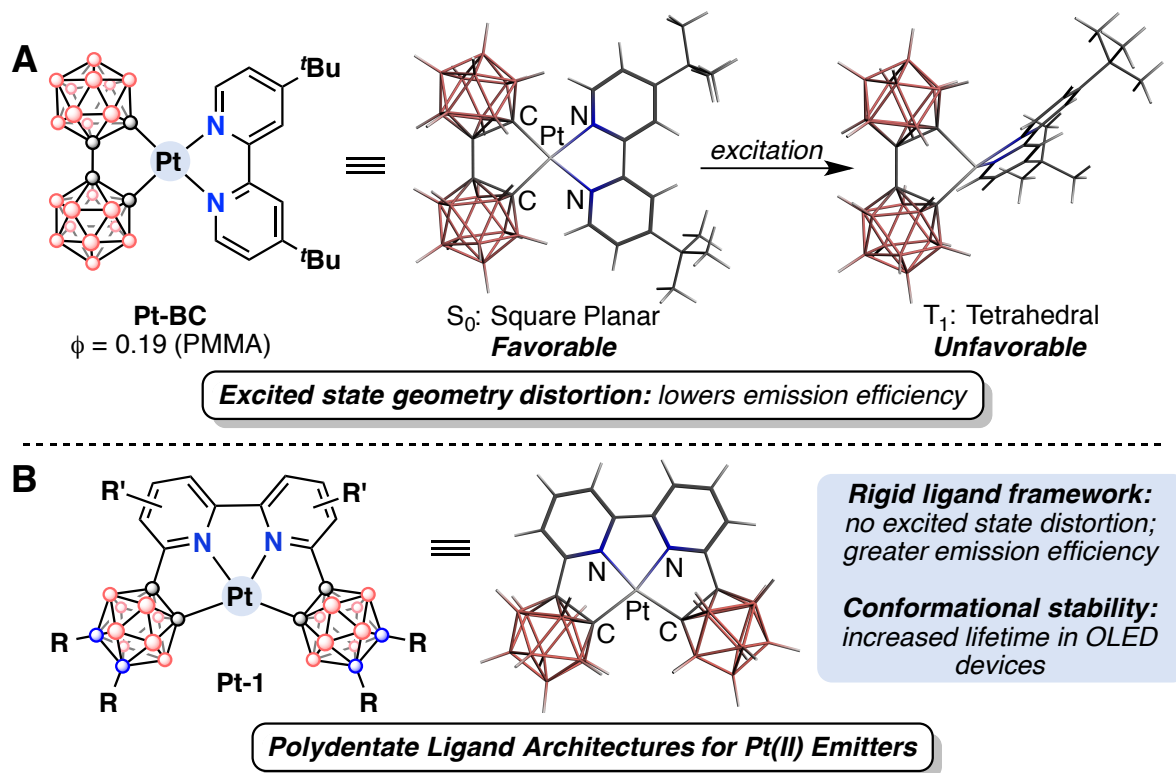
Figure 5.1 (A) Calculated S_0 and T_1 states for **Pt-BC** reveal a significant geometry distortion in the excited state (BP:TZP level of theory). (B) Proposed tetradentate carborane-based ligand scaffold for efficient and stable Pt(II) emitters.

Researchers have attempted to address the issues of low quantum yields in Pt(II) complexes by designing rigid, tetradentate cyclometalating ligands that are less susceptible to significant excited state distortions.[3] Due to the variety of potential tunable ligand frameworks available, the emission spectra from these complexes could be tuned across much of the visible spectrum with quantum yields approaching 0.90,[3e,f] though designing efficient blue emitters initially remained a challenge. It was shown that incorporating pyrazole,[4a] *N*-heterocyclic carbene (NHC),[4b] or carbazole[4c-e] moieties into the tetradentate ligand scaffold could sufficiently blue-shift the emission of the Pt(II) complex through an increase in the energy of the lowest

unoccupied molecular orbital (LUMO), resulting in blue emitters with quantum yields exceeding 0.80.[4] While these Pt(II) emitters exhibit favorable photophysical properties for use in OLEDs, such as high quantum yields ($\phi > 0.80$) and short excited state lifetimes ($\tau < 5$ μs), operational lifetimes of OLED devices incorporating azole- and NHC-based phosphorescent emitters were orders of magnitude lower than OLED devices containing red or green emitting phenylpyridine-based analogues.[4e] The low operational stability could be due to the poor energy mismatch between the high-lying LUMO energies of the azole- and NHC-based phosphorescent emitters with the LUMO energies of the organic host materials.[4e,5] In an attempt to circumvent this issue, Li and coworkers incorporated a 6-membered chelation ring designed to break conjugation between the donor and acceptor portions of the Pt(II) complex, resulting in a deep blue Pt(II) emitter with electrochemical properties that are better aligned with organic host materials.[4e] This strategy produced a blue OLED with exceptional operational stability (up to 30,000 hours at 100 cd/m^2). Although the color purity of this blue OLED was not suitable for use in lighting and display applications,[5a] this work presented a potentially useful strategy for designing stable and efficient blue phosphorescent emitters.

We hypothesized that incorporating a carboranyl unit into the tetradentate ligand would result in a Pt(II) complex with greater emission efficiency relative to that of **Pt-BC**, as well as high operational stability when incorporated into an OLED device (**Pt-1**, Figure 5.1B). Due to the large HOMO-LUMO gap of the carborane moiety (~ 8 eV),[6] we envisioned this ligand would have a similar conjugation-breaking effect to that of the 6-membered chelation ring,[4e] potentially resulting in a blue phosphorescent Pt(II) complex with electrochemical properties that are well-matched to organic host materials commonly employed in blue OLED devices. Furthermore, many square planar Pt(II) complexes are susceptible to aggregation as a consequence of the lack

of steric bulk above and below the square plane, leading to the formation of excimers with red-shifted emission spectra.[2b-e,3e] We have previously demonstrated that the three-dimensional steric bulk of the carborane-based ligand scaffold precludes these parasitic intermolecular interactions, so the emission properties of the resulting carborane-based Pt(II) complexes should be retained. This ligand system could potentially result in the next generation of highly efficient and robust deep blue phosphorescent Pt(II) emitters.

5.2 Results and Discussion

5.2.1 Targeted Pt(II) Complexes
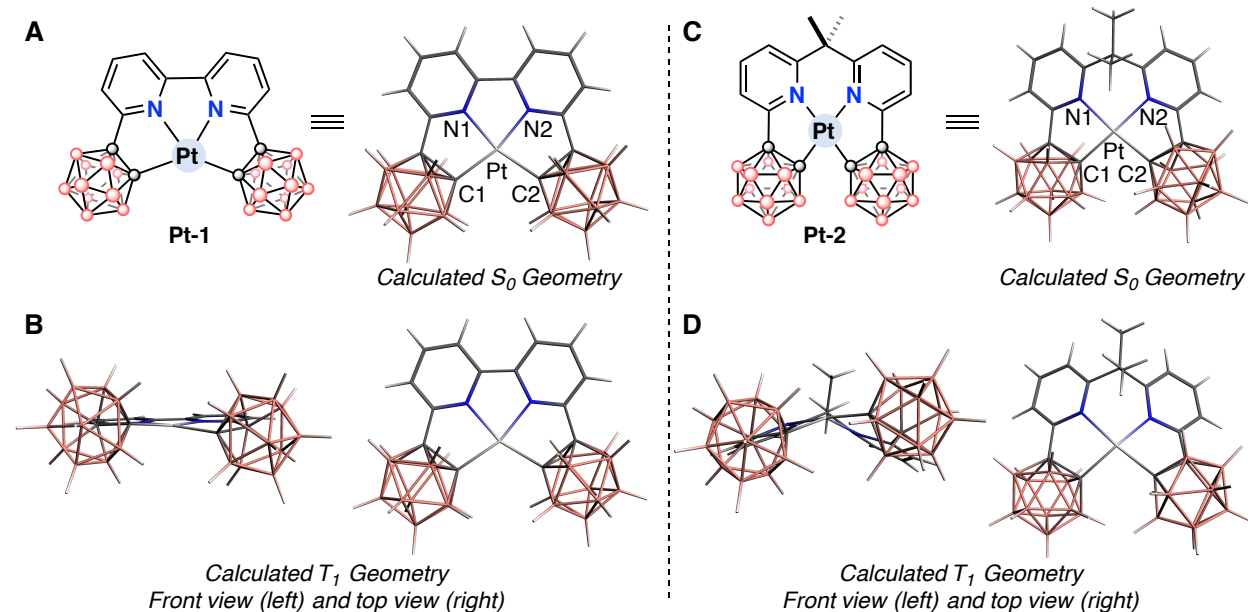
Figure 5.2 Molecular structure and calculated S_0 geometry (A) and T_1 geometry (B) for **Pt-1**. Molecular structure and calculated S_0 geometry (C) and T_1 geometry (D) for **Pt-2**. All calculations performed at the BP:TZP level of theory.

We initially designed two carborane-based tetradentate Pt(II) complexes, **Pt-1** and **Pt-2**, and calculated the optimized geometries of the S_0 and T_1 states for both molecules using DFT calculations (BP:TZP level of theory; Figure 5.2). The ligand structure for **Pt-1** has a bipyridine

backbone, and there is little distortion from the calculated S_0 geometry and the excited state T_1 geometry (Figures 5.2A and 5.2B, respectively). However, the calculated bond angles for C1–Pt–C2 and N1–Pt–N2 (109° and 80°, respectively) deviate significantly from the anticipated 90° for a square planar compound, suggesting the ligand framework might be too strained to accommodate a Pt(II) center. An alternative tetradentate ligand scaffold was designed to incorporate a methylene spacer between the pyridiyl units in order to better accommodate a Pt(II) ion (**Pt-2**, Figure 5.2C), and the calculated bond angles for C1–Pt–C2 and N1–Pt–N2 (100° and 92°, respectively) are in much better agreement with the anticipated 90° angles for a square planar Pt(II) complex. **Pt-2** also shows minimal distortion between the calculated S_0 and T_1 states, suggesting a more efficient emission process relative to that of **Pt-BC** (Figure 5.1A).

5.2.2 Synthesis of a Tetradentate Carborane-Based Ligand

Our synthetic route to the carborane-based tetradentate ligand (**5a**) is outlined in Figure 5.3.[7] The addition 2 equivalents of CH_3CN and 2 equivalents of NaH to a THF solution of the commercially available 2,6-dichloro-4-R-pyridine (R = H, **1a**; R = CH_3, **1b**) yields the bis-pyridyl-acetonitrile complexes **2a** and **2b**. As these compounds are isolated *via* filtration and washed with CH_2Cl_2, the yield of **2b** (29%) is significantly lower than that of **2a** (66%) due to the enhanced solubility of **2b** in CH_2Cl_2. Next, the methylene carbon is reduced by refluxing **2a** or **2b** in ethanol with a large excess of HCl (50 equivalents). Presumably, the nitrile group is hydrolyzed under acidic conditions and followed by a thermally induced decarboxylation to yield the desired bis-pyridyl-methane compounds. **3a** and **3b** can be isolated following workup and purification *via* silica gel column chromatography (70% and 61% yields, respectively).
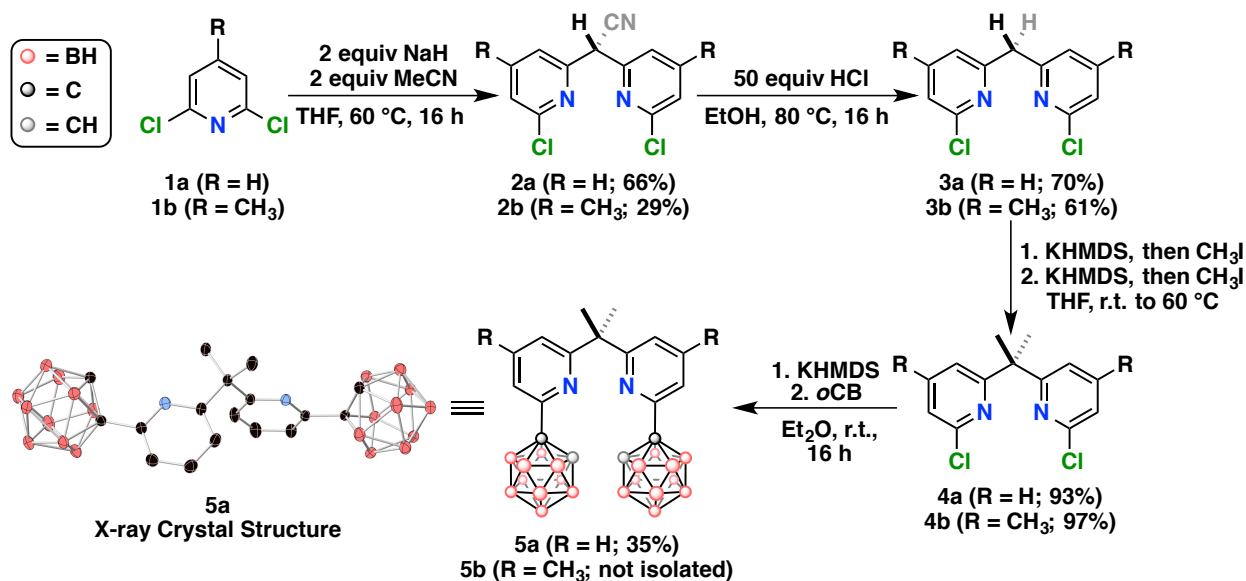
Figure 5.3 Synthesis of tetradentate carborane-based ligand **5a**. X-ray structure for **5a** drawn with 50% ellipsoid probability. H atoms are omitted for clarity.

The methylene carbon is then methylated twice following subsequent deprotonation and methylation steps. THF solutions of **3a** or **3b** are stirred with KHMDS for 3 hours at room temperature, followed by the addition of methyl iodide. After the reaction mixture is stirred at room temperature for 1 hour, KHMDS is added, and the reaction is stirred at room temperature for 1-2 hours. Finally, methyl iodide is added and the reaction mixture is heated to 60 °C overnight. Upon work up and purification *via* column chromatography, compounds **4a** and **4b** could be isolated in near quantitative yields (93% and 97%, respectively). Notably, this step differs from the previously reported method for synthesizing **4b**, which employed ^{n}BuLi as the base and required carefully-controlled reaction temperatures between -78 °C and room temperature throughout the reaction.[7a] In our hands, the use of ^{n}BuLi led to the formation of multiple products observed by GC-MS, including butylated pyridine-based products. We found KHMDS to be a superior base for this transformation as we did not observe any side products (even with the use of excess KHMDS), and the synthesis was operationally simpler as the reaction proceeded at room temperature until the final step, which required mild heating

165

overnight (60 °C). The final step for the installation of carborane is based upon our recently reported S_NAr-based method in which the deprotonated carborane can act as a nucleophile and attack the pyridyl chloride (**4a** or **4b**) to form the desired carboranyl-pyridine-based molecule.[7b] Crystals of **5a** suitable for X-ray diffraction were grown by the slow evaporation of a concentrated solution of acetone, and the diffraction study confirmed the proposed structure of **5a** (Figure 5.3). Under the optimized conditions for this reaction (*vide infra*), **5a** could be isolated in 35% yield. Despite the low yield, this reaction could be performed on the 1.5 mmol scale such that ~ 0.250 g **5a** could be isolated per reaction. Analogous reaction conditions were employed for the synthesis of **5b** at the 0.20 mmol scale, but the yield of **5b** determined by ^{1}H NMR spectroscopy was limited to 15-20% despite quantitative conversion of **4b**. The reaction for **5b** was not scaled up due to the low yield, and instead we focused our efforts on **5a** in subsequent reactions.

Table 5.1 Optimization of reaction conditions for **5a**.[a]

Entry	Solvent	# Equiv 4a	% Conversion 4a	Temperature	Isolated Yield,[b] 5a
1	MTBE	1.0	> 99%	55 °C	35%
2	MTBE	1.0	> 99%	r.t.	38%
3	Et$_2$O	1.0	> 99%	r.t.	38%
4	Et$_2$O	1.0	~ 50%	0 °C	17%
5	Et$_2$O	1.2	> 99%	r.t.	41%
6	Et$_2$O	1.4	> 99%	r.t.	41%
7	Et$_2$O	1.0	> 99%	r.t.	35%[b]

[a]Reactions performed at the 0.20 mmol scale unless otherwise specified. [b]Isolated yields reported after workup and purification *via* silica gel column chromatography (see section 5.4.6.7 for more details). [c]1.5 mmol scale. Optimized conditions are presented in Entry 7.

The optimization studies for the synthesis of **5a** are presented in Table 5.1. The optimized conditions previously reported[7b] for the S$_N$Ar-based C-vertex functionalization method were chosen as a starting point for the synthesis of **5a**: a methyl *tert*-butyl ether (MTBE) solution containing 2 equivalents of *o*-carborane and 6 equivalents of KHMDS was allowed to stir at room temperature for 1 hour, then added to a MTBE solution containing 1 equivalent of **4a**. The reaction mixture was then heated to 55 °C for 16 hours. Following workup and purification *via* silica gel column chromatography, **5a** was isolated in 35% yield (Entry 1) with quantitative conversion of **4a**. When the reaction temperature was lowered from 55 °C to room temperature, quantitative conversion of **4a** was observed, along with a slight improvement in the yield of **5a** (38%, Entry 2). This yield was reproduced when the solvent was switched from MTBE to Et$_2$O (38%, Entry 3), so further optimization studies were performed in Et$_2$O. The yield dropped precipitously when the reaction temperature was lowered to 0 °C due to incomplete conversion of **4a** (~ 50% conversion **4a**, 17% yield **5a**; Entry 4). Only a slight improvement in the isolated yield of **5a** was observed when 1.2-1.4 equivalents of **4a** were used (Entries 5 and 6, 41% yield **5a** in both cases). The conditions presented in entry 3 were scaled up from a 0.20 mmol scale to a 1.5 mmol scale, with minimal drop in the yield of **5a** observed (Entry 7, 35%).

Lastly, we found that this S$_N$Ar-based procedure was not compatible with **3a** or **3b**; that is, functionalization of the methylene position (**4a** or **4b**) was required for nucleophilic attack of the deprotonated carborane on the pyridyl chloride substrate to occur. Reaction conditions analogous to those presented in Table 5.1, Entry 7 were employed in these reactions, with **4a** replaced by **3a** or **3b**. Regardless of the number of equivalents of KHMDS added (2-10 equivalents), ethereal solvent used (Et$_2$O, MTBE, or THF), or reaction temperature employed (room temperature to 60 °C), the major species observed by ^{1}H and ^{11}B NMR spectroscopic

studies after allowing the reaction to proceed for 16 hours were unreacted **3a** or **3b** and *o*-carborane. At elevated temperatures in THF, ^{11}B NMR spectroscopic analysis of the crude reaction mixture suggested *nido*-carborane constituted 10-20% of the boron-containing species. Overall, we found it necessary to functionalize the methylene position of **3a** and **3b** in order for the S$_N$Ar-based carborane functionalization step to proceed under these conditions.

5.2.3 Attempts at Metalation of 5a

Table 5.2 Reactions between **5a** and Pt(SEt$_2$)$_2$Cl$_2$ or Pt(cod)Cl$_2$.[a]

Bulky carboranyl ligand likely prevents coordination of ligand
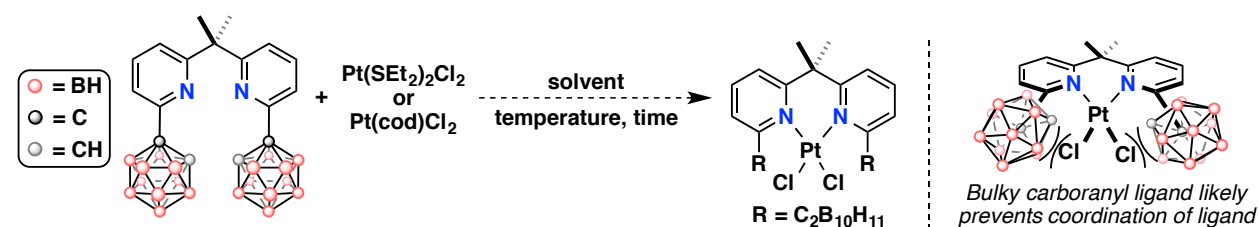
Entry	Solvent	Pt(II) source	Temperature	Time	Result
1	CH$_2$Cl$_2$	Pt(SEt$_2$)$_2$Cl$_2$	r.t.	16 h	> 99% starting materials[b]
2	1,2-dichloroethane	Pt(SEt$_2$)$_2$Cl$_2$	80 °C[c]	16 h	> 99% starting materials[b]
3	1,2-dichloroethane	Pt(SEt$_2$)$_2$Cl$_2$	140 °C[d]	2 h	> 99% starting materials[b]
4	MeOH	Pt(SEt$_2$)$_2$Cl$_2$	70 °C[c]	16 h	Pt metal
5	THF	Pt(cod)Cl$_2$	65 °C[c]	16 h	> 99% starting materials[b]

[a]Reactions conducted under N$_2$. [b]Determined by ^{1}H NMR spectroscopy. [c]Oil bath used. [d]Microwave irradiation used.

With the carborane-based tetradentate ligand **5a** in hand, we then set out to synthesize the corresponding tetradentate Pt(II) complex, **Pt-2**. Initially, we attempted to synthesize a Pt(II) dichloride complex in which the dipyridyl portion of **5a** binds to the Pt(II) center (Table 5.2), from which the desired cyclometalated Pt(II) complex could form upon introduction of an appropriate base.[8] For these experiments, **5a** and Pt(SEt$_2$)$_2$Cl$_2$ were combined in a reaction tube and dissolved in CH$_2$Cl$_2$, or 1,2-dichloroethane, and allowed to react for 2-16 hours at temperatures ranging from room temperature to 140 °C (Table 5.2, entries 1-3). In all cases, ^{1}H NMR spectroscopic analysis of the reaction mixture suggested > 99% starting materials

remained unreacted. When MeOH was used as the solvent, Pt metal coated the reaction tube after heating the reaction mixture to 70 °C for 16 hours, suggesting reduction of the starting Pt(II) complex to Pt metal (Entry 4). Lastly, when Pt(cod)Cl$_2$ was used as the Pt(II) source and the reaction was run in THF, only starting materials were observed by ^{1}H NMR spectroscopy after the reaction was allowed to proceed at 65°C for 16 hours (Entry 5). Based on these results, we hypothesized that the carboranyl moieties were likely too bulky for the desired Pt(II) dichloride complex to form, so we turned our attention to alternate routes to generate the tetradentate Pt(II) complex.
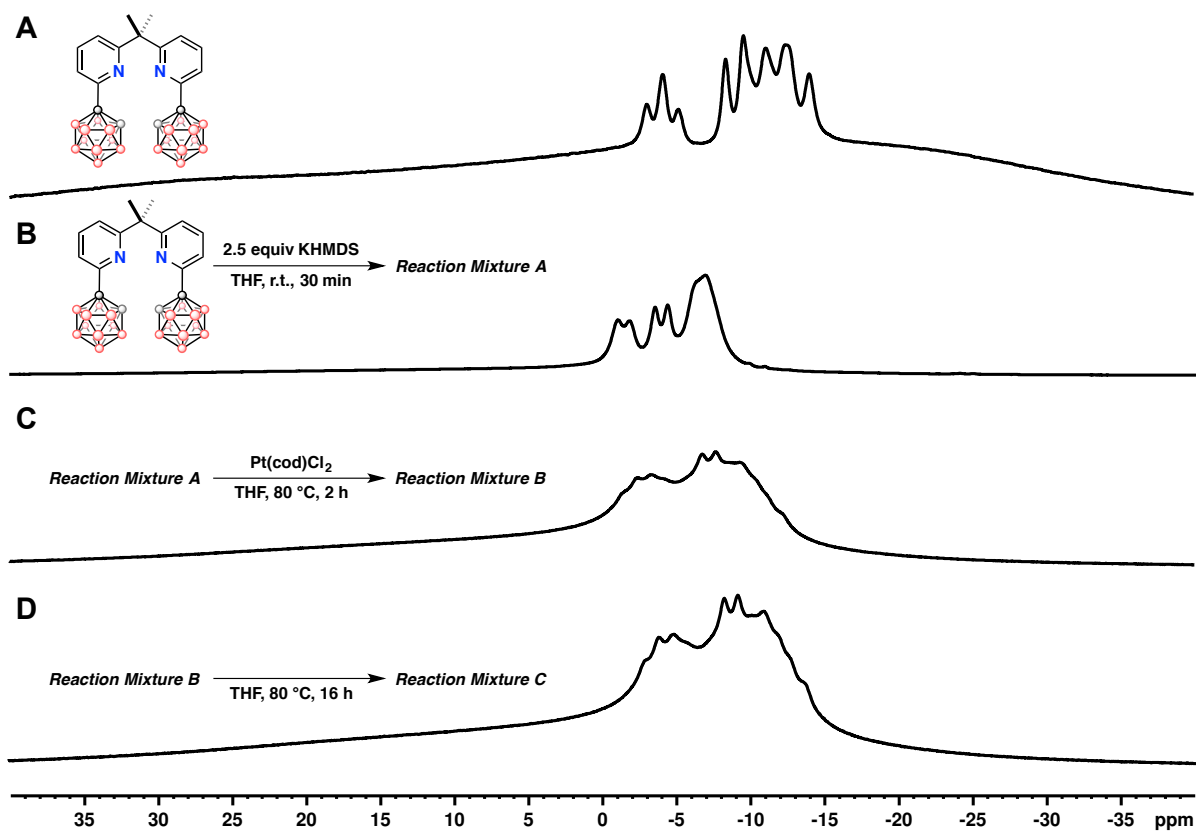

Figure 5.4 Sequential addition of reagents in to an NMR-scale reaction (under N$_2$, monitored by ^{11}B NMR spectroscopy). (A) ^{11}B NMR spectrum of **5a** in THF; (B) ^{11}B NMR spectrum of **5a** and 2.5 equivalents of KHMDS stirred at room temperature for 30 minutes in THF (*Reaction Mixture A*); (C) ^{11}B NMR spectrum obtained after the addition of Pt(cod)Cl$_2$ to *Reaction Mixture A* and refluxing for 2 hours (*Reaction Mixture B*); ^{11}B NMR spectrum obtained after refluxing *Reaction Mixture B* for 16 hours (*Reaction Mixture C*).

We considered a strategy in which the two acidic carboranyl C–H vertices of **5a** were deprotonated, followed by the addition of the deprotonated ligand to a Pt(II) precursor to yield **Pt-2**. First, we conducted an NMR-scale experiment to determine whether KHMDS was a suitable base for this transformation (Figure 5.4). After a THF solution of **5a** and 2.5 equivalents of KHMDS was stirred at room temperature for 30 minutes, an entirely new species was observed by ^{11}B NMR spectroscopy, suggesting complete deprotonation of the carboranyl C–H vertices of **5a** (Figure 5.4A-B). Next, Pt(cod)Cl$_2$ was added, and the reaction mixture was refluxed for 2 hours. The color of the reaction mixture changed to dark yellow, and a broadening of the ^{11}B NMR spectrum was observed (Figure 5.4C). The reaction mixture was refluxed for an additional 16 hours, yielding a dark brown mixture with a slight sharpening in some of the peaks in the ^{11}B NMR spectrum (Figure 5.4D). The broadened peaks in the ^{11}B NMR spectrum of the reaction mixture relative to those of the free ligand (Figure 5.4D and 5.4A, respectively) are consistent with metalation of the carboranyl-based ligand.[1] Following solvent removal *in vacuo*, the crude product was dissolved in acetone-d$_6$, and the ^{1}H NMR spectrum of the crude product was collected (Figure 5.5). A large mixture of products was observed in the ^{1}H NMR spectrum, and **5a** was completely consumed under these conditions. We then employed lower reaction temperatures, ranging from -78 °C to 60 °C, in an attempt to limit the formation of multiple products (Figure D1). While **5a** was completely consumed under these conditions, multiple products were still observed by ^{1}H NMR spectroscopy, suggesting modifying only the reaction temperature was not sufficient to bias this reaction towards the formation of a single product.
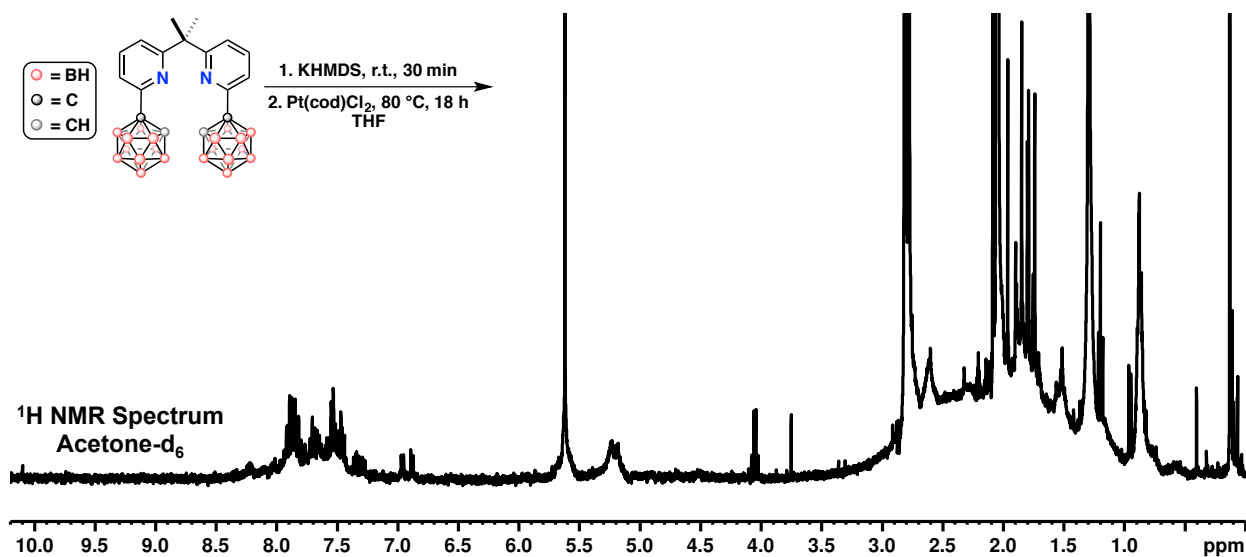
Figure 5.5 ^{1}H NMR spectrum for the crude product obtained from *Reaction Mixture C* in Figure 5.4D (Acetone-d₆).

We hypothesized that the presence of K⁺ after deprotonation of **5a** with KHMDS might adversely influence the outcome of the reaction and potentially inhibit the formation of **Pt-2**. Following the deprotonation of **5a**, the pyridyl moieties of **5a** could potentially coordinate to K⁺, complicating the reaction and limiting access for Pt(II) to approach the carboranyl-pyridyl fragment of the ligand and to cyclometalate. To test this hypothesis, we conducted an NMR-scale experiment in which we probed the influence of 18-crown-6 on the outcome of the reaction (Figure 5.6). Following the addition of 2 equivalents of KHMDS to a THF-d₈ solution of **5a**, full conversion of **5a** to one major species was observed by ^{1}H NMR spectroscopy after 30 minutes (presumably doubly deprotonated **5a**; Figure 5.6A-B). Next, 2 equivalents of 18-crown-6 were added, and the reaction mixture was allowed to react for 30 minutes at room temperature. The ^{1}H NMR spectrum obtained at this point revealed the formation of one new major species, suggesting 18-crown-6 does in fact segregate K⁺ ions from the deprotonated ligand (Figure 5.6C). Pt(cod)Cl₂ was then added to the reaction mixture, and after reacting for 30 minutes at room temperature, the species present in *Reaction Mixture B* was fully consumed, and multiple

new species were observed by ^{1}H NMR spectroscopy (Figure 5.6D). The reaction mixture was then heated to 60 °C for 16 hours, and the ^{1}H NMR spectrum obtained indicated the presence of multiple products in solution, with full conversion of Pt(cod)Cl$_2$ (Figure 5.6E). Interestingly, free ligand **5a** could be identified in the mixture of products observed in the ^{1}H NMR spectrum, suggesting the deprotonated **5a** species was protonated under these reaction conditions. When this reaction was repeated at lower temperatures (between -78 °C and room temperature), complex mixtures of products were observed by ^{1}H NMR spectroscopy (Figure D2).
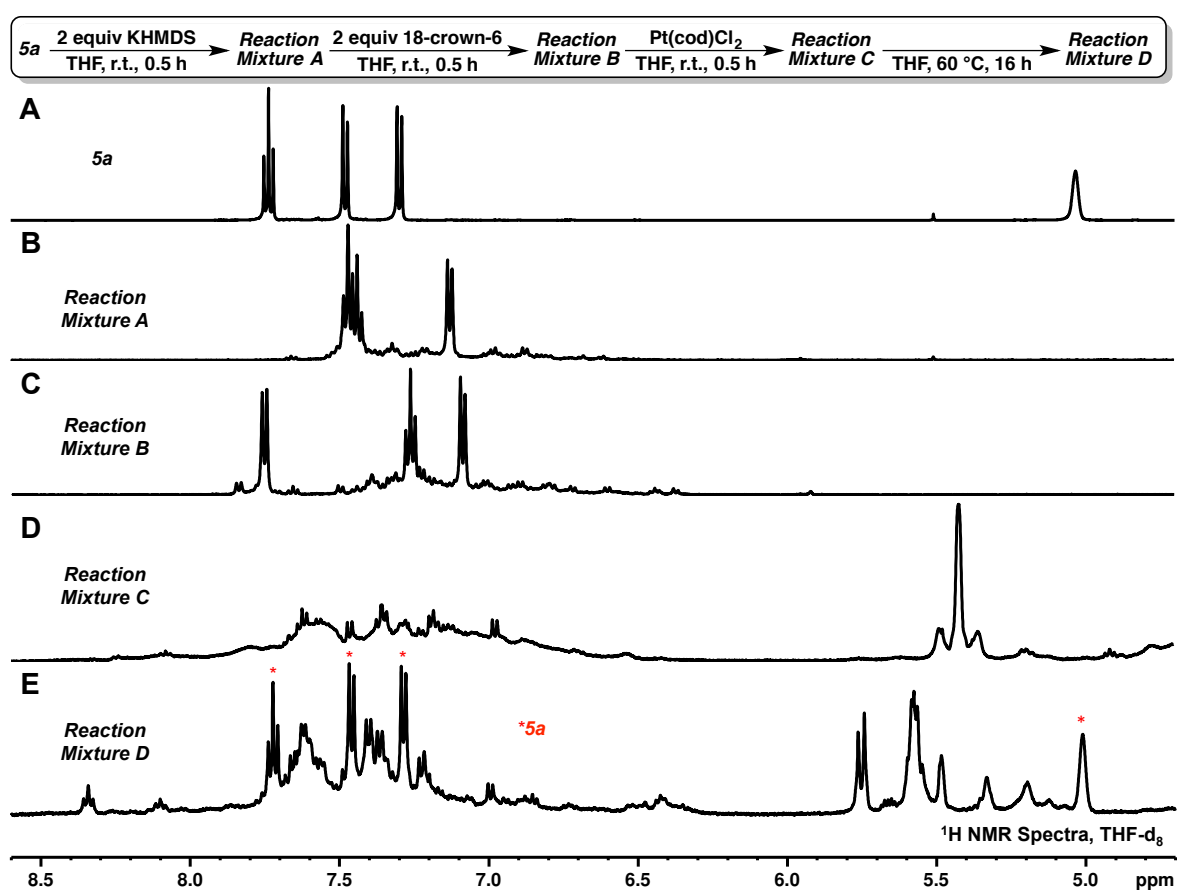

Figure 5.6 Sequential addition of reagents to an NMR-scale reaction prepared in an N$_2$-filled glove box (monitored by ^{1}H NMR spectroscopy, THF-d$_8$). (A) Free ligand **5a**; (B) The addition of 2 equivalents of KHMDS, yielding *Reaction Mixture A*; (C) The addition of 2 equivalents of 18-crown-6 to *Reaction Mixture A* to yield *Reaction Mixture B*; (D) The addition of Pt(cod)Cl$_2$ to *Reaction Mixture B* to yield *Reaction Mixture C*; (E) Heating *Reaction Mixture C* at 60 °C for 16 hours to yield *Reaction Mixture D*.

Based on these results and the mixture of products observed by ^{1}H NMR spectroscopy, we considered alternative strategies to synthesize **Pt-2**. First, we looked into a sequential deprotonation route in which each carboranyl-pyridine unit in **5a** would be cyclometalated in sequence, rather than at the same time, in an attempt to minimize the number of products formed (Figure D3). Under the conditions presented in Figure D4, a complex mixture of products formed, and attempts to isolate these products on silica were unsuccessful due to apparent decomposition of the crude product. Next, we conducted experiments with $Pt(acac)_2$ (acac = acetylacetonate) as the Pt(II) source (Table D1 and Figure D4). No reaction was observed by ^{1}H NMR spectroscopy when **5a** and $Pt(acac)_2$ were heated in acetonitrile for 2-16 hours, and only the free ligand, **5a**, and borates were observed by ^{11}B NMR spectroscopy when **5a** and $Pt(acac)_2$ were refluxed in benzonitrile overnight (Table D1). The lack of reactivity observed between **5a** and $Pt(acac)_2$ in acetonitrile might be attributed to the unfavorable pKa difference between the two reagents (pKa, carboranyl C–H $\sim$ 25 and pKa, $acac^-$ $\sim$ 17, respectively). In contrast, the formation of new products was observed by ^{1}H NMR spectroscopy when a THF solution of **5a**, 2 equivalents of KHMDS, and 2 equivalents of 18-crown-6 was added to a THF solution of $Pt(acac)_2$ and heated in either an oil bath or with microwave irradiation (Figure D4). Attempts to purify the crude products with silica or alumina column chromatography were unsuccessful, as the crude product did not appear to be stable in these media.

Next, we considered generating a cationic Pt(II) precursor as an alternative route to synthesize **Pt-2** (Figure D6). One equivalent of $AgSbF_6$ was added to a THF slurry of $Pt(cod)Cl_2$ and stirred for 30 minutes, then a THF solution of **5a**, 2 equivalents of KHMDS, and 2 equivalents of 18-crown-6 was added to this reaction mixture. After allowing the reaction to proceed overnight, a complex mixture of products was observed by ^{1}H NMR spectroscopy

(Figure D6B). Finally, we considered generating the Zn(II) analogue of **Pt-2**, as the Zn(II) ion could potentially be transmetalated with Pt(II) to afford the desired Pt(II) complex (Figure D6).[9] After a THF solution of **5a**, 2 equivalents of KHMDS, and 2 equivalents of 18-crown-6 was added to a THF solution of $ZnCl_2$ and stirred at room temperature overnight, a white precipitate formed. Upon filtration through a pad of Celite and solvent removal *in vacuo*, the crude product was dissolved in THF-d_8 and the ^{1}H NMR spectrum was obtained (Figure D7B). A complex mixture of products was observed, suggesting this was not a suitable route to a Zn(II)-based complex of **5a**.
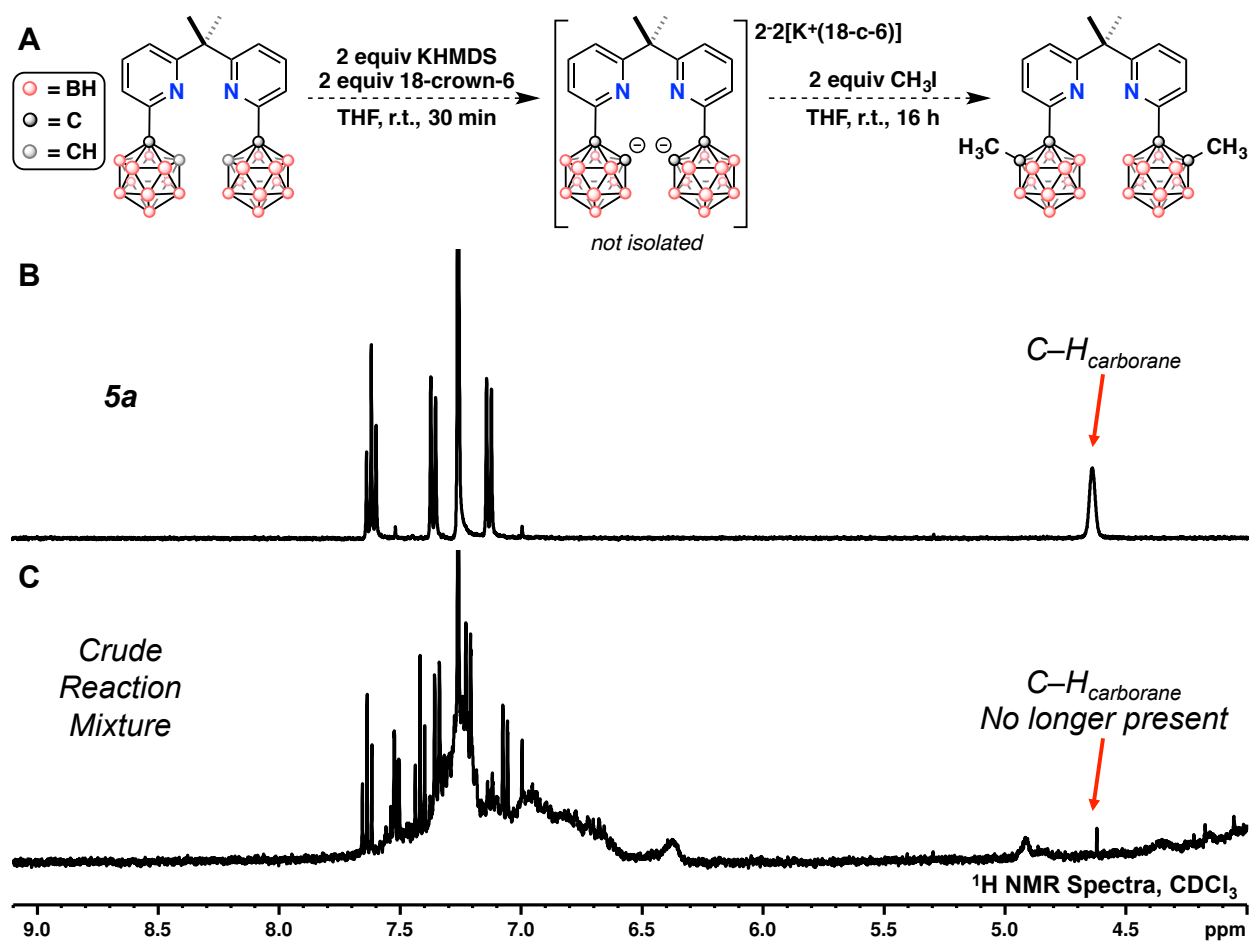

Figure 5.7 (A) Scheme for the C-methylation of **5a**. (B) ^{1}H NMR spectrum of **5a** in CDCl$_3$. (C) ^{1}H NMR spectrum of the crude product obtained from the reaction scheme presented in (A). Disappearance of the carboranyl C–H chemical shift suggests successful C-methylation of **5a**.

174

In order to determine whether the deprotonation of **5a** was occurring at the desired position (carboranyl C–H) rather than another position in the molecule, we attempted to quench the deprotonated **5a** species with methyl iodide (Figure 5.7). Following the addition of methyl iodide to a THF solution of **5a**, 2 equivalents of KHMDS, and 2 equivalents of 18-crown-6, the reaction mixture was allowed to stir at room temperature overnight. The solvent was removed under reduced pressure and the crude product dissolved in CDCl$_3$. The ^{1}H NMR spectrum suggested full conversion of **5a** as the diagnostic chemical shift corresponding to the carboranyl C–H was no longer present (Figure 5.6C). However, multiple products were observed in the ^{1}H NMR spectrum, suggesting deprotonation (or other undesired side reactions) might be occurring at other positions in **5a** and potentially complicating subsequent reactions involving Pt(II). We briefly explored the use of alternative bases, but it seems that both KH and Zn(HMDS)$_2$ are not suitable for the deprotonation of **5a** (Figures D7 and D8, respectively). Based on these results, a more detailed screen of potential bases for use in the deprotonation of **5a** is warranted.
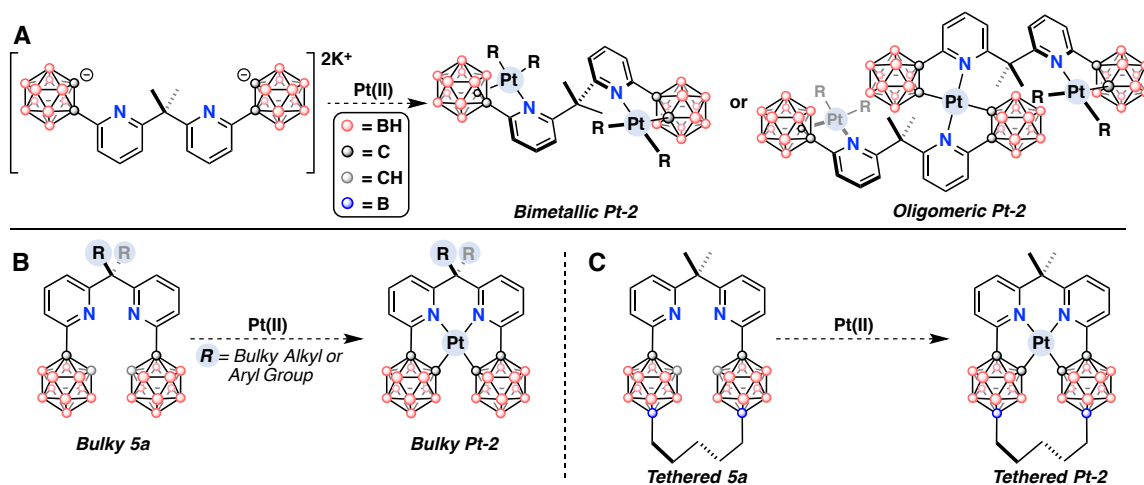

Figure 5.8 (A) Potential products that form during the attempted syntheses of **Pt-2**: Bimetallic Pt(II) species (**Bimetallic Pt-2**) or oligomeric Pt(II) species (**Oligomeric Pt-2**). Bulky functional groups at the methylene position of **5a** (B) or an alkyl-tethered analogue of **5a** (C) may potentially promote the formation of **Pt-2**-based complexes due to steric constraints that limit the propensity for undesired side reactions to occur during metalation.

The synthesis of **Pt-2** has not proved to be straightforward: while the ligand **5a** was entirely consumed under many of the reaction conditions employed, the formation of a clean, well-defined product has not been observed by ^{1}H NMR spectroscopy; rather, a complex mixture of products was commonly observed after sufficient reaction time (typically overnight). One potential reason for this could be due to the orientation of **5a** in solution and the rate of intermolecular versus intramolecular reactions with the Pt(II) source (Figure 5.8A). Based on the X-ray crystal structure for **5a** (Figure 5.3), each carboranyl-pyridine fragment is oriented in a way such that **5a** could potentially accommodate two Pt(II) centers to generate either a bimetallic species (**Bimetallic Pt-2**, Figure 5.8A), or an oliogmeric species in which the repeat unit consists of two distinct ligands bound to a single Pt(II) center (**Oligomeric Pt-2**, Figure 5.8A).[10] If the deprotonated **5a** species adopts a similar orientation in solution as **5a** does in the solid state, the formation of such multimetallic complexes is plausible. The complex mixture of products commonly observed by ^{1}H NMR spectroscopy and broadened ^{11}B and ^{11}B{^{1}H} NMR spectra typically seen for the crude products isolated after the metalation reactions presented in this chapter are consistent with the formation of either **Bimetallic Pt-2** or **Oligomeric Pt-2**. Careful control of reaction conditions, such as concentration and stoichiometry, might potentially mitigate the formation of multimetallic species by slowing the rate of intermolecular interactions between **5a** and the Pt(II) source and promoting the formation of the intramolecular reaction product, **Pt-2**. However, a more direct approach to addressing this issue involves the synthesis of derivatives of **5a** that will "lock" the tetradentate carborane-based ligand in the preferred orientation to promote formation of the desired monometallic **Pt-2**-based species. One design incorporates bulky alkyl or aryl groups at the methylene position of **5a** (**Bulky 5a**), which may potentially orient the ligand in such a way that the rate of intramoleclar reaction between the

ligand and the Pt(II) precursor is faster than the rate of intermolecular reaction between multiple ligands and Pt(II) sources, resulting in the formation of the desired **Pt-2**-based complex, **Bulky Pt-2** (Figure 5.8B). Alternatively, incorporating an alkyl tether between the two carboranyl moieties in **5a** (**Tethered 5a**, Figure 5.8C) could also provide a ligand platform that is more likely to form a monometallic Pt(II) species (**Tethered Pt-2**, Figure 5.8C) as rotation about the methylene spacer unit will be severely limited. These next generation tetradentate carborane-based ligands may potentially lead to the formation of the desired Pt(II) complexes, finally enabling the study of this class of carborane-based Pt(II) emitters.

5.3 Conclusions

Overall, we have identified two tetradentate carborane-based Pt(II) complexes, **Pt-1** and **Pt-2**, that may potentially exhibit high quantum yields due to minimal distortions between their calculated S_0 and T_1 geometries. Due to the large steric strain in the calculated ground state geometry for **Pt-1**, we chose to pursue **Pt-2**, as the ligand in this proposed complex appeared to be more capable of accommodating a Pt(II) center. We successfully synthesized the carborane-based tetradentate ligand, **5a**, by employing a S_NAr-based approach.[7b] Synthesis of the desired Pt(II) complex, **Pt-2**, proved to be challenging; metalation reactions involving **5a** typically formed a complex mixture of products observed by ^{1}H NMR spectroscopy, potentially due to the formation of multimetallic Pt(II)-based species, such as **Bimetallic Pt-2** and **Oligomeric Pt-2**. Future designs of **5a** should aim to "lock" the ligand into the preferred orientation to promote the synthesis of the desired monometallic Pt(II) complex. Two such strategies include the incorporation of bulky groups at the methylene position of **5a** (**Bulky 5a**), and tethering the carboranyl fragments of **5a** together with an alkyl chain (**Tethered 5a**). From there, synthesis of the desired carborane-based tetradentate Pt(II) complex may potentially be achieved. With many

reports of vertex-selective functionalization methods for carborane emerging,[11] it is conceivable that this carborane-based ligand framework can be derivatized in a straightforward manner, potentially leading to a new family of efficient, deep blue phosphorescent Pt(II) emitters that will be suitable for use in OLED-based devices and applications.

5.4 Appendix D

5.4.1 General Considerations

All experiments were set up in a nitrogen-filled glovebox or performed under an atmosphere of nitrogen using standard Schlenk and cannula techniques. All work-up and characterization was performed under ambient conditions. The "ambient conditions" for this manuscript refer to room temperature (20 - 25 °C) and uncontrolled laboratory air. Tetrahydrofuran (THF) and diethyl ether used for reactions were sparged through argon and passed through activated alumina before use.

5.4.2 Materials

Deuterated solvents, other than THF-d_8, were purchased from Cambridge Isotope Laboratories and stored over 3Å molecular sieves prior to use. Pt(cod)Cl$_2$,[1] Pt(SEt$_2$)$_2$Cl$_2$,[2] were synthesized according to previously reported procedures. K$_2$[PtCl$_6$], potassium bis(trimethylsilyl)amide (KHMDS), 18-crown-6, methyl iodide, concentrated hydrochloric acid, ZnCl$_2$, THF-d_8, diethyl sulfide, potassium hydride, 1,5-cyclooctadiene, and silver hexafluoroantimonate were purchased from Sigma-Aldrich. Pt(acac)$_2$ was purchased from Strem Chemicals. 2,6-dichloropyridine (**1a**) and 2,6-dichloro-4-methylpyridine (**1b**) were purchased from Oakwood Chemical. Organics. *o*-Carborane (1,2-C$_2$B$_{10}$H$_{12}$) was purchased from Boron Specialties (USA) and was purified prior to use in the following procedure: a round-bottomed

flask was charged with *o*-carborane (15 g, 10.4 mmol) and MeOH (150 mL). Concentrated HCl (50 mL) was added slowly to the reaction vessel, and the resulting mixture was heated to 50 °C and stirred overnight. The solution was then cooled, H_2O (200 mL) was added, and the resulting white solid was isolated by vacuum filtration, washed with water, and air-dried. The solid was then dissolved in CH_2Cl_2, dried with $MgSO_4$, and filtered through Celite. The solution was dried *in vacuo* to afford a white powder. The powder was then sublimed at 60 °C under dynamic vacuum. After sublimation away from the yellow residue, the white sublimate was dissolved in 1,2-dichloroethane. Activated carbon/charcoal (ca. 3–5 g) was added, and the mixture was stirred for 6 hours at about 75°C. The suspension was then filtered, and the filtrate was concentrated under vacuum. The resulting white solid was again sublimed at 60 °C to afford purified *o*-carborane. All reagents were used as received unless otherwise indicated.

5.4.3 Instruments

^{1}H, ^{11}B, and ^{11}B{^{1}H} NMR spectra were obtained on a Bruker AV400 or Bruker DRX500 spectrometer; ^{13}C{^{1}H} NMR spectra were obtained on a Bruker AV400 spectrometer. Bruker Topspin software was used to process the NMR data. ^{1}H and ^{13}C{^{1}H} NMR spectra were referenced to residual solvent resonances in deuterated solvents (THF-d_8: ^{1}H, 3.580 ppm, ^{13}C, 67.210 ppm; acetone-d_6: ^{1}H, 2.050 ppm, ^{13}C: 29.840 ppm; CDCl$_3$: ^{1}H, 7.260 ppm, ^{13}C, 77.160 ppm; Note: due to high humidity H_2O resonances are often present). ^{11}B NMR spectra were referenced to an external BF$_3$·Et$_2$O (0 ppm) standard.

5.4.4 X-Ray Data Collection and Processing Parameters

For **5a** a single crystal was mounted on a nylon loop using perfluoropolyether oil and cooled rapidly to 100 K with a stream of cold dinitrogen. Diffraction data were measured using a Bruker APEX-II CCD diffractometer using Mo-$K\alpha$ radiation. The cell refinement and data

reduction were carried out using Bruker SAINT and the structure was solved with SHELXS-97. All subsequent crystallographic calculations were performed using SHELXL-2013. Solvent molecules with significant disorder were rendered using the SQUEEZE method.

5.4.5 DFT Calculation Details

Geometries **Pt-1** and **Pt-2** optimized with DFT calculations using standard triple-ξ polarization (TZP) basis sets available in the Amsterdam Density Functional 2014.04 Rev. 44409 (ADF)[3] software suite, with Becke[4] and Perdew[5] (BP) Slater-type orbitals (STOs) on a 6 core Apple computer. The local density approximation (LDA) was made with BP and exchange and correlation corrections available by default in the ADF 2014.04 suite. Single point calculations were performed using the B3LYP[6,7] level of theory and a TZ2P basis set. The COSMO solvation model (THF) was used for both geometry optimizations and single point calculations. All-electron basis sets were used for all atoms (cores remained un-frozen). Electron spins were restricted for S_0 calculations, and electron spins were unrestricted for T_1 calculations. Relativistic correlations were made using Zero-Order Relativistic Approximation (ZORA)[8-10] for Pt.

5.4.6 Synthetic Procedures

5.4.6.1 2,2-bis(6-chloropyrid-2-yl)acetonitrile (2a)

Inside a N_2 filled glove box, 2,6-dichloropyridine (5.00 g, 33.8 mmol), NaH (1.62 g, 67.6 mmol), acetonitrile (3.52 mL, 67.6 mmol), and THF (100 mL) were added to a 200 mL Schlenk flask to yield a gray slurry. The flask was removed from the glove box and heated at 65 °C under N_2 for 17 hours. The brown reaction mixture was then cooled to room temperature and diluted with Et_2O (~ 20 mL). Brine (~ 50 mL) was added, then the organic and aqueous layers were

separated. The aqueous layer was washed with Et_2O (~ 75 mL x 3), and the organic portions were combined and dried with Na_2SO_4. After filtration through a pad of Celite and removal of solvent under reduced pressure, an orange, viscous solid was isolated. Next, CH_2Cl_2 was added and the mixture was filtered to yield a yellow-brown solid (which was isolated) and an orange filtrate (which was discarded). The solid was collected from the filter frit and vacuum dried (2.95 g, 66%). This product was used without further purification for the next step. **^{1}H NMR** (acetone-d_6, 400 MHz) δ 7.93-7.70 (br m, 2H, Ar), 7.22-7.18 (m, 2H, Ar), 6.33 (dd, 2H, Ar); **^{13}C{^{1}H} NMR** (acetone-d_6, 100 MHz) δ 162.28, 149.40, 137.32, 129.08, 115.52, 110.16, 70.61. *Note: C–H$_{methylene}$ not observed via ^{1}H NMR spectroscopy.*

5.4.6.2 2,2-bis(6-chloro-4-methylpyrid-2-yl)acetonitrile (2b)

Inside a N_2 filled glove box, 2,6-dichloro-4-methylpyridine (10.00 g, 61.7 mmol), NaH (2.95 g, 123 mmol), acetonitrile (6.45 mL, 123 mmol), and THF (200 mL) were added to a 500 mL Schlenk flask to yield a gray slurry. The flask was removed from the glove box and heated at 65 °C under N_2 for 17 hours. The brown reaction mixture was then cooled to room temperature and diluted with EtOAc (~ 20 mL). Brine (~ 100 mL) was added, then the organic and aqueous layers were separated. The aqueous layer was washed with Et_2O (~ 75 mL x 4), and the organic portions were combined and dried with Na_2SO_4. After filtration through a pad of Celite and removal of solvent under reduced pressure, a green, viscous solid was isolated. Next, CH_2Cl_2 was added and the mixture was filtered to yield a green solid (which was isolated) and an orange filtrate (which was discarded). The solid was collected from the filter frit and vacuum dried (2.60 g, 29%). This product was used without further purification for the next step. **^{1}H NMR** (acetone-d_6, 400 MHz) δ 7.68 (br s, 2H, Ar), 6.18 (br s, 2H, Ar), 2.13 (s, 6H, Ar–CH$_3$); *Note: C–H$_{methylene}$*

not observed via ^{1}H NMR spectroscopy. These data are consistent with those reported in reference 9.

5.4.6.3 Bis(6-chloropyrid-2-yl)methane (3a)

2a (5.00 g, 18.9 mmol), HCl (12 M, 78.9 mL, 947 mmol), and ethanol (70 mL) were combined in a 500 mL round bottom flask and heated to 80 °C for 20 hours. The deep yellow reaction mixture was cooled in an ice bath and neutralized with NaOH up to a pH of 8 (~ 30-35g NaOH in ~ 100 mL H_2O). The aqueous layer was extracted with EtOAc (100 mL x 4), and the organic layers were combined and dried with Na_2SO_4, then passed through a pad of Celite. The solvent was removed *via* rotary evaporation to yield a light brown solid. The crude product was purified *via* silica gel column chromatography (R_f = 0.50, CH_2Cl_2) to yield a white solid after solvent removal and drying under vacuum (3.18 g, 70%). **^{1}H NMR** (CDCl$_3$, 400 MHz) δ 7.57 (t, 2H, Ar), 7.19 (t, 4H, Ar), 4.26 (s, 2H, CH$_2$); **^{13}C{^{1}H} NMR** (CDCl$_3$, 100 MHz) δ 159.56, 150.96, 139.37, 122.42, 122.30, 46.33.

5.4.6.4 Bis(6-chloro-4-methylpyrid-2-yl)methane (3b)

2b (2.50 g, 8.56 mmol), HCl (12 M, 35.6 mL, 428 mmol), and ethanol (30 mL) were combined in a 300 mL round bottom flask and heated to 80 °C for 16 hours. The deep yellow reaction mixture was cooled in an ice bath and neutralized with NaOH up to a pH of 8 (~ 17g NaOH in ~ 50 mL H_2O). The aqueous layer was extracted with EtOAc (75 mL x 4), and the organic layers were combined and dried with Na_2SO_4, then passed through a pad of Celite. The solvent was removed *via* rotary evaporation to yield a yellow solid. The crude product was purified *via* silica gel column chromatography (R_f = 0.70, CH_2Cl_2) to yield a white solid after solvent removal and drying under vacuum (1.40 g, 61%). **^{1}H NMR** (acetone-d$_6$, 400 MHz) δ 7.14 (d, 4H, Ar), 4.12 (s, 2H, CH$_2$), 2.33 (s, 6H, Ar–CH$_3$); **^{13}C{^{1}H} NMR** (acetone-d$_6$, 100 MHz)

δ 160.36, 152.37, 151.22, 124.33, 123.37, 46.28, 20.58. *These data are consistent with those reported in reference 9.*

5.4.6.5 2,2-Bis(6-chloropyrid-2-yl)propane (4a)

Inside a N_2 filled glove box, **3a** (2.39 g, 10 mmol), KHMDS (2.19 g, 11 mmol), and THF (100 mL) were added to a 250 mL round bottom flask and stirred at room temperature for 2.5 hours to yield a dark brown reaction mixture. Next, CH_3I (0.685 mL, 11 mmol) was added at room temperature, and the reaction mixture immediately turned bright green. After stirring at room temperature for 1 hour, KHMDS (2.99 g, 15 mmol) was added as a solid at room temperature to yield a deep red reaction mixture, which was then allowed to stir at room temperature for 1.5 hours. Next, CH_3I (0.93 mL, 15 mmol) was added at room temperature, and the reaction mixture turned gray within a few minutes. The flask was then heated to 60 °C under N_2 for 16 hours. The reaction was quenched with NH_4Cl, and the organic and aqueous layers were separated. The aqueous layer was extracted with EtOAc (75 mL x 3), and the organic layers were combined and dried with Na_2SO_4, then passed through a pad of Celite. After solvent removal *via* rotary evaporation, the crude product was purified *via* silica gel column chromatography (R_f = 0.70, CH_2Cl_2) to yield a white solid after solvent removal and drying under vacuum (2.47 g, 93%). If the final product is yellow, it can be dissolved in CH_2Cl_2 and stirred with charcoal at room temperature overnight, filtered through a pad of Celite, and isolated under reduced pressure to remove colored impurities. **^{1}H NMR** ($CDCl_3$, 400 MHz) *δ* 7.53 (t, 2H, Ar), 7.15-7.08 (m, 4H, Ar), 1.77 (s, 6H, CH_3); **^{13}C{^{1}H} NMR** ($CDCl_3$, 100 MHz) *δ* 168.00, 150.36, 138.91, 121.87, 120.08, 48.21, 28.24.

5.4.6.6 2,2-Bis(6-chloro-4-methylpyrid-2-yl)propane (4b)

Inside a N_2 filled glove box, **3b** (1.34 g, 5.02 mmol), KHMDS (1.10 g, 5.52 mmol), and THF (50 mL) were added to a 200 mL round bottom flask and stirred at room temperature for 3 hours to yield a red-orange reaction mixture. Next, CH_3I (0.340 mL, 5.52 mmol) was added at room temperature, and the reaction mixture immediately turned green. After stirring at room temperature for 1 hour, KHMDS (1.50 g, 7.52 mmol) was added as a solid at room temperature to yield a red-orange reaction mixture, which was then allowed to stir at room temperature for 1.5 hours. Next, CH_3I (0.470 mL, 7.52 mmol) was added at room temperature, and the reaction mixture turned gray within a few minutes. The flask was then heated to 60 °C under N_2 for 18 hours. The reaction was quenched with NH_4Cl, and the organic and aqueous layers were separated. The aqueous layer was extracted with EtOAc (50 mL x 3), and the organic layers were combined and dried with Na_2SO_4, then passed through a pad of Celite. After solvent removal *via* rotary evaporation, the crude product was purified *via* silica gel column chromatography ($R_f =$ 0.80, CH_2Cl_2) to yield a white solid after solvent removal and drying under vacuum (1.44 g, 97%). If the final product is yellow, it can be dissolved in CH_2Cl_2 and stirred with charcoal at room temperature overnight, filtered through a pad of Celite, and isolated under reduced pressure to remove colored impurities. **¹H NMR** (CDCl₃, 400 MHz) δ 7.11 (m, 4H, Ar), 2.32 (s, 6H, Ar– CH₃), 1.71 (s, 6H, methylene CH₃). *These data are consistent with those reported in reference 11.*

5.4.6.7 2,2-Bis(6-(1-*o*-carboranyl)pyrid-2-yl)propane (5a)

Inside a N_2 filled glove box, *o*-carborane (0.431 g, 3.00 mmol), KHMDS (1.79 g, 9.00 mmol), and Et_2O (20 mL) were added to a 100 mL round bottom flask and stirred at room temperature for 30 minutes to yield a yellow-gold solution. This solution was then added

dropwise to a solution of **bis(6-chloropyrid-2-yl)propane** (0.400 g, 1.50 mmol) in Et_2O (20 mL), and the red-orange reaction mixture was allowed to stir in the glove box at room temperature for 15 hours. The brown reaction mixture was removed from the glove box and quenched with NH_4Cl. The organic and aqueous layers were separated, and the aqueous layer was extracted with EtOAc (50 mL x 3). The organic layers were combined, dried with Na_2SO_4, passed through a layer of Celite, and solvent was removed *via* rotary evaporation. The crude product was purified *via* silica gel column chromatography (R_f = 0.45, 9:1 hexanes:CH_2Cl_2) to yield an orange solid after removal of solvent under reduced pressure. This solid was then dissolved in CH_2Cl_2 (~ 10 mL) and stirred with charcoal at room temperature overnight. This mixture was then passed through a pad of Celite and solvent was removed under reduced pressure to yield an off-white solid. Unreacted *o*-carborane is removed *via* sublimation (60 °C, dynamic vacuum, 3 hours), and the desired product (material that did not sublime) is isolated (0.250 g, 35%). **^{1}H NMR** (CDCl$_3$, 400 MHz) δ 7.64 (t, 2H, Ar), 7.36 (d, 2H, Ar), 7.14 (d, 2H, Ar), 4.65 (s, 2H, C–H$_{carborane}$), 1.72 (s, 6H, CH$_3$), 3.11-1.35 (br, 20H, B–H); **^{11}B NMR** (CDCl$_3$, 160 MHz) δ -3.77 (m, 4B), -11.21 (m, 16B); **^{13}C{^{1}H} NMR** (CDCl$_3$, 100 MHz) δ 166.37, 149.68, 137.89, 121.74, 119.03, 75.52, 56.69, 48.44, 28.07.

5.4.7 Supplementary Figures and Tables
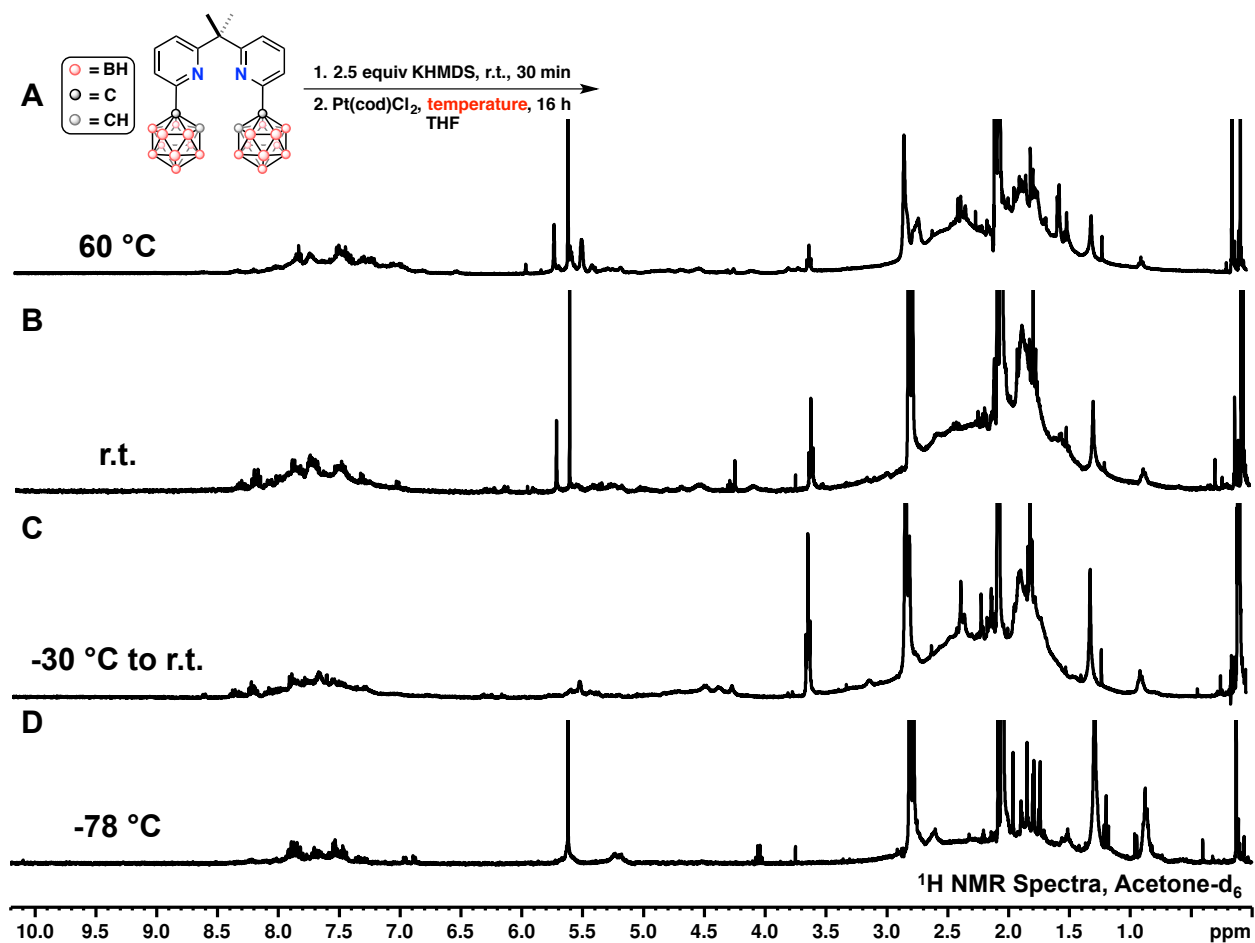
Figure D1 Varying the reaction temperature for the addition of a THF solution of **5a** and 2.5 equivalents of KHMDS to Pt(cod)Cl$_2$. After 16 hours at 60 °C (A), room temperature (B), -30 °C to room temperature (C), or -78 °C (D), solvent was removed *in vacuo*, the crude reaction mixture was dissolved in acetone-d$_6$, and the ^{1}H NMR spectrum for each reaction was obtained.
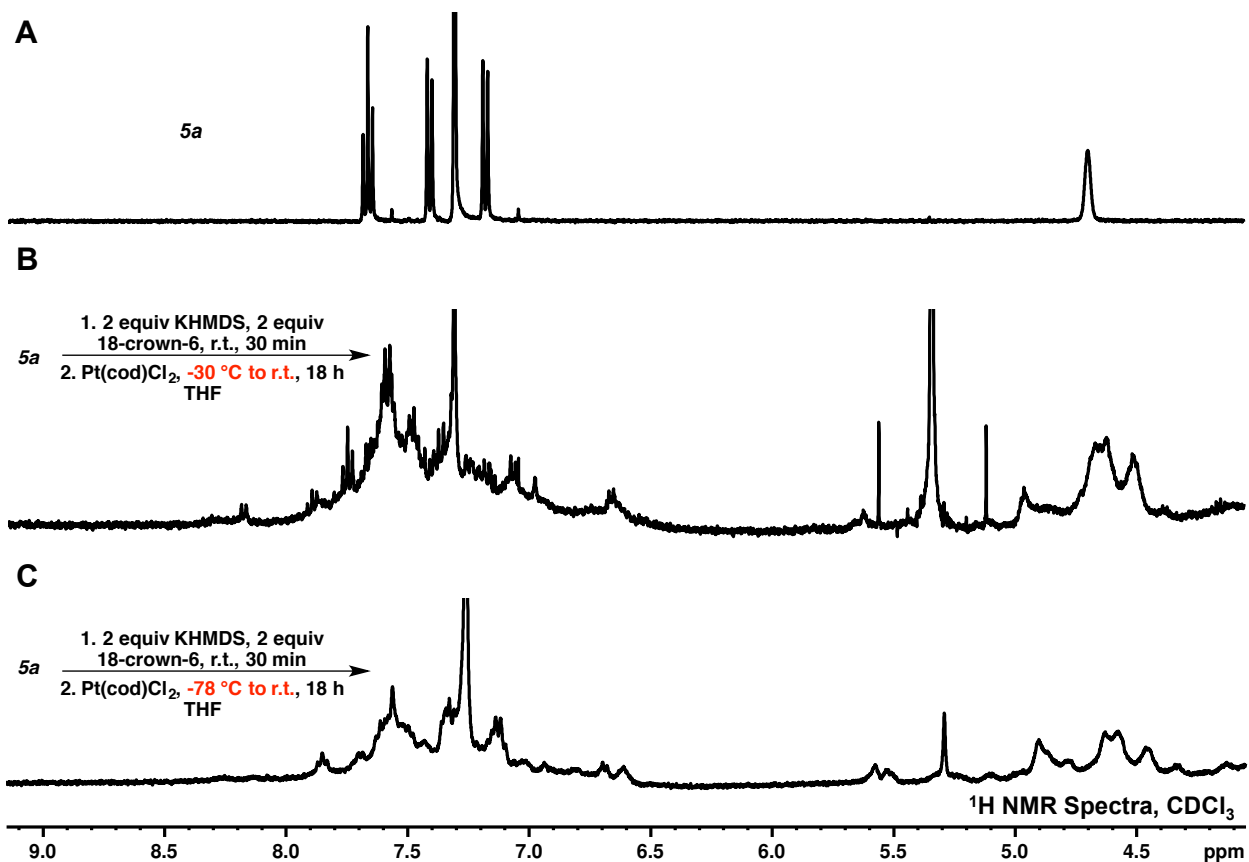
Figure D2 (A) ^{1}H NMR spectrum of **5a** in CDCl$_3$. (B) and (C) Varying the reaction temperature for the addition of a THF solution of **5a**, 2 equivalents of KHMDS, and 2 equivalents of 18-crown-6 to Pt(cod)Cl$_2$. The reaction was allowed to warm from -30 °C to room temperature (B), or -78 °C to room temperature (C) over the course of 16 hours. Following removal of solvent *in vacuo*, the crude product from each reaction was dissolved in CDCl$_3$, and the ^{1}H NMR spectrum was obtained.
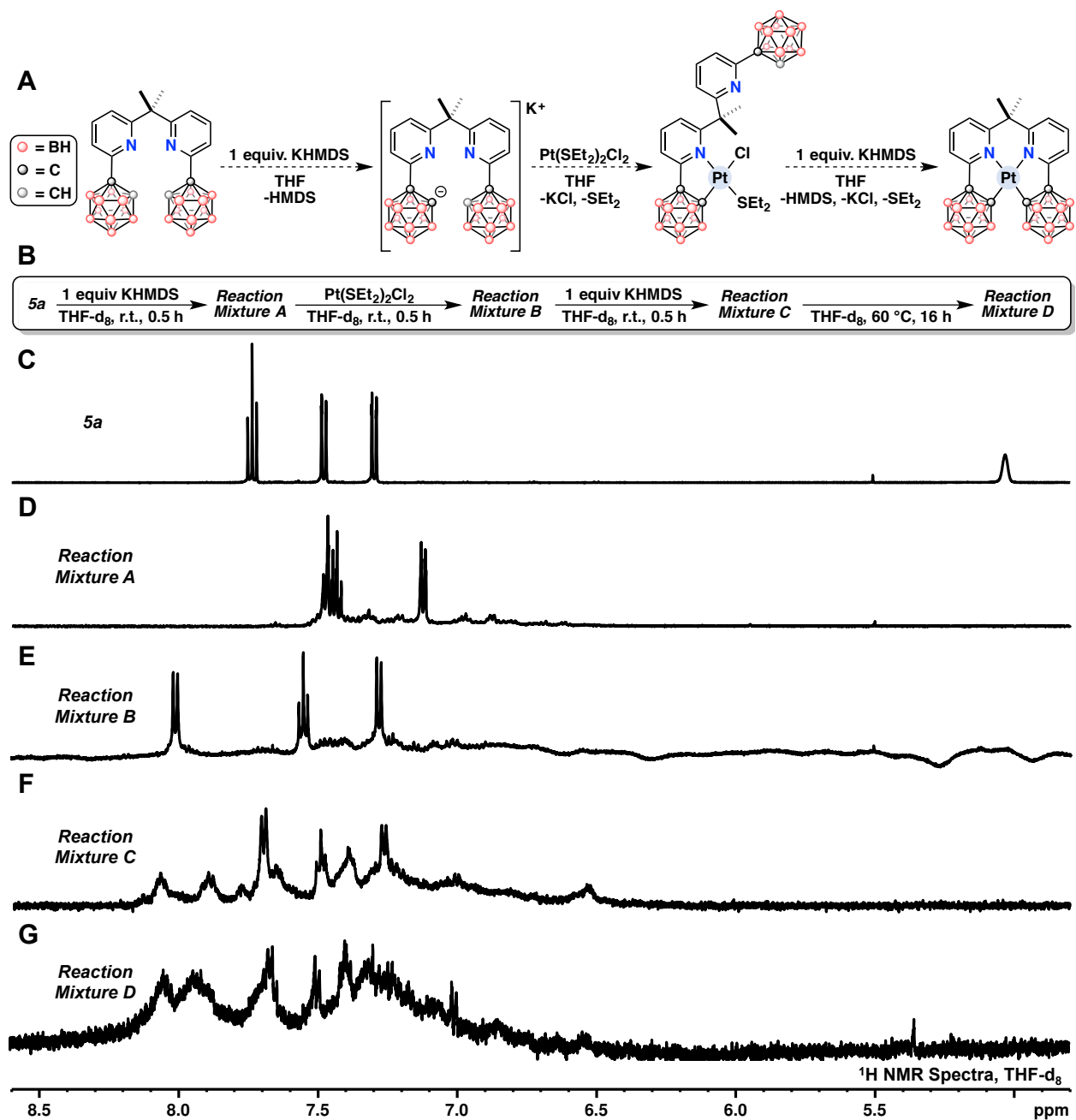
Figure D3 (A) Scheme for the proposed sequential deprotonation and cyclometalation of **5a**. (B) Overview of the NMR-scale experiment conducted. (C) ^{1}H NMR spectrum of **5a** in THF-d$_8$. (D) ^{1}H NMR spectrum of **5a** and 1 equivalent of KHMDS in THF-d$_8$ following stirring at room temperature for 30 minutes (*Reaction Mixture A*). (E) ^{1}H NMR spectrum acquired after Pt(SEt$_2$)$_2$Cl$_2$ was added to *Reaction Mixture A* and stirred for 30 minutes at room temperature (*Reaction Mixture B*). (F) ^{1}H NMR spectrum obtained after 1 equivalent of KHMDS was added to *Reaction Mixture B* and stirred at room temperature for 30 minutes (*Reaction Mixture C*). (G) ^{1}H NMR spectrum acquired after *Reaction Mixture C* was heated to 60 °C overnight (*Reaction Mixture D*).

Table D1 Reactions between **5a** and Pt(acac)$_2$.[a]
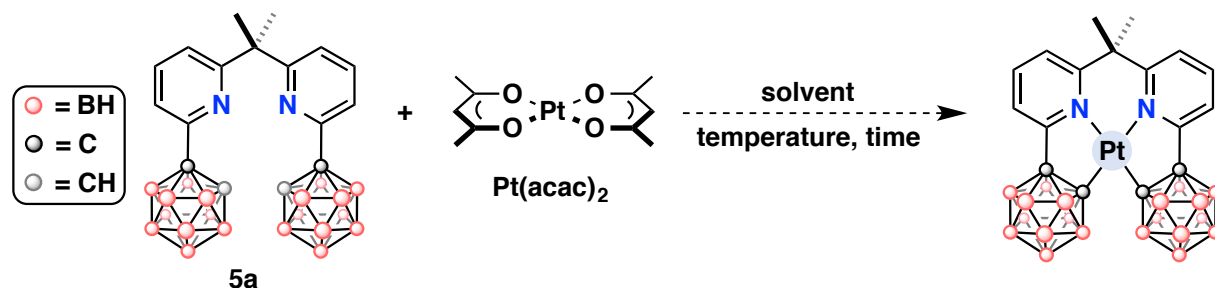
Entry	Solvent	Temperature	Heating Method	Time	Result
1	CH$_3$CN	80 °C	Oil Bath	16 hr	> 99% starting materials[b]
2	CH$_3$CN	140 °C	Microwave	2 hr	> 99% starting materials[b]
3	C$_6$H$_5$CN	170 °C	Oil Bath	16 hr	**5a** + borates[c]

[a]Reactions conducted under N$_2$. [b]Determined by ^{1}H NMR spectroscopy. [c]Determined by ^{11}B NMR spectroscopy.
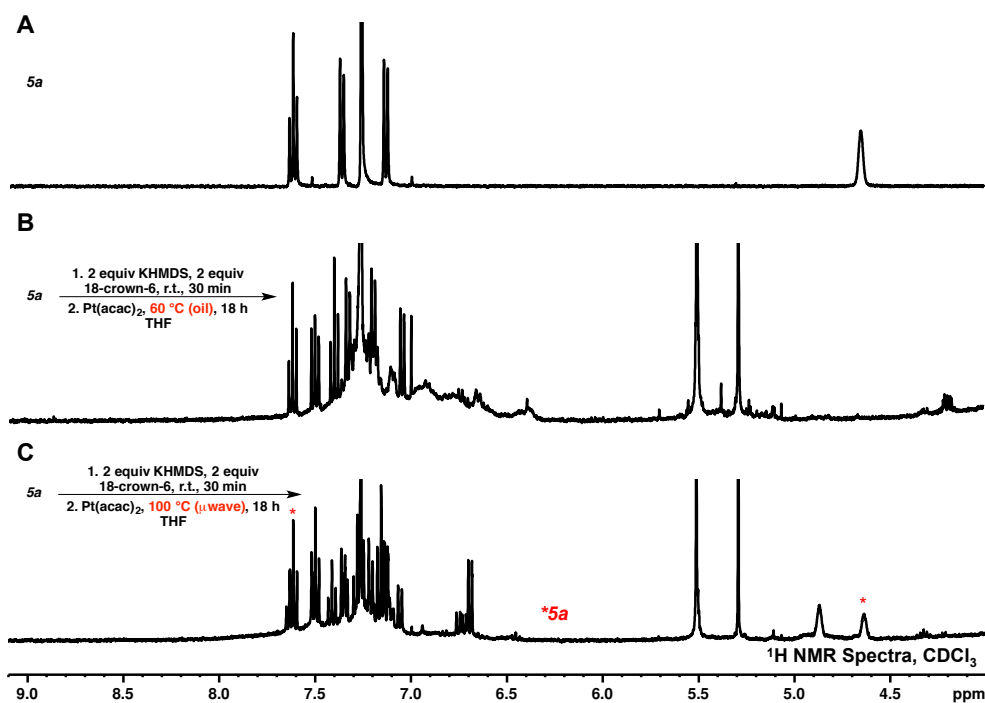
Figure D4 (A) ^{1}H NMR spectrum of **5a** in CDCl$_3$. (B) ^{1}H NMR spectrum of the crude product obtained after a THF solution of **5a**, 2 equivalents of KHMDS, and 2 equivalents of 18-crown-6 was added to a THF solution of Pt(acac)$_2$ and heated to 60 °C in an oil bath for 16 hours. (C) ^{1}H NMR spectrum of the crude product obtained after a THF solution of **5a**, 2 equivalents of KHMDS, and 2 equivalents of 18-crown-6 was added to a THF solution of Pt(acac)$_2$ and heated to 100 °C under microwave irradiation for 16 hours.
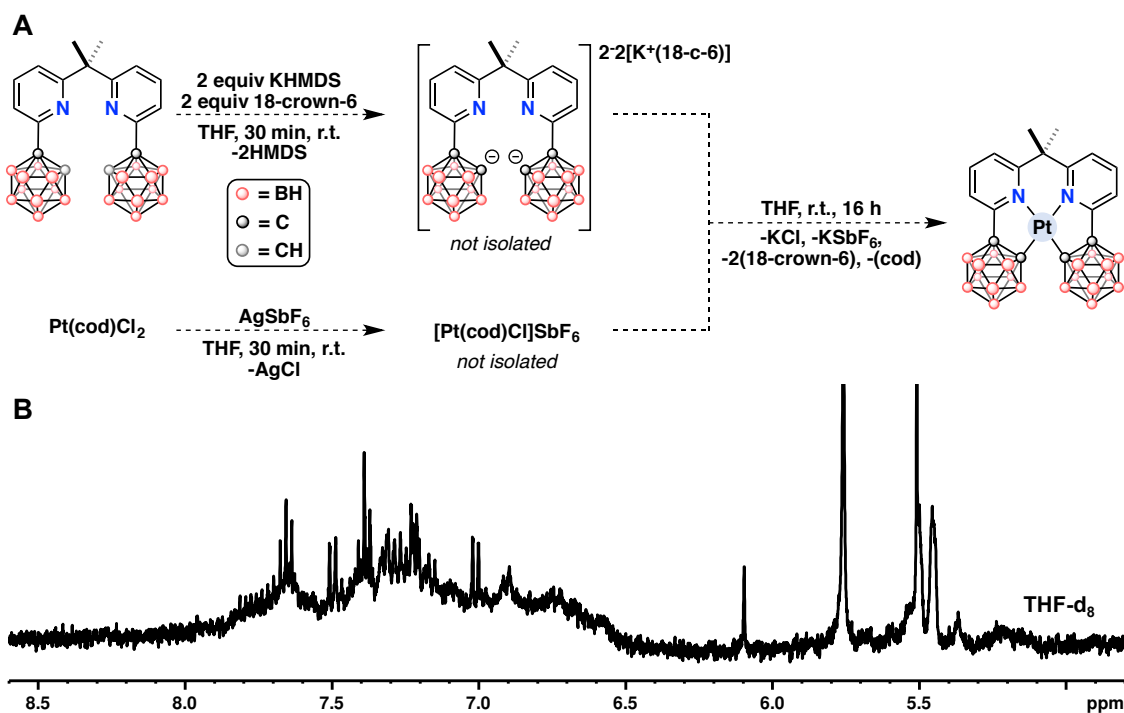
Figure D5 (A) Scheme for reaction involving a cationic Pt(II) precursor. A THF solution of **5a**, 2 equivalents of KHMDS, and 2 equivalents of 18-crown-6 was added to a THF slurry of Pt(cod)Cl$_2$ and 1 equivalent of AgSbF$_6$, then stirred at room temperature overnight. (B) ^{1}H NMR spectrum (THF-d$_8$) obtained from the crude product from the reaction scheme presented in (A).
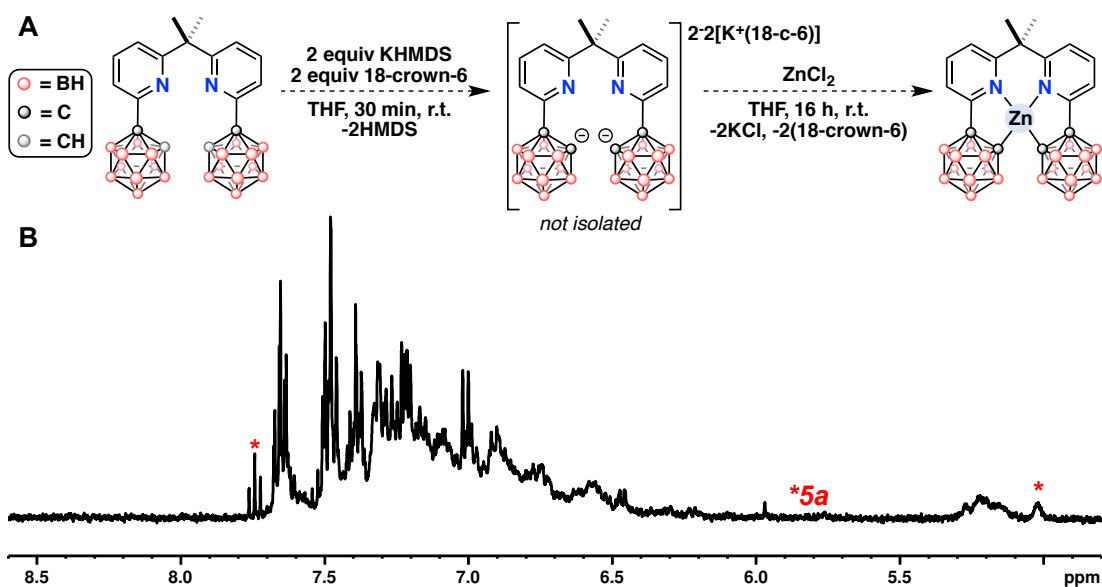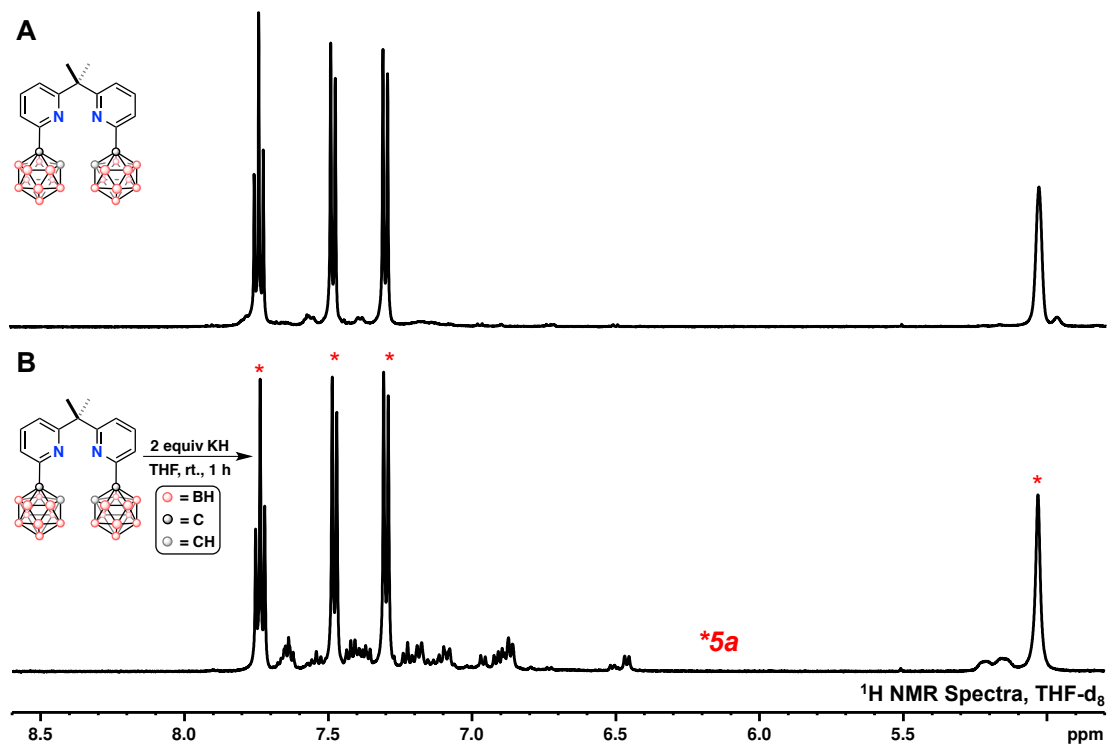

Figure D6 (A) Scheme for the potential synthesis of a Zn(II) analogue of **Pt-2**. A THF solution of **5a**, 2 equivalents of KHMDS, and 2 equivalents of 18-crown-6 was added to a THF slurry of ZnCl$_2$ and stirred at room temperature overnight. (B) ^{1}H NMR spectrum obtained (THF-d$_8$) from the crude product from the reaction scheme presented in (A).

Figure D7 (A) ^{1}H NMR spectrum of **5a** in THF-d$_8$. (B) ^{1}H NMR spectrum obtained after 2 equivalents of KH were added to the THF-d$_8$ solution of **5a** from (A) and allowed to react at room temperature for 1 hour. The major species observed in solution is unreacted **5a**.
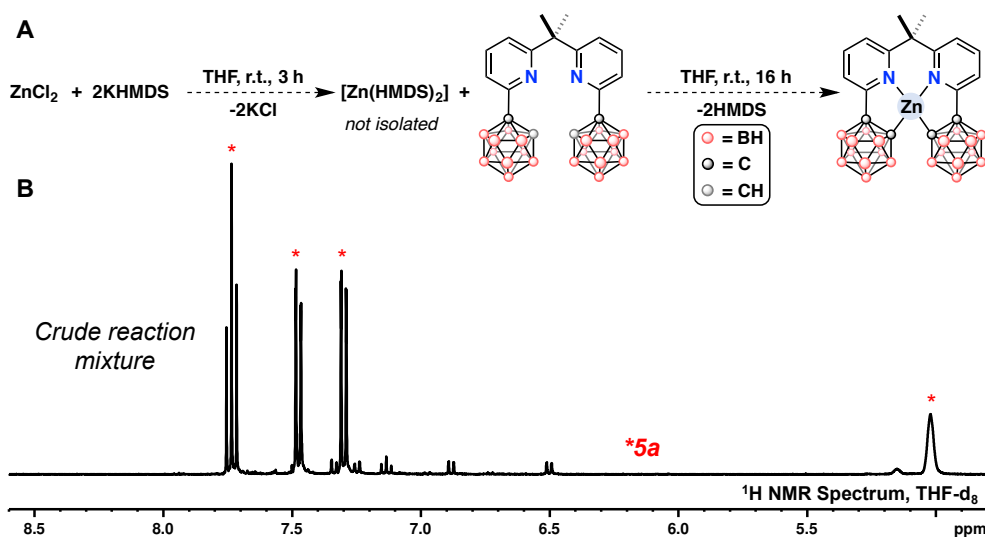
Figure D8 (A) Scheme for the potential synthesis of a Zn(II) analogue of **Pt-2** using Zn(HMDS)$_2$ as the base to deprotonate **5a**. A THF solution of ZnCl$_2$ and 2 equivalents of KHMDS is stirred at room temperature for 3 hours. Next, **5a** is added, and the reaction is allowed to stir at room temperature overnight. (B) ^{1}H NMR spectrum obtained (THF-d$_8$) from the crude product from the reaction scheme presented in (A).
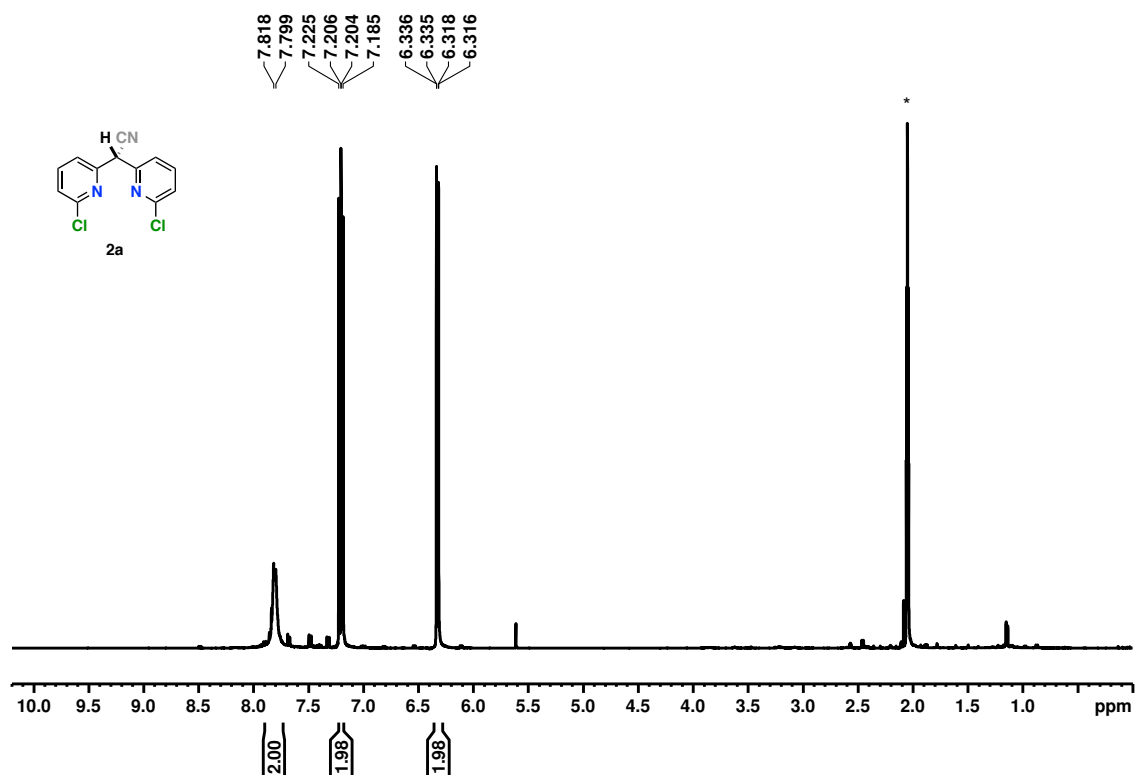
Figure D9 ^{1}H NMR spectrum of **2a**.
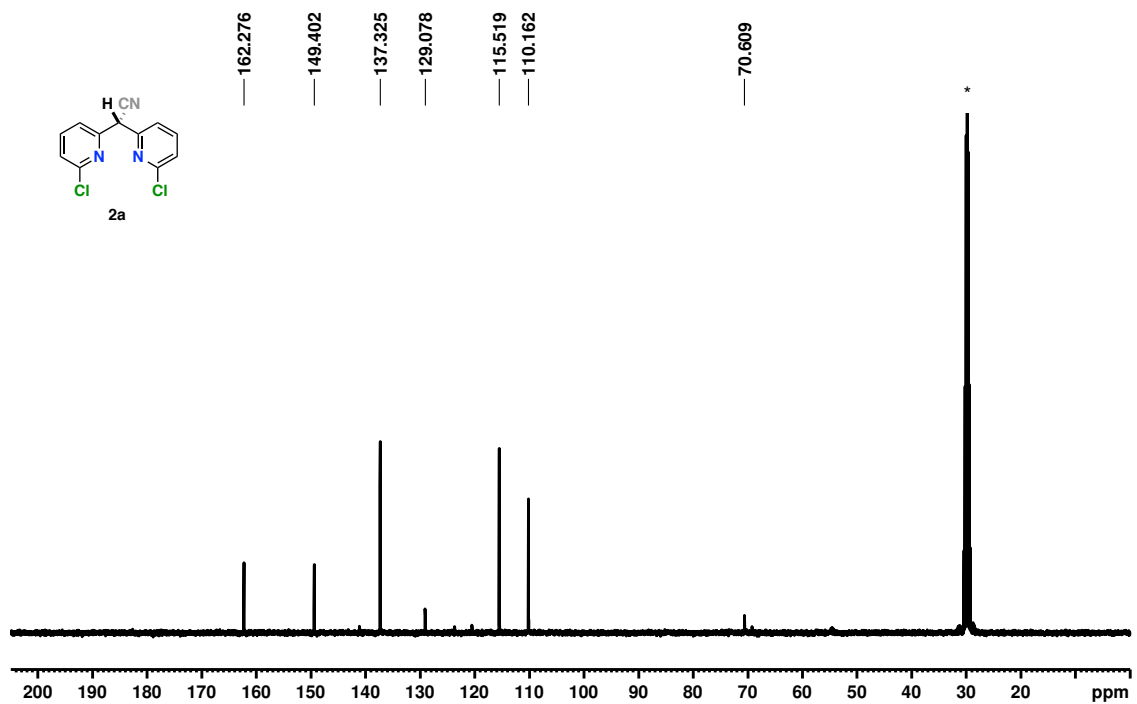
Figure D10 ^{13}C{^{1}H} NMR spectrum of **2a**. *CDCl$_3$.
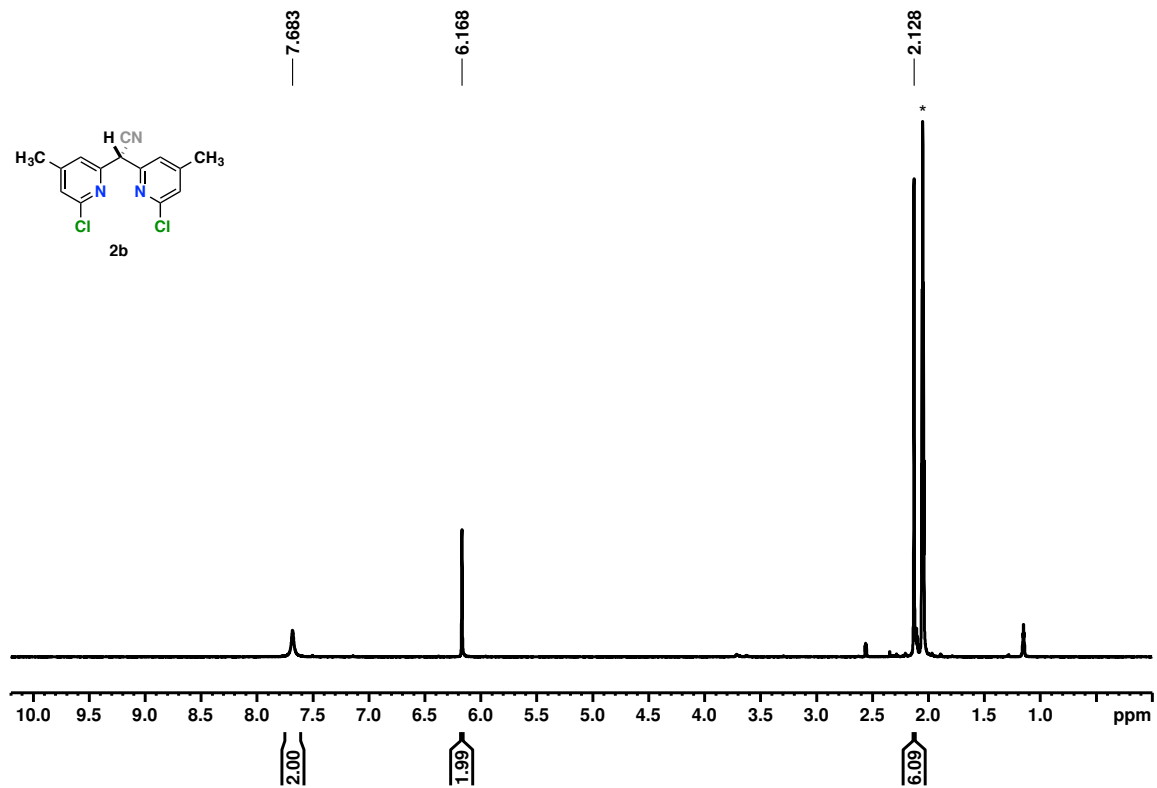
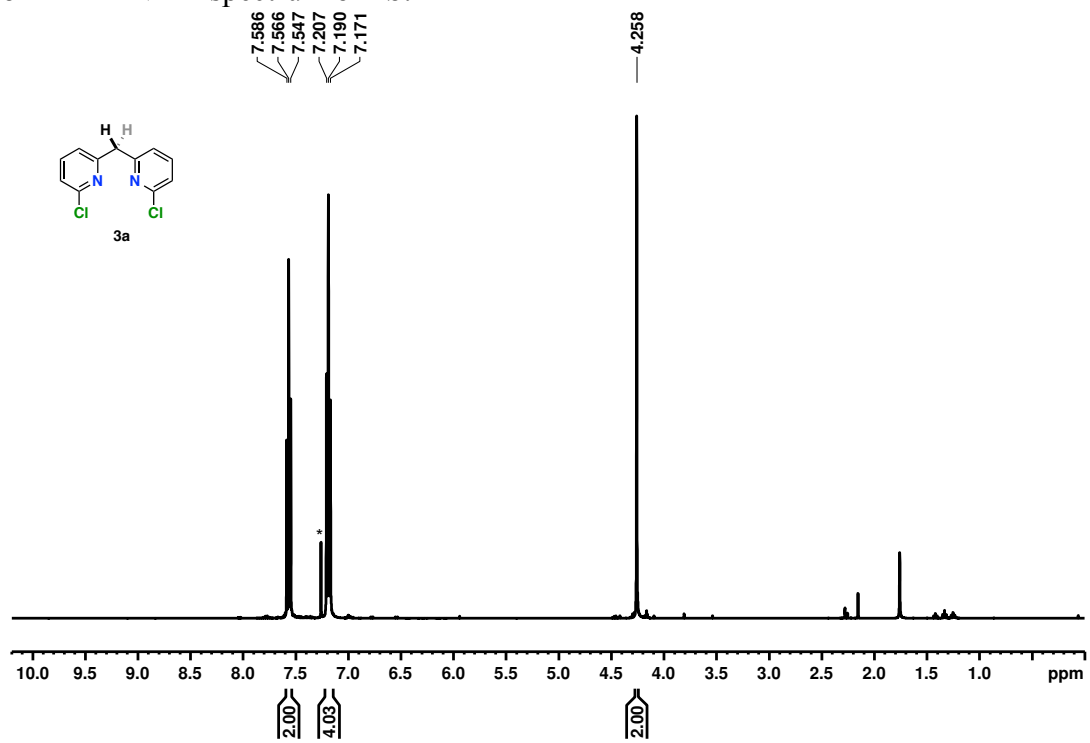**Figure D11** ^{1}H NMR spectrum of **2b**.

Figure D12 ^{1}H NMR spectrum of **3a**. *CDCl$_3$.

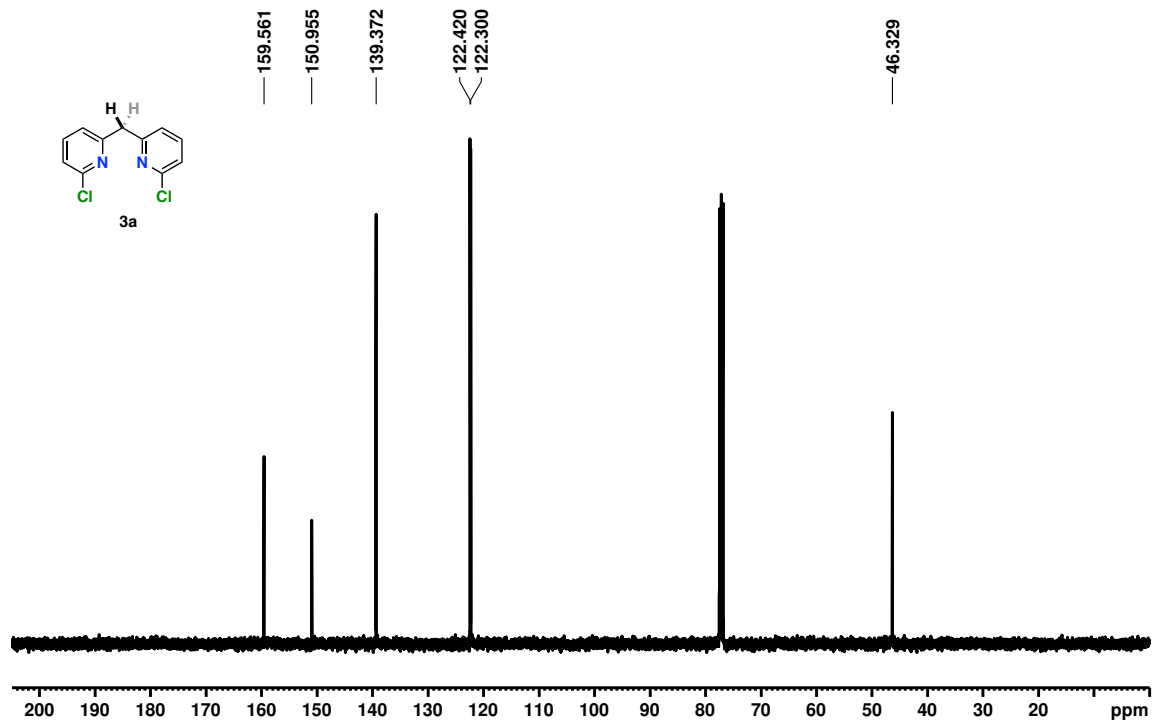**Figure D13** $^{13}C\{^1H\}$ NMR spectrum of **3a**.
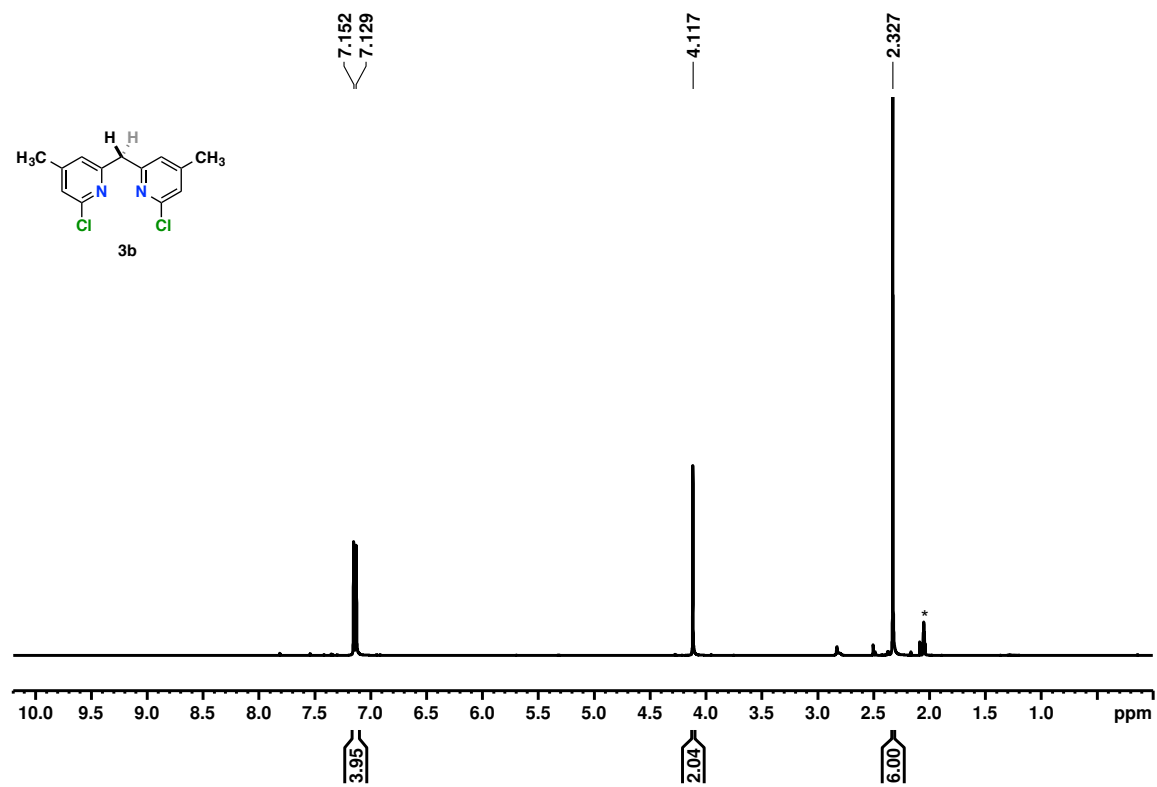

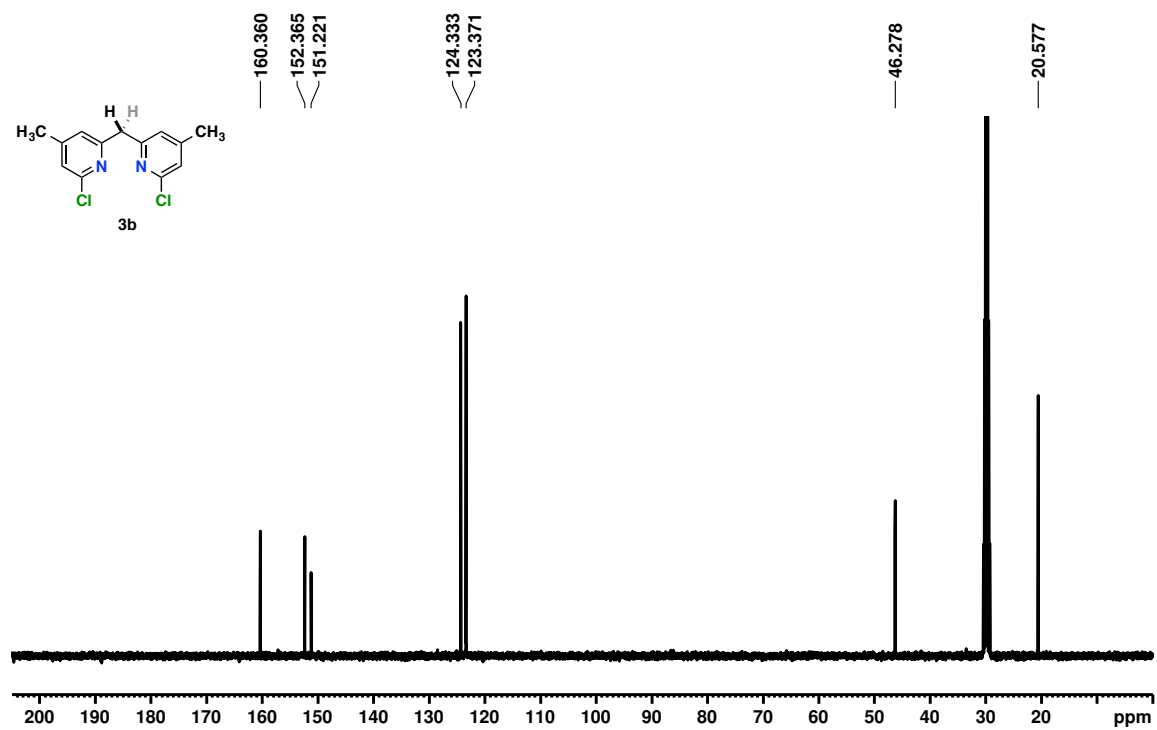**Figure D14** ^1H NMR spectrum of **3b**. *Acetone-d_6.
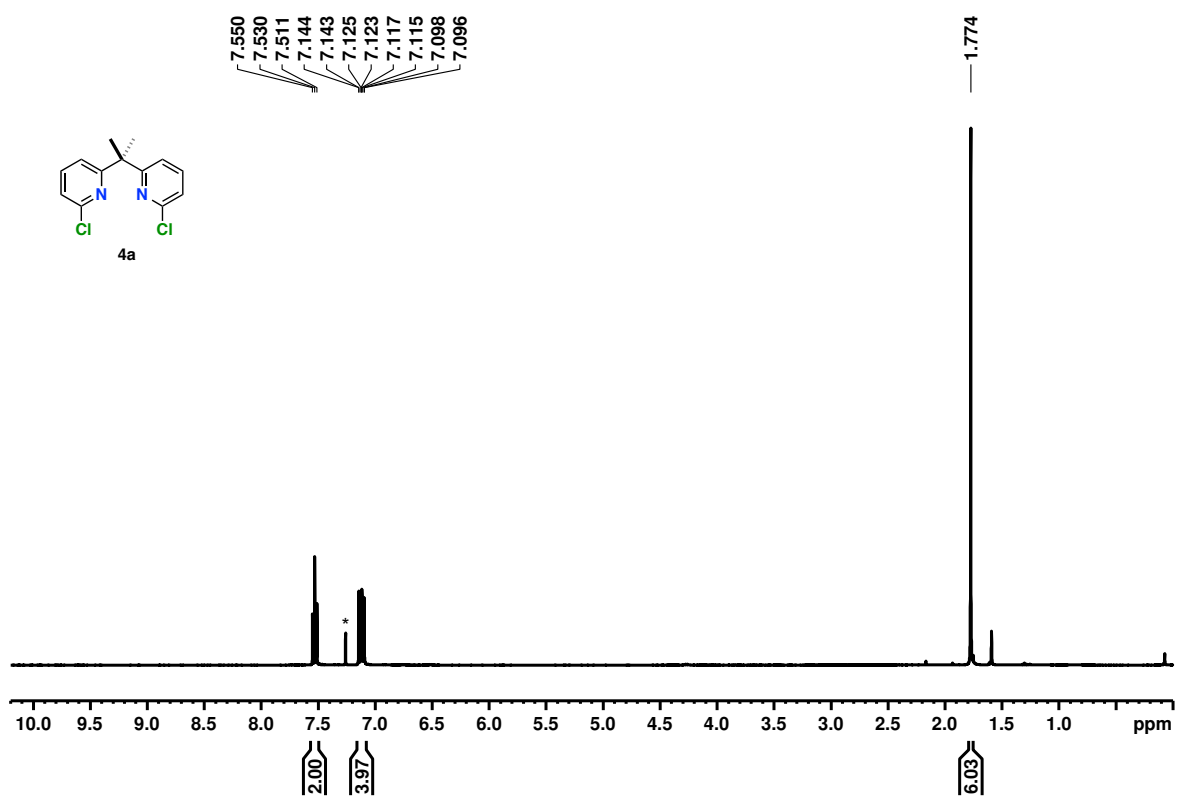
Figure D15 $^{13}C\{^1H\}$ NMR spectrum of **3b**.

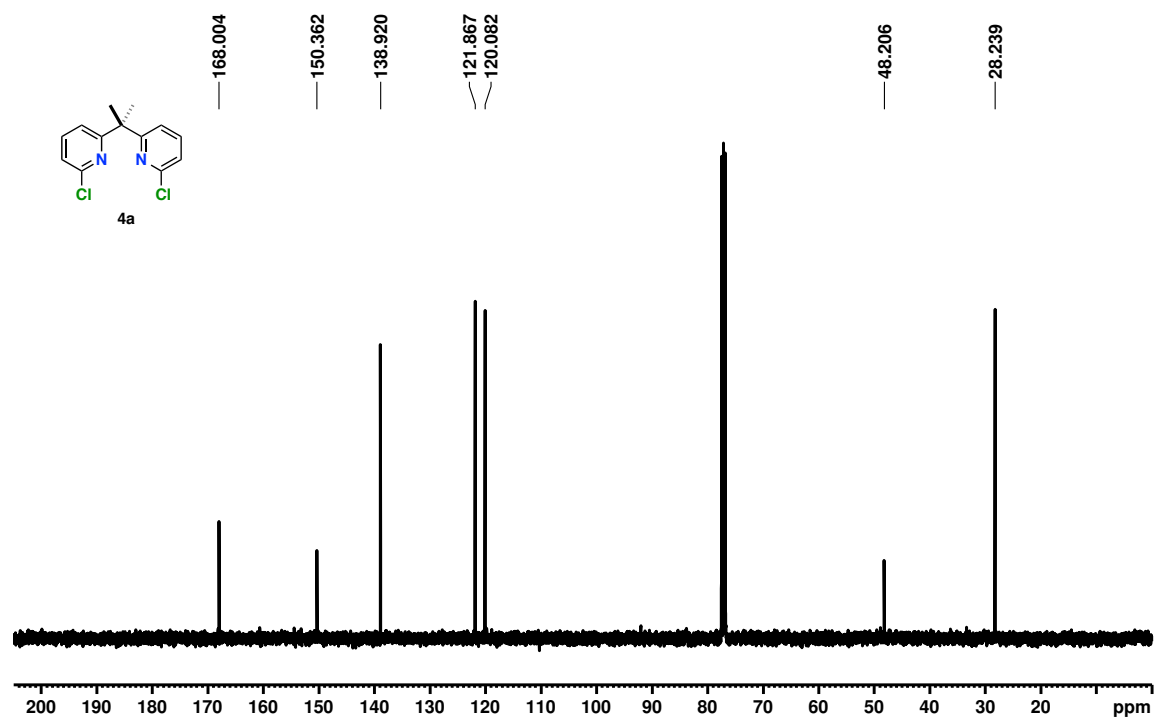**Figure D16** ^1H NMR spectrum of **4a**. *CDCl₃.
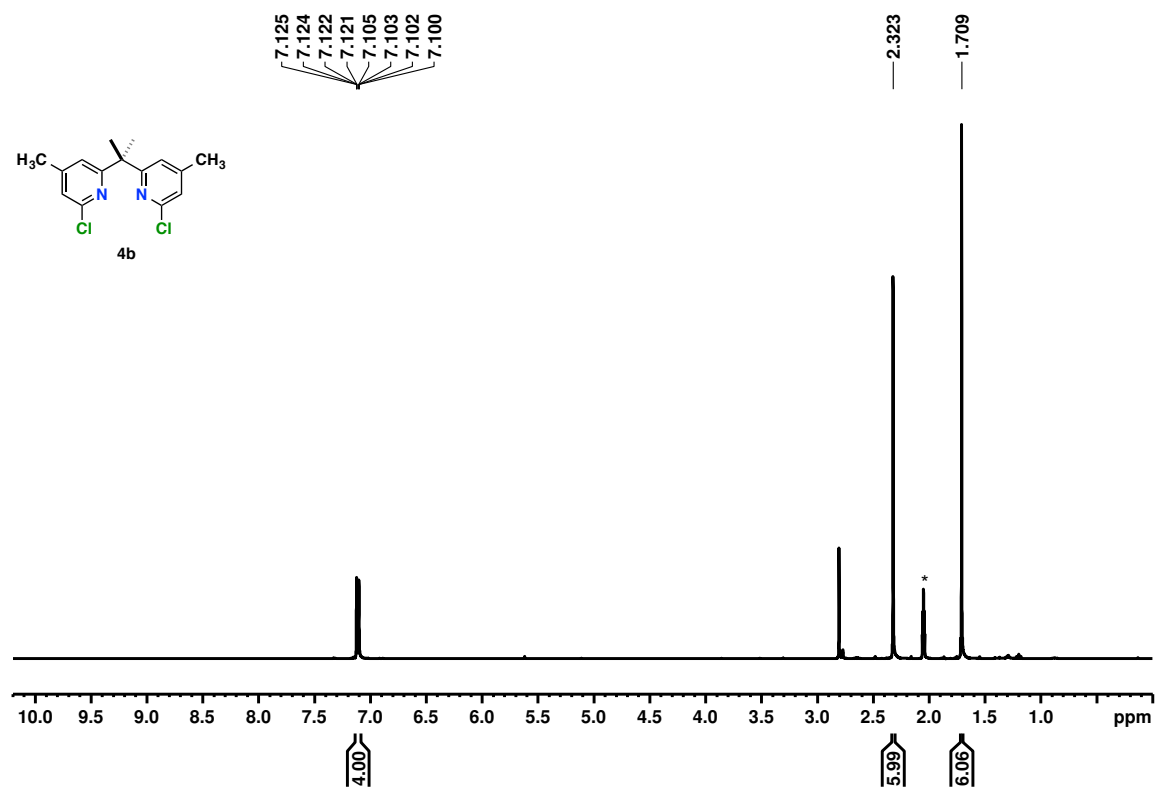
Figure D17 $^{13}C\{^1H\}$ NMR spectrum of **4a**.

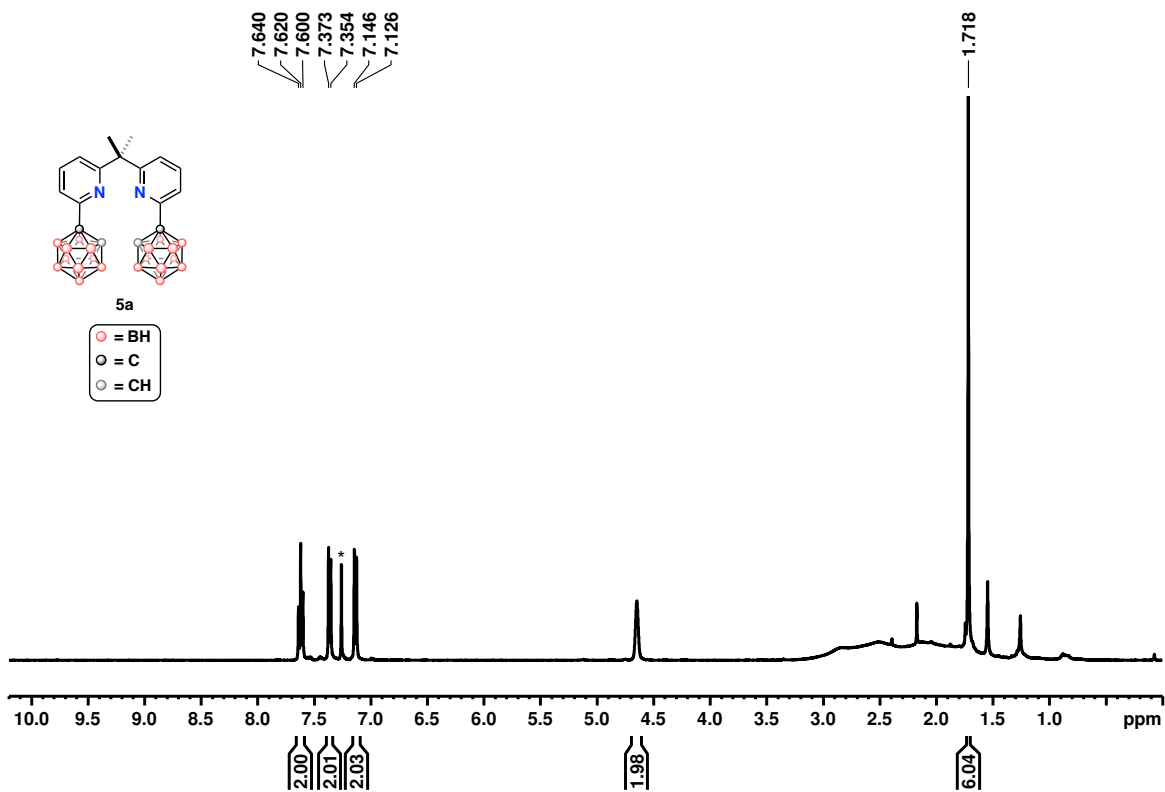**Figure D18** ^1H NMR spectrum of **4b**. *Acetone-d$_6$.
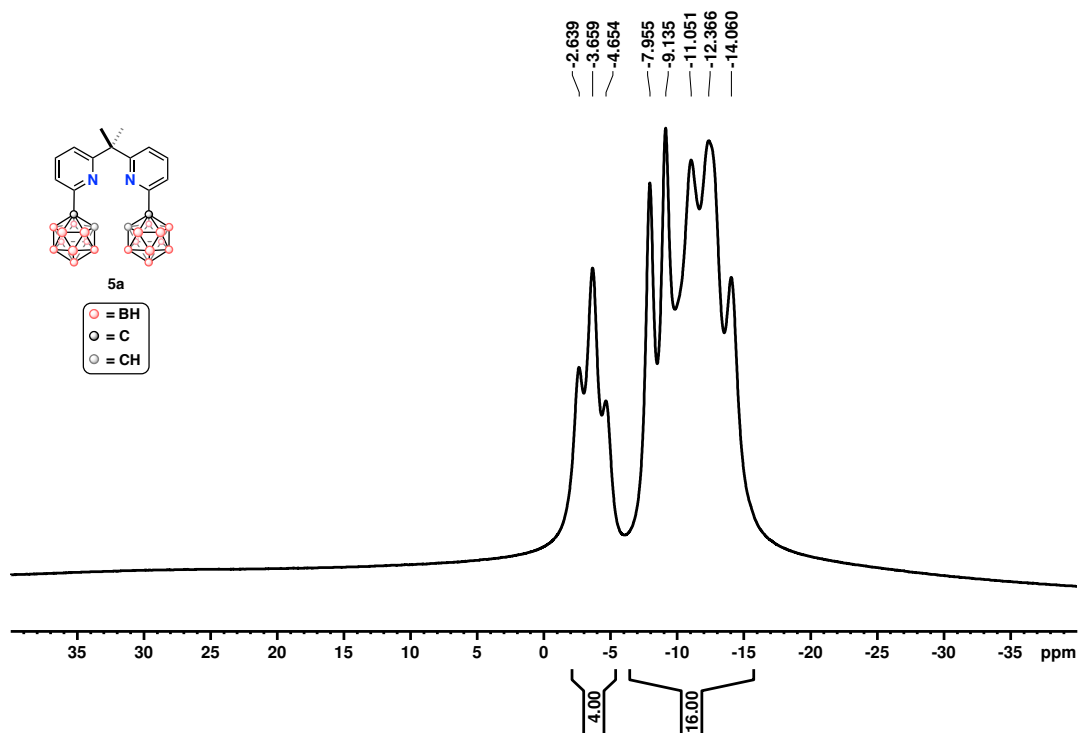
Figure D19 ^{1}H NMR spectrum of **5a**. *CDCl$_3$.

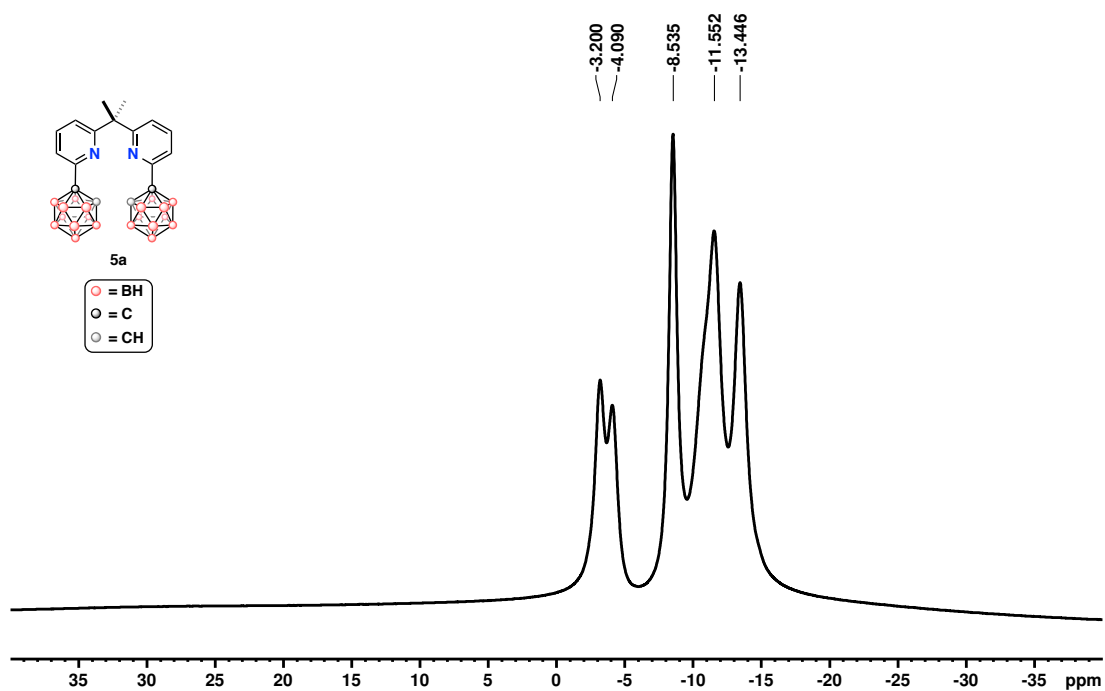**Figure D20** ^{11}B NMR spectrum of **5a**.
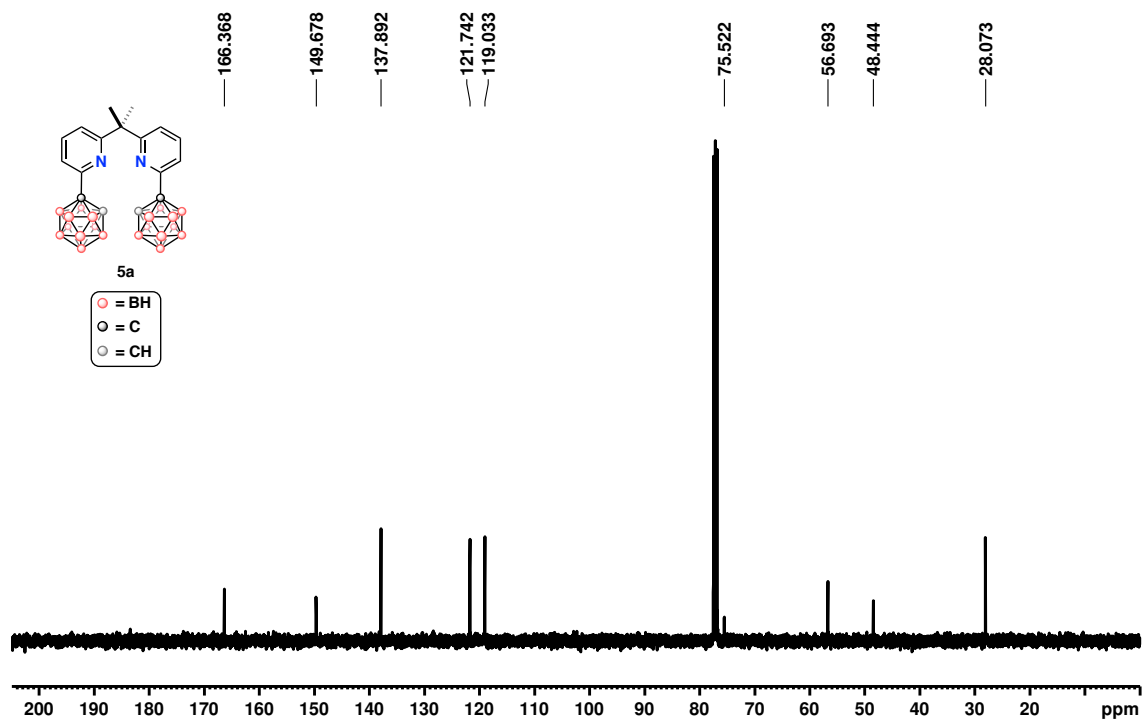
Figure D21 $^{11}B\{^1H\}$ NMR spectrum of **5a**.

Figure D22 $^{13}C\{^1H\}$ NMR spectrum of **5a**.

5.4.8 References For Appendix D

1. J. X. McDermott, J. F. White, G. M. Whitesides, *J. Am. Chem. Soc.* **1976**, *98*, 6521-6528.
2. A. G. De Crisci, A. J. Lough, K. Multani, U. Fekl, *Organometallics* **2008**, *27*, 1765-1779.
3. C. F. Guerra, J. G. Snijders, G. te Velde, E. J. Baerends, *Theo. Chem. Acc.* **1998**, *99*, 391-403; G. te Velde, F. M. Bickelhaupt, E. J. Baerends C. F. Guerra, S. J. A. Van Gisbergen, J. G. Snijders, T. Ziegler, *J. Comput. Chem.* **2001**, *22*, 931-967; ADF 2014/GUI 2014, SCM, Amsterdam, The Netherlands, http://www.scm.com, E.J. Baerends, T. Ziegler, J. Autschbach, D. Bashford, A. Bérces, F.M. Bickelhaupt, C. Bo, P.M. Boerrigter, L. Cavallo, D.P. Chong, L. Deng, R.M. Dickson, D.E. Ellis, M. van Faassen, L. Fan, T.H. Fischer, C. Fonseca Guerra, M. Franchini, A. Ghysels, A. Giammona, S.J.A. van Gisbergen, A.W. Götz, J.A. Groeneveld, O.V. Gritsenko, M. Grüning, S. Gusarov, F.E. Harris, P. van den Hoek, C.R. Jacob, H. Jacobsen, L. Jensen, J.W. Kaminski, G. van Kessel, F. Kootstra, A. Kovalenko, M.V. Krykunov, E. van Lenthe, D.A. McCormack, A. Michalak, M. Mitoraj, S.M. Morton, J. Neugebauer, V.P. Nicu, L. Noodleman, V.P. Osinga, S. Patchkovskii, M. Pavanello, P.H.T. Philipsen, D. Post, C.C. Pye, W. Ravenek, J.I. Rodríguez, P. Ros, P.R.T. Schipper, H. van Schoot, G. Schreckenbach, J.S. Seldenthuis, M. Seth, J.G. Snijders, M. Solà, M. Swart, D. Swerhone, G. te Velde, P. Vernooijs, L. Versluis, L. Visscher, O. Visser, F. Wang, T.A. Wesolowski, E.M. van Wezenbeek, G. Wiesenekker, S.K. Wolff, T.K. Woo, A.L. Yakovlev.
4. A. D. Becke, *Phys. Rev. A* **1988**, *38*, 3098-3100.
5. J. P. Perdew, *Phys. Rev. B* **1986**, *33*, 8822-8824.
6. A. D. Becke, *J. Chem. Phys.* **1993**, *98*, 5648-5652.
7. C. Lee, W. Yang, R. G. Parr, *Phys. Rev. B* **1988**, *37*, 785.
8. E. van Lenthe, E. J. Baerends, J. G. Snijders, *J. Chem. Phys.* **1993**, *99*, 4597-4610.
9. E. van Lenthe, E. J. Baerends, J. G. Snijders, *J. Chem. Phys.* **1994**, *101*, 9783-9792.
10. E. van Lenthe, A. Ehlers, E. J. Baerends, *J. Chem. Phys.* **1999**, *110*, 8943-8953.
11. G. Kottas, Z. Elshenawy, G. Szigethy, C. Xia. Organic Electroluminescent Materials and Devices. U.S. Patent US20160285014A1. March 23, 2015

5.5 References

1. (a) K. O. Kirlikovali, J. C. Axtell, A. Gonzalez, A. C. Phung, S. I. Khan, A. M. Spokoyny, *Chem. Sci.* **2016**, *7*, 5132-5138; (b) K. O. Kirlikovali, J. C. Axtell, K. Anderson, P. I. Djurovich, A. L. Rheingold, A. M. Spokoyny, *Organometallics* **2018**, *37*, 3122-3131.
2. (a) J. Brooks, Y. Babayan, S. Lamansky, P. I. Djurovich, I. Tsyba, R. Bau, M. E. Thompson, *Inorg. Chem.* **2002**, *41*, 3055-3066; (b) D. Bandyopadhyay, P. Bandyopadhyay, A. Chakravorty, F. A. Cotton, L. R. Falvello, *Inorg. Chem.* **1983**, *22*, 1315-1321; (c) L. Chassot, E. Müller, A. von Zelewsky, *Inorg. Chem.* **1984**, *23*, 4249-4253; (d) M. Ghedini, D. Pucci, A. Crispini, G. Barberio, *Organometallics* **1999**, *18*, 2116-2124; (e) K. E. Dungey, B. E. Thompson, N. A. P. Kane-Maguire, L. L. Wright, *Inorg. Chem.* **2000**, *39*, 5192-5196.
3. (a) Y.-Y. Lin, S.-C. Chan, M. C. W. Chan, Y.-J. Hou, N. Zhu, C.-M. Che, Y. Liu, Y. Wang, *Chem. Eur. J.* **2003**, *9*, 1263-1272; (b) C.-M. Che, S.-C. Chan, H.-F. Xiang, M. C. W. Chan, Y. Liu, Y. Wang, *Chem. Commun.* **2004**, 1484-1485; (c) D. A. K. Vezzu, J. C. Deaton, J. S. Jones, L. Bartolotti, C. F. Harris, A. P. Marchetti, M. Kondakova, R. D. Pike, S. Huo, *Inorg. Chem.* **2010**, *49*, 5107-5119; (d) C.-M. Che, C.-C. Kwok, S.-W. Lai, A. F. Rauch, W. J.

Finkenzeller, N. Zhu, H. Yersin, *Chem. Eur. J.* **2010**, *16*, 233-247; (e) S. C. F. Kui, P. K. Chow, G. S. M. Tong, S.-L. Lai, G. Cheng, C.-C. Kwok, K.-H. Low, M. Y. Ko, C.-M. Che, *Chem. Eur. J.* **2013**, *19*, 69-73; (f) S. C. F. Kui, P. K. Chow, G. Cheng, C.-C. Kwok, C. L. Kwong, K.-H. Low, C.-M. Che, *Chem. Commun.* **2013**, *49*, 1497-1499; (g) K. Feng, C. Zuniga, Y.-D. Zhang, D. Kim, S. Barlow, S. R. Marder, J. L. Brédas, M. Weck, *Marcomolecules* **2009**, *42*, 6855-6864; (h) S. Huo, C. F. Harris, D. A. K. Vezzu, J. P. Gagnier, M. E. Smith, R. D. Pike, Y. Li, *Polyhedron* **2013**, *52*, 1030-1040.

4. (a) K. Lai, G. Cheng, C. Ma, X. Guan, W.-M. Kwok, Y. Chen, W. Lu, C.-M. Che, *Chem. Sci.* **2013**, *4*, 2630-2644; (b) E. Turner, N. Bakken, J. Li, *Inorg. Chem.* **2013**, *52*, 7344-7351; (c) X.-C. Hang, T. Fleetham, E. Turner, J. Brooks, J. Li, *Angew. Chem. Int. Ed.* **2013**, *52*, 6753-6756; (d) T. Fleetham, G. Li, L. Wen, J. Li, *Adv. Mater.* **2014**, *26*, 7116-7121; (e) T. B. Fleetham, L. Huang, K. Klimes, J. Brooks, J. Li, *Chem. Mater.* **2016**, *28*, 3276-3282.

5. (a) Y. Im, S. Y. Byun, J. H. Kim, D. R. Lee, C. S. Oh, K. S. Yook, J. Y. Lee, *Adv. Funct. Mater.* **2017**, *27*, 1603007; (b) Y. Zhang, J. Lee, S. R. Forrest, *Nat. Commun.* **2014**, *5*, 5008; (c) C.-H. Hsieh, F.-I. Wu, C.-H. Fan, M.-J. Huang, K.-Y. Lu, P.-Y. Chou, Y.-H. O. Yang, S.-H. Wu, I.-C. Chen, S.-H. Chou, K.-T. Wong, C.-H. Cheng, *Chem. Eur. J.* **2011**, *17*, 9180-9187; (d) R. J. Holmes, S. R. Forrest, T. Sajoto, A. Tamayo, P. I. Djurovich, M. E. Thompson, J. Brooks, Y. J. Tung, B. W. D'Andrade, M. S. Weaver, R. C. Kwong, J. J. Brown, *Appl. Phys. Lett.* **2005**, *87*, 243507; (e) J. Lee, H.-F. Chen, T. Batagoda, C. Coburn, P. I. Djurovich, M. E. Thompson, S. R. Forrest, *Nat. Mater.* **2016**, *15*, 92-98.

6. (a) M. Scholz, E. Hey-Hawkins, *Chem. Rev.* **2011**, *111*, 7035-7062; (b) J. M. Oliva, P. v. r. Schleyer, G. Aullón, J. I. Burgos, A. Fernández-Barbero, I. Alkorta, *Phys. Chem. Chem. Phys.* **2010**, *12*, 5101-5108.

7. (a) The syntheses of **4a** and **4b** are slightly modified from the synthesis of **4b** reported in this patent: G. Kottas, Z. Elshenawy, G. Szigethy, C. Xia. Organic Electroluminescent Materials and Devices. U.S. Patent US20160285014A1. March 23, 2015; (b) The synthesis of **5a** is based on the S_NAr method recently reported: K. P. Anderson, H. A. Mills, C. Mao, K. O. Kirlikovali, J. C. Axtell, A. L. Rheingold, A. M. Spokoyny, *Tetrahedron* **2019**, *75*, 187-191.

8. G. R. Newkome, D. W. Evans, G. E. Kiefer, K. J. Therlot, *Organometallics* **1988**, *7*, 2537-2542.

9. (a) W.-L. Tong, S.-M. Yiu, M. C. W. Chan, *Inorg. Chem.* **2013**, *52*, 7114-7124; (b) E. C. Escudero-Adán, J. Benet-Buchholz, A. W. Kleij, *Inorg. Chem.* **2007**, *46*, 7265-7267; (c) L. S. Felices, E. C. Escudero-Adán, J. Benet-Buchholz, A. W. Kleij, *Inorg. Chem.* **2009**, *48* 846-853.

10. (a) B. Ma, J. Li, P. I. Djurovich, M. Yousufuddin, R. Bau, M. E. Thompson, *J. Am. Chem. Soc.* **2005**, *127*, 28-29; (b) A. Tronnier, T. Strassner, *Dalton Trans.* **2013**, *42*, 9847-9851; (c) T. Strassner, *Acc. Chem. Res.* **2016**, *49*, 2680-2689; (d) H. Leopold, M. Tenne, A. Tronnier, S. Metz, I. Münster, G. Wagenblast, T. Strassner, *Angew. Chem. Int. Ed.* **2016**, *55*, 15779-15782; (e) P. Pinter, Y. Unger, T. Strassner, *ChemPhotoChem* **2017**, *1*, 113-115.

11. (a) S. Duttwyler, *Pure Appl. Chem.* **2018**, *90*, 733-744; (b) Y. Quan, Z. Qui, Z. Xie, *Chem. Eur. J.* **2018**, *24*, 2795-2805; (c) R. M. Dziedzic, J. L. Martin, J. C. Axtell, L. M. A. Saleh, T.-C. Ong, Y.-F. Yang, M. S. Messina, A. L. Rheingold, K. N. Houk, A. M. Spokoyny, *J. Am. Chem. Soc.* **2017**, *139*, 7729-7732; (d) R. M. Dziedzic, L. M. A. Saleh, J. C. Axtell, J. L. Martin, S. L. Stevens, A. T. Royappa, A. L. Rheingold, A. M. Spokoyny, *J. Am. Chem. Soc.* **2016**, *138*, 9081-9084; (e) R. Cheng, B. Li, J. Wu, J. Zhang, Z. Qiu, W. Tang, S.-L. You, Y. Tang, Z. Xie, *J. Am. Chem. Soc.* **2018**, *140*, 4508-4511; (f) R. Cheng, Z. Qiu, Z. Xie, *Nat.*

Commun. **2017**, *8* 14827-14833; (f) R. M. Dziedzic, A. M. Spokoyny, *Chem. Commun.* **2019**, *55*, 430-442.